From intermolecular forces, via crystal engineering, to mechanical flexibility in the organic solid-state

by

Amila Marie Abeysekera

B.Pharm., University of Sri Jayewardenepura, 2010
M.Sc., University of Colombo, 2015

AN ABSTRACT OF A DISSERTATION

submitted in partial fulfillment of the requirements for the degree

DOCTOR OF PHILOSOPHY

Department of Chemistry
College of Arts and Sciences

KANSAS STATE UNIVERSITY
Manhattan, Kansas

2021

Abstract

To better understand the structural influence of competing hydrogen- and halogen-bond interactions, we have investigated the solid-state landscape of a family of amide-substituted pyridines, belonging to four series; (N-(pyridin-2-yl)benzamides (Bz), N-(pyridin-2-yl)picolinamides (2Pyr), N-(pyridin-2-yl)nicotinamides (3Pyr) and N-(pyridin-2-yl) isonicotinamides (4Pyr) functionalized with three different halogen atoms (chlorine, bromine and iodine). We analyzed crystal structures of these sixteen compounds and identified their primary intermolecular interactions. The calculated molecular electrostatic potential (MEP) of the halogen atoms increased in the order of chlorine< bromine<iodine. Halogen bonding, either competitive or complementary (in comparison with the unhalogenated parent) was only shown by the iodinated target and this was consistent with its higher MEP.

Next we explored the influence of an unactivated halogen atom in co-crystal assembly with targets from the three series N-(pyridin-2-yl)picolinamides (2Pyr-X), N-(pyridin-2-yl)nicotinamides (3Pyr-X), N-(pyridin-2-yl)isonicotinamides (4Pyr-X) with ten aliphatic dicarboxylic acids. A total of 100 experiments were carried out. The 4Pyr-I target was the only compound to show competitive halogen bonding both in homomeric assemblies as well as in heteromeric co-crystals.

To investigate halogen-bond binding preferences, we co-crystallized sixteen targets from four families (Bz, 2Pyr, 3Pyr and 4Pyr) with two well halogen-bond donors 1,4-diiodotetrafluorobenzene(DITFB) and 1,3,5-trifluoro-2,4,6-triiodobenzene(TITFB). A total of 13 co-crystals were analyzed by single-crystal X-ray diffraction (SCXRD). The intermolecular hydrogen bonding present in the homomeric targets (those belonging to Bz, 3Pyr and 4Pyr) were

broken to enable co-crystal formation in 9/10 cases. In the three co-crystals from 2Pyr series, where an intramolecular hydrogen bond (HB) is present, a halogen bond (XB) occurred to either a vacant (oxygen or nitrogen) binding site. Overall, the acceptor sites selected by the halogen-bond donors were distributed as follows; N(pyr)=77%, O=C (19%) or π (4%).

Next, we deliberately increased the strength of the halogen-bonding sites (Cl, Br and I) of the Bz, 2Pyr, 3Pyr and 4Pyr targets by activating the halogen atoms via an *sp*-hybridized carbon atom. The analogues ethynyl hydrogen functionalized targets were also synthesized. SCXRD data for fourteen of sixteen compounds were obtained. Upon activation, the MEP of chlorine is in the range of the unactivated iodine atom. Within each series (Bz, 2Pyr, 3Pyr and 4Pyr) the σ-hole values rank in the order of chloroethynyl~iodine<bromoethynyl<iodoethynyl. However, the halogen-bond forming frequency varies in the order of chloroethynyl<iodine~bromoethynyl<iodoethynyl. Chloroethynyl, iodine and bromoethynyl typically formed halogen bonds to π or nitrogen acceptors. The iodoethynyl moiety emerged as the superior XB donor forming halogen bonds 4/4 times, and the interaction was always to a pyridyl nitrogen. The ethynyl hydrogen-bond donor had a MEP between halogens of bromoethynyl and iodoethynyl, and selected a carbonyl oxygen as an acceptor site in all three cases.

We next investigated the self-aggregation of N-(pyridin-2-yl)alkylamides (substituted at the 5 position), which may be considered as the alkyl version of the previously explored Bz targets. These molecules can primarily aggregate through chain or dimer formation. We synthesized twenty targets with substituents Cl, Br, I, H or methyl combined with different alkyl chains (acetyl, propyl, butyl, and pentyl). IR and SXCRD were used to assess the mode of assembly and we found that IR data alone could be used to elucidate which of the two primary motifs were present in the solid state. Broadly speaking chains were more common with the two shorter alkyl chains (7/10)

and dimers with the two longer alkyl chains (7/10). As a strategy for altering the assembly of compounds carrying shorter alkyl chains, we introduced an iodoethynyl and ethynyl hydrogen groups as potential structural 'disruptors'. We successfully switched the assembly from chains to dimers 4/4 times.

In order to synthesize new (and very rare) examples of ternary co-crystals, we developed assembly strategies that combined NH-N and iodoethynyl moieties to act as recognition sites for a carboxylic acid and a pyridyl nitrogen acceptor site respectively. Two target molecules, N-(5-(iodoethynyl)pyridin-2-yl)acetamide and N-(5-(iodoethynyl)pyridin-2-yl)benzamide, were synthesized and screened against three aromatic acids and either five or seven halogen bond acceptors. A total of 36 attempted syntheses of ternary co-crystals were carried out, and based on IR and DSC data, we identified 29 positive hits corresponding to a remarkable success rate 80%. We also managed to grow a single-crystal of one of these co-crystals which demonstrated that our postulated strategy did indeed deliver the intended binding modes.

Finally, we discovered that one of our co-crystals, N-(5-iodopyridin-2-yl) propionamide:benzoic acid displayed remarkable mechanical flexibility, and given the broad interest in understanding how flexibility of crystalline materials is related to structure (packing features), we began to explore the structure-property relationships of similar co-crystals (i.e. formed by N-(pyridin-2-yl)alkylamides and carboxylic acids). A total of ten co-crystals were obtained. The three co-crystals obtained from the target bearing an acetyl chain were brittle, while the seven co-crystals obtained from a target bearing a propyl or butyl chain were flexible. Five of these displayed elastic deformation while two displayed plastic deformation. The three different responses (brittle, plastic, and elastic deformation) to external mechanical stimuli, could be explained by specific intermolecular interactions and packing features in each crystal structure.

From intermolecular forces, via crystal engineering, to mechanical flexibility in the organic solid-state

by

Amila Marie Abeysekera

B.Pharm., University of Sri Jayewardenepura, 2010
M.Sc., University of Colombo, 2015

A DISSERTATION

submitted in partial fulfillment of the requirements for the degree

DOCTOR OF PHILOSOPHY

Department of Chemistry
College of Arts and Sciences

KANSAS STATE UNIVERSITY
Manhattan, Kansas

2021

Approved by:

Major Professor
Dr. Christer B. Aakeröy

Copyright

Abstract

To better understand the structural influence of competing hydrogen- and halogen-bond interactions, we have investigated the solid-state landscape of a family of amide-substituted pyridines, belonging to four series; (N-(pyridin-2-yl)benzamides (Bz), N-(pyridin-2-yl)picolinamides (2Pyr), N-(pyridin-2-yl)nicotinamides (3Pyr) and N-(pyridin-2-yl) isonicotinamides (4Pyr) functionalized with three different halogen atoms (chlorine, bromine and iodine). We analyzed crystal structures of these sixteen compounds and identified their primary intermolecular interactions. The calculated molecular electrostatic potential (MEP) of the halogen atoms increased in the order of chlorine< bromine<iodine. Halogen bonding, either competitive or complementary (in comparison with the unhalogenated parent) was only shown by the iodinated target and this was consistent with its higher MEP.

Next we explored the influence of an unactivated halogen atom in co-crystal assembly with targets from the three series N-(pyridin-2-yl)picolinamides (2Pyr-X), N-(pyridin-2-yl)nicotinamides (3Pyr-X), N-(pyridin-2-yl)isonicotinamides (4Pyr-X) with ten aliphatic dicarboxylic acids. A total of 100 experiments were carried out. The 4Pyr-I target was the only compound to show competitive halogen bonding both in homomeric assemblies as well as in heteromeric co-crystals.

To investigate halogen-bond binding preferences, we co-crystallized sixteen targets from four families (Bz, 2Pyr, 3Pyr and 4Pyr) with two well halogen-bond donors 1,4-diiodotetrafluorobenzene(DITFB) and 1,3,5-trifluoro-2,4,6-triiodobenzene(TITFB). A total of 13 co-crystals were analyzed by single-crystal X-ray diffraction (SCXRD). The intermolecular hydrogen bonding present in the homomeric targets (those belonging to Bz, 3Pyr and 4Pyr) were broken to enable co-crystal formation in 9/10 cases. In the three co-crystals from 2Pyr series, where

an intramolecular hydrogen bond (HB) is present, a halogen bond (XB) occurred to either a vacant (oxygen or nitrogen) binding site. Overall, the acceptor sites selected by the halogen-bond donors were distributed as follows; N(pyr)=77%, O=C (19%) or π (4%).

Next, we deliberately increased the strength of the halogen-bonding sites (Cl, Br and I) of the Bz, 2Pyr, 3Pyr and 4Pyr targets by activating the halogen atoms via an *sp*-hybridized carbon atom. The analogues ethynyl hydrogen functionalized targets were also synthesized. SCXRD data for fourteen of sixteen compounds were obtained. Upon activation, the MEP of chlorine is in the range of the unactivated iodine atom. Within each series (Bz, 2Pyr, 3Pyr and 4Pyr) the σ-hole values rank in the order of chloroethynyl~iodine<bromoethynyl<iodoethynyl. However, the halogen-bond forming frequency varies in the order of chloroethynyl<iodine~bromoethynyl<iodoethynyl. Chloroethynyl, iodine and bromoethynyl typically formed halogen bonds to π or nitrogen acceptors. The iodoethynyl moiety emerged as the superior XB donor forming halogen bonds 4/4 times, and the interaction was always to a pyridyl nitrogen. The ethynyl hydrogen-bond donor had a MEP between halogens of bromoethynyl and iodoethynyl, and selected a carbonyl oxygen as an acceptor site in all three cases.

We next investigated the self-aggregation of N-(pyridin-2-yl)alkylamides (substituted at the 5 position), which may be considered as the alkyl version of the previously explored Bz targets. These molecules can primarily aggregate through chain or dimer formation. We synthesized twenty targets with substituents Cl, Br, I, H or methyl combined with different alkyl chains (acetyl, propyl, butyl, and pentyl). IR and SXCRD were used to assess the mode of assembly and we found that IR data alone could be used to elucidate which of the two primary motifs were present in the solid state. Broadly speaking chains were more common with the two shorter alkyl chains (7/10) and dimers with the two longer alkyl chains (7/10). As a strategy for altering the assembly of

compounds carrying shorter alkyl chains, we introduced an iodoethynyl and ethynyl hydrogen groups as potential structural ‘disruptors’. We successfully switched the assembly from chains to dimers 4/4 times.

In order to synthesize new (and very rare) examples of ternary co-crystals, we developed assembly strategies that combined NH-N and iodoethynyl moieties to act as recognition sites for a carboxylic acid and a pyridyl nitrogen acceptor site respectively. Two target molecules, N-(5-(iodoethynyl)pyridin-2-yl)acetamide and N-(5-(iodoethynyl)pyridin-2-yl)benzamide, were synthesized and screened against three aromatic acids and either five or seven halogen bond acceptors. A total of 36 attempted syntheses of ternary co-crystals were carried out, and based on IR and DSC data, we identified 29 positive hits corresponding to a remarkable success rate 80%. We also managed to grow a single-crystal of one of these co-crystals which demonstrated that our postulated strategy did indeed deliver the intended binding modes.

Finally, we discovered that one of our co-crystals, N-(5-iodopyridin-2-yl) propionamide:benzoic acid displayed remarkable mechanical flexibility, and given the broad interest in understanding how flexibility of crystalline materials is related to structure (packing features), we began to explore the structure-property relationships of similar co-crystals (i.e. formed by N-(pyridin-2-yl)alkylamides and carboxylic acids). A total of ten co-crystals were obtained. The three co-crystals obtained from the target bearing an acetyl chain were brittle, while the seven co-crystals obtained from a target bearing a propyl or butyl chain were flexible. Five of these displayed elastic deformation while two displayed plastic deformation. The three different responses (brittle, plastic, and elastic deformation) to external mechanical stimuli, could be explained by specific intermolecular interactions and packing features in each crystal structure.

Table of Contents

List of Figures

List of Tables

Acknowledgements

First and foremost, I acknowledge my major advisor Prof. Christer B. Aakeröy, for giving me the opportunity to be a part of his research group. It's been an amazing journey! I'm grateful for his inspiration and motivation which encourages me to always strive to try to do my level best. I'm indebted for his extreme patience, support, advice, and kindness that has helped me pull through! I'm grateful for his selfless sacrifice in collecting data and solving crystal structures (around the clock), without which this thesis wouldn't be the same.

Thank you to my committee members, Prof. Tendai Gadzikwa, Prof. Christine Aikens, Prof. Ruth Welti, Prof. Brian Geisbrecht for their valuable time and feedback, flexibility in exam scheduling and support.

I wish to acknowledge everyone who solved crystal structures. Thank you to Dr. Boris Averkiev (especially for being so enthusiastic!), Dr. Abhijeet Sinha, Dr. Victor Day and Dr. Pierre LeMagueres for their valuable contribution in making this work possible.

Department of Chemistry for funding throughout my studies at KSU. I wish to acknowledge Boehringer Ingelheim for the summer internship opportunity (2018) and Dr. Nina Gonella for her supervision. Johnson Cancer Research Centre (summer 2019), John Berschied and Donna Derstadt Fellowship in Chemistry (summer 2020) and NOTICXE Graduate Student Fellowship (spring 2021) for support which made this work possible. Thank you to PLU, Graduate Student Council, Arts and Sciences Travel Scholarship at Kansas State University for providing funding for attending conferences. I wish to express my thanks to the General Sir John Kotelawela Defence University and my colleagues for supporting my stay at KSU for studies.

Everyone at the department of chemistry, KSU for being very friendly and supportive. Special thanks to Prof. Ryan Rafferty for his support during the application process, Dr. Yasmin

Patell for making our group gathering enjoyable and entertaining, Mr. Michael Hinton for his support in teaching scheduling and Dr. Daniel Higgins for navigating the Department amidst a pandemic! Dr. Leila Maurmann for the initial NMR training, Dr. Simon Sham for keeping the new instruments in terrific condition, Mr. Jim Hodgson, Mr. Tobe Eggers, Mr. Ron Jackson for their creative solutions to lab issues and for being ever willing to help-out! Ms. Mary Dooley, Ms. Kim Ross and everyone else for all the work they do behind the scenes to keep everything running smoothly.

Special thanks to Aakeröy group members (past and present) for all the support throughout my time at KSU. A big thank you to Dr. Bhupinder Sandhu for her guidance and encouragement as I was starting out in lab. Thank you to Dr. Nandini Sarkar, Dr. Janaka Gamekkanda and Dr. Manomi Perera for helping me in numerous ways. I'm grateful for your support, the good-times and memories with all of you including Vinu Panikkattu, Viraj de Silva and Kelly Shunje.

I am grateful to Dr. David Littrell, Dr. Cora Cooper, Dr. Rachel Dirks and the Department of Music for all the opportunities and support given to me.

I wish to thank friends in the Department of Chemistry, Department of Music and on campus for making my time at KSU memorable, and friends from back home for their support.

Last but not least, I thank all my family for their love and support!

Preface

Research carried out at Kansas State University for this dissertation led to the following publications in scientific journals.

1. Mapping out the Relative Influence of Hydrogen and Halogen and Bonds in Crystal Structures of a Family of Amide-Substituted Pyridines by Amila M. Abeysekera, Victor W. Day, Abhijeet S. Sinha, and Christer B. Aakeröy; *Crystal Growth & Design* http://dx.doi.org/10.1021/acs.cgd.0c01086 (Chapter 2)
2. The Impact of Halogen Substituents on the Synthesis and Structure of Co-Crystals of Pyridine Amides by Amila M. Abeysekera, Abhijeet S. Sinha and Christer B. Aakeröy; *Molecules* https://doi.org/10.3390/molecules26041147 (Chapter 3)
3. Establishing halogen-bond preferences in molecules with multiple acceptor sites by Amila M. Abeysekera, Boris B. Averkiev, Abhijeet S. Sinha, Pierre Le Magueres and Christer B. Aakeröy; submitted for review to *ChemPlusChem* (Chapter 4)

Chapter 1 - Introduction and outline of the thesis

1.1 Significance of structure property relationships

The practical usefulness and performance of any material is governed by its structure. For example, at the molecular level the stereochemistry of a drug molecule would render it either toxic or therapeutic; the drug Thalidomide prescribed as a sedative led to birth defects as a result of administration of the incorrect stereoisomer.[1] At a supramolecular level, the binding of a hormone or a drug molecule to a receptor site, or a substrate to an enzyme will rely on a specific orientation between the interacting components[2,3] (Figure 1.1).

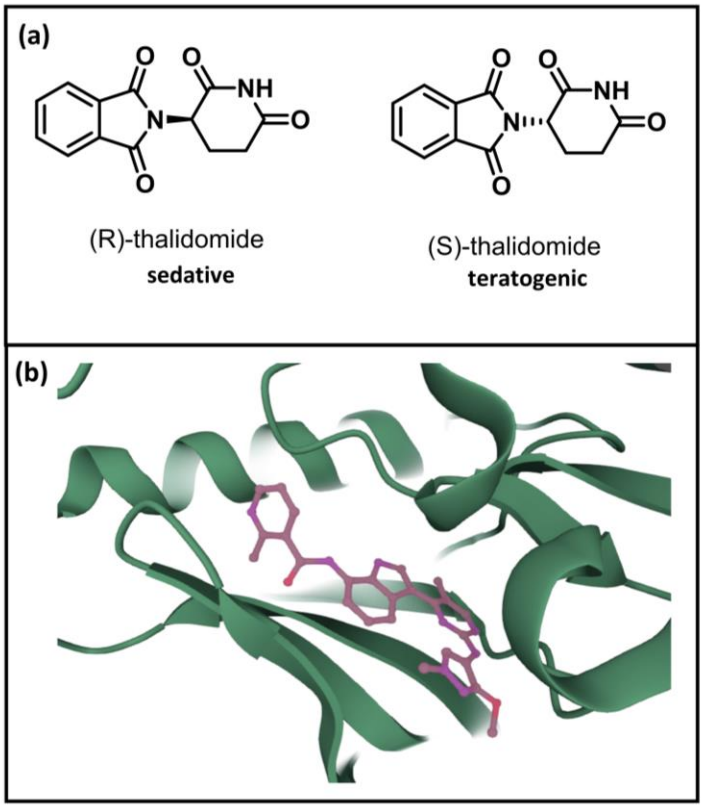

Figure 1.1. Structure property relationships at (a) molecular level (b) supramolecular level[4]

In the solid-state, the three-dimensional orientation and organization of molecules *i.e* the crystal structure, ultimately determines many fundamental physical properties of that particular material,

e.g. solubility[5], thermal stability,[6,7] hygroscopicity,[8] and mechanical strength and behavior[9] (Figure 1.2).

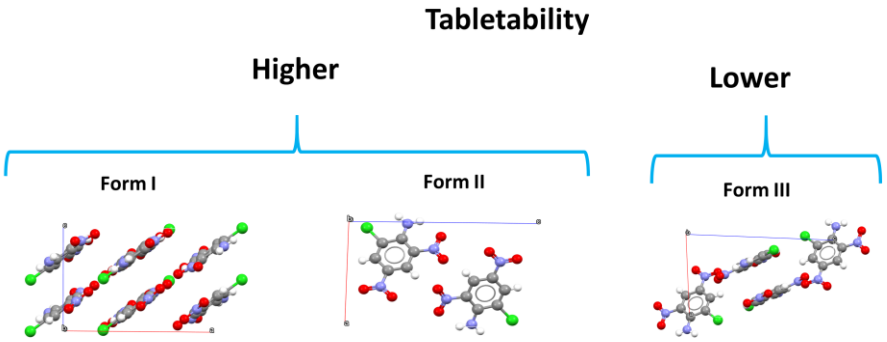

Figure 1.2. Importance of solid-state structure to physical property[10]

Consequently, an ability to control, predict, and change the crystal structure of both known and unknown compounds would be of enormous significance to both manufacturers and consumers of solid specialty chemicals. The importance of the solid-state and the connections between structure and activity are felt particularly strongly in areas related to pharmaceuticals,[11,12,13,14] agrochemicals,[15,16] food,[17,18] dyes[19,20], detergents, and energetic materials.[21,22,23] For example, bioavailability is governed by solubility, tableting behavior, filterability, and bulk density, and all these features are ultimately determined by size and particle shape, which, in turn, are related to internal structure of a the solid.

1.2 Different types of intermolecular interactions

Of critical importance to this field is our understanding of how the balance and competition between a variety of intermolecular forces determine whether individual molecules, recognize and bind, accept or reject, each other on the path from solution (supramolecular chemistry) via nucleation and crystallization to a solid-state materials (crystal engineering) with specific bulk properties. In this context, we may think about the connections between covalent synthesis, which

allows us to build new molecules that have never been seen before, and supramolecular synthesis, which allows us to assemble and organize individual molecules into assemblies and groups which ultimately determine solid-state structure and properties (Figure 1.3)

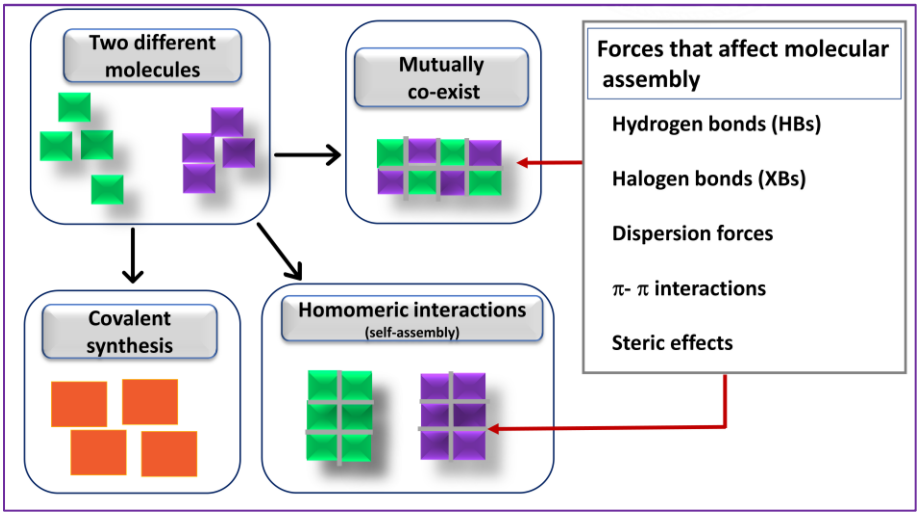

Figure 1.3. Schematic difference between covalent *vs*. non-covalent synthesis

Crystal engineering has been defined as "the understanding of intermolecular interactions in the context of crystal packing and in the utilization of such understanding in the design of new solids with desirable physical and chemical properties"[24] Molecular recognition[25] events in solution are the prelude to observed solid-state assemblies. Since intermolecular interactions in solution also play a key role in biological processes such as protein-ligand binding, drug-target binding both theoretical[26] and experimental studies in the field of crystal engineering can also provide valuable insights into existing challenges in biochemistry, biology and medicinal chemistry[27,28]

Many parallels have been drawn between the similarities of supramolecular synthesis and covalent synthesis and, subsequently, the influence of intermolecular interactions and covalent bonds upon those activities, respectively. Due to the comparatively weaker and reversible nature of non-covalent interactions, predicting the structural outcomes of such forces remains a challenge. The

hydrogen bond (HB)[29,30,31] is the most frequently exploited and best understood interaction in supramolecular synthesis, while the halogen bond (XB)[32,33] is now increasingly being explored.

1.3 The halogen bond

1.3.1 The halogen bond (XB) and hydrogen bond (HB)

The report by Colin, nearly 200 years ago, of the complex formed between iodine and ammonia was the first noted example of a halogen bond.[34] In 2011, the IUPAC defined halogen bonding as the non-covalent interaction between an electrophilic halogen substituent, X and a Lewis base, LB.[35] Thus, it bears similarity to hydrogen bonding (Figure 1.4).

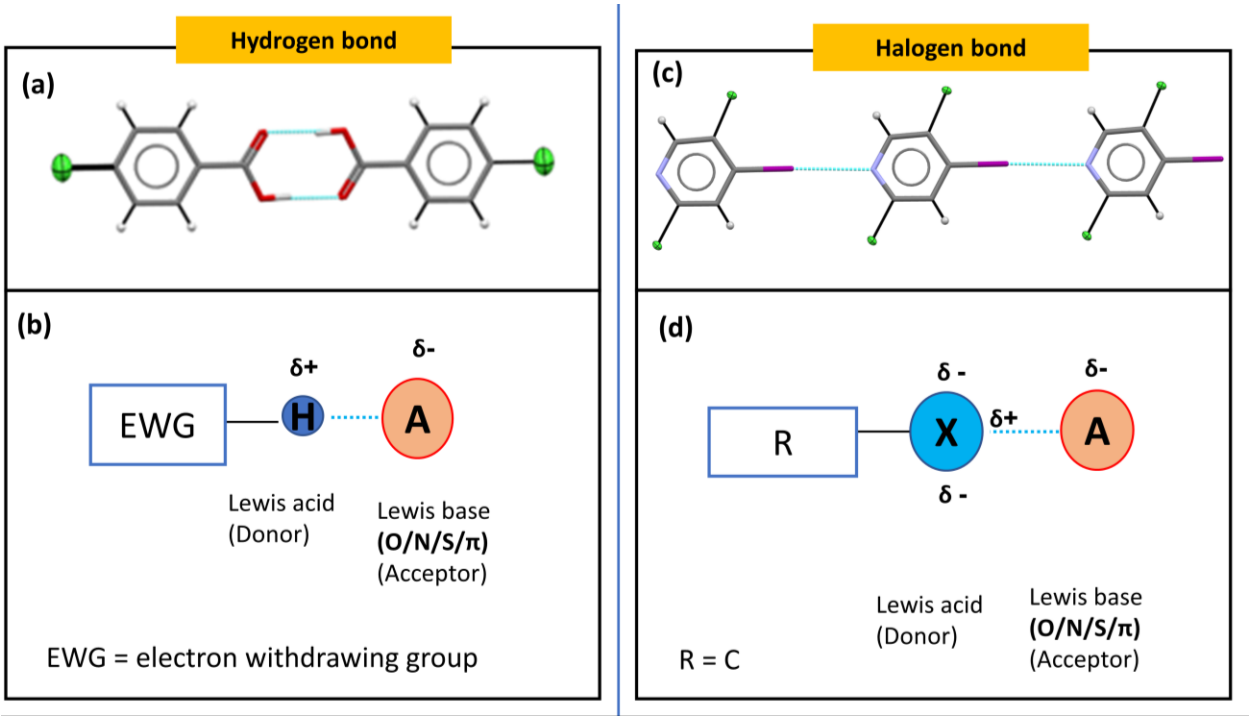

Figure 1.4. Similarity between hydrogen bonds and halogen bonds

(a) Hydrogen bonded carboxylic acid[36] (b) Schematic representation of hydrogen bond (c) Halogen bonding in an iodopyridine compound[37] (d) Schematic representation of halogen bonding

Two theories are used to explain the phenomenon of halogen bonding;[38]

i) Based on electronic origin: The attractive fore of a halogen bond is explained by a n- σ* partial electron transfer from the non-bonding orbital of the Lewis base into the antibonding orbital of the R-X bond.

ii) Based on electrostatic origin: Molecular electrostatic potential calculations reveal that there is a region of electron deficiency at the tip of the halogen atom along the extension of the R-X bond as a result of anisotropic electron distribution.

1.3.2 Factors which make halogen bonds different to hydrogen bonds

- Halogen bonds have a high directionality with R-X----LB ≈ 180°.[39] This is a consequence of repulsion of lone pairs on the halogen to those on the Lewis base at obtuse angles.
- They offer a higher tunability.

  -Increasing Lewis acidity occurs in the order of Cl<Br<I (with increasing polarizability of the halogen atom).[40]

  -The halogen bond strength will vary significantly depending on the hybridization of the connecting carbon in the order of $sp^3 < sp^2 < sp$.[41]

  -The presence of electron withdrawing groups such as fluorine[42] and nitro groups[43] lead to higher Lewis acidity of the halogen atom and subsequently greater halogen bonding ability.
- The halogen atoms/bonds are generally more hydrophobic than hydrogen bonds.[44]

1.3.3 The challenge of using in HBs and XBs simultaneously in supramolecular chemistry

Halogen bonds are more directional and tunable,[45,46] yet, due to their fundamental similarities to hydrogen bonds, they may both compete for the same acceptor sites and/or functional groups in

their molecular recognition events (Figure 1.5) Thus, identifying, recognizing, and utilizing reliable motifs that can be used in the bottom-up design of materials design, where both types of interactions are present simultaneously, remains a huge challenge.

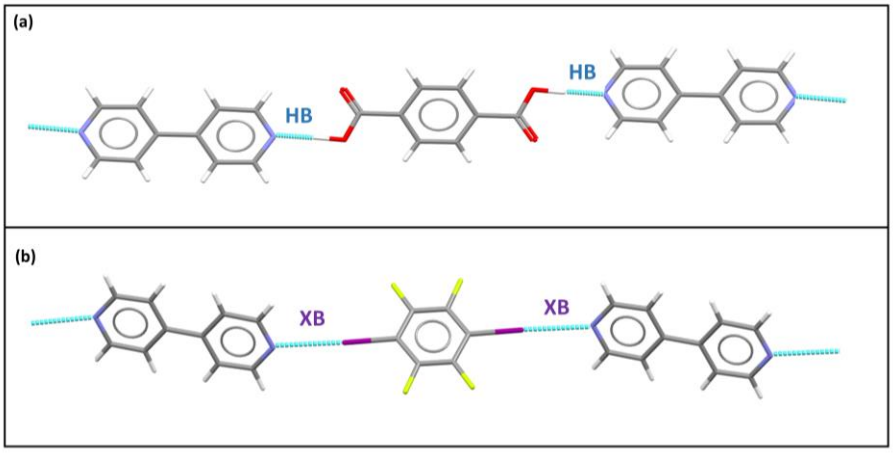

Figure 1.5. Same acceptor molecule used by (a) hydrogen-bond donors[47] and (b) halogen-bond donors.[48]

1.4 Specific goals of this thesis

The overriding scientific challenges that will be addressed in this thesis (chapters 2-8) can essentially be split into three parts; (i) Evaluating the balance between competing intermolecular forces (HB/XB/non-polar components) in the organic solid state, (ii) Using intermolecular forces for practical crystal engineering of ternary co-crystals, and (iii) establishing structure-property relationships in mechanically responsive crystals based on strengths of intermolecular forces (Figure 1.6).

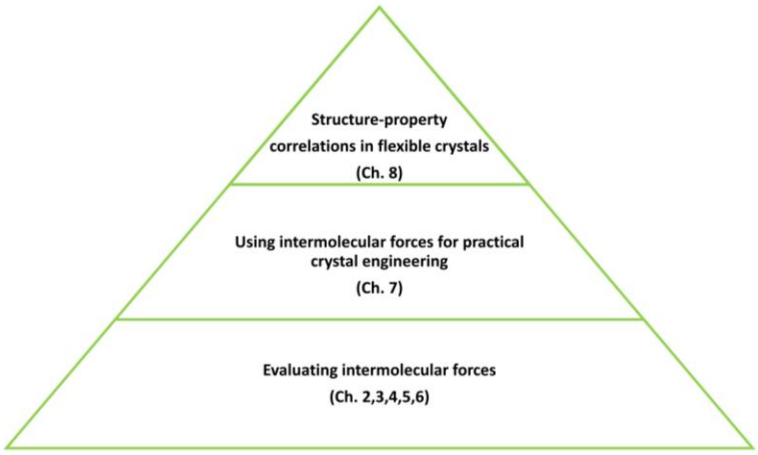

Figure 1.6. Road map of this thesis

Chapter 2 explores the balances between hydrogen and unactivated halogen bond interactions in the self-assembly of a family of amide-substituted pyridines.

Chapter 3 evaluates the structural impact of halogen atoms on the synthesis of co-crystals of pyridine amides.

Chapter 4 deals with establishing halogen-bond preferences in molecules with multiple acceptor sites

Chapter 5 focuses on evaluating halogen bond binding preferences as a function of molecular electrostatic potential

Chapter 6 explores the role of non-polar components in self-assembly of 2-aminopyridines

Chapter 7 combines knowledge gained about intermolecular interactions in previous chapter for a practical crystal engineering purpose (building ternary co-crystals)

Chapter 8 analyzes the effect of intermolecular force in structure property relationships in a group of mechanically responsive co-crystals.

1.5 References

[1] McBride, W. G. Thalidomide and congenital abnormalities. Lancet, **1961**, 2, 90927-8.
[2] Li, J.; Wang, J.; Gavalas, V. G.; Atwood, D. A.; Bachas, L. G. Alumina− pepsin hybrid nanoparticles with orientation-specific enzyme coupling. *Nano Lett.*, **2003**, *3*, 55-58.
[3] Pauff, J. M.; Zhang, J.; Bell, C. E.; Hille, R. *J.* Substrate orientation in xanthine oxidase: crystal structure of enzyme in reaction with 2-hydroxy-6-methylpurine. *Biol. Chem.* **2008**, *283*, 4818-4824.
[4] PDB 6SMB, Sehnal, D. R. A. S.; Rose, A. S.; Koca, J.; Burley, S.; Velankar, S. Mol*: towards a common library and tools for web molecular graphics. In *Workshop on Molecular Graphics and Visual Analysis of Molecular Data. The Eurographics Association* **2018**, (Vol. 10).
[5] Llinas, A.; Burley, J. C.; Box, K. J.; Glen, R. C.; Goodman, J. M. Diclofenac solubility: independent determination of the intrinsic solubility of three crystal forms. *J. Med. Chem*.**2007**, 50, 979-983.
[6] Liu, G.; Xiong, Y.; Gou, R.; Zhang, C. Difference in the Thermal Stability of Polymorphic Organic Crystals: A Comparative Study of the Early Events of the Thermal Decay of 2, 4, 6, 8, 10, 12-Hexanitro-2, 4, 6, 8, 10, 12-hexaazaisowurtzitane (CL-20) Polymorphs under the Volume Constraint Condition. *J. Phys. Chem. C* **2019**, 123,16565-16576.
[7] Vadivel, S.; Sultan, A. B.; Samad, S. A.; Shunmuganarayanan, A.; Muthu, R. Synthesis, structural elucidation, thermal, mechanical, linear and nonlinear optical properties of hydrogen bonded organic single crystal guanidinium propionate for optoelectronic device application. *Chem. Phys. Lett.* **2018,** 707, 165-171.
[8] Downton, G. E.; Flores-Luna, J. L.; King, C. J. Mechanism of stickiness in hygroscopic, amorphous powders. Ind. *Eng. Chem. Fundam*. **1982**, 21, 447-451.
[9] Elemans, J. A.; Lei, S.; De Feyter, S. Molecular and Supramolecular Networks on Surfaces: From Two-Dimensional Crystal Engineering to Reactivity. *Angew. Chem. Int.* **2009**, 48, 7298-7332.
[10] Wang, C.; Sun, C. C. Identifying slip planes in organic polymorphs by combined energy framework calculations and topology analysis. *Cryst. Growth Des,* **2018**, *18*, 1909-1916
[11] Babu, N.J.; Cherukuvada, S.; Thakuria, R.; Nangia, A. Conformational and synthon polymorphism in furosemide (Lasix). *Cryst. Growth Des.* **2010,** *10*, 1979-1989.
[12] Kavanagh, O. N.; Croker, D. M.; Walker, G. M.; Zaworotko, M. J. Pharmaceutical cocrystals: from serendipity to design to application. *Drug Discov. Today.* **2019**, *24*, 796-804
[13] Gong, N.; Yang, D.; Jin, G.; Liu, S.; Du, G.; Lu, Y. Structure, characterization, solubility and stability of podophyllotoxin polymorphs. *J. Mol. Struct.* **2019**, *1195*, 323-330.
[14] Yan, Y.; Chen, J. M.; Lu, T. B; Simultaneously enhancing the solubility and permeability of acyclovir by crystal engineering approach. *CrystEngComm*, **2013**, 15, 6457-6460.
[15] Sandhu, B.; Sinha, A. S.; Desper, J.; Aakeröy, C. B. Modulating the physical properties of solid forms of urea using co-crystallization technology. *Chem. Commun.* **2018**, 54, 4657-4660.
[16] Nauha, E.; Kolehmainen, E.; Nissinen, M. Packing incentives and a reliable N–HN–pyridine synthon in co-crystallization of bipyridines with two agrochemical actives. *CrystEngComm.* **2011**, 13, 6531–6537.
[17] Roos, Y. R., Karel, M. A. Crystallization of amorphous lactose. *J. Food Sci.* **1992**, 57, 775-777.
[18] Patel, A. R.; Dewettinck, K. Current update on the influence of minor lipid components, shear and presence of interfaces on fat crystallization. *Curr. Opin. Food Sci.* **2015,** 3, 65-70.
[19] Lim, S. I.; Ryu, K. H.; Jeon, D. Y.; Yang, C. M.; De Sio, L.; Kim, D. Y.; Jeong, K. U. Crystal Engineering of Amphiphilic Organic Dye for Metallic Coloration. *Cryst. Growth Des.* **2020,** 20,5896-5902.
[20] Taden, A.; Landfester, K.; Antonietti, M. Crystallization of dyes by directed aggregation of colloidal intermediates: a model case. Langmuir. **2014,** 20, 957-961.
[21] Grilli, N.; Koslowski, M. The effect of crystal orientation on shock loading of single crystal energetic materials. *Comput. Mater. Sci*.**2018**, *155*, 235-245.
[22] Gamekkanda, J.C., Sinha, A.S., Aakeröy, C.B. Cocrystals and Salts of Tetrazole-Based Energetic Materials. *Cryst. Growth Des.* **2020**, *20*, 2432–2439.
[23] Zhang, C.; Jiao, F.;Li, H. Crystal engineering for creating low sensitivity and highly energetic materials. *Cryst. Growth Des*, **2018,** 18, 5713-5726.
[24] Desiraju. G. R. Crystal Engineering. The Design of Organic Solids, Elsevier, Amsterdam, 1989.
[25] J. Rebek. Molecular recognition with model systems. Angew. *Chem., Int. Ed. Engl*. **1990**, 29, 245-255.

[26] Price, S. S. L. Computed crystal energy landscapes for understanding and predicting organic crystal structures and polymorphism. *Acc. Chem. Res.* **2009**, 42, 117-126.
[27] Fersht, A. R.The hydrogen bond in molecular recognition. *Trends Biochem. Sci.***1987,** 12, 301-304.
[28] Zhou, J.; Yu, G.; Huang, F. Supramolecular Chemotherapy Based on Host–Guest Molecular Recognition: A Novel Strategy in the Battle against Cancer with a Bright Future. Chem. Soc. Rev 2017, 46, 7021–7053.
[29] Aakeröy, C.B.; Seddon, K.R. The hydrogen bond and crystal engineering. *Chem. Soc. Rev.* **1993**, *22*, 397–407.
[30] Steiner, T. The hydrogen bond in the solid state. Angew. Chem. Int. Ed. 2002, 41, 48-76.
[31] Hisaki, I.; Suzuki, Y.; Gomez, E.; Ji, Q.; Tohnai, N.; Nakamura, T.; Douhal, A. Acid responsive hydrogen-bonded organic frameworks. *J. Am. Chem. Soc.* **2019,** *141*, 2111-2121
[32] Wang, H.; Bisoyi, H.K.; Urbas, A.M.; Bunning, T.J.; Li, Q. The halogen bond: an emerging supramolecular tool in the design of functional mesomorphic materials. *Chem. Eur. J.* **2019,** *25*, 1369-1378
[33] Meazza, L.; Foster, J. A.; Fucke, K.; Metrangolo, P.; Resnati, G.; & Steed, J. W. Halogen-bonding-triggered supramolecular gel formation. *Nature chemistry*. **2013**, *5*, 42-47
[34] Catalano, L.; Cavallo, G.; Metrangolo, P.; Resnati, G.; Terraneo, G. Halogen bonding in hypervalent iodine compounds. Hypervalent Iodine Chemistry, **2016,** 289-309.
[35] Arunan, E.: Desiraju, G.R.; Klein, R.A.; Sadlej, J.; Scheiner, S.; Alkorta, I.; Clary, D.C.; Crabtree, R.H.; Dannenburg, J.J.; Hobza, P.; Kjaergaard, G.; Legon, A.C.; Mennucci, B.; Nesbitt, D.J. Definition of the hydrogen bond (IUPAC Recommendations 2011). Pure Appl. Chem 2011, 83, 1637–1641
[36] D.El Sayed, *CSD Communication* **(2019)**
[37] Snégaroff, K.; Nguyen, T. T.; Marquise, N.; Halauko, Y. S.; Harford, P. J.; Roisnel, T.; Mongin, F. Deprotonative Metalation of Chloro-and Bromopyridines Using Amido-Based Bimetallic Species and Regioselectivity-Computed CH Acidity Relationships *Chem.-Eur.J.* **2011**, 17, 13284-13297
[38] Wolters, L. P.; Schyman, P.; Pavan, M. J.; Jorgensen, W. L.; Bickelhaupt, F. M.; Kozuch, S., The many faces of halogen bonding: a review of theoretical models and methods. *Wiley Interdiscip. Rev. Comput. Mol. Sci.* **2014,** *4*, 523-540
[39] Stone, A. J. Are halogen bonded structures electrostatically driven? *J. Am. Chem. Soc.* **2013,** *135*, 7005-7009.
[40] Desiraju, G. R.; Harlow, R. L. Cyano-Halogen Interactions and Their Role in the Crystal Structures of the 4-Halobenzonitriles. *J. Am. Chem. Soc.* **1989,** *111*, 6757−6764
[41] Metrangolo, P.; Meyer, F.; Pilati, T.; Resnati, G.; Terraneo, G. Halogen Bonding in Supramolecular Chemistry. Angew. Chem., Int. Ed. **2008**, *47*, 6114−6127
[42] Kniep, F.; Stefan H.J.; Qi, Z.; Sebastian M. W,: Severin, S.; Ingo, S.; Eberhardt, H.; Stefan, M. H. "Organocatalysis by neutral multidentate halogen-bond donors. *Angew. Chem., Int. Ed.* 52, no. 27 **2013**, *52*, 7028-7032
[43] Aakeröy, C. B.; Wijethunga, T. K.; Desper, J.;Daković, M. Crystal engineering with iodoethynylnitrobenzenes: a group of highly effective halogen-bond donors. *Cryst. Growth Des.* **2015**. *15*, 3853-3861
[44] Bergamaschi, G., Lascialfari, L., Pizzi, A., Espinoza, M. I. M., Demitri, N., Milani, A., Gori. A. Metrangolo, P. A halogen bond-donor amino acid for organocatalysis in water. *Chem. Commun.* **2018,** 54,10718-10721.
[45] Desiraju, G. R.; Harlow, R. L. Cyano-Halogen Interactions and Their Role in the Crystal Structures of the 4-Halobenzonitriles. *J. Am. Chem. Soc.* **1989,** *111*, 6757−6764
[46] Metrangolo, P.; Panzeri, W.; Recupero, F.; Resnati, G. Perfluorocarbon-Hydrocarbon Self-Assembly Part 16. 19F NMR Study of the Halogen Bonding between Halo-Perfluorocarbons and Heteroatom Containing Hydrocarbons. *J. Fluorine Chem.* **2002,** *114*, 27−33
[47] Rao, V. K.; Zeller. M.; Lovelace-Cameron S.R. *Acta Crystallogr.,Sect.E:Struct.Rep.Online*. **2012**, *68*, o1711,
[48] Walsh R.B.; Padgett, C.W.; Metrangolo, P.; Resnati, G.; Hanks, T. W.; Pennington, W.T. Crystal engineering through halogen bonding: complexes of nitrogen heterocycles with organic iodides. *Cryst.Growth Des.* **2001**, *1*, 165-175

Chapter 2 - Mapping out the relative influence of hydrogen- and halogen-bonds in crystal structures of a family of amide-substituted pyridines

2.1 Introduction

The hydrogen bond[1,2] has long been established as the primary driver for intermolecular assembly and organization, but halogen[3,4] and chalcogen bonds[5,6] are now also being recognized as valuable tools in practical crystal engineering.[7] All three interactions share a considerable reliance on electrostatics for both strength and directionality, but as most molecules contain multiple sites capable of forming electrostatically-based intermolecular bonds, it is difficult to predict, *a priori*, what the most likely pairing/binding between electron poor (donor) and electron rich (acceptor) sites will be. As a result, even relatively simple and rigid molecules can produce drastically different molecular aggregates in the solid state (Figure 2.1) which creates considerable challenges for bottom-up supramolecular synthesis.[8,9]

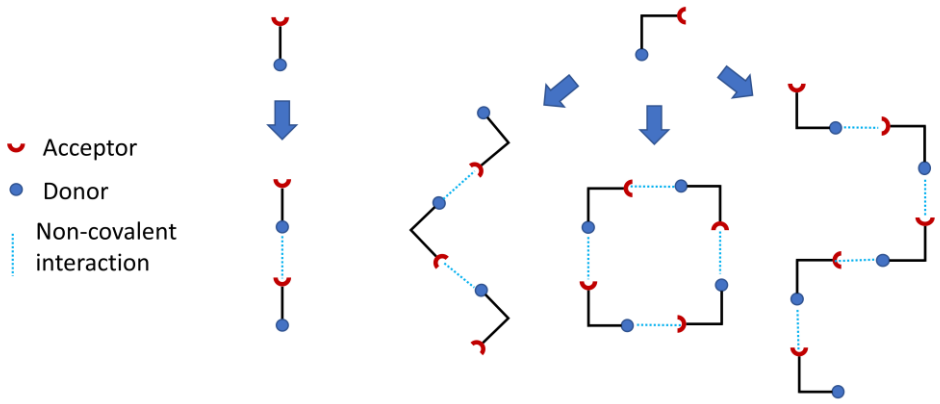

Figure 2.1. A few examples of intermolecular assembly based on the relative orientations of donor and acceptor site.

The relative orientation of molecules within a crystalline material ultimately plays an important role in the resulting physical properties and has significant implications for the performance of high value solids such as pharmaceuticals.[10,11,12] In addition, an improved understanding of interactions prevailing between individual components can also help to develop effective synthetic strategies for co-crystallizations.[13,14] A key concept that has become very helpful for identifying frequently occurring molecular recognition events in the solid state is the 'synthon'; "a structural unit within a supermolecule which can be formed and or assembled by known or conceivable synthetic operations involving intermolecular interactions".[15] In order to further transition this concept into versatile and reliable synthetic strategies, we need systematic structural studies on closely related compounds so that we directly connect functional groups and molecular structure to specific and predictable molecular recognition events in the solid state.[16,17,18,19]

In has been shown that the preferred synthon in a competitive assembly can often be rationalized using calculated molecular electrostatic potentials (MEPs), where the best acceptor (presenting the largest negative MEP) interacts with the best donor (presenting the most positive MEP on the molecular surface).[20] However, in systems with donors of different elements (*e.g* hydrogen and halogen), and where acceptors are not of the same element, a direct comparison of electrostatic potentials alone may not lead to reliable protocols for identifying which synthons are most likely to appear in the resulting crystal structure. Detailed studies that address such questions are relatively rare, and therefore we have carried out a systematic structural examination of four complementary series of relatively simple organic molecules that contain a variety of hydrogen-bond/halogen-bond donors and acceptors in order to map out the structural landscape of the amide group. Related studies include work on methyl-n-(pyridyl) benzamides[21], fluoro-n-(pyridyl) benzamides[22] and monochlorobenzamides[23] where N-H···N interactions were shown to dominate

over N-H···O=C interactions. However, the molecules under consideration in those studies include only one pyridine nitrogen and do not include iodine which is the halogen atom most capable of eliciting halogen bonding.[24]

In this study, sixteen molecules grouped into four series (Bz, 2Pyr, 3Pyr and 4Pyr) have been structurally interrogated by increasing the supramolecular and steric complexity (Figure 2.2)

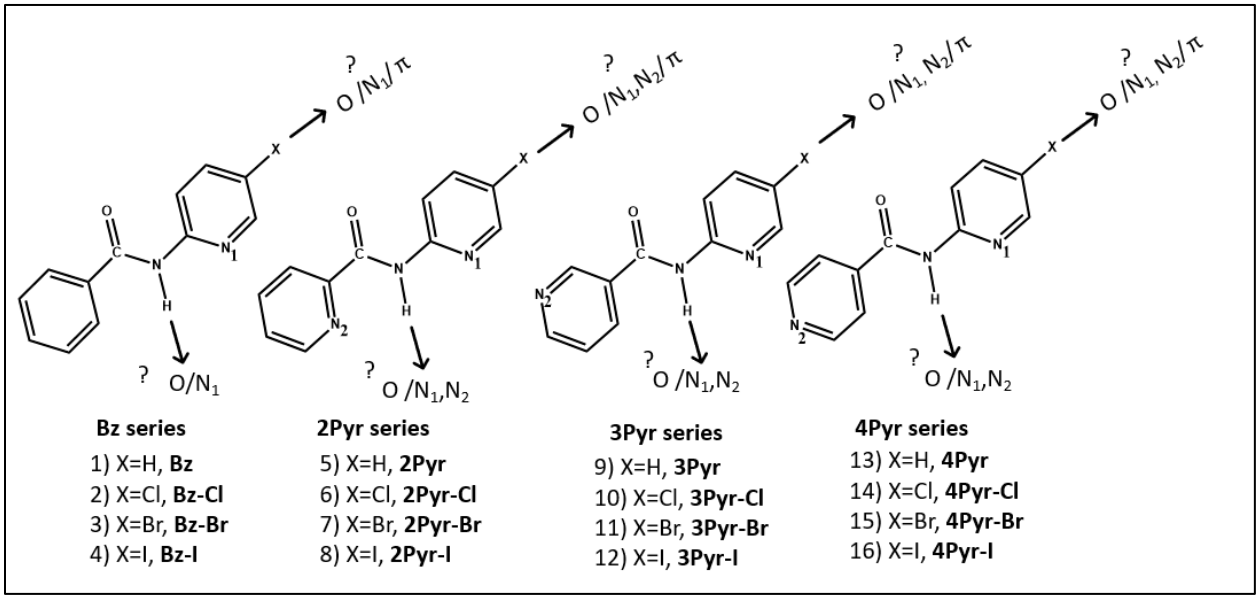

Figure 2.2. Molecular structures of compounds in this study and likely sites of binding for amide hydrogen and the halogen atom in each case.

In the course of this work we wanted to address several key question regarding molecular aggregation and recognition including to what extent MEPs can help to rationalize observed synthons, and whether the presence of a halogen atom can significantly alter the supramolecular assembly and, if so, will all halogen atoms have the same effect, Figure 2. To the best of our knowledge there are no systematic structural studies of hydrogen-bond motifs in the solid state of molecules bearing the core structure (i.e. the unhalogenated compound) of the Bz series. Reported structures25 to date bearing the 2Pyr core structure mainly form assemblies within larger molecules26 and contain only fluorine as a halogen atom substituent.27 The 3Pyr and 4Pyr core

structures (unhalogenated compounds) have been utilized in metal complexation28 but exhaustive data on solid state self-assembly of these compounds with potential halogen bond donors have not been reported.

In addition, we wanted to establish which of the two most likely motifs, chains or dimers, Figure 3, will prevail in the Bz series, and how the assembly process is affected by increasing molecular complexity and steric variability by the addition of a competing acceptor site as in series 2Pyr, 3Pyr and 4Pyr, respectively. The most likely interactions and the resulting aggregates have been presented schematically (Figure 2.3)

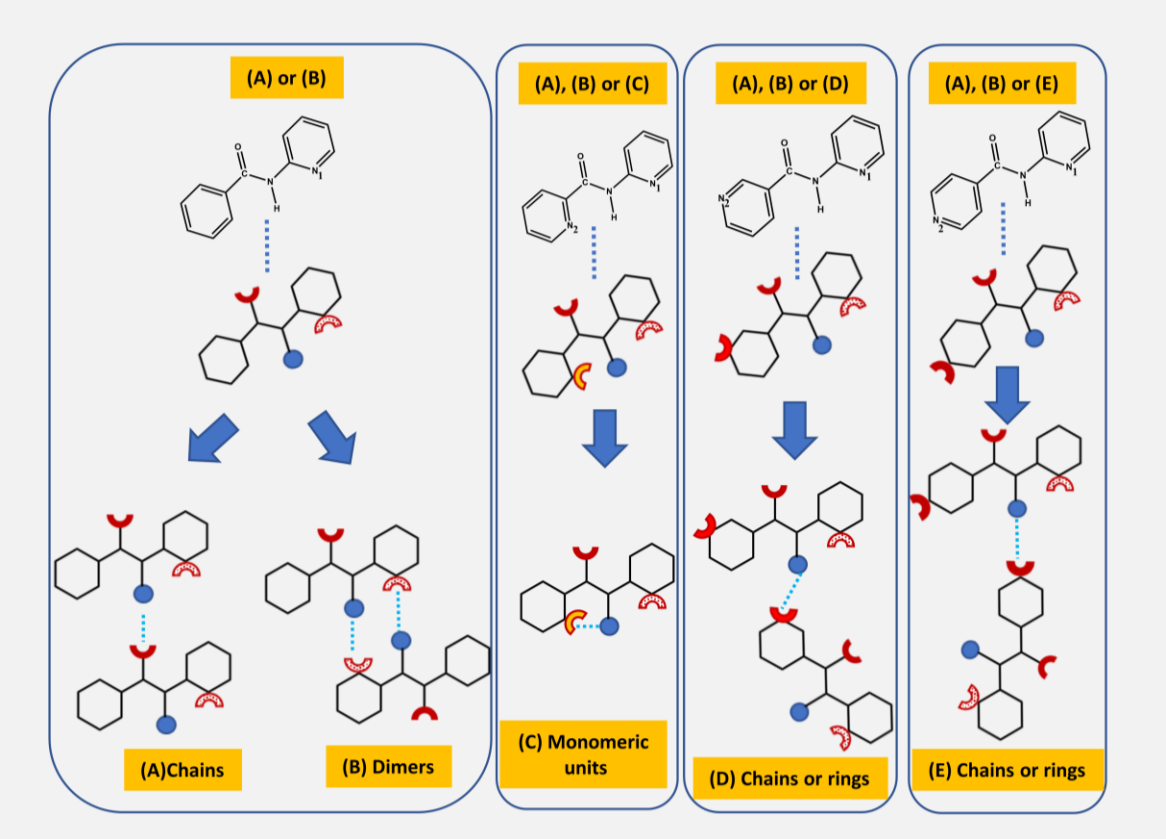

Figure 2.3. Schematic representation on possible structural consequences of increasing the number of acceptor sites and their relative positions

2.2 Experimental

2.2.1 General

All precursors, solvents were purchased from commercial sources and used without further purification. ^{1}H NMR spectra and ^{13}C NMR spectra were recorded on Bruker 400 spectrometer. Melting points were recorded on a Fisher-Johns melting point apparatus or a TA Instruments DSC Q20 differential scanning calorimeter. IR spectra were recorded with a Nicolet 380 FT-IR spectrometer using an attenuated total reflection (ATR) technique and ZnSe as the crystal. Electrostatic potentials were calculated with density functional B3LYP level of theory using 6-311++G** basis set in vacuum, using Spartan 08' software.

2.2.2 Synthesis

Bz series: Synthesis of N-(pyridin-2-yl)benzamides was done according to an available literature procedure.[29] (Sections 2.2.2.1 - 2.2.2.4)

2Pyr series: Synthesis of N-(pyridin-2-yl)picolinamides was done according to an available literature procedure.[30] (Sections 2.2.2.5 - 2.2.2.8)

3Pyr series: Synthesis of N-(pyridin-2-yl)nicotinamides was done according to an available literature procedure. [31](Sections 2.2.2.9 - 2.2.2.12)

4Pyr series: Synthesis of N-(pyridin-2-yl) isonicotinamides was done according to an available literature procedure.[31] (2.2.2.13 – 2.2.2.16)

2.2.2.1 Synthesis of N-(pyridin-2-yl)benzamide

2-Aminopyridine (1.03 g, 11.0 mmol) was dissolved in 50 mL of pyridine and cooled in an ice bath. Benzoyl chloride (1.85 mL, 16.0 mmol) was added dropwise maintaining the temperature between 0-5 ºC. After the addition was complete the solution was stirred at room temperature until no further starting material (2-amino-5-pyridine) was detected by TLC. Upon completion, chilled water (100 mL) was added and stirred for 15 minutes. The reaction contents were extracted with dichloromethane. The organic layer was washed with saturated sodium bicarbonate solution, brine, water and dried with anhydrous magnesium sulfate, filtered and concentrated in vacuo to isolate the pure product. Yield 80%, m.p 92-94 °C. (lit. 80-82 °C).[32] ^{1}H NMR (400 MHz, DMSO-d_6) δ 10.78 (s, 1H), 8.44 – 8.35 (m, 1H), 8.20 (dd, J = 8.4, 1.1 Hz, 1H), 8.07 – 8.00 (m, 2H), 7.88 – 7.79 (m, 1H), 7.59 (td, J = 7.3, 1.3 Hz, 1H), 7.51 (ddd, J = 8.4, 6.7, 1.3 Hz, 2H), 7.16 (ddd, J = 7.4, 4.8, 1.1 Hz, 1H).^{13}C NMR (101 MHz, DMSO-d_6) δ 166.46, 152.68, 148.40, 138.57, 134.57, 132.38, 128.81(2C), 128.46(2C), 120.26, 115.20

2.2.2.2 Synthesis of N-(5-chloropyridin-2-yl)benzamide

2-Amino-5-chloropyridine (1.40 g, 11.0 mmol) was dissolved in 50 mL of pyridine and cooled in an ice bath. Benzoyl chloride (1.85 mL, 16.0 mmol) was added dropwise maintaining the temperature between 0-5 ºC . After the addition was complete the contents were stirred at room temperature till no further starting material (2-amino-5-chloropyridine) was detected by TLC. Upon completion, chilled water (100 mL) was added and stirred for 15 minutes. The reaction contents were extracted with dichloromethane and the organic layer was washed with saturated sodium bicarbonate solution, brine, water and dried with anhydrous magnesium sulfate, filtered and concentrated in vacuo to isolate the pure product. Yield 85 %, m.p 123-125 °C. (lit. 124-125 ºC).[33] ^{1}H NMR (400 MHz, DMSO-d_6) δ 10.99 (s, 1H), 8.44 (d, J = 2.7 Hz, 1H), 8.25 (d, J = 8.9

Hz, 1H), 8.03 (dt, J = 7.1, 1.4 Hz, 2H), 7.95 (dd, J = 9.0, 2.7 Hz, 1H), 7.64 – 7.55 (m, 1H), 7.51 (dd, J = 8.2, 6.8 Hz, 2H). ^{13}C NMR (101 MHz, DMSO-d_6) δ 166.56, 151.36, 146.73, 138.28, 134.28, 132.52, 128.81, 128.52, 126.00, 116.24

2.2.2.3 Synthesis of N-(5-bromopyridin-2-yl)benzamide

2-Amino-5-bromopyridine (1.90 g, 11.0 mmol) was dissolved in 50 mL of pyridine and cooled in an ice bath. Benzoyl chloride (1.85 mL, 16.0 mmol) was added dropwise maintaining the temperature between 0-5 ºC. After the addition was complete the contents were stirred at room temperature till no further starting material (2-amino-5-bromopyridine) was detected by TLC. Upon completion, chilled water (100 mL) was added and stirred for 15 minutes. The reaction contents were extracted with dichloromethane and the organic layer was washed with saturated sodium bicarbonate solution, brine, water and dried with anhydrous magnesium sulfate, filtered and concentrated in vacuo to isolate the pure product. Yield 82 %, m.p 119-121°C.(lit. 223 ºC).[29,34] ^{1}H NMR (400 MHz, DMSO-d_6) δ 10.98 (s, 1H), 8.55 – 8.48 (m, 1H), 8.19 (dd, J = 8.9, 0.7 Hz, 1H), 8.07 (dd, J = 8.9, 2.6 Hz, 1H), 8.06 – 7.98 (m, 2H), 7.64 – 7.56 (m, 1H), 7.55 – 7.47 (m, 2H). ^{13}C NMR (101 MHz, DMSO-d_6) δ 166.17, 151.24, 148.52, 140.61, 133.86, 132.13, 128.42, 128.10, 116.36, 114.02

2.2.2.4 Synthesis of N-(5-iodopyridin-2-yl)benzamide

2-Amino-5-iodoopyridine (2.20 g, 11.0 mmol) was dissolved in 50 mL of pyridine and cooled in an ice bath. Benzoyl chloride (1.85 mL, 16.0 mmol) was added dropwise maintaining the temperature between 0-5 ºC. After the addition was complete the solution was stirred at room temperature till no further starting material (2-amino-5-iodopyridine) was detected by TLC. Upon completion, chilled water (100 mL) was added and stirred for 15 minutes. The reaction contents were extracted with dichloromethane and the organic layer was washed with saturated sodium

bicarbonate solution, brine, water and dried with anhydrous magnesium sulfate, filtered and concentrated in vacuo to isolate the pure product. Yield 85 %, m.p 121-123°C.(lit. 121-122 °C).[35] ^{1}H NMR (400 MHz, DMSO-d_6) δ 10.92 (s, 1H), 8.60 (d, J = 2.3 Hz, 1H), 8.17 (dd, J = 8.8, 2.3 Hz, 1H), 8.09 (d, J = 8.8 Hz, 1H), 8.02 (dd, J = 8.2, 1.4 Hz, 2H), 7.64 – 7.55 (m, 1H), 7.50 (t, J = 7.5 Hz, 2H). ^{13}C NMR (101 MHz, DMSO-d_6) δ 166.55, 153.85, 151.90, 146.36, 134.31, 132.52, 128.81, 128.50, 117.16, 87.21.

2.2.2.5 Synthesis of N-(pyridin-2-yl)picolinamide

Picolinic acid (1.00 g, 8.13 mmol), (2-(1H-benzotriazol-1-yl)-1,1,3,3-tetramethyluronium hexafluorophosphate (4.00 g, 10.5 mmol), triethylamine (3.40 mL, 24.4 mmol) and 2-aminopyridine (0.836 g, 8.90 mmol) were dissolved in 60 mL DMF. The reactants were stirred at room temperature for 14 hours, diluted with ethyl acetate and washed with water. The organic later was dried with anhydrous magnesium sulfate and concentrated by rotary evaporation to obtain the crude product which was purified by column chromatography using hexane:ethyl acetate (90:10) elution to obtain pure product. Yield 50%, m.p 117-119°C. (lit. 107–108 °C) [36] ^{1}H NMR (400 MHz, DMSO-d_6) δ 10.43 (s, 1H), 8.77 (ddd, J = 4.8, 1.7, 1.0 Hz, 1H), 8.44 – 8.37 (m, 1H), 8.29 (dt, J = 8.3, 1.0 Hz, 1H), 8.22 (dt, J = 7.8, 1.1 Hz, 1H), 8.12 (td, J = 7.7, 1.7 Hz, 1H), 7.91 (ddd, J = 8.8, 7.3, 1.9 Hz, 1H), 7.74 (ddd, J = 7.6, 4.7, 1.3 Hz, 1H), 7.22 (ddd, J = 7.4, 4.9, 1.0 Hz, 1H). ^{13}C NMR (101 MHz, DMSO-d_6) δ 161.55, 150.15, 148.35, 148.08, 138.28, 138.14, 127.20, 121.86, 119.88, 112.74.

2.2.2.6 Synthesis of N-(5-chloropyridin-2-yl)picolinamide

Picolinic acid (1.00 g, 8.13 mmol), (2-(1H-benzotriazol-1-yl)-1,1,3,3-tetramethyluronium hexafluorophosphate (4.00 g, 10.5 mmol), triethylamine (3.40 mL, 24.4 mmol) and 2-amino-5-chloropyridine (1.14 g, 8.90 mmol) were dissolved in 60 mL DMF. The reactants were stirred at room temperature for 14 hours, diluted with ethyl acetate and washed with water. The organic later was dried with anhydrous magnesium sulfate and concentrated by rotary evaporation to obtain the

crude product which was purified by column chromatography using hexane:ethyl acetate (90:10) elution to obtain pure product. Yield 55%, m.p 153-155°C. ^{1}H NMR (400 MHz, DMSO-d_6) δ 10.53 (s, 1H), 8.76 (ddd, J = 4.8, 1.7, 0.9 Hz, 1H), 8.46 (dd, J = 2.6, 0.7 Hz, 1H), 8.31 (dd, J = 8.9, 0.7 Hz, 1H), 8.22 (dt, J = 7.8, 1.1 Hz, 1H), 8.12 (td, J = 7.7, 1.7 Hz, 1H), 8.04 (dd, J = 8.9, 2.6 Hz, 1H), 7.74 (ddd, J = 7.6, 4.8, 1.3 Hz, 1H). ^{13}C NMR (101 MHz, DMSO-d_6) δ 162.76, 149.93, 149.45, 148.94, 147.51, 139.23, 139.06, 128.38, 126.66, 123.05, 115.00.

2.2.2.7 Synthesis of N-(5-bromopyridin-2-yl)picolinamide

Picolinic acid (1.00 g, 8.13 mmol), (2-(1H-benzotriazol-1-yl)-1,1,3,3-tetramethyluronium hexafluorophosphate (4.00 g, 10.5 mmol), triethylamine (3.40 mL, 24.4 mmol) and 2-amino-5-bromopyridine (1.54 g, 8.90 mmol) were dissolved in 60 mL DMF. The reactants were stirred at room temperature for 14 hours, diluted with ethyl acetate and washed with water. The organic later was dried with anhydrous magnesium sulfate and concentrated by rotary evaporation to obtain the crude product which was purified by column chromatography using hexane:ethyl acetate (90:10) elution to obtain pure product. Yield 53%, m.p 149-151°C. ^{1}H NMR (400 MHz, DMSO-d_6) δ 10.50 (s, 1H), 8.74 (d, J = 4.8 Hz, 1H), 8.50 (d, J = 2.5 Hz, 1H), 8.22 (dd, J = 17.5, 8.3 Hz, 2H), 8.16 – 8.06 (m, 2H), 7.73 (dd, J = 7.6, 4.8 Hz, 1H) 13C NMR (101 MHz, DMSO-d_6) δ 162.76, 150.22, 149.68, 149.43, 148.93, 141.76, 139.21, 128.38, 123.04, 115.50, 115.05

2.2.2.8 Synthesis of N-(5-iodopyridin-2-yl)picolinamide

Picolinic acid (1.00 g, 8.13 mmol), (2-(1H-benzotriazol-1-yl)-1,1,3,3-tetramethyluronium hexafluorophosphate (4.00 g, 10.5 mmol), triethylamine (3.40 mL, 24.4 mmol) and 2-amino-5-iodopyridine (1.96 g, 8.90 mmol) were dissolved in 60 mL DMF. The reactants were stirred at room temperature for 14 hours, diluted with ethyl acetate and washed with water. The organic later was dried with anhydrous magnesium sulfate and concentrated by rotary evaporation to obtain the

crude product which was purified by column chromatography using hexane:ethyl acetate (90:10) elution to obtain pure product. Yield 55%, m.p 124-126°C. ^{1}H NMR (400 MHz, DMSO-d_6) δ 10.46 (s, 1H), 8.75 (ddd, J = 4.8, 1.7, 0.9 Hz, 1H), 8.60 (dd, J = 2.2, 0.8 Hz, 1H), 8.27 – 8.17 (m, 2H), 8.12 (ddd, J = 15.6, 8.1, 1.3 Hz, 2H), 7.73 (ddd, J = 7.5, 4.8, 1.3 Hz, 1H). 13C NMR (101 MHz, DMSO-d_6) δ 162.56, 154.39, 150.23, 149.22, 148.76, 146.90, 139.00, 128.15, 122.81, 115.67, 87.70.

2.2.2.9 Synthesis of N-(pyridin-2-yl)nicotinamide

Nicotinic acid (1.21 g, 9.83 mmol) and triethylamine (1.40 mL, 10.0 mmol) were added to 30 mL of chloroform and cooled in an ice bath. Thionyl chloride (0.73 mL, 10.0 mmol) was added dropwise under nitrogen. After the addition of thionyl chloride was complete, the mixture was heated under reflux for 3 h. The mixture was cooled to room temperature and a solution of 2-aminopyridine (0.94 g,10.0 mmol) and triethylamine (1.40 mL, 10.0 mmol) in 30 mL acetonitrile was added in-situ. The contents were stirred overnight at room temperature. The organic layer was washed with water and the solvent removed in-vacuo. The product was purified by column chromatography using hexane:ethyl acetate (90:10) to isolate the pure product. Yield 28%, m.p 137-139 °C.(lit. 136-137 °C)[31] ^{1}H NMR (400 MHz, DMSO-d_6) δ 11.07 (s, 1H), 9.13 (dd, J = 2.4, 0.9 Hz, 1H), 8.75 (dd, J = 4.8, 1.7 Hz, 1H), 8.40 (ddd, J = 4.8, 2.0, 0.9 Hz, 1H), 8.37 – 8.30 (m, 1H), 8.19 (dt, J = 8.4, 1.0 Hz, 1H), 7.86 (ddd, J = 8.5, 7.4, 2.0 Hz, 1H), 7.54 (ddd, J = 8.0, 4.8, 0.9 Hz, 1H), 7.19 (ddd, J = 7.4, 4.8, 1.0 Hz, 1H). ^{13}C NMR (101 MHz, DMSO-d_6) δ 165.40, 153.00, 152.61, 149.68, 148.68, 138.91, 136.41, 130.55, 124.07, 120.75, 115.40.

2.2.2.10 Synthesis of N-(5-chloropyridin-2-yl)nicotinamide

Nicotinic acid (1.21 g, 9.83 mmol) and triethylamine (1.40 mL, 10.0 mmol) were added to 30 mL of chloroform and cooled in an ice bath. Thionyl chloride (0.73 mL, 10.0 mmol) was added

dropwise under nitrogen. After the addition of thionyl chloride was complete, the mixture was heated under reflux for 3 h. The mixture was cooled to room temperature and a solution of 2-amino-5-chloropyridine (1.28 g,10.0 mmol) and triethylamine (1.40 mL, 10.0 mmol) in 30 mL acetonitrile was added in-situ. The contents were stirred overnight at room temperature. The organic layer was washed with water and the solvent removed in-vacuo. The product was purified by column chromatography using hexane:ethyl acetate (90:10) to isolate the pure product. Yield 28%, 193-195 m.p °C. ^{1}H NMR (400 MHz, DMSO-d_6) δ 11.27 (s, 1H), 9.13 (d, J = 2.3 Hz, 1H), 8.76 (dd, J = 4.9, 1.7 Hz, 1H), 8.47 (d, J = 2.7 Hz, 1H), 8.34 (dt, J = 8.0, 2.0 Hz, 1H), 8.24 (d, J = 8.9 Hz, 1H), 7.99 (dd, J = 8.9, 2.7 Hz, 1H), 7.59 – 7.51 (m, 1H). ^{13}C NMR (101 MHz, DMSO-d_6) δ 164.92, 152.51, 150.69, 149.09, 146.45, 138.03, 135.87, 129.73, 125.87, 123.47, 115.85.

2.2.2.11 Synthesis of N-(5-bromopyridin-2-yl)nicotinamide

Nicotinic acid (1.21 g, 9.83 mmol) and triethylamine (1.40 mL, 10.0 mmol) were added to 30 mL of chloroform and cooled in an ice bath. Thionyl chloride (0.73 mL, 10.0 mmol) was added dropwise under nitrogen. After the addition of thionyl chloride was complete, the mixture was heated under reflux for 3 h. The mixture was cooled to room temperature and a solution of 2-amino-5-bromopyridine (1.73 g,10.0 mmol) and triethylamine (1.40 mL, 10.0 mmol) in 30 mL acetonitrile was added in-situ. The contents were stirred overnight at room temperature. The organic layer was washed with water and the solvent removed in-vacuo. The product was purified by column chromatography using hexane:ethyl acetate (90:10) to isolate the pure product. Yield 28%, 190-192 m.p °C. ^{1}H NMR (400 MHz, DMSO-d_6) δ 11.25 (s, 1H), 9.12 (dd, J = 2.4, 0.9 Hz, 1H), 8.75 (dd, J = 4.8, 1.7 Hz, 1H), 8.57 – 8.50 (m, 1H), 8.37 – 8.29 (m, 1H), 8.19 (dd, J = 8.9, 0.8 Hz, 1H), 8.09 (dd, J = 8.9, 2.5 Hz, 1H), 7.54 (ddd, J = 8.0, 4.8, 0.9 Hz, 1H), 2.08 (s, 2H). 13C

NMR (101 MHz, DMSO-d_6) δ 164.92, 152.51, 150.99, 149.09, 148.62, 140.75, 135.85, 129.72, 123.45, 116.34, 114.30, 30.73.

2.2.2.12 Synthesis of N-(5-iodopyridin-2-yl)nicotinamide

Nicotinic acid (1.21 g, 9.83 mmol) and triethylamine (1.40 mL, 10.0 mmol) were added to 30 mL of chloroform and cooled in an ice bath. Thionyl chloride (0.73 mL, 10.0 mmol) was added dropwise under nitrogen. After the addition of thionyl chloride was complete, the mixture was heated under reflux for 3 h. The mixture was cooled to room temperature and a solution of 2-amino-5-iodopyridine (2.20 g,10.0 mmol) and triethylamine (1.40 mL, 10.0 mmol) in 30 mL acetonitrile was added in-situ. The contents were stirred overnight at room temperature. The organic layer was washed with water and the solvent removed in-vacuo. The product was purified by column chromatography using hexane:ethyl acetate (90:10) to isolate the pure product. Yield 25%, 192-194 m.p °C. ^{1}H NMR (400 MHz, DMSO-d_6) δ 11.21 (s, 1H), 9.15 – 9.10 (m, 1H), 8.76 (dd, J = 4.8, 1.7 Hz, 1H), 8.65 – 8.60 (m, 1H), 8.34 (dt, J = 8.1, 2.0 Hz, 1H), 8.20 (dd, J = 8.8, 2.3 Hz, 1H), 8.12 – 8.05 (m, 1H), 7.55 (ddd, J = 8.0, 4.8, 0.9 Hz, 1H). ^{13}C NMR (101 MHz, DMSO-d_6) δ 164.90, 153.53, 152.49, 151.24, 149.08, 146.09, 135.83, 129.75, 123.44, 116.72, 87.18.

2.2.2.13 Synthesis of N-(pyridin-2-yl)isonicotinamide

Isonicotinic acid (1.21 g, 9.83 mmol) and triethylamine (1.40 mL, 10.0 mmol) were added to 30 mL of chloroform and cooled in an ice bath. Thionyl chloride (0.73 mL, 10.0 mmol) was added dropwise under nitrogen. After the addition of thionyl chloride was complete, the mixture was heated under reflux for 3 h. The mixture was cooled to room temperature and a solution of 2-aminopyridine (0.94 g,10.0 mmol) and triethylamine (1.40 mL, 10.0 mmol) in 30 mL acetonitrile was added in-situ. The contents were stirred overnight at room temperature. The organic layer was washed with water and the solvent removed in-vacuo. The product was purified by column

chromatography using hexane:ethyl acetate (90:10) to isolate the pure product. Yield 32%, m.p 136-138 °C. (lit. 136-138 °C)[31] ^{1}H NMR (400 MHz, DMSO-d_6) δ 8.77 (d, J = 6.0 Hz, 2H), 8.42 (d, J = 3.7 Hz, 1H), 8.19 (d, J = 8.3 Hz, 1H), 7.92 (d, J = 6.1 Hz, 2H), 7.88 (s, 1H), 7.22 (s, 1H). ^{13}C NMR (101 MHz, DMSO-d_6) δ 164.94, 152.01, 150.49, 148.35, 141.50, 138.60, 122.08, 120.59, 115.15.

2.2.2.14 Synthesis of N-(5-chloropyridin-2-yl)isonicotinamide

Isonicotinic acid (1.21 g, 9.83 mmol) and triethylamine (1.40 mL, 10.0 mmol) were added to 30 mL of chloroform and cooled in an ice bath. Thionyl chloride (0.73 mL, 10.0 mmol) was added dropwise under nitrogen. After the addition of thionyl chloride was complete, the mixture was heated under reflux for 3 h. The mixture was cooled to room temperature and a solution of 2-amino-5-chloropyridine (1.28 g,10.0 mmol) and triethylamine (1.40 mL, 10.0 mmol) in 30 mL acetonitrile was added in-situ. The contents were stirred overnight at room temperature. The organic layer was washed with water and the solvent removed in-vacuo. The product was purified by column chromatography using hexane:ethyl acetate (90:10) to isolate the pure product. Yield 30%, m.p 158-160 °C. ^{1}H NMR (400 MHz, DMSO-d_6) δ 11.31 (s, 1H), 8.77 (d, J = 5.8 Hz, 2H), 8.47 (d, J = 2.6 Hz, 1H), 8.23 (d, J = 8.9 Hz, 1H), 7.99 (dd, J = 8.9, 2.7 Hz, 1H), 7.90 (d, J = 5.9 Hz, 2H). ^{13}C NMR (101 MHz, DMSO-d_6) δ 165.01, 150.64, 150.44, 146.67, 141.18, 138.25, 126.28, 122.04, 116.15.

2.2.2.15 Synthesis of N-(5-bromopyridin-2-yl)isonicotinamide

Isonicotinic acid (1.21 g, 9.83 mmol) and triethylamine (1.40 mL, 10.0 mmol) were added to 30 mL of chloroform and cooled in an ice bath. Thionyl chloride (0.73 mL, 10.0 mmol) was added dropwise under nitrogen. After the addition of thionyl chloride was complete, the mixture was heated under reflux for 3 h. The mixture was cooled to room temperature and a solution of 2-

amino-5-bromopyridine (1.73 g,10.0 mmol) and triethylamine (1.40 mL, 10.0 mmol) in 30 mL acetonitrile was added in-situ. The contents were stirred overnight at room temperature. The organic layer was washed with water and the solvent removed in-vacuo. The product was purified by column chromatography using hexane:ethyl acetate (90:10) to isolate the pure product. Yield 28%, m.p 166-168 °C. ^{1}H NMR (400 MHz, DMSO-d_6) δ 11.30 (s, 2H), 8.80 – 8.74 (m, 4H), 8.54 (d, J = 2.5 Hz, 2H), 8.18 (d, J = 8.9 Hz, 2H), 8.10 (dd, J = 8.9, 2.5 Hz, 2H), 7.93 – 7.87 (m, 4H), 2.53 – 2.47 (m, 1H). ^{13}C NMR (101 MHz, DMSO-d_6) δ 165.26, 151.18, 150.67, 149.09, 141.41, 141.22, 122.26, 116.88, 114.99.

2.2.2.16 Synthesis of N-(5-iodopyridin-2-yl)isonicotinamide

Isonicotinic acid (1.21 g, 9.83 mmol) and triethylamine (1.40 mL, 10.0 mmol) were added to 30 mL of chloroform and cooled in an ice bath. Thionyl chloride (0.73 mL, 10.0 mmol) was added dropwise under nitrogen. After the addition of thionyl chloride was complete, the mixture was heated under reflux for 3 h. The mixture was cooled to room temperature and a solution of 2-amino-5-iodopyridine (2.20 g,10.0 mmol) and triethylamine (1.40 mL, 10.0 mmol) in 30 mL acetonitrile was added in-situ. The contents were stirred overnight at room temperature. The organic layer was washed with water and the solvent removed in-vacuo. The product was purified by column chromatography using hexane:ethyl acetate (90:10) to isolate the pure product. Yield 30%, m.p 194-196°C. ^{1}H NMR (400 MHz, DMSO-d_6) δ 11.25 (s, 1H), 8.81 – 8.74 (m, 2H), 8.63 (dd, J = 2.4, 0.8 Hz, 1H), 8.21 (dd, J = 8.7, 2.3 Hz, 1H), 8.08 (dd, J = 8.8, 0.8 Hz, 1H), 7.93 – 7.87 (m, 2H). ^{13}C NMR (101 MHz, DMSO-d_6) δ 165.04, 153.80, 151.24, 150.47, 146.38, 141.25, 122.05, 117.05, 87.72.

2.2.3 Crystal growth

In order to obtain crystals suitable for single-crystal X-ray diffraction, slow evaporation from a variety of solvents was used for all sixteen compounds, Table 2.1.

Table 2.1. Solvents used for crystal growth and crystal descriptions

Compound	Code	Solvent	Color and morphology
N-(pyridin-2-yl)benzamide	**Bz**	Ethanol	Colorless, Rectangular
N-(5-chloropyridin-2-yl)benzamide	**Bz-Cl**	Ethanol	Colorless, Blocks
N-(5-bromopyridin-2-yl)benzamide	**Bz-Br**[37]	Ethanol	Colorless Blocks
N-(5-iodopyridin-2-yl)benzamide	**Bz-I**	Ethanol	Colorless, Squares
N-(pyridin-2-yl)picolinamide	**2Pyr**	Acetone	Colorless, Rectangular
N-(5-chloropyridin-2-yl)picolinamide	**2Pyr-Cl**	Methanol: Ethyl acetate (50:50)	Colorless, Rectangular
N-(5-bromopyridin-2-yl)picolinamide	**2Pyr-Br**	Acetonitrile	Colorless, Needle
N-(5-iodopyridin-2-yl)picolinamide	**2Pyr-I**	Hexane: Ethyl acetate (80:20)	Colorless, Needle
N-(pyridin-2-yl)nicotinamide	**3Pyr**	Toluene	Colorless, Rectangular
N-(5-chloropyridin-2-yl)nicotinamide	**3Pyr-Cl**	Methanol	Colorless needle
N-(5-bromopyridin-2-yl)nicotinamide	**3Pyr-Br**	Methanol	Yellow, Rectangular
N-(5-iodopyridin-2-yl)nicotinamide	**3Pyr-I**	Tetrahydrofuran	Colorless, Rectangular
N-(pyridin-2-yl)isonicotinamide	**4Pyr**[38]	Methanol	Yellow, Plate
N-(5-chloropyridin-2-yl)isonicotinamide	**4Pyr-Cl**	Toluene	Colorless, Rectangular
N-(5-bromopyridin-2-yl)isonicotinamide	**4Pyr-Br**	Methanol	Colorless, Rectangular
N-(5-iodopyridin-2-yl)isonicotinamide	**4Pyr-I-i**	Hexane: Ethyl acetate (80:20)	Yellow, Parallelepiped
	4Pyr-I-ii*	Ethyl acetate	Colorless, Needle

*Obtained from a failed co-crystallization experiment of 4Pyr-I with dodecanoic acid in 1:1 molar ratio.

2.3 Results

2.3.1 Molecular electrostatic potentials

The calculated MEP values are shown in Figure 2.4

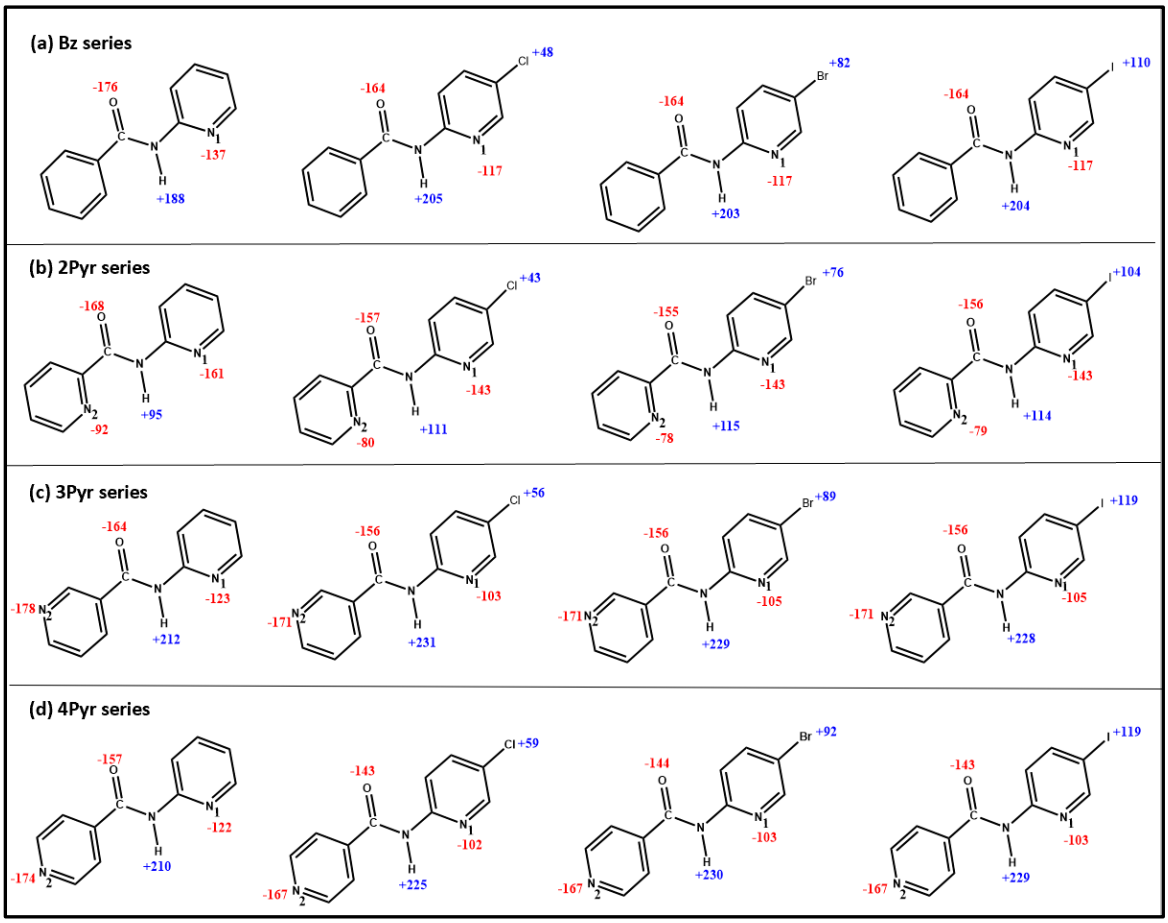

Figure 2.4. MEP values at most likely donor and acceptor sites in the sixteen target compounds.

2.3.2 X-ray crystallography results

In every one of the four crystal structures from the Bz family, the primary intermolecular interaction is a N-H···N(py)/N(py)···H-N synthon that produced symmetry-related dimers (Figure 2.5a). The only additional interaction of note is a C-I···π halogen bond in **Bz-I**. The analogous chloro and bromo compounds do not display any other notable short-contacts to neighboring molecules. The relevant hydrogen- and halogen and bond geometries in these four crystal structures are given in Table 2.

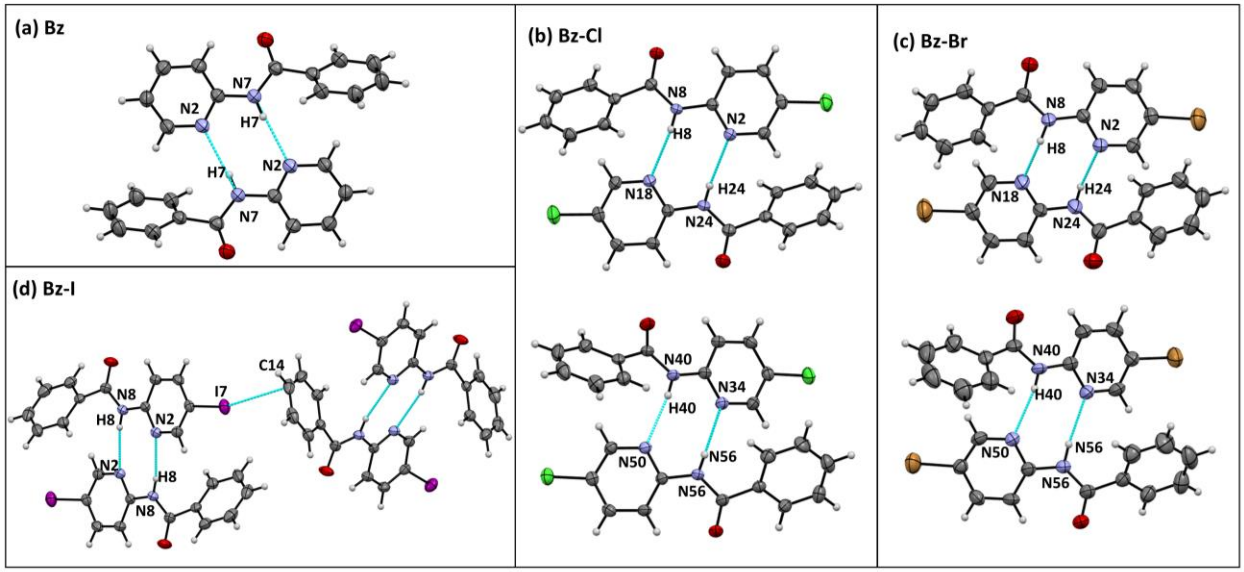

Figure 2.5. Primary interactions seen in single crystal structures of (a) Bz, (b) Bz-Cl, (c) Bz-Br, (d) Bz-I

Table 2.2. Hydrogen- and halogen-bond parameters of crystal structures in the Bz series

	D-H/I···A	D/I···A (A)	D-H···A (deg)
Bz	N7-H7···N2	3.0557(16)	166.5(16)
Bz-Cl	N8-H8···N18	3.189(2)	153.3(19)
	N24-H24···N2	3.203(2)	152.(2)
	N40-H40···N50	2.967(2)	159.9(19)
	N56-H56···N34	3.108(2)	163.5(19)
Bz-Br	N8-H8···N18	3.211(5)	150.(5)
	N24-H24···N2	3.227(5)	150.(5)
	N40-H40···N50	2.987(5)	149.(3
	N56-H56···N34	3.113(5)	156.(4)
Bz-I	N8-H8···N2	3.238(3)	163.(3)
	C4-I7···C14	3.580(3)	162.37(9)

The primary non-covalent interactions in the four crystal structures from the 2Pyr series are shown in Figure 2.6. The addition of a pyridyl substituent with the nitrogen atom in close proximity to the N-H hydrogen-bond donor of the amide moiety, leads to the formation of a very persistent N-H···N(py) intramolecular interaction in all four structures, which effectively prevents the formation of pairwise dimers in the solid state. Again, the iodo-analogue is the only member of this group that displays a structure-directing halogen bond and, interestingly, the iodine atom acts as a halogen-bond donor and acceptor simultaneously. The relevant hydrogen- and halogen and bond geometries in these four crystal structures are given in Table 2.3.

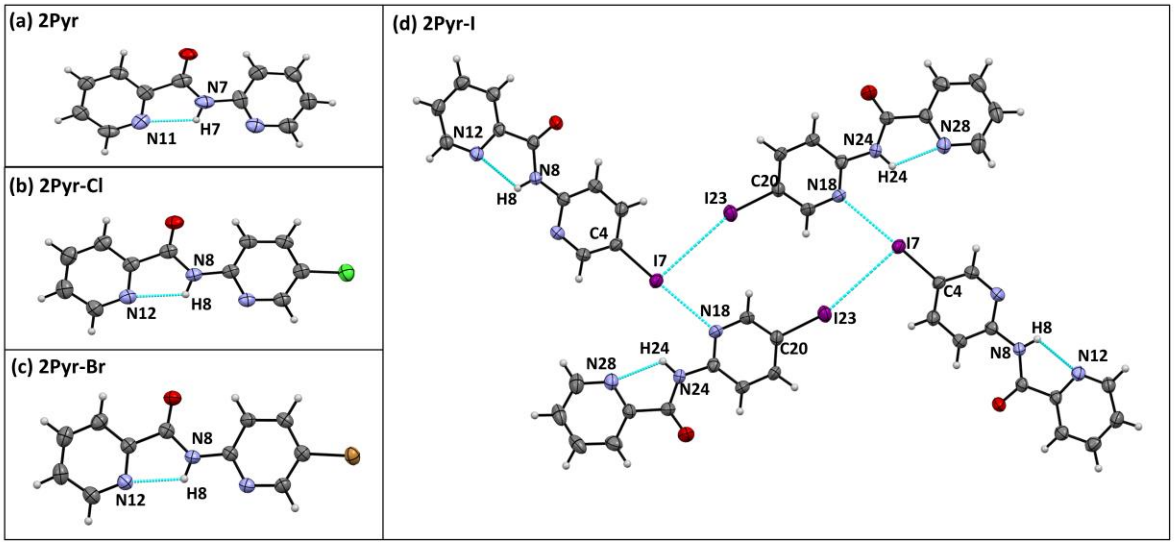

Figure 2.6. Primary interactions seen in single crystal structures of (a) 2Pyr (b)2Pyr-Cl, (c)2Pyr-Br, (d) 2Pyr-I

Table 2.3. Hydrogen- and halogen-bond parameters of crystal structures of 2Pyr series

	D-H/I···A	D/I···A (A)	D-H/I···A (deg)
2Pyr	N7-H7···N11	2.668(4)	113.4
2Pyr-Cl	N8-H8···N12	2.647(3)	113(3)
2Pyr-Br	N8-H8···N12	2.645(4)	114(3)
2Pyr-I	N8-H8···N12	2.658(6)	115.(5)
	N24-H24···N28	2.655(6)	115.(5)
	C4-I7···N18	3.018(4)	176.06(17)
	C20-I23···I7	3.9173(5)	164.48(15)

In all four crystal structures of the 3Pyr series the primary non-covalent interaction is a N-H···N(py) synthon (Figure 2.7). There are no additional structure directing interactions shown by any of the halogenated compounds. The *trans*-conformation with respect to the two ring nitrogen atoms is the preferred option in three of the four structures, while 3Pyr-Br is the only compound

showing a *cis*-arrangement. The relevant hydrogen- and halogen and bond geometries in these four crystal structures are given in Table 2.4.

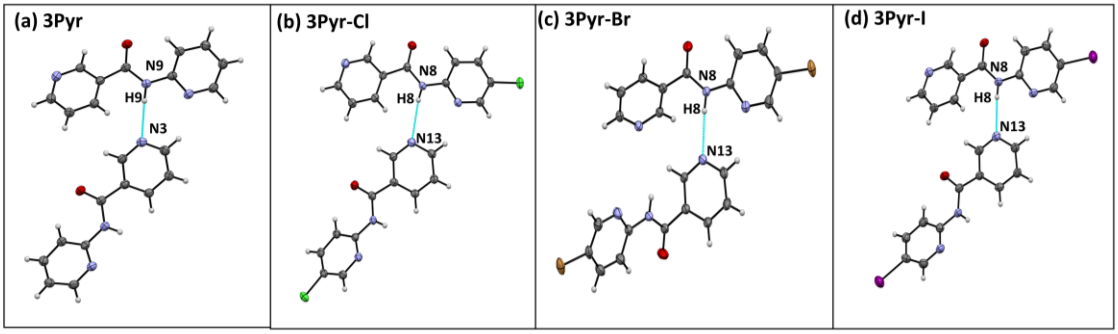

Figure 2.7. Primary interactions seen in single crystal structures of (a) 3Pyr, (b)3Pyr-Cl, (c)3Pyr-Br, (d) 3Pyr-I

Table 2.4. Hydrogen- and halogen-bond parameters of crystal structures of 3Pyr series

	D-H/I···A	D/I···A (Å)	D-H/I···A (deg)
3Pyr	N9-H9···N3	3.154(2)	176(2)
3Pyr-Cl	N8-H8···N13	3.233(2)	171(2)
3Pyr-Br	N8-H8···N13	3.079(3)	172(3)
3Pyr-I	N8-H8···N13	3.035(11)	169(9)

The primary non-covalent interactions in the crystal structures from the 4Pyr series are shown in Figure 2.8. The primary hydrogen bond interaction in 4Pyr is a N-H···N(py) to the nitrogen N_2 (Figure 8). Both 4Pyr-Cl and 4Pyr-Br also follow this pattern in hydrogen bonding and form four-membered rings. In 4Pyr-I-i the halogen bond C-I···N to nitrogen $–N_2$, and dimeric unit formation by N-H···N(py)/N(py)···H-N synthon is seen. The C-I···N (to $–N_2$) interaction is once again present in 4Pyr-I-ii, while the hydrogen bond interaction changes to a N-H···O synthon. The relevant hydrogen- and halogen bond geometries in these four crystal structures are given in Table 2.5.

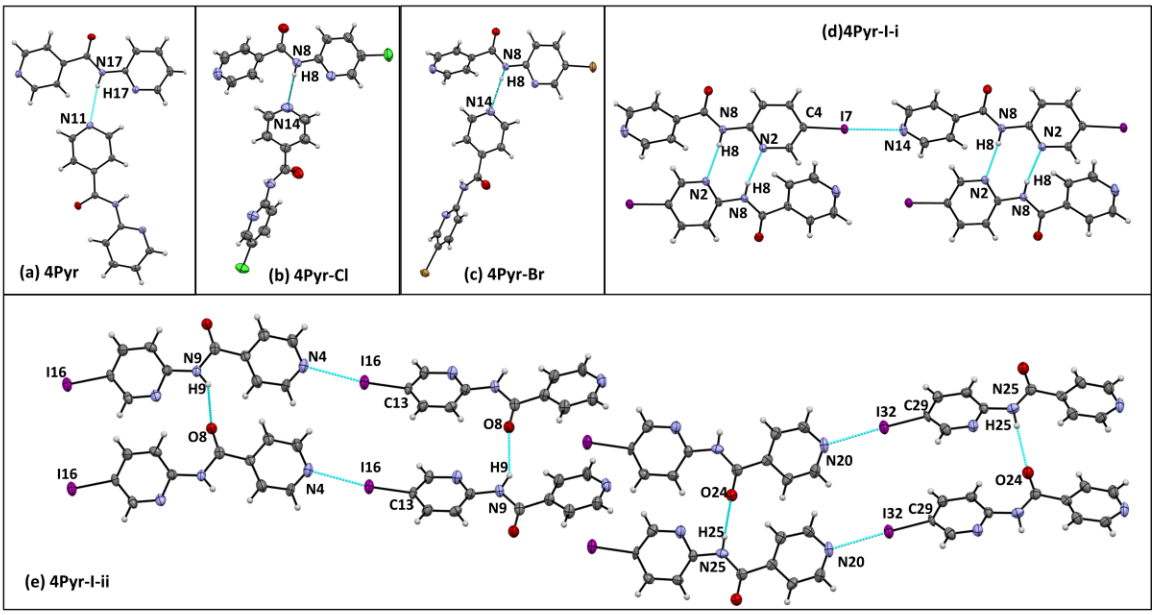

Figure 2.8. Primary interactions seen in single crystal structures of (a) 4Pyr, (b)4Pyr-Cl, (c)4Pyr-Br, (d) 4Pyr-I-i, (e) 4Pyr-I-ii

Table 2.5. Hydrogen- and halogen-bond parameters of crystal structures of 4Pyr series

	D-H/I···A	D/I···A (Å)	D-H/I···A (deg)
4Pyr	N17-H17···N11	3.3308(12)	170.1(11)
4Pyr-Cl	N8-H8···N14	3.0169(18)	179.0(19)
4Pyr-Br	N8-H8···N14	2.997(3)	171.(2)
4Pyr-I-i	N8-H8···N2	3.011(3)	166.(5)
	C4-I7···N14	3.013(2)	177.95(9)
4Pyr-I-ii	N9-H9··· O8	3.086(13)	147.(12)
	C13-I16···N4	2.998(9)	171.5(4)
	N25-H25···O24	3.129(13)	171.(15)
	C29-I32···N20	2.969(10)	177.4(4)

The primary hydrogen- and halogen bonds in the sixteen crystal structures are summarized in Figure 2.9.

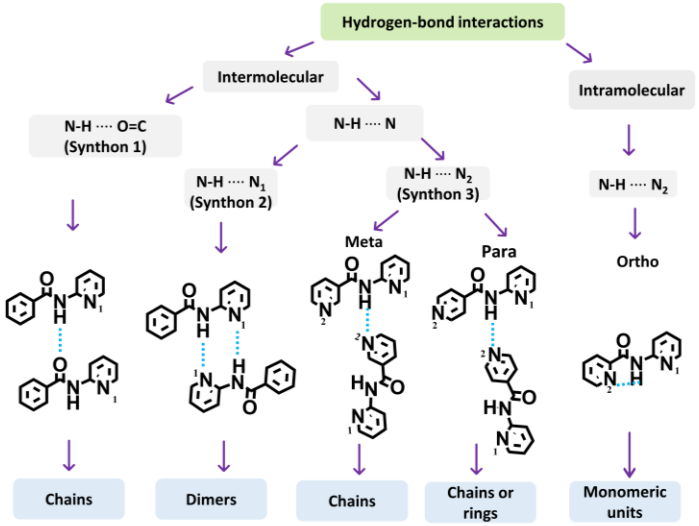

Bz series	$\frac{0}{4}$	$\frac{4}{4}$	n/a	n/a	n/a	I---π
2Pyr series	$\frac{0}{4}$	$\frac{0}{4}$	n/a	n/a	$\frac{4}{4}$	I---I and I---N_1
3Pyr series	$\frac{0}{4}$	$\frac{0}{4}$	$\frac{4}{4}$	n/a	n/a	none
4Pyr series	$\frac{1}{5}$	$\frac{1}{5}$	n/a	$\frac{3}{5}$ ($\frac{1}{5}$ chain + $\frac{2}{5}$ ring)	n/a	I---N_2

Halogen-bond interactions

Figure 2.9. Summary of the primary hydrogen- and halogen-bond interactions in the sixteen compounds.

As seen above, except for the two polymorphs of 4Pyr-I, the hydrogen bonds are identical among compounds within each series. To gain insight into the nature of the hydrogen bonding shown by these compounds in the solution phase, the chemical shift of the amide hydrogen in DMSO was investigated. The data appears clustered in three sets (Figure 2.10) and the connection between each of these sets to crystal structures are addressed in detail in the discussion.

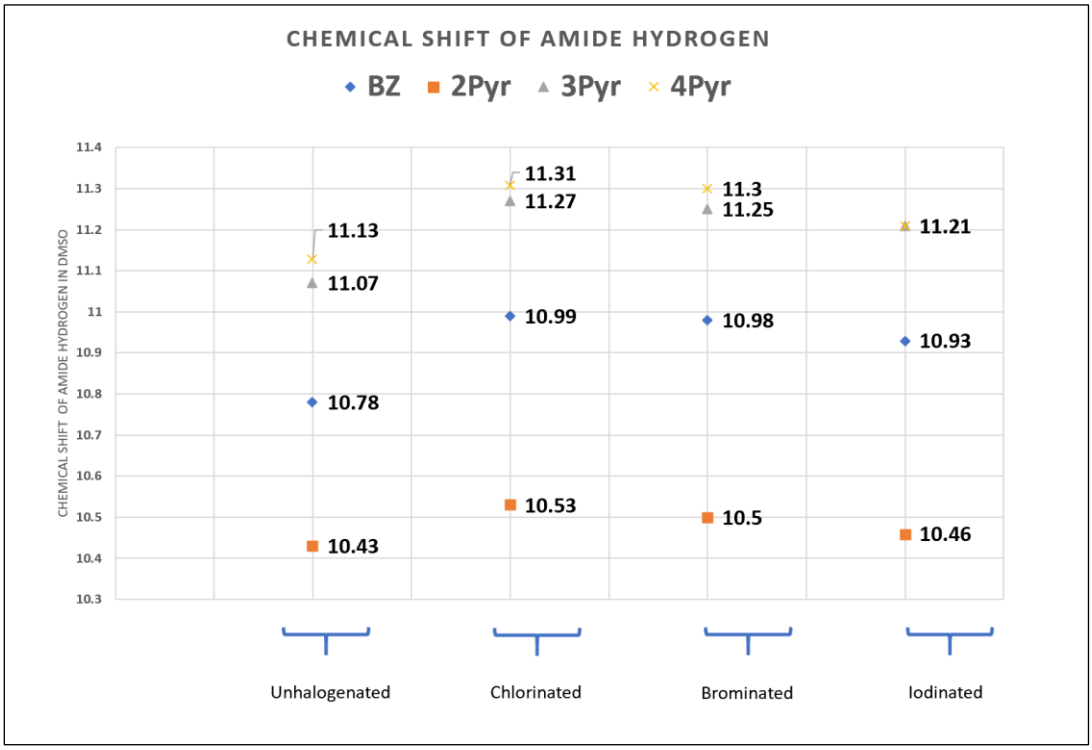

Figure 2.10. ^{1}H NMR chemical shift of the amide hydrogen atoms grouped by series.

2.4 Discussion

We hypothesized initially that the Bz compounds would engage in one of two different synthons, N-H···O=C or N-H···N (py) hydrogen bonds, resulting in infinite chains or discrete dimers, respectively. In fact, in all four cases, only the latter interaction was observed in the solid state (Figure 9). A CSD search was conducted to compare the prevalence of this N-H···N(py)/N(py)···H-N interaction in molecules bearing a similar backbone *i.e.* N-(pyridin-2-yl)benzamide. To make the analysis most relevant to our systems, only molecules with a single N-(pyridin-2-yl)benzamide unit and without any other potential hydrogen-bond donors (such as OH) or acceptors were included. The search identified 22 structures and all but three of them contain

the N-H···N(py)/N(py)···H-N interaction. In the three 'outliers' (YOVKIG, JIXCUO and JIXDAV) the N-H···O=C is instead present. Thus, the combined percentage for dimers in all 26 structures under consideration here is 88% while chain formation is 12%. The dominant assembly observed in the solution phase is likely to serve as an important precursor to or indication of what will ultimately appear in the solid state and vice versa.[39] Separate NMR signals which may arise due to different synthons at play are averaged out in the resultant spectrum. All the N-H peaks of compounds in this series occur within a 0.20 ppm range and in a separate 'band' compared to the other series (Figure 2.10). We can therefore confidently assume that the NMR data for all Bz compounds in this series indicate that they are similar to each other and predominantly form dimers in DMSO.

In the Bz series, the introduction of the halogen atoms altered the MEP of the donor and acceptor sites by increasing the donor potential and reducing the acceptor potential (less negative). The presence of electron withdrawing groups is known to decrease electron density from donor sites making them potentially stronger donors while the electron withdrawal from acceptor sites lead to decreased electron density and weaker acceptors. Thus, in this case the electron withdrawing nature of the halogen atom leads to the observed alterations of molecular electrostatic potentials.[40] Despite this, the N-H···N synthon was favored resulting in dimer formation in each of the four cases. As the reported crystal structures also have varying MEP at the donor and acceptor sites it is clear that changes in the MEP potential at these sites do not lead to a change in the resulting supramolecular assembly. However, in the crystal structure of Bz-I, an additional interaction, an iodine-π halogen bond, is also present. The relatively limited polarizability of the chlorine and bromine analogues explain why similar short contacts did not appear in Bz-Cl and Bz-Br, respectively. The Bz-Cl and Bz-Br are also isostructural.[41] The I···π halogen bond is unlikely to

be very strong as it has not been 'activated' through electron-withdrawing groups[42] or via an *sp*-hybridized carbon atom.[43]

In the 2Pyr series, all four compounds showed intramolecular hydrogen bonding to $–N_2$. The free rotation about the ring provides the perfect orientation between $–N_2$ and the amide hydrogen for intramolecular hydrogen bonding. Even though the electrostatic potential on $–N_2$ is higher than that of $–N_1$, an intramolecular hydrogen bond is generally going to be favored over intermolecular hydrogen bonds. Again, the chloro and bromo compounds are isostructural to each other. The CSD analysis of the core 2Pyr structure reveals the presence of the basic N-(pyridin-2-yl)picolinamide unit as a subunit in larger molecules wherein the intramolecular hydrogen bonding has been used for constructing functional materials such as aqua pores(EPIDEO)[44] or pharmaceutical agents (FIDROB).[45] In 2Pyr-I the vacant N_1 acts as a halogen bond acceptor to an iodine atom on an adjacent molecule. The negatively charged 'equator' of the same donor iodine acts a halogen bond acceptor to another 2Pyr-I molecule. Thus, there are two crystallographically unique 2Pyr-I molecules in this structure. This also serves to explain the presence of two amide hydrogen peaks in the infrared spectrum. Once again, the increased polarizability of the iodine atom in comparison to the other halogen atoms enabled it to act as a halogen bond donor while chlorine and bromine did not. The solution phase (NMR data) indicated the absence of multiple assembly modes by the amide hydrogen. Moreover, the amide peaks of the compounds in this series occur in a different "band" compared to the other series. This indicates that the solution phase assembly is quite distinct to those of the other series and reflects the nature of the observed outcome in the solid state. The NMR data also indicate that there are no dimers present in solution as was the case with the Bz compounds.

With shifting of the second pyridyl site in 3Pyr, intramolecular hydrogen bonding is no longer an option. The postulated possibilities for hydrogen bonding were via synthon 1, synthon 2 or synthon 3. Synthon 3 is observed in all four structures in the solid state. Despite the donor potential of amide hydrogen increasing and acceptor potential decreasing with the introduction of the halogen the same motif is observed throughout the series. The selection of synthon 3 over synthon 2 can be rationalized based on the higher negative electrostatic potential of the acceptor nitrogen.[20] The CSD structure analysis revealed one compound 2-chloro-N-(6-methyl-2-pyridinyl)nicotinamide (MEDJUB)[46] where the molecules assemble via synthon 3. In this compound the two pyridyl nitrogen atoms are arranged cis to each other. 3Pyr-Br in this study was the only structure out of the four to also show a cis arrangement of the pyridyl nitrogen atoms. The solution phase NMR shows that all four compounds behave similarly. The chemical shift range for the compounds in this series are quite distinct to that observed for the Bz and 2Pyr series. This nature of difference in the synthon is also reflected in the solid state.

The expected synthons for the 4Pyr series were synthon 1, synthon 2 or synthon 3. 4Pyr, 4Pyr-Cl and 4Pyr-Br assemble via synthon 3. In this series too, the chloro and bromo compounds exhibit isostructurality. All halogen atoms produced a similar alteration of the potentials at amide hydrogen (making it stronger) and the acceptor sites (making it weaker). Despite this change, the hydrogen bond synthon remained identical in these three compounds. We obtained two crystal structures for 4Pyr-I, both of which showed different hydrogen bonding compared to the other compounds in the series. In 4Pyr-I-i synthon 2 is observed and halogen bonding between iodine and $-N_2$ is seen. The other polymorph, 4Pyr-I-ii was obtained from a failed co-crystallization experiment between 4Pyr-I and dodecanoic acid. In 4Pyr-I-ii, again halogen bond formation between iodine and $-N_2$ is seen. The solution phase data (NMR) indicate that the amide hydrogen

appeared clustered in the same general range as the 3Pyr series. This similarity of the binding mode observed in the solution phase is also reflected in the solid state as all these compounds (except for 4Pyr-I) assemble via synthon 3. The NMR of 4Pyr is from a crystal of 4Pyr-I-i. Although the amide hydrogen forms dimers in 4Pyr-I-i they are not 'isolated' dimers as in the case of Bz series. This may explain why it appears more downfield than compounds in the Bz series. Additionally, the deviation of chemical shift to the bromo and chloro compounds in the series is different to the deviation of the other series (nearly 0.09 vs 0.05) and it may also reflect the chemical nature of the amide hydrogen due to the presence of synthon 1 seen in 4Pyr-I-ii.

3Pyr-I was the only iodinated compound which did not show any halogen bonds or close contacts. In order to verify that the crystal of 3Pyr-I grown, is representative of the solid-state arrangement of the compound PXRDs of experimental and simulated were examined (Appendix). The experimental PXRD did not reveal additional crystalline forms. The MEP value of the iodine in 3Pyr-I is more positive than the iodinated compounds in the Bz and 2Pyr series and is identical to that of 4PyrI. Thus, the absence of any halogen bond or contact formation by 3Pyr-I may be due to steric effects.

2.5 Conclusions

We find that the head-to-head dimer is the prevailing interaction in compounds of the Bz series in the four compounds of this study and amongst N-(pyridin-2-yl)benzamide compounds reported in the literature. With the introduction of the halogen in all series the acceptors became weaker and the donor stronger. Considering all four series, irrespective of which halogen atom, within a series, the electrostatics at each donor and acceptor site is altered to the same extent. i.e., MEP at the acceptor sites (carbonyl oxygen and pyridine nitrogen) is decreased and increased donor potential (of amide hydrogen) in comparison to the non-halogenated compound. In three out of the four

series (Bz, 2Pyr and 4Pyr) the chloro and bromo compounds are isostructural. Out of the thirteen crystal structures obtained for the halogenated compounds, despite the MEP changes, the hydrogen bonding motif was altered in only two out of thirteen (2/13) structures with respect to the non-halogenated compound. Although the hydrogen bond motif was not altered, both Bz-I and 2Pyr-I showed halogen bond/contact formation. Overall, only the iodinated targets exhibit halogen bond/contact formation (Table 2). This observation is in accordance with the halogen bonding theory where higher polarizability of the halogen atom leads to a bigger σ-hole as reflected in the calculated MEPs. Thus, the introduction of a halogen atom leads to significant changes in assembly in 4/13 cases, and all the changes occurred in the presence of the iodine substituent. It is worth noting that in the case of 4Pyr-I, halogen bonding occurs competitively to hydrogen bonding despite the iodine not being activated.

In these compounds when another donor site of sufficient donor ability (iodine) is introduced the overall assembly was changed in comparison to the parent (un-halogenated) compounds. Since, the hydrogen bonding motif remained identical to that of the non-halogenated, chlorinated and brominated derivatives in 2/4 structures (Bz-I and 2Pyr-I) and in the other 2/4 cases (both the 4PyrI structures) the hydrogen bond motif is different, the halogen bonding iodine site acted auxiliary 50% of the time acted competitively 50% of the time to the amide hydrogen, Figure 2.11.

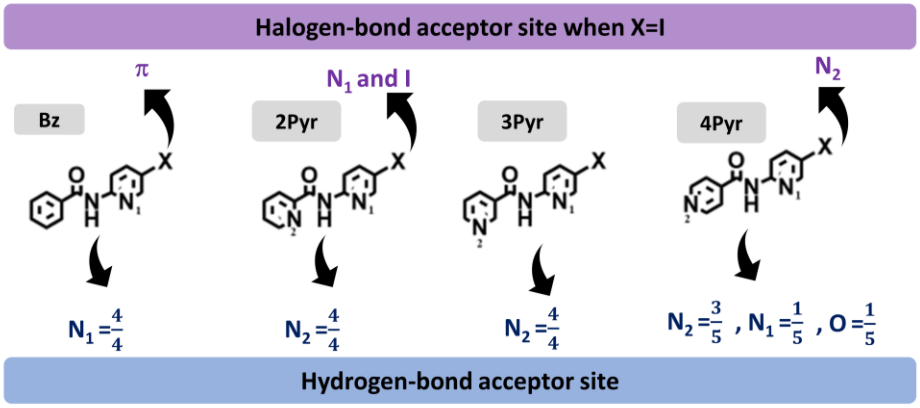

Figure 2.11. A summary of the motifs in the sixteen compounds analyzed herein, grouped by series.

2.6 References

[1] Steiner, T. The hydrogen bond in the solid state. *Angew. Chem. Int. Ed*. **2002,** *41*, 48-76.
[2] Hisaki, I.; Suzuki, Y.; Gomez, E.; Ji, Q.; Tohnai, N.; Nakamura, T.; Douhal, A. Acid responsive hydrogen-bonded organic frameworks. *J. Am. Chem. Soc*. **2019,** *141*, 2111-2121
[3] Wang, H.; Bisoyi, H.K.; Urbas, A.M.; Bunning, T.J.; Li, Q. The halogen bond: an emerging supramolecular tool in the design of functional mesomorphic materials. *Chem. Eur. J*. **2019,** *25*, 1369-1378.
[4] Meazza, L.; Foster, J. A.; Fucke, K.; Metrangolo, P.; Resnati, G.; & Steed, J. W. Halogen-bonding-triggered supramolecular gel formation. *Nature chemistry*. **2013**, *5*, 42-47
[5] Scilabra, P.; Terraneo, G.; Resnati, G. The chalcogen bond in crystalline solids: A world parallel to halogen bond. *Acc. Chem. Res.* **2019,** *52*, 1313-1324.
[6] Vogel, L.; Wonner, P.; Huber, S. M. Chalcogen bonding: An overview. *Angew. Chem. Int. Ed*. **2019,** *58*, 1880-1891.
[7] Resnati, G.; Boldyreva, E.; Bombicz, P.; Kawano P. Supramolecular interactions in the solid-state. *IUCrJ*. **2015**, *2*, 675−690.
[8] Aakeröy, C.B.: Wijethunga, T.K.; Desper, J. Constructing molecular polygons using halogen bonding and bifurcated N-oxides. *CrystEngComm.* **2014**, *16*, 28-31
[9] Mandal, S.; Mukhopadhyay, T.; K., Mandal, N.; Datta, A. Hierarchical Noncovalent Interactions between Molecules Stabilize Multicomponent Cocrystals. *Crystal Growth & Design*. **2019**, *19*, 4802-4809.
[10] Babu, N.J.; Cherukuvada, S.; Thakuria, R.; Nangia, A. Conformational and synthon polymorphism in furosemide (Lasix). *Cryst. Growth Des.* **2010,** *10*, 1979-1989.
[11] Gong, N.; Yang, D.; Jin, G.; Liu, S.; Du, G.; Lu, Y. Structure, characterization, solubility and stability of podophyllotoxin polymorphs. *J. Mol. Struct.* **2019**, *1195*, 323-330.
[12] Kavanagh, O. N.; Croker, D. M.; Walker, G. M.; Zaworotko, M. J. Pharmaceutical cocrystals: from serendipity to design to application. *Drug Discov. Today.* **2019**, *24*, 796-804
[13] Kacso, I.; Rus, L.M.; Martin, F.; Miclaus, M.; Filip, X.; Dan, M. Solid-state compatibility studies of Ketoconazole-Fumaric acid co-crystal with tablet excipients. *J. Therm. Anal. Calorim*. **2020,** 1-8.

[14] Gołdyn, M.; Larowska, D.; Nowak, W.; Bartoszak-Adamska, E. Synthon hierarchy in theobromine cocrystals with hydroxybenzoic acids as coformers. *CrystEngComm*. **2019**, *21*, 7373-738
[15] Desiraju, G.R. Supramolecular synthons in crystal engineering—a new organic synthesis. *Angew. Chem. Int. Ed*. **1995,** *34*, 2311-2327.
[16] Corpinot MK.; Bučar D.K. A Practical guide to the design of molecular crystals. *Cryst Growth & Des*. **2019**, *19*, 1426-1453
[17] Khavasi, H. R.; Hosseini, M.; Tehrani, A. A.; Naderi, S. Strengthening N··· X halogen bonding via nitrogen substitution in the aromatic framework of halogen-substituted arylpyrazinamides. *CrystEngComm*. **2014**, *16*, 4546-4553
[18] Liu, H.; Yang, X.; Chen, J.; Zhang, M.; Parkin, S.; Cao, S.; Li, T.; Yang, Z.; Yu, F.; Long, S. Steric Effect Determines the Formation of Lactam-Lactam Dimer or Amide C= O… NH (Lactam) Chain Motif in N-phenyl-2-hydroxynicotinanilides. *Cryst. Growth Des.* **2020**, *20*, 4346-4357
[19] Goswami, A.; Garai, M.; Biradha, K. Interplay of halogen bonding and hydrogen bonding in the cocrystals and salts of dihalogens and trihalides with N, N′-bis (3-pyridylacrylamido) derivatives: phosphorescent organic salts. *Cryst. Growth Des.* **2019**, *19*, 2175-2188
[20] Perera, M.D.; Desper, J.; Sinha, A.S.; Aakeröy, C.B. Impact and importance of electrostatic potential calculations for predicting structural patterns of hydrogen and halogen bonding. *CrystEngComm*. **2016,** *18*, 8631-8636.
[21] Mocilac, P.; Tallon, M.; Lough, A. J.; Gallagher, J. F. Synthesis, structural and conformational analysis of a 3× 3 isomer grid based on nine methyl-N-(pyridyl) benzamides. *CrystEngComm*. **2010**. *12*, 3080-309
[22] Mocilac, P.; Donnelly, K.; Gallagher, J. F. Structural systematics and conformational analyses of a 3× 3 isomer grid of fluoro-n-(pyridyl) benzamides: Physicochemical correlations, polymorphism and isomorphous relationships. *Acta Crystallographica Section B: Structural Science*. **2012**. *68*, 189-203
[23] Gallagher, J. F.; Farrell, M.; Hehir, N.; Mocilac, P.; Aubert, E.; Espinosa, E.; Benoît, G.; Jelsch, C. At the Interface of Isomorphous Behavior in a 3× 3 Isomer Grid of Monochlorobenzamides: Analyses of the Interaction Landscapes via Contact Enrichment Studies. *Cryst. Growth Des*. **2019.** *19*, 6141-6158
[24] Wolters, L. P.; Schyman, P.; Pavan, M. J.; Jorgensen, W. L.; Bickelhaupt, F. M.; Kozuch, S. The many faces of halogen bonding: a review of theoretical models and methods. *Wiley Interdisciplinary Reviews: Computational Molecular Science*, **2014**. *4*, 523-540
[25] The Cambridge Structural Database, Groom, C.R., Bruno, I.J., Lightfoot, M.P., Ward, S.C., Acta Cryst., **2016**, *B72*, 171-179
[26] Liu, Y. Z.; Wang, H.; Chan, C. K.; Mu, X.; Robeyns, K.; Wang, C. C.; Singleton, M. L. Structure-Dependent Guest Recognition with Flexible Ferrocene-Based Aromatic Oligoamide β-Sheet Mimics. *Chem. Eur. J.* **2010**, *26*, 181-185
[27] Gan, Q.; Ferrand, Y.; Bao, C.; Kauffmann, B.; Grélard, A.; Jiang, H.; Huc, I. Helix-rod host-guest complexes with shuttling rates much faster than disassembly. *Science*. **2011**, *331*, 1172-1175
[28] McMoran, E. P.; Dominguez, M. N.; Erwin, E. M.; Powell, D. R.; Rowe, G. T.; Yang, L. Structural diversity, spectral characterization and computational studies of Cu (I) complexes with pyridylamide ligands. *Inorg. Chim. Acta.* **2016.** *446*, 150-160
[29] Rai, D.; & Singh, R. K. Synthesis and antibacterial activity of benzamides and sulfonamide derived from 2-amino-5-bromo/nitropyridine against bacterial strains isolated from clinical patients. *Indian J. Chem*. **2011,** 50B, 931-936
[30] Vu, H.N.; Kim, J.Y.; Hassan, A.H.; Choi, K.; Park, J.H.; Park, K.D.; Lee, J.K.; Pae, A.N.; Choo, H.; Min, S.J.; Cho, Y.S.; Synthesis and biological evaluation of picolinamides and thiazole-2-carboxamides as mGluR5 (metabotropic glutamate receptor 5) antagonists. *Bioorg. Med. Chem. Lett.* **2016,** *26*, 140-144.
[31] Aakeröy, C.B.; Panikkattu, S.V.; DeHaven, B.; Desper, J. Establishing supramolecular control over solid-state architectures: a simple mix and match strategy. *Cryst. Growth Des*. **2012,** *12*, 2579-2587.
[32] Yang, S.; Yan, H.; Ren, X.; Shi, X.; Li, J.; Wang, Y.; Huang, G. Copper-catalyzed dehydrogenative reaction: synthesis of amide from aldehydes and aminopyridine. *Tetrahedron*. **2013,** *69*, 6431-6435.
[33] Nicolas, L.; Angibaud, P.; Stansfield, I.; Meerpoel, L.; Reymond, S.; Cossy, J. Copper-catalysed amidation of 2-chloro-pyridines. *RSC advances*. **2013**, *3*, 18787-18790.
[34] This reported melting point of this compound is likely to be in error.

[35] Searls, T.; Chen, D.L.; Lan, T.; McLaughlin, L.W. Nucleoside Analogue Substitutions in the Trinucleotide DNA Template Recognition Sequence 3 '-(CTG)-5 'and Their Effects on the Activity of Bacteriophage T7 Primase. *Biochemistry*. **2000**, *39*, 4375-4382.
[36] Wang, K.; Shen, M.; Sun, W.H. N-(Pyridin-2-yl) picolinamide tetranickel clusters: Synthesis, structure and ethylene oligomerization. *Polyhedron*. **2010**, *29*, 564-568.
[37] The crystal structure of this compound was published during the course of this project; Pappula, V., Ravi, C., Samanta, S., Adimurthy, S., Oxidative Amidation of Methylarenes anf Heteroamines under Metal-Free Conditions, *Chem. Select Comm*., **2017**, *2*, 5887-5890.
[38] Kumar, D. K.; Jose, D. A.; Dastidar, P.; Das, A. Nonpolymeric hydrogelator derived from N-(4-pyridyl) isonicotinamide. *Langmuir*. **2004**, *20*, 10413-10418.
[39] Osmiałowski, B.; Kolehmainen, E.; Dobosz, R.; Gawinecki, R.; Kauppinen, R.; Valkonen, A., Juha, K,; Rissanen, K. (2010). Self-organization of 2-acylaminopyridines in the solid state and in solution. *J. Phys. Chem. A.* **2010,** *114*, 10421–10426
[40] Aakeröy, C. B.; Rajbanshi, A.; Li, Z. J.; Desper, J. Mapping out the synthetic landscape for re-crystallization, co-crystallization and salt formation. *CrystEngComm*, **2010**, *12*, 4231-4239
[41] Mukherjee, A.; Desiraju, G. R. Halogen bonds in some dihalogenated phenols: applications to crystal engineering. *IUCrJ*. **2014**, *1*, 49-60
[42] Bamberger, J.; Ostler, F.; Mancheño, O. G. Frontiers in Halogen and Chalcogen-Bond Donor Organocatalysis. *ChemCatChem*. **2019**, *11*, 5198-5211.
[43] Bosch, E.; Kruse, S. J.; Groeneman, R. H. Infinite and discrete halogen bonded assemblies based upon 1, 2-bis (iodoethynyl) benzene. *CrystEngComm.* **2019**, *21*, 990-993
[44] Zhao, H.; Sheng, S.; Hong, Y.; Zeng, H. Proton gradient-induced water transport mediated by water wires inside narrow aquapores of aquafoldamer molecules. *J. Am. Chem. Soc.* **2014**, *136*,14270–14276
[45] Gottschalk, S.; Engelmann, J.; Rolla, G. A.; Botta, M.; Parker, D.; Mishra, A. Comparative in vitro studies of MR imaging probes for metabotropic glutamate subtype-5 receptor targeting. *Org. Biomol. Chem.* **2013**,*11*, 6131-6141
[46] Fernandes, E. L.; Magalhaes, A.; Paes, K. C.; De Souza, M. V.; Vasconcelos, T. R.; Wardell, J. L.; Wardell, S. M. Cyclisation of 2-Chloro-N-(2-Pyridinyl) Nicotinamides to 5-Oxo-5, 6-Dihydrodipyrido [1, 2-a: 3′, 2′-e] Pyrimidin-11-Ium Chlorides. *J.Chem.Res.* **2006,** 93-97

Chapter 3 - The impact of halogen substituents on the synthesis and structure of co-crystals of pyridine amides

3.1 Introduction

Practical crystal engineering is driven by the use of intermolecular forces, primarily hydrogen-bonding [1], for connecting discrete molecular building blocks or coordination complexes into extended crystalline architectures[2,3,4,5]. A "second-phase" of research in this area has added (i) synthetic complexity by taking advantage of additional structure-directing interactions such as halogen[6] and chalcogen bonds[7] and (ii) compositional complexity by building multi-component architectures such as binary, ternary[8,9,10] and higher-order co-crystals[11]. Most of these efforts have been in the area of basic science, with the goal of establishing guidelines for how different molecules and functional groups recognize and bind to each other via non-covalent interactions.[12]Such insights can enable forays into applied materials science by applying co-crystal technology to the synthesis of new solid forms of pharmaceutically relevant compounds,[13,14] agrochemicals,[15,16] energetic materials[17,18] and other high-value solids.[19] In order to learn more about competing molecular-recognition events in supramolecular assembly, we previously examined the outcomes of co-crystallization of N-(pyridin-2-yl)nicotinamide and N-(pyridin-2-yl)isonicotinamide with di-carboxylic acids and identified reliable recognition events between both the N2(py) and N1(py)—NH sites of the target molecules to the dicarboxylic acids. Additionally, the fundamental nature of the observed architectures (rings or chains) could be correlated to the geometries of the binding sites of target molecules and the relative position of —COOH groups in odd and even chained acids.[20]

In order to expand and refine practical crystal engineering strategies, we wanted to systematically map out the structural influence exerted by a potential halogen bonding site on the supramolecular

framework in the same set of target compounds. Furthermore, we also wanted to establish if it is reasonable to hypothesize that differences between crystal structures of halogenated and non-halogenated homomeric assemblies would lead to similar differences in co-crystals of the same set of targets. The work presented herein utilized a systematic structural study of co-crystals of closely related compounds, Figure 3.1, in order to learn more about the balance between competing interactions in heteromeric molecular architectures.

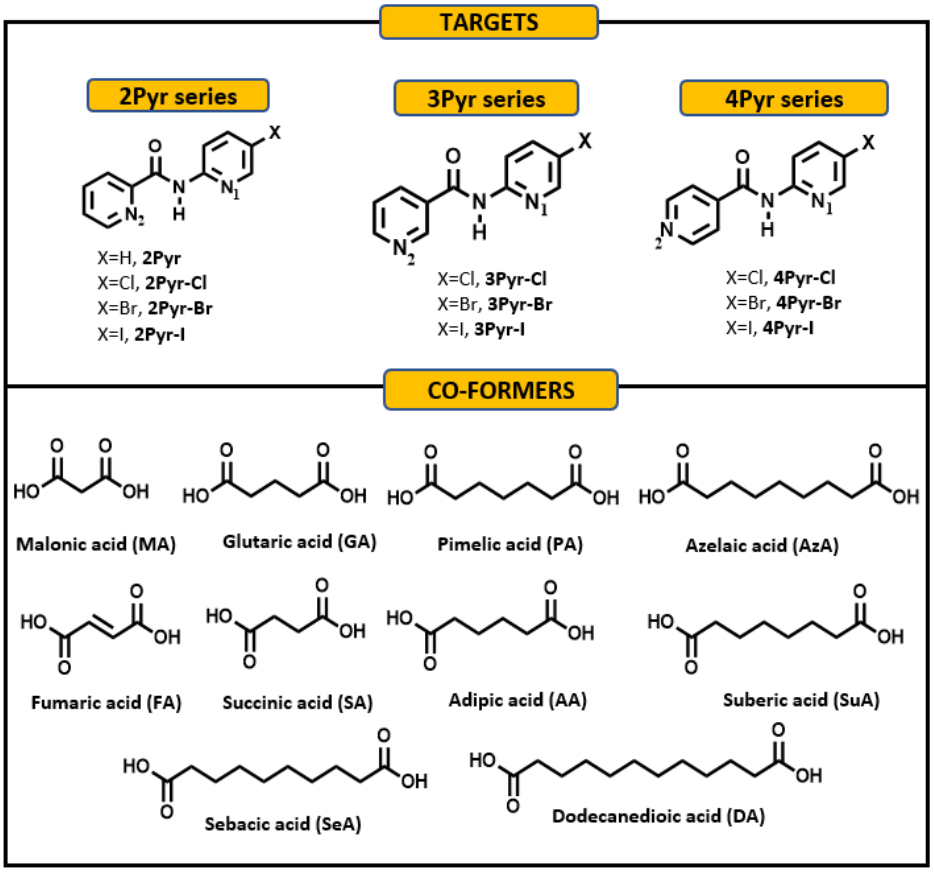

Figure 3.1. Schematics of target molecules and co-formers in this study

We previously identified the prevailing hydrogen-bond interactions in the ten targets.[21] The 2Pyr compounds all displayed intramolecular N-H···N_2 hydrogen bonding, whereas this was not geometrically possible in the 3Pyr/4Pyr analogues. This allowed us to hypothesize that even though all three isomers contain identical hydrogen-bonding sites, the presence of an intramolecular five-membered "ring" in 2Pyr would preclude these target compounds from forming co-crystals with carboxylic acids through pairs of N-H···O=C/N···H-O hydrogen bonds (Figure 3.2).

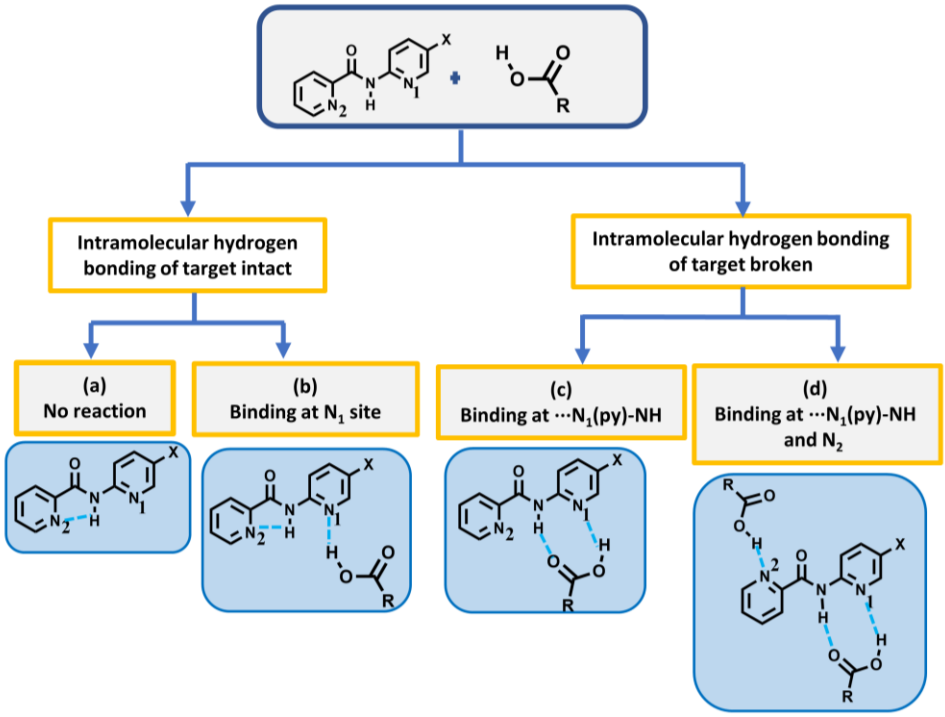

Figure 3.2 Possible outcomes of co-crystallization experiments of 2Pyr series compounds.

Outcomes (a) No reaction and (b) Binding at N_1 may occur with intramolecular hydrogen bonding intact. Outcomes (c) Binding at ···N_1(py)-NH and (d) Binding at ···N_1(py)-NH and N_2(py) are assumed not to take place because of the likely presence of an intramolecular hydrogen-bonded five-membered ring.

In this study we wanted to address five specific questions.

- What is the effect of co-crystallization ability in targets where the NH hydrogen of the N_1(py)-NH pocket is engaged in intramolecular hydrogen bonding to N_2
- How does the presence of the halogen atoms alter the supramolecular assembly of co-crystals?
- Are any observed alterations consistent amongst targets in the same series?
- Are there any instances in which the (potential) halogen-bond donor competes with the hydrogen-bond donor?
- So isostructural targets exhibit isostructurality in their corresponding co-crystals?

Three possible outcomes in the presence of a halogen atom on the molecular framework of co-crystals in 3Pyr and 4Pyr series may be postulated, as shown in Figure 3.3.

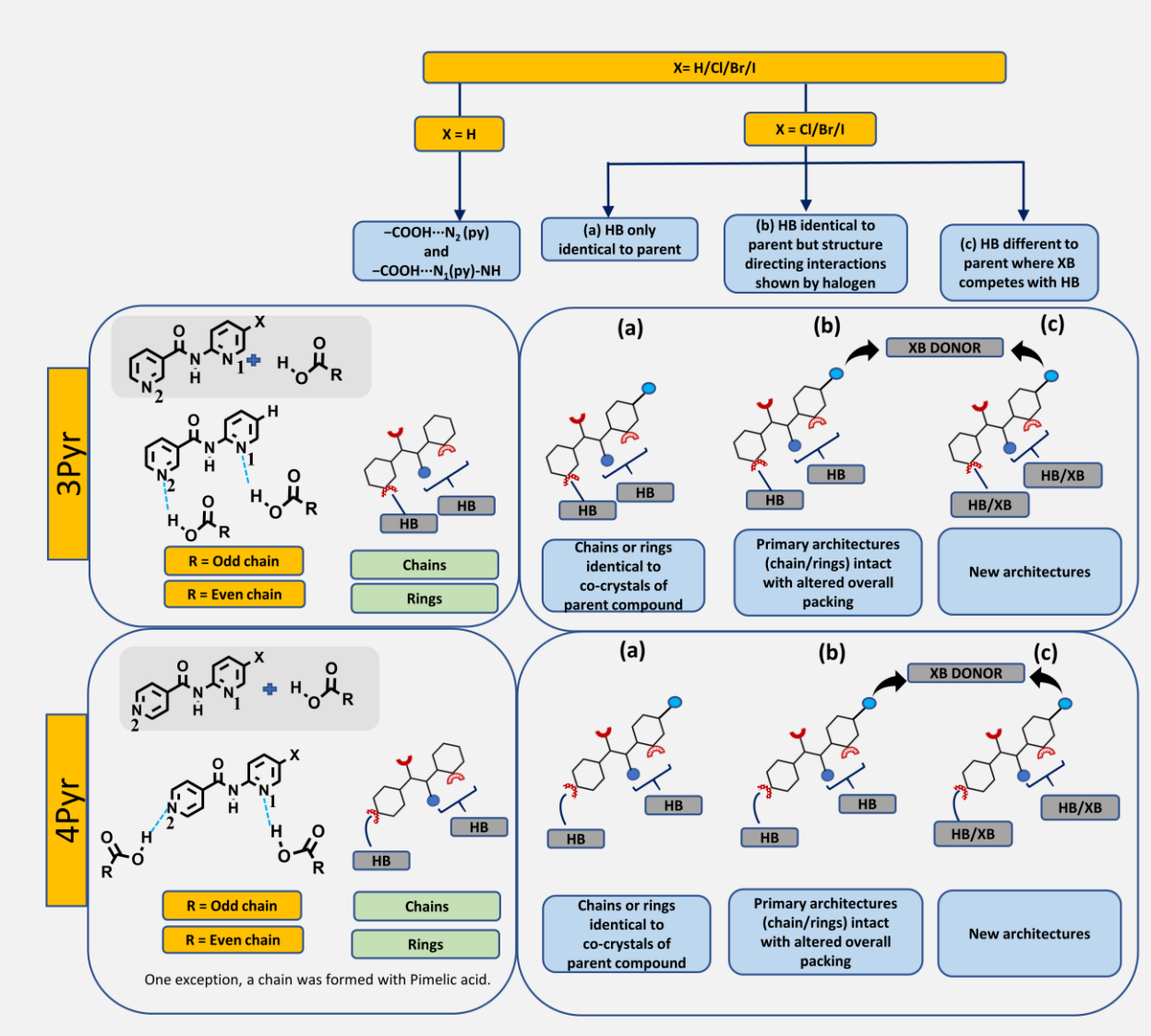

Figure 3.3. Postulated structural outcomes in co-crystals of halogenated target molecules in 3Pyr/4Pyr series and carboxylic acids.

HB = hydrogen bonding, XB = halogen bonding where (a) HB only, (b) HB and structure directing non-competitive XB interactions, (c) XB competes with HB leading to new architecture with halogenated 3Pyr (top) and 4Pyr (bottom) targets respectively.

3.2 Experimental

The target compounds were prepared as previously reported.21 Co-crystal screening with ten aliphatic dicarboxylic acids (Figure 3.1) was carried out using liquid assisted grinding with stoichiometric 1:1 amounts of target and co-former, followed by IR characterization of the ground powder. A total of 100 experiments were performed. Broad stretches near 1850 cm−1 and 2450 cm−1 indicative of intermolecular O-H···N hydrogen bonds were used for confirming the presence of a co-crystal.[20] IR spectra of cocrystal screening experiments were recorded with a Nicolet 380 FT-IR spectrometer using an attenuated total reflection (ATR) technique and ZnSe as the crystal. Melting points were measured using a Fisher-Johns melting point apparatus or a TA Instruments DSC Q20 differential scanning calorimeter. Datasets for single-crystal X-ray diffraction analysis were collected on a Bruker Kappa APEX II system using CuKα radiation

3.3 Results

The outcome of the IR screening results is given in Table 1. The relevant IR data is provided in the Appendix B.

3.3.1 Results of co-crystal screen

Table 3.1. Results of co-crystal screening experiments**.**

	Malonic Acid	Glutaric Acid	Pimelic Acid	Azelaic Acid	Fumaric Acid	Succinic Acid	Adipic Acid	Suberic Acid	Sebacic Acid	Dodecanedioic Acid
2Pyr	×	×	×	×	×	×	×	×	×	×
2Pyr-Cl	×	×	×	×	×	×	×	×	×	×
2Pyr-Br	×	×	×	×	×	×	×	×	×	×
2Pyr-I	×	×	×	×	×	×	×	×	×	×
3Pyr-Cl	✓	×	✓	×	×	✓	✓	✓	×	×
3Pyr-Br	✓	✓	×	×	✓	✓*	✓	✓*	×	×
3Pyr-I	✓*	✓	×	×	✓	✓	✓*	✓*	✓*	×
4Pyr-Cl	✓	✓	✓*	✓	✓*	✓	✓*	✓	✓	✓
4Pyr-Br	✓	✓	✓	✓	✓*	✓	✓*	✓	✓	✓
4Pyr-I	✓	✓	✓	✓	✓*	✓*	✓*	✓	✓*	×

(×= negative, ✓= positive, * = single crystal structure obtained).

3.3.2 Crystal growth

The resultant solids that showed co-crystal formation were dissolved in a variety of solvents to obtain crystals of diffraction quality; see Table 2 for details. Out of the 47 co-crystals that were obtained, 15 produced crystals suitable for single-crystal X-ray diffraction (SCXRD). The resultant solids that showed co-crystal formation were dissolved in a variety of solvents to obtain crystals of diffraction quality; see Table 3.2 for details. Out of the 47 co-crystals that were obtained, 15 produced crystals suitable for single-crystal X-ray diffraction (SCXRD).

Table 3.2. Solvents used for crystal growth and crystal descriptions

Co-Crystal	Code	Solvent	Melting point	Color and Morphology
(*N*-(5-bromopyridin-2-yl)nicotinamide) Succinic acid (1:1)	3Pyr-Br:SA	Ethyl acetate: MeOH(1:1)	185–187 °C	Colorless, Parallelepiped
(*N*-(5-bromopyridin-2-yl)nicotinamide) Suberic acid (1:1)	3Pyr-Br:SuA	Ethyl acetate: MeOH(1:1)	149–151 °C	Colorless, Rectangular
(*N*-(5-iodopyridin-2-yl)nicotinamide) Adipic acid (1:1)	3Pyr-I:AA	Ethyl acetate	163–165 °C	Yellow, Rectangular
(*N*-(5-iodopyridin-2-yl)nicotinamide) Suberic acid (1:1)	3Pyr-I:SuA	Ethyl acetate	148–150 °C	Colorless, Rectangular
(*N*-(5-iodopyridin-2-yl)nicotinamide) Sebacic acid (1:1)	3Pyr-I:SeA	Ethyl acetate	139–141 °C	Yellow, Rectangular
(*N*-(5-iodopyridin-2-yl)nicotinamide) Malonic acid (1:1)	3Pyr-I:MA	Chloroform: MeOH(1:1)	169–171 °C	Colorless, Rectangular
(*N*-(5-chloropyridin-2-yl)isonicotinamide) Adipic acid (1:1)	4Pyr-Cl:AA	Ethyl acetate	169–171 °C	Colorless, Rectangular
(*N*-(5-bromopyridin-2-yl)isonicotinamide) Adipic acid (1:1)	4Pyr-Br:AA	Acetonitrile	161–163 °C	Colorless, Rectangular
(*N*-(5-chloropyridin-2-yl)isonicotinamide) Pimelic acid (1:1)	4Pyr-Cl:PA	Ethyl acetate	163–165 °C	Colorless, Rectangular
(*N*-(5-iodopyridin-2-yl)isonicotinamide) Adipic acid (2:1)	4Pyr-I:AA	Acetonitrile	159–161 °C	Colorless, Chunk
(*N*-(5-iodopyridin-2-yl)isonicotinamide) Suberic acid (2:1)	4Pyr-I:SuA	Ethyl acetate: MeOH(1:1)	146–148 °C	Colorless, Rectangular
(*N*-(5-iodopyridin-2-yl)isonicotinamide) Sebacic acid (2:1)	4Pyr-I:SeA	Ethyl acetate	147–149 °C	Colorless, Rhombus
(*N*-(5-chloropyridin-2-yl)isonicotinamide) Fumaric acid (1:1)	4Pyr-Cl:FA	Ethyl acetate	231–233 °C	Colorless, Irregular
(*N*-(5-bromopyridin-2-yl)isonicotinamide) Fumaric acid (1:1)	4Pyr-Br:FA	Methanol	240–242 °C	Colorless, Chunk
(*N*-(5-iodopyridin-2-yl)isonicotinamide) Fumaric acid (1:1)	4Pyr-I:FA	Ethyl acetate	237–239 °C	Colorless, Blocks

3.3.3 X-ray crystallography results

Six co-crystals of 3Pyr-X targets suitable for SCXRD were successfully grown. In the five co-crystals with even-chain acids (3Pyr-Br:SA, 3Pyr-Br:SuA, 3Pyr-I:AA, 3Pyr-I:SuA, 3Pyr-I:SeA) and the one with an odd-chain acid (3Pyr-I:MA), each target interacted with two acid molecules. With the even chain acids, 3Pyr-Br and 3Pyr-I formed two identical synthons, –COOH···N2(py) and –COOH···N1(py)-NH, which overall led to a tetrameric ring (Figure 3.4a–e) in a 1:1 stoichiometric ratio. In addition, both Br and I engaged in halogen bonds to the hydroxylic oxygen, thereby linking neighboring rings into an infinite ribbon (Figure 3.3a–e). The Br···O interactions showed a reduction of combined van der Waals radii of 5%, while the I···O showed a 10% reduction. In the structure of 3Pyr-I:MA, the hydrogen bonds (HBs) were once again –COOH···N2(py) and –COOH···N1(py)-NH but now led to chain-like architectures. The iodine atom formed two halogen bonds to both OH groups of a neighboring carboxylic acid molecule with van der Waals reductions of 10% and 3%, respectively. Thus, the halogen bonding effectively linked chains together (Figure 3.4f).

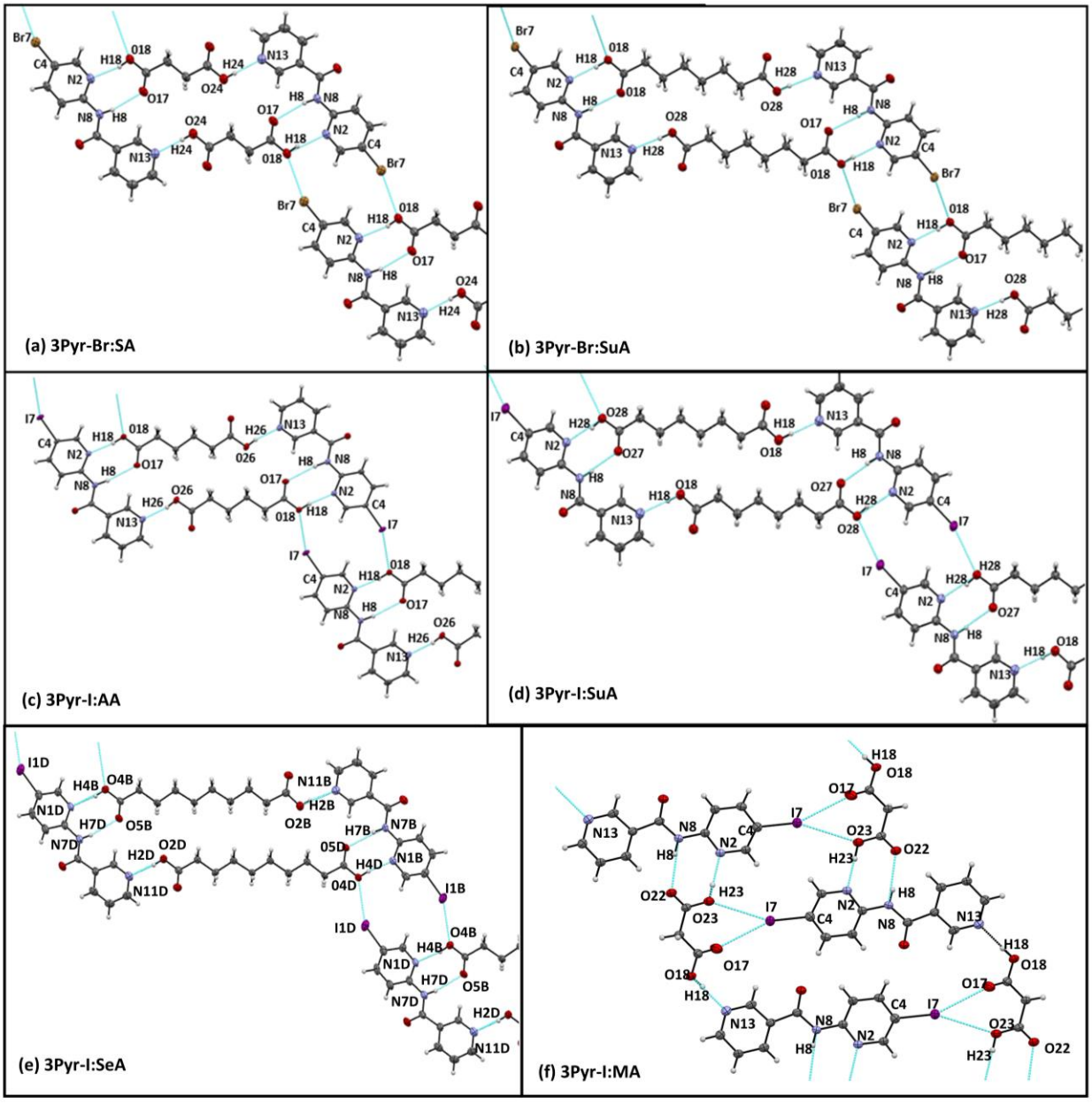

Figure 3.4. Primary interactions seen in single crystal structures of (a) 3Pyr-Br:SA, (b) 3Pyr-Br:SuA, (c) 3Pyr-I:AA, (d) 3Pyr-I:SuA, (e) 3Pyr-I:SeA*, and (f) 3Pyr-I:MA.

* Please see Appendix for image with all crystallographically unique molecules displayed.

The relevant hydrogen- and halogen-bond geometries in the six co-crystals from the 3Pyr series are given in Table 3.3.

Table 3.3. Hydrogen- and halogen-bond parameters in the Six 3Pyr-X Co-Crystals.

Code	D-H/X⋯A	D/X⋯A (Å)	D-H/X⋯A (deg)
3Pyr-Br:SA	N8-H8⋯O17	3.071(3)	167.(3)
	O18-H18⋯N2	2.732(3)	165.(5)
	O24-H24⋯N13	2.691(3)	172.(4)
	C4-Br7⋯O18	3.191(2)	158.56(8)
3Pyr-Br:SuA	N8-H8⋯O17	2.938(3)	166.(3)
	O18-H18⋯N2	2.692(3)	175.(3)
	O28-H28⋯N13	2.754(3)	177.(4)
	C4-Br7⋯O18	3.1979(19)	159.79(8)
3Pyr-I:AA	N8-H8⋯O17	3.198(4)	173.(4)
	O18-H18⋯N2	2.668(4)	171.(9)
	O26-H26⋯N13	2.683(4)	169.(7)
	C4-I7⋯O18	3.186(3)	155.15(11)
3Pyr-I:SuA	N8-H8⋯O27	2.970(5)	170.(4
	O18-H18⋯N13	2.766(6)	167.(7)
	O28-H28⋯N2	2.679(5)	167.(5)
	C4-I7⋯O28	2.086(4)	159.81(14)
3Pyr-I:SeA	O4B-H4B⋯N1D	2.692(5)	169.5
	N7D-H7D⋯O5B	3.088(6)	162.4(3)
	O2D-H2D ⋯N11D	2.718(6)	172.6
	C3D-I1D⋯O4D	3.227(4)	151.4(2)
	O2B-H2B⋯N11B	2.704(6)	165.0
	O4D-H4D⋯N1B	2.660(5)	171.2
	N7B-H7B⋯O5D	3.043(5)	170.1(3)
	C3B-I1B⋯O4B	3.229(4)	152.5(2)
	O4A-H4A⋯N1C	2.673(5)	171.3
	N7C-H7C⋯O5A	3.043(6)	168.0(3)
	O4C- H4C ⋯N11C	2.706(6)	172.2
	C3C-I1C⋯O2C	3.267(4)	150.9(2)
	O2A-H2A⋯N11A	2.705(6)	165.2
	O2C-H2C⋯N1A	2.685(5)	168
	N7A-H7A⋯O3C	3.068(6)	169.2(3)
	C3A-I1A⋯O4A	3.298(4)	151.1(2)
	04F-H4F⋯N1E	2.661(6)	169.4
	N7E-H7E⋯05F	3.050(6)	161.8(3)
	O18- H18 ⋯N1F	2.714(6)	169.1
	C3E-I1E⋯O4E	3.201(4)	152.4(2)
	O4E-H4E⋯N1F	2.665(5)	170.5
	N7F-H7F⋯O5E	3.068(5)	162.4(3)
	O23-H23⋯ N11F	2.661(6)	169.4
	C16-I1F⋯O4F	3.229(4)	152.5(2)
3Pyr-I:MA	N8-H8⋯O22	2.979(5)	170.(5)
	O18-H18⋯N13	2.634(5)	165.(6)
	O23-H23⋯N2	2.689(5)	173.(8)
	C4-I7⋯O17	3.231(4)	156.63(14)
	C4-I7⋯O23	3.452(3)	150.84(13)

A total of nine co-crystals of 4Pyr-X targets suitable for SCXRD were successfully grown. Eight of these contained even-chain acids as co-formers. Except for three of the iodinated co-crystals

(4Pyr-I:AA, 4Pyr-I:SuA, and 4Pyr-I:SeA), each target molecule in all the other co-crystals formed hydrogen bonding to two carboxylic acid molecules. In the co-crystals of 4Pyr-Cl:AA, 4Pyr-Br:AA, and 4Pyr-Cl:PA, two identical hydrogen-bonding (HB) interactions, −COOH···N_2(py) and −COOH···N_1(py)-NH, with the carboxylic acid led to chain-like architectures. There were no structure directing interactions shown by bromine or the chlorine atoms in these structures, Figure 3.5 a–c.

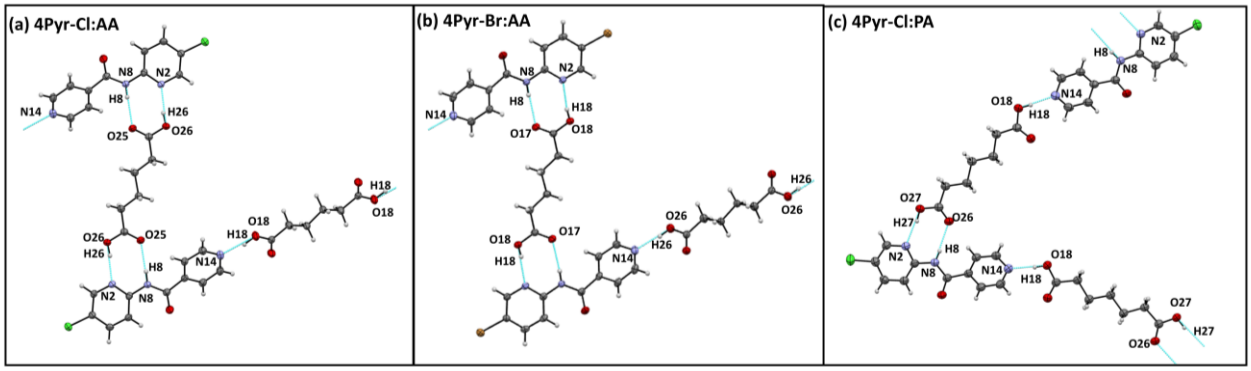

Figure 3.5. Primary interactions seen in single crystal structures of (a) 4Pyr-Br: AA, (b) 4Pyr-Br: AA, (c) 4Pyr-Cl-PA.

In three co-crystals 4Pyr-I:AA, 4Pyr-I:SuA, and 4Pyr-I:SeA, only −COOH···N_1(py)-NH interaction was seen between the target and co-former. In addition, −I···N_2 (py) intermolecular interactions were formed between target molecules. With each acid, the target compound combined in a 2:1 stoichiometry. The overall architecture can be described as having a "ladder-like" architecture (Figure 3.6a–c). Within these three co-crystals, 4Pyr-I:SuA contrasted to the other two as it had the carbonyl groups of halogen-bonded target molecules arranged trans to each other.

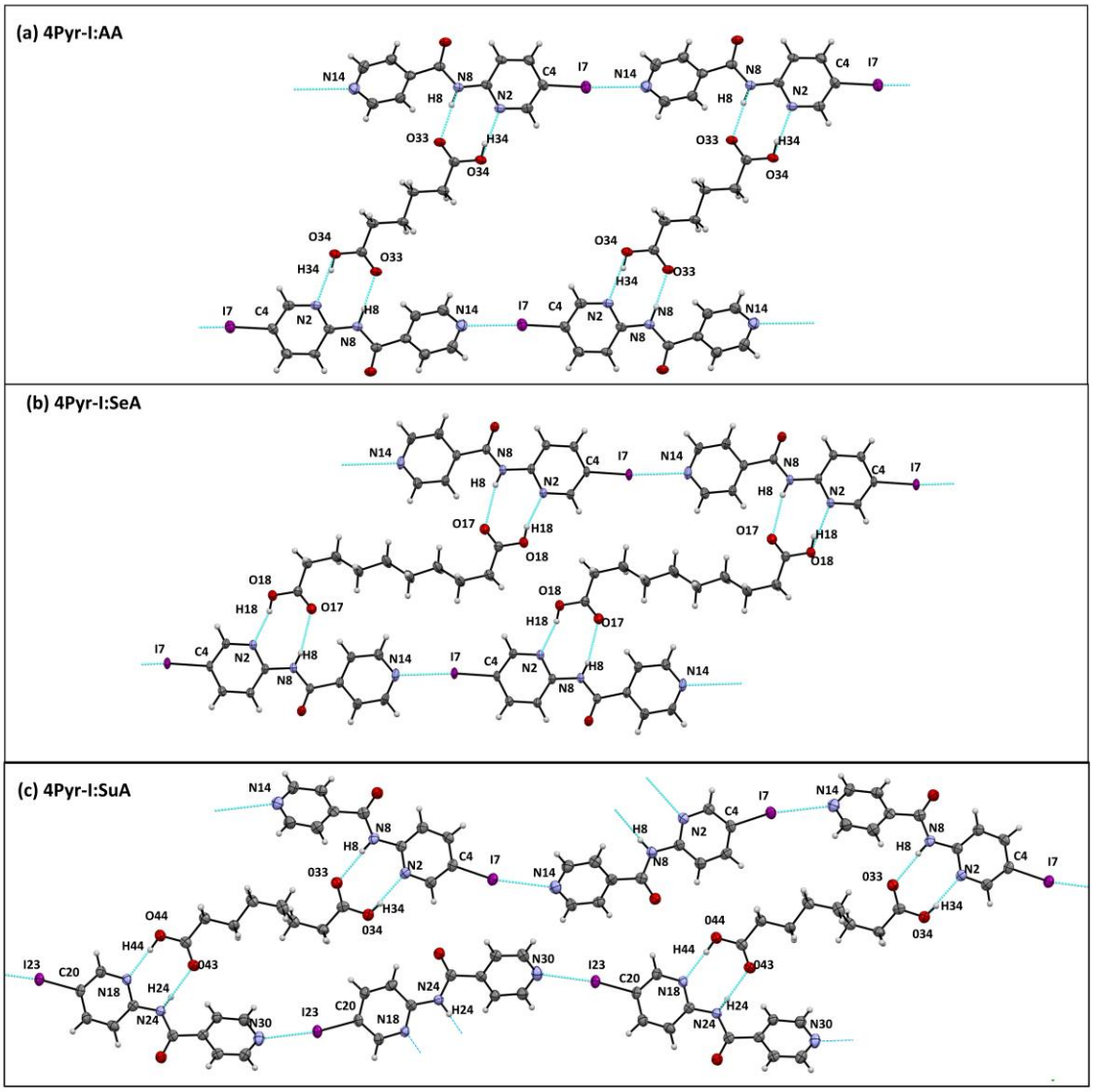

Figure 3.6. Primary interactions seen in single crystal structures of (a) 4Pyr-I:AA*, (b) 4Pyr-I:SeA, (c) 4Pyr-I:SuA.

* Please see Appendix for image with all crystallographically unique molecules displayed.

The three co-crystals of 4Pyr-Cl:FA, 4Pyr-Br:FA, and 4Pyr-I:FA showed identical HB patterns. Both the N_1(py)-NH and N_2(py) sites were engaged in hydrogen bonding to the carboxylic acid. Each target bound to two carboxylic acid molecules, forming −COOH···N2(py) and −NH···O=C

hydrogen bonds (Figure 3.7). In addition, a halogen–halogen (Type I) interaction was seen in both 4Pyr-Br:FA and 4Pyr-I:FA, with van der Waals reductions of 2% and 8%, respectively.

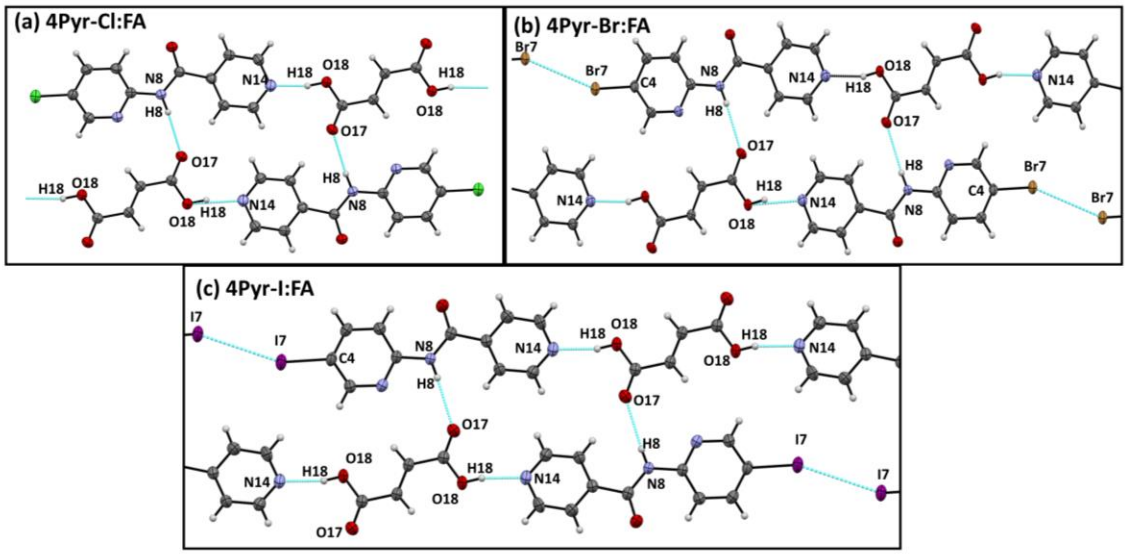

Figure 3.7. Primary interactions in crystal structures of (a) 4Pyr-Cl:FA, (b) 4Pyr-Br:FA, and (c) 4Pyr-I:FA.

The relevant hydrogen- and halogen-bond geometries in the nine co-crystals from the 4Pyr series are given in Table 3.4.

Table 3.4. Hydrogen- and halogen-bond parameters in the Nine 4Pyr-X Co-Crystals.

Code	D-H/I···A	D/I···A (Å)	D-H···A (deg)
4Pyr-Cl:AA	N8-H8···O25	2.7376(19	176(2)
	O18-H18···N14	2.678(2)	166(3)
	O26-H26···N2	2.7376(19)	172(3)
4Pyr-Br:AA	N8-H8···O17	2.942(2)	172(3)
	O18-H18···N2	2.735(2)	172(4)
	O26-H26···N14	2.683(3)	172(4)
4Pyr-I:AA	N8-H8···O33	2.828(4)	175.(5)
	N24-H24···O38	2.874(4)	167.(5)
	O34-H34···N2	2.689(4)	170.(6)
	O39-H39··· N18	2.718(4)	180.(10)
	C4-I7···N14	2.910(3)	173.99(10)
	C20-I23···N30	2.938(4)	177.38(13)
4Pyr-I:SuA	N8-H8···O33	2.877(6)	173.(5)
	N24-H24···O43	2.814(6)	167.(6)
	O34-H34···N2	2.765(6)	164.(16)
	O44-H44···N18	2.738(6)	172.(7)
	C4-I7···N14	3.140(5)	168.28(19)
	C4-I23···N30	2.931(5)	170.09(18)
4Pyr-I:SeA	N8-H8···O17	3.104(3)	166.(4)
	O18-H18···N2	2.697(3)	160.(6)
	C4-I7···N14	2.910(3)	173.99(10)
4Pyr-Cl:PA	N8-H8···O26	2.973(3)	174(3)
	O18-H18···N14	2.705(3)	174(4)
	O27-H27···N2	2.737(3)	169(3)
4Pyr-Cl:FA	N8-H8···O17	3.0940(15)	175.2(18)
	O18-H18···N14	2.6129(16)	168(2)
4Pyr-Br:FA	N8-H8···O17	3.094(2)	176.(3)
	O18-H18···N14	2.619(2)	162.1
	C4-Br7··· Br7	3.6187(5)	155.69(7)
4Pyr-I:FA	N8-H8···O17	3.118(4)	175.(3)
	O18-H18···N14	2.653(3)	167.(4)
	C4-I7··· I7	3.6478(7)	157.54(8)

3.4 Discussion

None of the compounds in the 2Pyr series formed co-crystals while eighteen out of thirty experiments gave positive results in the 3Pyr series and twenty-nine out of thirty experiments gave positive results for the 4Pyr series halogenated compounds (Figure 3.8).

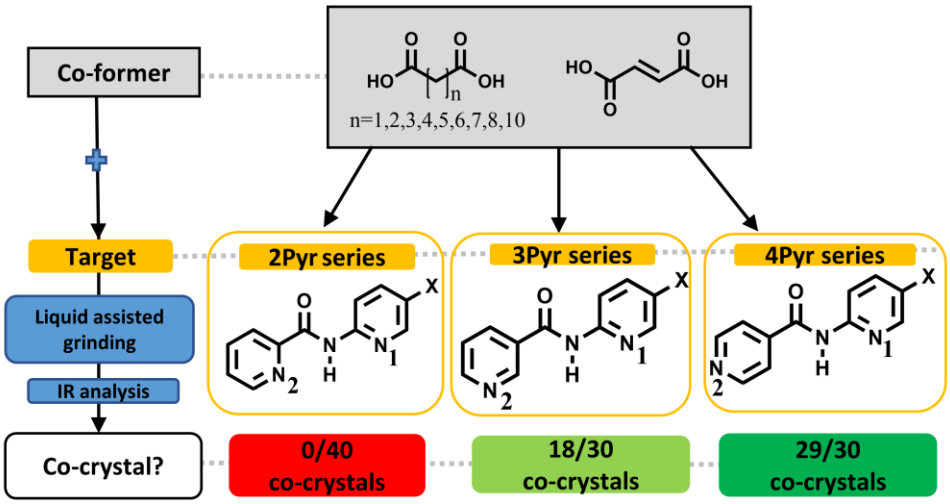

Figure 3.8. Summarized results of co-crystal screen.

The absence of co-crystal formation by any compound in the 2Pyr series demonstrates the stability of this five-membered hydrogen-bonded N-H···N_2 ring, which effectively precludes intermolecular hydrogen bonding (essential for co-crystal synthesis) at that binding site. In addition, carboxylic acid binding at the N_1 position was not observed either. Single-point hydrogen bonding by carboxylic acids to pyridine nitrogen atoms can be found in the Cambridge Structural Database (CSD).[24] However, the vast majority of those reported co-crystals are formed in the presence of aromatic carboxylic acids. In comparison there are a handful reported with aliphatic carboxylic acids.[25,26] Several of these have additional structure-directing interactions,[27,28,29] and it is conceivable that these interactions facilitate intermolecularly driven assembly.

All six co-crystals from the 3Pyr-X series showed identical hydrogen bonding as compared to those of the co-crystals of the same co-formers with the unhalogenated target. Thus, the combination of 3Pyr-X and odd-chain acids led to hydrogen-bonded chains, and 3Pyr-X and even-chain acids gave hydrogen-bonded rings. However, the halogen atom (bromine and iodine) showed structure directing interactions of the type X···O(OH) linking the hydrogen-bonded motifs

together (Figure 3.9). The van der Waals reduction was 10% with the iodinated compounds and 5% in the brominated co-crystals, which is consistent with what is expected from the relative magnitudes of their corresponding sigma-holes.[21]

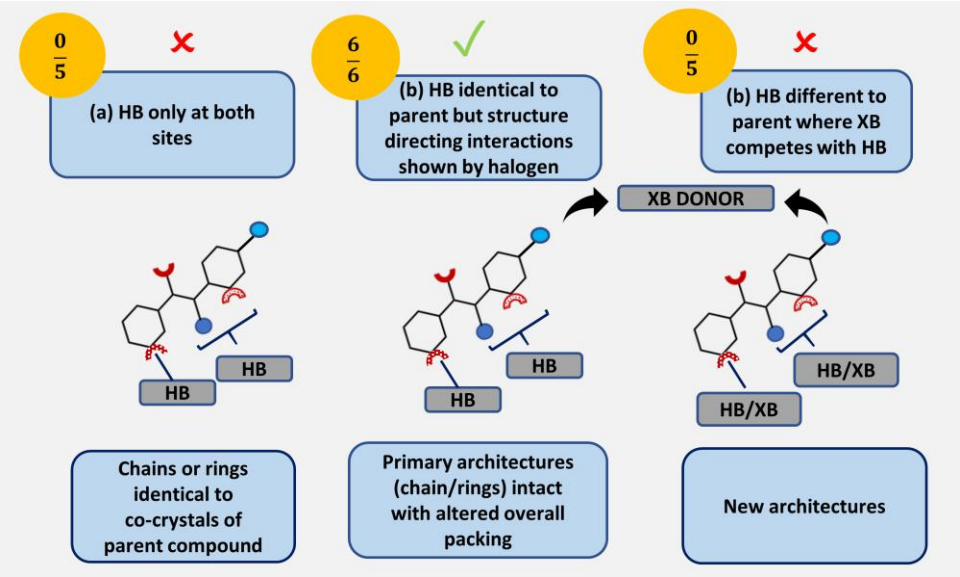

Figure 3.9. Schematic representation of effect of halogen on aggregation of molecules with halogens in crystal structures of 3Pyr-X.

In the co-crystals of the 4Pyr series halogenated compounds, all except 4Pyr-I:AA, 4Pyr-I:SuA, and 4Pyr-I:SeA showed hydrogen bonding at both the N_2(py) and N_1(py)-NH sites. In the three co-crystals of fumaric acid, both pockets were occupied by hydrogen bonding. However, –NH···O=C hydrogen bond interactions were observed instead of –COOH···N_1(py)-NH seen in other co-crystals. Although, Type I short X···X contacts in 4Pyr-Br:FA and 4Pyr-I:FA were observed, these two co-crystals were isostructural to 4PyrCl:FA, and therefore these short contacts are more likely to be the result of simple close-packing instead of due to any structure directing interactions (Figure 3.10). The 4Pyr-I target showed hydrogen bonding only at the ···N_1(py)-NH pocket, whilst the iodine atom formed an I···N_2 near-linear halogen bond. This is the only instance where we saw the halogen bond competing with hydrogen bonding. The 4Pyr-I target was also the

only compound in which the iodine atom exhibited competitive halogen bonding (with respect to hydrogen bonding) in the individual homomeric structures.

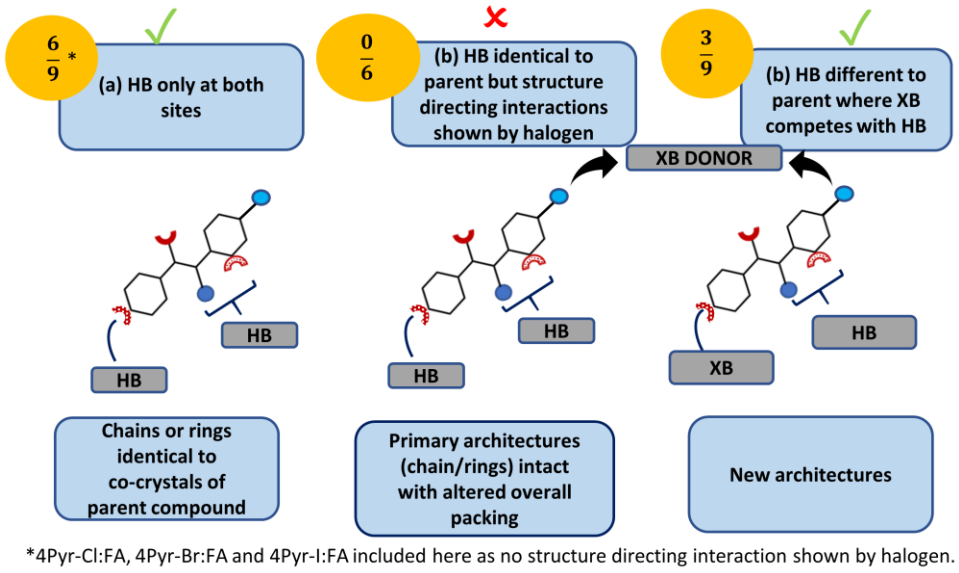

Figure 3.10. Schematic representation of effect of halogen on aggregation of molecules with halogens in crystal structures of 4Pyr-X.

The torsion angle between the two aromatic rings in the crystal structures of the in-dividual 3Pyr-X target molecules ranged from ~30° to 50°, which is similar to the range found in the structures of the 4Pyr-X analogues, ~30° to 60°.[21] However, in the co-crystals of 3Pyr series, the target molecules were near planar, with torsion angles ranging from ~0° to 10°, whereas they fell in the ~10° to 45° range for the target molecules of the 4Pyr co-crystals. There is no obvious reason as to why the two groups behaved differently, but since the torsion in these targets followed a relatively shallow potential energy curve, crystal packing would clearly influence the molecular geometry in each group. It is notable that even though the individual targets 3Pyr and 3Pyr-I were isostructural, the analogues co-crystals were not, due to the I···O(OH) halogen bond. In contrast, although 3Pyr-Br and 3Pyr-I were not isostructural, the co-crystals formed by these two targets

were. In the 4Pyr series, although the co-crystal formed by the three targets (4Pyr, 4Pyr-Cl, and 4Pyr-Br) were isostructural, these two halogenated targets were not isostructural with the corresponding parent. The co-crystal formed with the odd-chain pimelic acid and 4Pyr-Cl led to a chain rather than expected ring architecture, analogues to 4Pyr. Therefore, we can conclude that isostructurality is not directly transferrable from single component to multi-component systems (Figure 3.11).

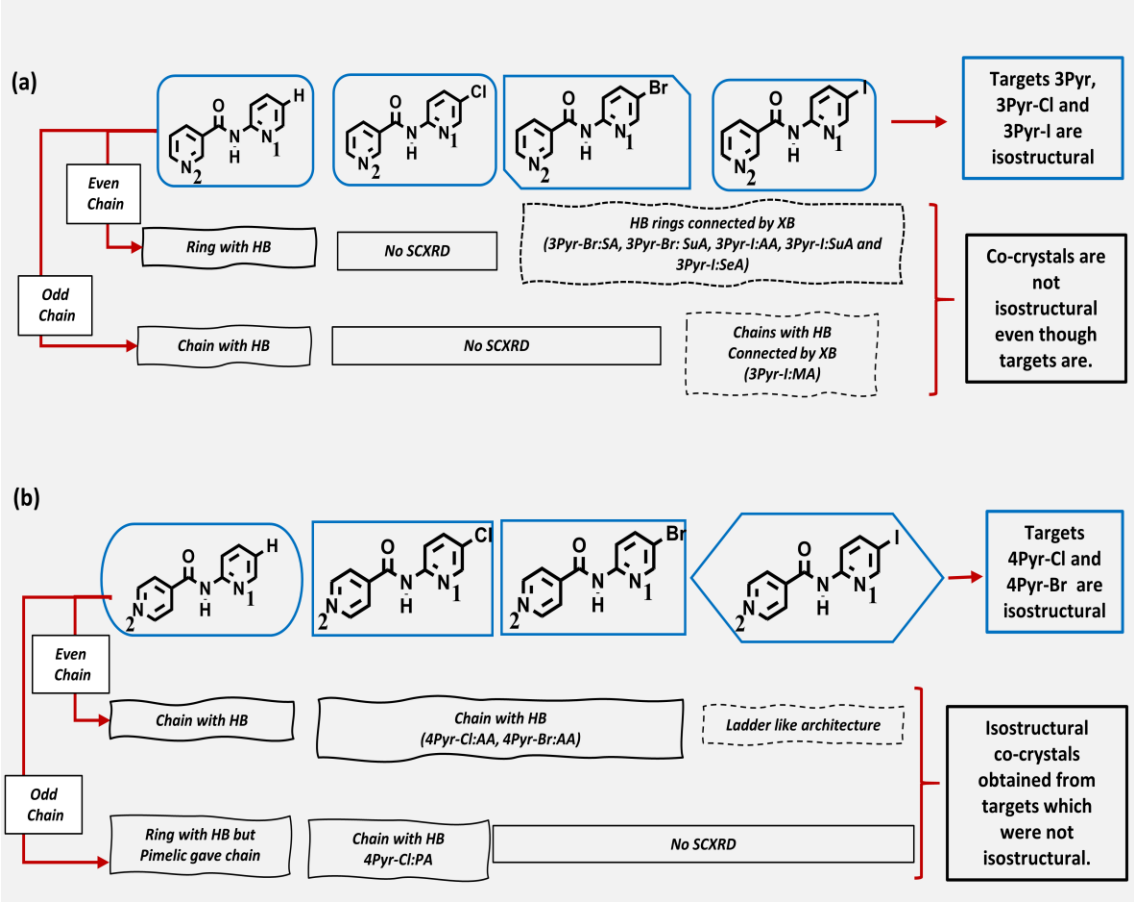

Figure 3.11. Map of isostructurality between targets and co-crystals of (a) 3Pyr and (b) 4Pyr series compounds.

The shape of the box around targets indicate if they are isostructural or not.

3.5 Conclusions

No co-crystals were obtained with the 2Pyr series since the omnipresent intramolecular hydrogen bonding prevented any opportunities for co-crystal synthesis via intermolecular interactions with any co-former. In the structures obtained from the 3Pyr and 4Pyr series where halogen atoms were engaged in halogen bonding (XB), the extent of these interactions, as indicated by reduction in combined van der Waals radii, was in the order of Cl < Br < I. Only 4Pyr-I exhibited halogen bonding in the homomeric state, as well as in three of four co-crystals. In the other six co-crystals of the 4Pyr series, no structure directing effects were shown by the halogen atoms. In the six co-crystals of the 3Pyr series, all showed complementary interactions to hydrogen bonding. Thus, in the fifteen co-crystals obtained from 3Pyr-X and 4Pyr-X targets, structure directing influence shown by the halogen was either none (6/15), complementary (6/15), or competitive (3/15) to hydrogen bonding. Since isostructural targets did not always lead to isostructural co-crystals, and since isostructural co-crystals were obtained with targets that were not isostructural, it is clear that isostructurality is not necessarily transferrable from single- to multi-component systems.

3.6 References

1. Arunan, E.: Desiraju, G.R.; Klein, R.A.; Sadlej, J.; Scheiner, S.; Alkorta, I.; Clary, D.C.; Crabtree, R.H.; Dannenburg, J.J.; Hobza, P.; Kjaergaard, G.; Legon, A.C.; Mennucci, B.; Nesbitt, D.J. Definition of the hydrogen bond (IUPAC Recommendations 2011). *Pure Appl. Chem* **2011**, *83*, 1637–1641.
2. Kollman, P.A.; Allen, L.C. Theory of the hydrogen bond. *Chem. Rev.* **1972**, *72*, 283–303.
3. Aakeröy, C.B.; Seddon, K.R. The hydrogen bond and crystal engineering. *Chem. Soc. Rev.* **1993**, *22*, 397–407.
4. MacGillivray, L.R. Organic synthesis in the solid state via hydrogen-bond-driven self-assembly. *J. Org. Chem* **2008**, *73*, 3311–3317.
5. Guo, X.; Tian, Y.; Zhang, M.; Li, Y.; Wen, R.; Li, X.; Li, X.; Xue, Y.; Ma, L.; Xia, C.; Li, S. Mechanistic insight into hydrogen-bond-controlled crystallinity and adsorption property of covalent organic frameworks from flexible building blocks. *Chem. Mater.* **2018**, *30*, 2299–2308.
6. Desiraju, G.R.; Ho, P.S.; Kloo, L.; Legon, A.C.; Marquardt, R.; Metrangolo, P.; Politzer, P.; Resnati, G.; Rissanen, K. Definition of the halogen bond (IUPAC Recommendations 2013). *Pure Appl. Chem* **2013**, *85*, 1711–1713.
7. Aakeroy, C.B.; Bryce, D.L.; Desiraju, G.R.; Frontera, A.; Legon, A.C.; Nicotra, F.; Rissanen, K.; Scheiner, S.; Terraneo, G.; Metrangolo, P.; Resnati, G. Definition of the chalcogen bond (IUPAC Recommendations 2019). *Pure Appl. Chem* **2019**, *91*, 1889–1892.

8. Tothadi, S.; Desiraju, G. Designing ternary cocrystals with hydrogen bonds and halogen bonds. *ChemComm* **2013**, *4*, 7791–7793.
9. Bolla, G.; Nangia, A Multicomponent ternary cocrystals of the sulfonamide group with pyridine-amides and lactams. *ChemComm* **2015**, *51*, 15578–15581.
10. Lemmerer, A. All good things come in threes: First example of a trimorphic, ternary molecular salt complex. *CrystEngComm* **2020**, *22*, 6091–6095.
11. Paul, M.; Desiraju, G. From a binary to a quaternary cocrystal: An unusual supramolecular synthon. *Angew. Chem* **2019**, *58*, 12027–12031.
12. Ramon, G.; Davies, K.; Nassimbeni, L.R. Structures of benzoic acids with substituted pyridines and quinolines: Salt versus co-crystal formation. *CrystEngComm* **2014**, *16*, 5802–5810.
13. Thayyil, A.R.; Juturu, T.; Nayak, S.; Kamath, S. Pharmaceutical Co-Crystallization: Regulatory Aspects, Design, Characterization, and Applications. *Adv. Pharm Bull.* **2020**, *10*, 203.
14. Pagire, S.K.; Seaton, C.C.; Paradkar, A. Improving Stability of Effervescent Products by Co-Crystal Formation: A Novel Application of Crystal Engineered Citric Acid. *Cryst. Growth Des.* **2020**, *20*, 4839–4844.
15. Sandhu, B.; Sinha, A.S.; Desper, J.; Aakeröy, C.B. Modulating the physical properties of solid forms of urea using co-crystallization technology. *ChemComm* **2018**, *54*, 4657–4660.
16. Nauha, E., Kolehmainen, E.; Nissinen, M. Packing incentives and a reliable N–HN–pyridine synthon in co-crystallization of bipyridines with two agrochemical actives. *CrystEngComm* **2011**, *13*, 6531–6537.
17. Şen, N.; Dursun, H.; Hope, K.S.; Nazir, H.; Acar, N.; Atakol, O. Towards low-impact-sensitivity through crystal engineering: New energetic co-crystals formed between Picric acid, Trinitrotoluene and 9-Vinylanthracene. *J. Mol. Struct* **2020**, *1219*, 128614.
18. Gamekkanda, J.C., Sinha, A.S., Aakeröy, C.B. (2020). Cocrystals and Salts of Tetrazole-Based Energetic Materials. *Cryst. Growth Des.* 2020, *20*, 2432–2439.
19. Lu, B., Fang, X., Yan, D. (2020). Luminescent polymorphic co-crystals: A promising way to the diversity of molecular assembly, fluorescence polarization, and optical waveguide. *ACS Appl. Mater. Interfaces* **2020**, *12*, 31940–31951.
20. Aakeröy, C.B.; Panikkattu, S.V.; DeHaven, B.; Desper, J. Establishing supramolecular control over solid-state architectures: a simple mix and match strategy. *Cryst. Growth Des.* **2012**, *12*, 2579–2587.
21. Abeysekera, A.M.; Day, V.W.; Sinha, A.S.; Aakeröy, C.B. Mapping out the Relative Influence of Hydrogen and Halogen Bonds in Crystal Structures of a Family of Amide-Substituted Pyridines. *Cryst. Growth Des.* **2020**, *20*, 7399–7410.
22. Remenar, J.F.; Morissette, S.L.; Peterson, M.L.; Moulton, B.; MacPhee, J.M.; Guzma'n H. R.; Almarsson, O¨. Crystal engineering of novel cocrystals of a triazole drug with 1, 4-dicarboxylic acids. *J. Am. Chem. Soc.* **2003**, *125*, 8456–8457.
23. Draguta, S.; Fonari, M.S.; Bejagam, S.N.; Storms, K.; Lindline, J.; Timofeeva, T.V. Structural similarities and diversity in a series of crystalline solids composed of 2-aminopyridines and glutaric acid. *Struct Chem.*, **2016**, *27*, 1303–1315.
24. Groom, C.R.; Bruno, I.J.; Lightfoot, M.P.; Ward, S.C. The Cambridge Structural Database. *Acta Cryst.*, **2016**, *B72*, 171–179.
25. Aakeröy, C.B.; Wijethunga, T.K.; Desper, J. Molecular electrostatic potential dependent selectivity of hydrogen bonding. *New J. Chem*, **2015**, *39*, 822–828.
26. Haynes, D.A.; Jones, W.; Motherwell, W.S. Cocrystallisation of succinic and fumaric acids with lutidines: A systematic study. *CrystEngComm*, **2006**, *8*, 830–840.
27. Aakeröy, C.B.; Forbes, S., Desper, J. Altering physical properties of pharmaceutical co-crystals in a systematic manner. *CrystEngComm*, **2014**, *16*, 5870–5877.
28. Orola, L.; Veidis, M.V. Nicotinamide fumaric acid supramolecular cocrystals: Diversity of stoichiometry. *CrystEngComm*, **2009**, *11*, 415–417.
29. Lemmerer, A.; Bernstein, J.; Kahlenberg, V. One-pot covalent and supramolecular synthesis of pharmaceutical co-crysts using the API isoniazid: a potential supramolecular reagent. *CrystEngComm*, **2010**, *12*, 2856–2864.

Chapter 4 - Establishing halogen-bond preferences in molecules with multiple acceptor sites

4.1 Introduction

Molecular recognition[1,2] a key concept in fundamental chemical[3] and biochemical[4,5,6] processes, relies on a delicate balance between molecular size7, shape8 and functional-group complementarity. In addition, the competition between a variety of directional intermolecular forces is ultimately responsible for selectivity and binding reversibility, which are key characteristics of any practically useful recognition events[9,10,11.12,13] A subsequent transition from solution to solid-state events takes us into the realm of crystal engineering14 which requires the ability to systematically assemble molecules into specific architectural features via non-covalent interactions. The most commonly utilized and best understood supramolecular synthetic driver is the hydrogen bond.[15] However, the halogen bond (XB)[16] and many other σ-hole interactions are also being investigated for the purpose of synthetic crystal engineering.[17] The halogen bond displays a slightly higher directionality and tunability than the hydrogen bond (HB),[18,19] but due to the importance of the electrostatic component in both interactions, they are capable of competing for the very same binding sites. Therefore, in order to develop more reliable and transferable protocols for supramolecular synthesis, we need to know in advance if a particular XB-donor will displace a certain HB-donor from an acceptor site. A schematic example of how the outcome of such a competition can lead to very different supramolecular assemblies is illustrated (Figure 4.1).

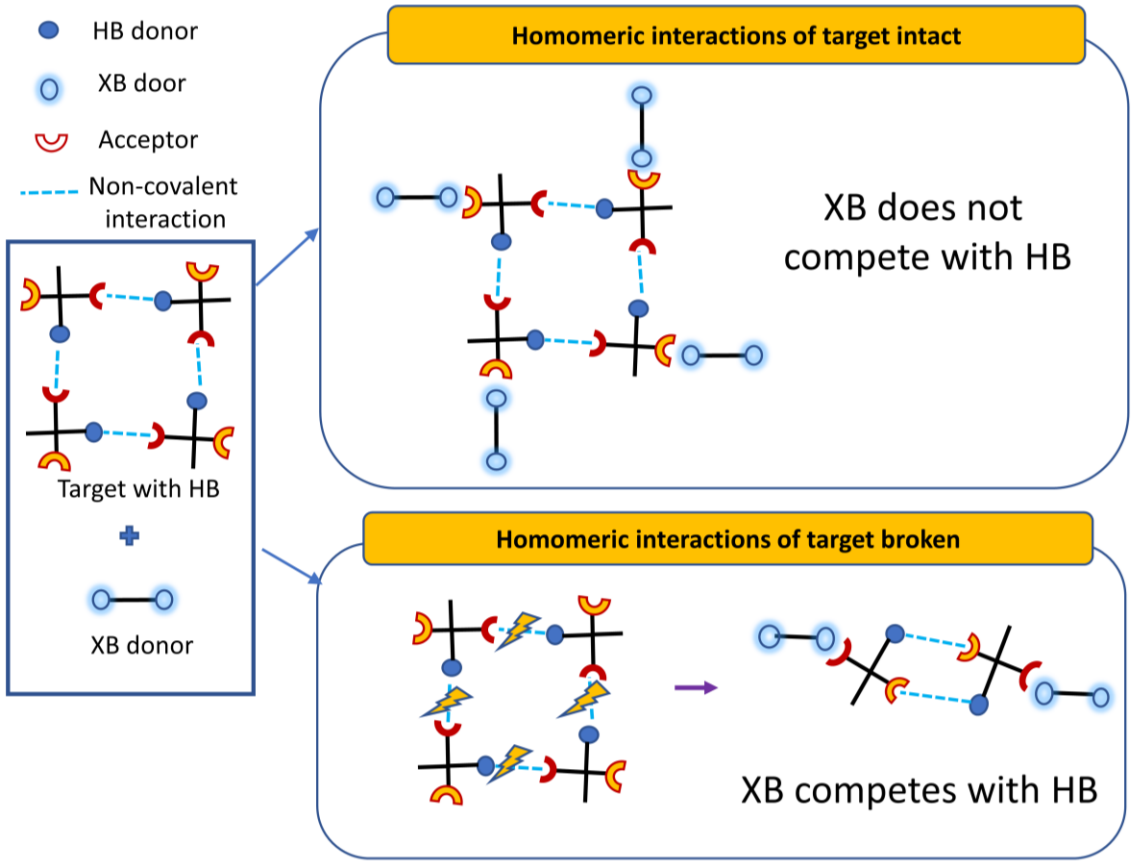

Figure 4.1. Postulated outcomes when a multi-functional supramolecular target is interrogated by a powerful halogen-bond donor.

In order to add more insight into the structural competition between hydrogen- and halogen bonding, we have carried out a systematic co-crystal screen of halogen-bond donors and targets carrying both nitrogen- and oxygen-based acceptor sites. The structural preferences of the targets themselves is well established, which makes them a very useful starting point for attempted co-crystallizations with molecular competitors. The sixteen target molecules all contain one conventional HB donor and two or three acceptor sites (Figure 4.2), and we selected two co-formers that are well known to form co-crystals with a variety of species; 1,4-

diiodoterafluorobenzene[20,21] , and 1,3,5-triiodo-2,4,6,-tetrafluorobenzene (co-formers), (Figure 4.2).

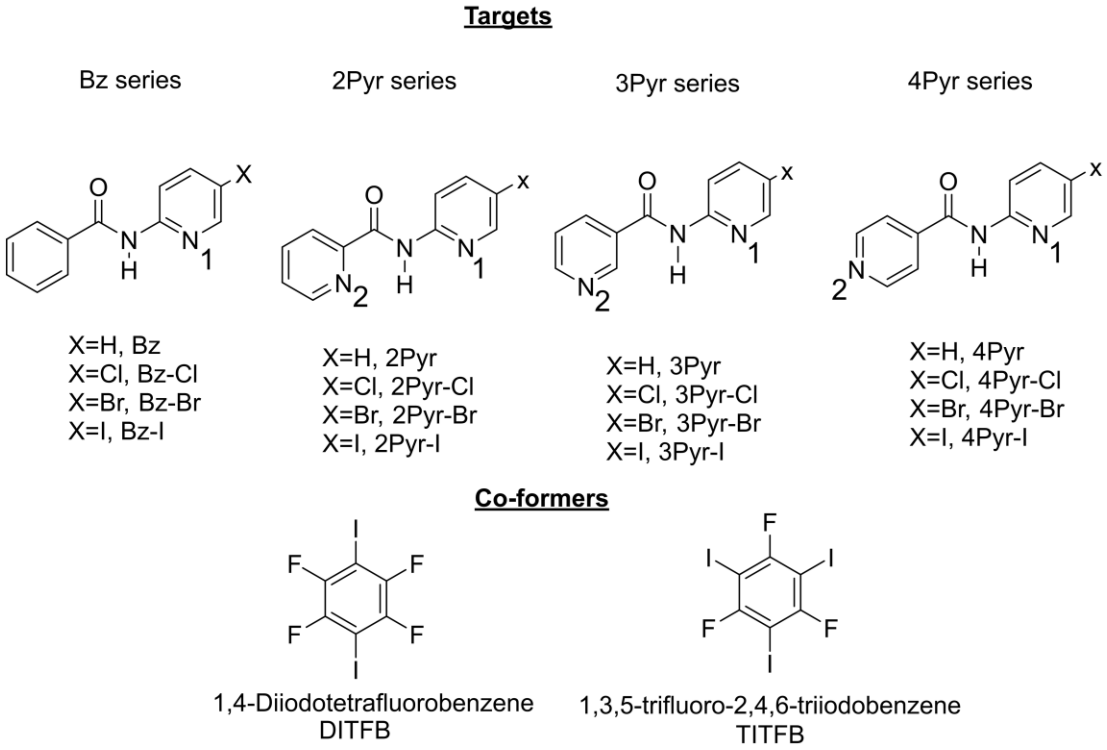

Figure 4.2. Target molecules (top) and co-formers (bottom) in this study.

The sixteen target molecules offer the advantage of being equipped with a carbonyl oxygen, an acceptor site which has not been frequently utilized for assessing XB binding preferences (such investigations have mostly included nitrogen containing heterocycles as potential acceptors).[22,23] The crystal structures of the individual targets have previously been investigated[24] and the compounds in the Bz series form −NH···N_1 dimers, the 2Pyr molecules form −NH···N_2 intramolecular hydrogen bond, whereas both the 3Pyr and the 4Pyr molecules form −NH···N_2 hydrogen-bonds (with the exception of 4Pyr-I which produced either an NH···N_1 dimer (Form I)

or an NH···O=C interaction (Form II). As a result, we can postulate which kind of binding sites may be targeted by the XB donors in the study presented herein (Figure 3.3).

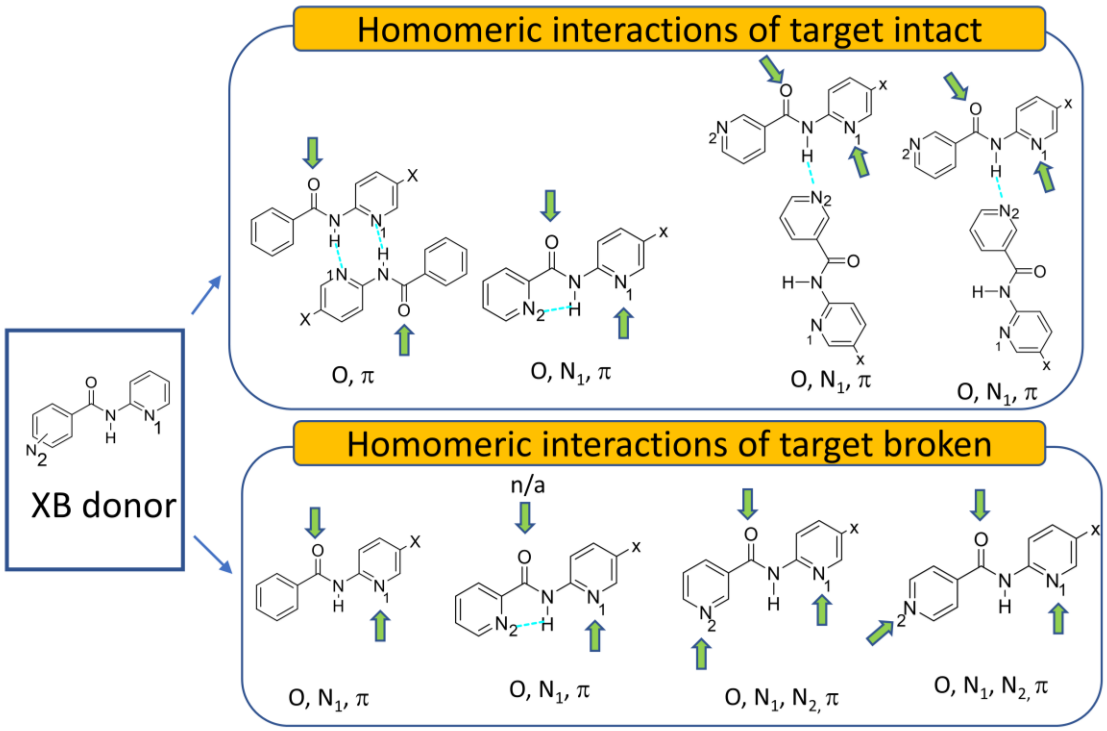

Figure 4.3. Possible acceptor sites on the targets that can be occupied by XB donors.

In this study we address the following questions;

1. Does the XB donor favor a specific acceptor type, i.e. oxygen, nitrogen or π system?

2. Are the hydrogen bonds observed in the target structures broken or intact in the resulting co-crystals?

3. Can we use any vibrational spectroscopic signatures to identify key structural features in the halogen-bonded co-crystals?

4.2 Experimental

The target compounds were prepared as reported in chapter 1. Co-crystal screening with the two halogen bond donors was carried out using liquid assisted grinding with stoichiometric 1:1 amounts of target and co-former, followed by IR characterization of the ground powder. A total of 32 experiments were performed. Peak shifts of ~3 cm−1 in several modes of both the target and co-former was used as the criterion to assess co-crystal formation paying special attention to peak shifts in amide (~3300-3400 cm−1) and carbonyl regions (~1600-1700 cm−1). IR spectra of cocrystal screening experiments were recorded with a Nicolet 380 FT-IR spectrometer using an attenuated total reflection (ATR) technique and ZnSe as the crystal. The melting points were measured using a Fisher-Johns melting point apparatus or a TA Instruments DSC Q20 differential scanning calorimeter.

4.3 Results

All the 32 co-crystal screening experiments gave a positive result as determined by IR spectroscopy. The relevant IR data is provided in the Appendix. The ground solids were dissolved in methanol to obtain crystals of diffraction quality.

4.3.1 Crystal growth

A total of 13 experiments produced crystals suitable for single-crystal X-ray diffraction (SCXRD), (Table 4.1).

Table 4.1. Some physical properties of co-crystals obtained.

Co-Crystal	Code	Melting Point	Color and Morphology
(N-(pyridin-2-yl)benzamide)1,4Diiodotetrafluorobenzene (1:1)	Bz:DITFB	88–90 °C	Colorless, Plate
(N-(pyridin-2-yl)benzamide)1,3,5-trifluoro-2,4,6-triiodobenzene (1:1)	Bz:TITFB	98–100 °C	Colorless, Plate
(N-(5-iodopyridin-2-yl)benzamide)1,4Diiodotetrafluorobenzene (2:1)	Bz-I:DITFB	165–165 °C	Colorless, Block
(N-(pyridin-2-yl)picolinamide)1,4Diiodotetrafluorobenzene (1:1)	2Pyr:DITFB	85–87 °C	Colorless, Block
(N-(5-bromopyridin-2-yl)picolinamide)1,4Diiodotetrafluorobenzene (2:1)	2Pyr-Br:DITFB	141–143 °C	Colorless, Rectangular
(N-(5-iodopyridin-2-yl)picolinamide) 1,4Diiodotetrafluorobenzene (2:1)	2Pyr-I:DITFB	137–139 °C	Colorless, Rectangular
(N-(pyridin-2-yl)nicotinamide)1,4Diiodotetrafluorobenzene (1:1)	3Pyr:DITFB	110–112 °C	Colorless, Needle
(N-(5-iodopyridin-2-yl)nicotinamide)1,4Diiodotetrafluorobenzene (1:1)	3Pyr-I: DITFB	178–180 °C	Colorless, Parallelepiped
(N-(5-iodopyridin-2-yl)nicotinamide)1,3,5-trifluoro-2,4,6-triiodobenzene (1:1)	3Pyr-I:TITFB	180–182 °C	Colorless, Needle
(N-(pyridin-2-yl)isonicotinamide)1,4Diiodotetrafluorobenzene (1:1)	4Pyr:DITFB	110–112 °C	Colorless, Needle
(N-(pyridin-2-yl)isonicotinamide) 1,3,5-trifluoro-2,4,6-triiodobenzene (1:1)	4Pyr:TITFB	135–137 °C	Colorless, Plate
(N-(5-chloropyridin-2-yl)isonicotinamide)1,3,5-trifluoro-2,4,6-triiodobenzene (1:1)	4Pyr-Cl:TITFB	149–151 °C	Colorless, Needle
(N-(5-bromopyridin-2-yl)isonicotinamide)1,4Diiodotetrafluorobenzene (1:1)	4Pyr-Br:TITFB	154–155 °C	Colorless, Needle

4.3.2 X-ray crystallography results

Three co-crystals of Bz targets suitable for single-crystal X-ray diffraction (SCXRD) were successfully grown. In the two co-crystals obtained from the non-halogenated target, Bz:DITFB and Bz:TFTIB (Figure 3a-b), the homomeric N-H···N_1(py)/N_1(py)···H-N interactions present in the structure of the target itself are broken. In Bz:DITFB, C-I···N_1 and C-I···π halogen bonds are observed, resulting in chains. The N-H···O=C hydrogen bond connects neighboring chains into an infinite 2-D architecture. In the crystal structure of Bz:TFTIB, alternating C-I···O=C and C-I···N_1 halogen bonds connect target and co-former into chains. Only two of the three iodine atoms of the co-former act as XB donors, a behavior which is relatively common.[25] Finally, there is also an N-H···I hydrogen bond in this structure; the negative equatorial "belt" of the iodine atom acts as the acceptor site.[26] In the crystal structure of Bz-I:DITFB (Figure 4.4c), a C-I···O=C halogen bond is

observed (the two iodine atoms are crystallographically equivalent), while the homomeric H···N_1(py)/N_1(py)···H-N motif, which was found in the structure of the target, remains intact. In addition, the iodine atom of the target molecule is oriented towards the negative belt of the iodine atom of the co-former in a Type II halogen bond.[27]

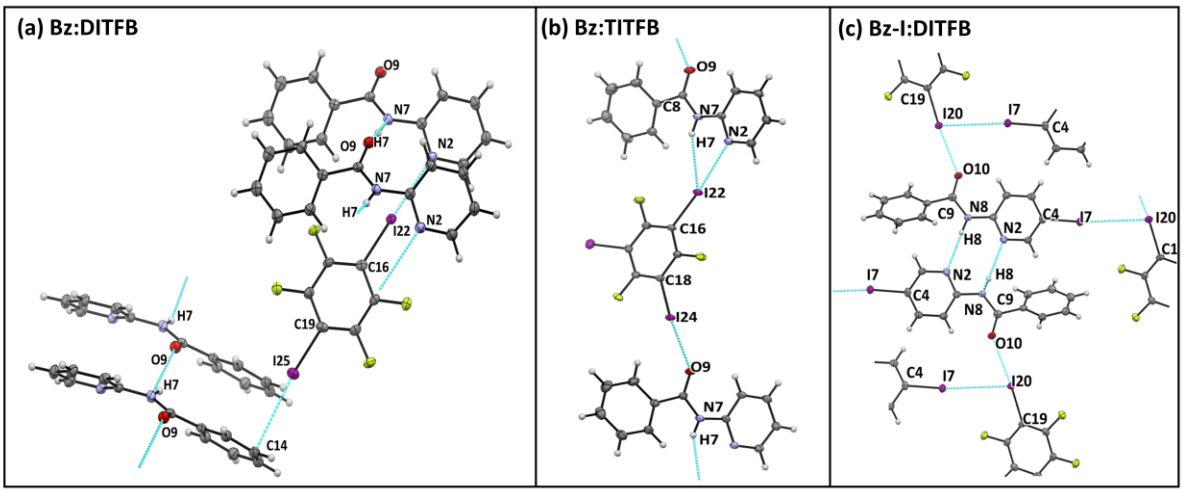

Figure 4.4. Primary interactions in crystal structures of (a) Bz:DITFB, (b) Bz:TITFB, and (c) Bz-I:DITFB

The relevant hydrogen- and halogen-bond geometries in the three co-crystals from the Bz series are given (Table 4.2)

Table 4.2. Hydrogen- and halogen-bond parameters in the three Bz series co-crystals.

Co-crystal	**D-H/X··A**	**D/X···A (Å)**	**D-H/X···A (deg)**
Bz:DITFB	C16-I22···N2	2.820(3)	179.03(2)
	N7-H7···O9	2.947(4)	147.0(2)
	C19-I25···C14	3.296(4)	143.49(2)
Bz:TITFB	C16-I22···N2	2.860(2)	174.96(6)
	N7-H7···I22	3.636(2)	139.45(3)
	C18-I24···O9	2.911(1)	174.28(1)
Bz-I:DITFB	C19-I20···O18	2.830(3)	174.07(1)
	N8-H8···N2	3.064(4)	167.13(2)
	C4-I20···I7	3.939(3)	170.41(1)

Three crystal structures of co-crystals of 2Pyr targets were obtained (Figure 4.5a-c). As expected, the homomeric −NH···N_2 intramolecular hydrogen bond of the target compounds remained intact in all three co-crystals and halogen bonding occurred to the "vacant" nitrogen/oxygen atoms in the target molecule. In 2Pyr-DITFB, alternating C-I···O=C and C-I···N_1 link the target and co-former into infinite chains. The two co-crystals of 2Pyr-Br:DITFB and 2Pyr-I:DITFB are isostructural and the co-former is residing on an inversional center resulting in a 2:1 stoichiometry between target and co-former. Both iodine atoms of DITFB form C-I···N_1 halogen bonds.

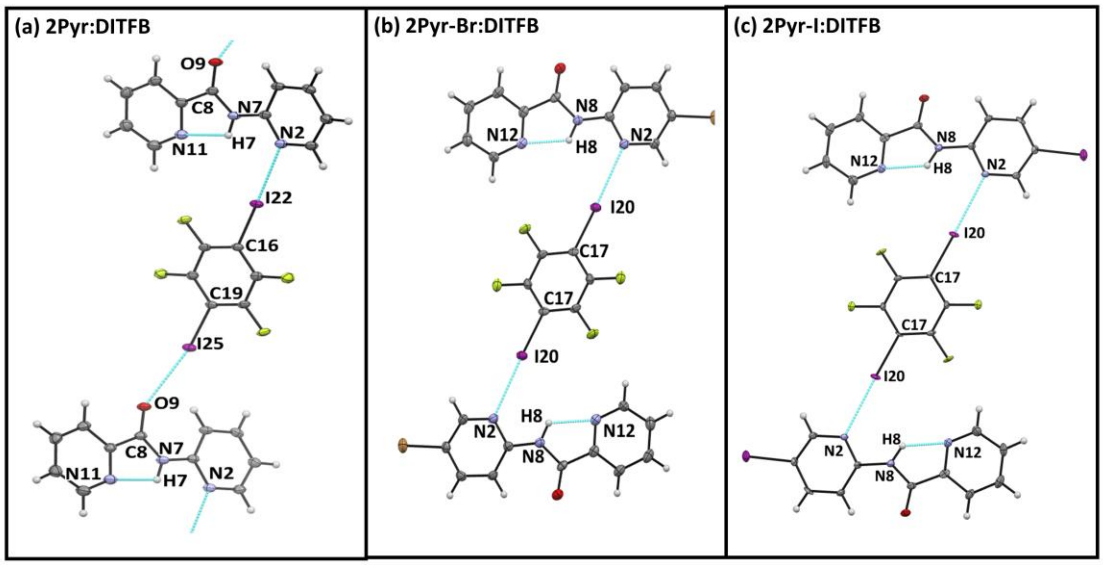

Figure 4.5. Primary interactions in crystal structures of (a) 2Pyr:DITFB, (b) 2Pyr-Br:DITFB, and (c) 2Pyr-I:DITFB

The relevant hydrogen- and halogen-bond geometries in the three co-crystals from the 2Pyr series are given (Table 4.3).

Table 4.3. Hydrogen- and halogen-bond parameters in the three 2Pyr series co-crystals.

Co-crystal	**D-H/X··A**	**D/X···A (Å)**	**D-H/X···A (deg)**
2Pyr:DITFB	N7-H7···N11	2.615(3)	113.07(2)
	C16-I22···N2	2.847(2)	177.64(8)
	C9-I25···O9	2.984 (2)	167.11(7)
2Pyr-Br:DITFB	N8-H8···N12	2.615(7)	118.(5)
	C17-I20···N2	2.921(2)	177.74 (1)
2Pyr-I:DITFB	N8-H8···N12	2.600(7)	121.(6)
	C17-I20···N2	2.925(6)	178.40(2)

Three crystal structures of co-crystals of 3Pyr targets were obtained (Figure 4.6a-c). In all three, the homomeric NH···N2(py interactions present in the structure of the target itself are broken. In the structure of 3Pyr:DITFB, both iodine atoms form C-I···N_1 and C-I···N_2 halogen bonds leading to the formation of tetrameric rings (Figure 4.6a). Additionally, the N-H···O=C hydrogen bond connect tetramers into a ladder like architecture. The crystal structure of 3Pyr-I:DITFB is isostructural with 3Pyr:DITFB. In the structure of 3Pyr-I:TITFB, C-I···N_1 and C-I···N_2 interactions are formed by a linking co-former which leads to infinite chains. Once again, the hydrogen bond motif N-H···O=C leads to stacking of chains. In addition, the third iodine atom of the co-former TITFB (which does not interact with the target molecule), forms a Type II halogen bond of van der Waals reduction of ~7%, to the iodine atom forming a XB bond to N_2.

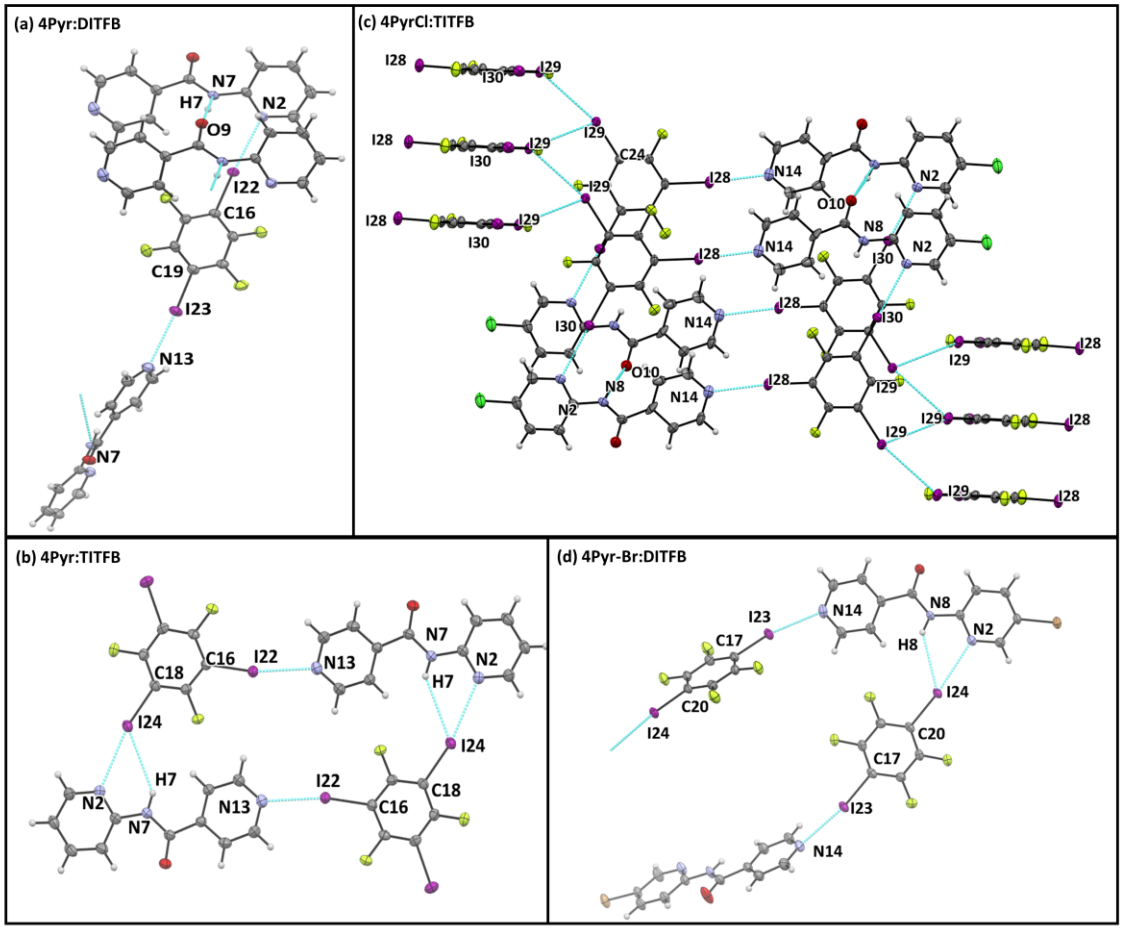

Figure 4.6. Primary interactions in crystal structures of (a) 3Pyr:DITFB, (b) 3Pyr-I:DITFB, and (c) 3Pyr-I:DITFB

Table 4.4. Hydrogen- and halogen-bond parameters in the three 3Pyr series co-crystals

Co-crystal	**D-H/X··A**	**D/X···A (Å)**	**D-H/X···A (deg)**
3Pyr:DITFB	N7-H7···O9	3.022(4)	151.00(1)
	C16-I22···N12	2.820(2)	178.56(7)
	C19-I25···N2	2.892(2)	177.12(7)
3Pyr-I:DITFB	N7-H7···O9	2.984(9)	150.(9)
	C17-I23···N13	2.839(7)	176.7(2)
	C20-I26···N2	2.939(6)	178.3(2)
3Pyr-I:TITFB	N8-H8···O10	2.907 (7)	143.87 (1)
	C19-I24···N13	2.830 (1)	175.67 (2)
	C17-I23···N2	2.913 (6)	179.26(2)
	C21-I25···I24	3.704 (1)	164.45 (2)

Four crystal structures of co-crystals of 4Pyr targets were obtained (Figure 4.7a-d). In all four, the homomeric NH···N_2 interactions present in the structure of the target itself are broken. In the structure of 4Pyr:DITFB, both iodine atoms form C-I···N_1 and C-I···N_2 halogen bonds with different target molecules leading to the formation of "z" shaped chains (Figure 4.7b). These chains are cross-linked by N-H···O=C hydrogen bonds (with stacking of like molecules). In 4Pyr:TFTIB, two of the iodine atoms form C-I···N_1 and C-I···N_2 halogen bonds, leading to the formation of tetrameric rings. These tetrameric rings stack while there is also an N-H···I hydrogen bond in this structure; the negative equatorial "belt" of the iodine atom acts as the acceptor site. In the co-crystal of 4Pyr-Cl:TFTIB, again two iodine atoms form C-I···N_1 and C-I···N_2 halogen bonds leading to the formation of tetrameric rings. The stacked tetrameric rings are cross-linked by NH···O=C interactions. In 4Pyr-Br:DITFB C-I···N_1 and C-I···N_2 halogen bonds lead to chain formation. The chains arrange in a spiral fashion (with target and co-former molecules stacking

over targets and co-formers respectively). There is also an N-H···I interaction, to the negative belt of the iodine atom.

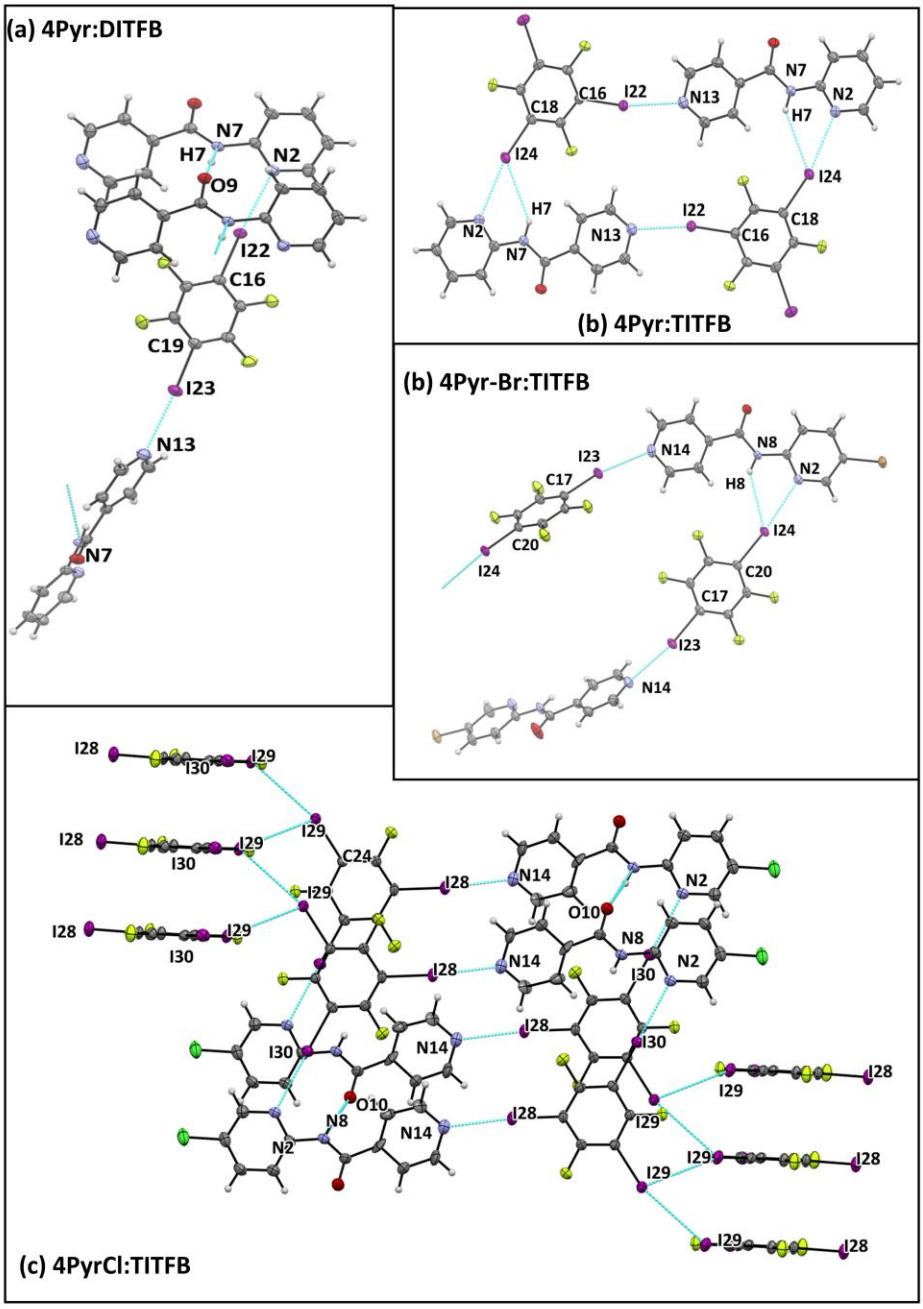

Figure 4.7. Primary interactions in crystal structures of (a) 4Pyr:DITFB, (b) 4Pyr:DITFB, (c) 4Pyr-Cl:DITFB, and (d) 4Pyr-Br:DITFB

Table 4.5. Hydrogen- and halogen-bond parameters in the four 4Pyr series co-crystals

Co-crystal	**D-H/X··A**	**D/X···A (Å)**	**D-H/X···A (deg)**
4Pyr:DITFB	N7-H7···O9	2.916 (2)	146.76(1)
	C16-I22···N2	2.865 (2)	175.41(5)
	C19-I23···N13	2.900(2)	171.48(5)
4Pyr:TITFB	N7-H7···I24	3.750(3)	141.4(2)
	C18-I24···N2	3.000(4)	167.50(1)
	C16-I22···N13	2.813(4)	168.85(1)
4Pyr-Cl:TITFB	N8-H8···O10	2.986(6)	160.03(5)
	C22-I28···N14	2.845 (4)	174.70(1)
	C26-I30···N2	2.894 (4)	179.20 (1)
	C24-I29···I29	3.839 (4)	153.24 (5)
4Pyr-Br:DITFB	N8-H8···I24	3.696 (8)	141.61 (1)
	C20-I24···N2	2.973 (6)	173.561(2)
	C17-I23···N14	2.882(6)	168.80 (4)

4.4 Discussion

As expected, the intramolecular hydrogen bonding was intact in co-crystal of 2Pyr series targets. Considering the 10 co-crystals obtained from targets exhibiting intermolecular hydrogen bonding (Bz, 3Pyr and 4Pyr series) in the homomeric state, the prevalent intermolecular interactions of homomeric assembly was broken 9/10 times (Figure 4.8).

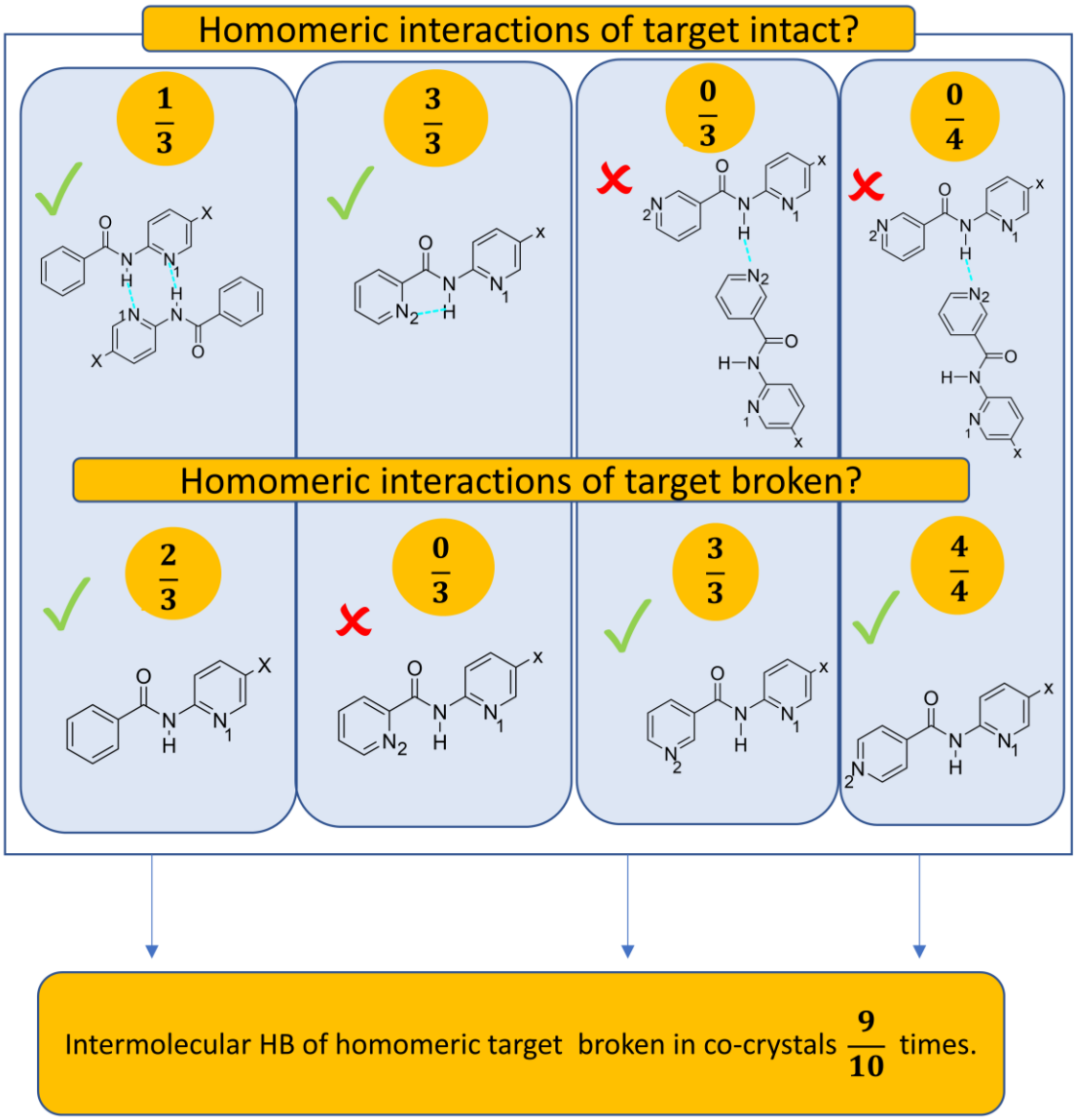

Figure 4.8. Summary of outcomes to HB interactions in target upon co-crystal formation

In the nine cases where the intermolecular N-H···$N_{1/2}$ motif was broken, either a N-H···O=C or N-H···I, interaction was formed instead. In all four crystals obtained with TITFB only two of the iodine atoms formed halogen bonds with the target. In all co-crystals obtained with DITFB both iodine atoms formed halogen bonds with the target molecule. Thus, in all 13 structures combined, a total 26 XBs are formed between the targets and XB donor. The majority of the time XB bond

formation was to a pyridyl nitrogen (20/26), while the carbonyl oxygen was the next most popular site (5/26) and halogen bonding to π system occurring only once (1/26) (Figure 4.9).

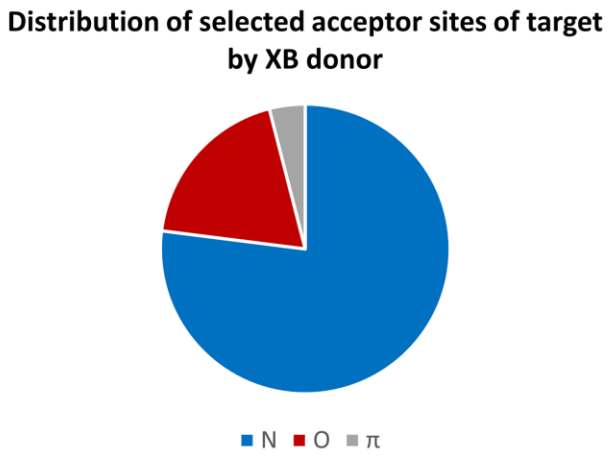

Figure 4.9. Distribution of selected acceptor sites on target

The key vibrational (IR) changes observed in the ground mixtures, when compared to the analogous modes in the target structures, and between the target and co-former in the co-crystals, are summarized (Table 4.6).

Table 4.6. Summarized IR data and interactions in targets and co-crystals

Target	Main HB in target itself	Location of IR bands for N-H, and C=O modes, respectively (cm^{-1}).	Co-Crystal	Are HBs of target changed when co-crystal is formed ?	Primary interactions in co-crystal	Key IR peak positions in co-crystal for NH and O=C. (cm^{-1})	Relative change of key IR positions in co-crystal vs. target	Acceptor site selected by XB donor
Bz	−NH···N_1	a, 1669	Bz:DITFB	Yes	C-I···N_1 C-I···π N-H···O=C	3338, 1656	*,-13	N_1, π
Bz	−NH···N_1	a, 1669	Bz:TITFB	Yes	C-I···O=C C-I'···N_1 N-H···I'	3410, 1672	*, +3	O, N_1
Bz-I	−NH···N_1	a, 1672	Bz-I:DITFB	No	C-I···O=C	a, 1667	**, -5	O, O
2Pyr	−NH···N_2 (intramolecular)	3342, 1686	2Pyr:DITFB	No	C-I···O=C C-I···N_1	3285, 1682	-57, -4	O, N_1
2Pyr-Br	−NH···N_2 (intramolecular)	3344, 1691	2Pyr-Br:DITFB	No	C-I···N_1 C-I···N_1	3286, 1694	-58, +3	N_1, N_1
2Pyr-i	−NH···N_2 (intramolecular)	3350 and 3331, 1689 and 1683	2Pyr-I:DITFB	No	C-I···N_1 C-I···N_1	3290, 1692	-60 and -41, +3 and +9	N_1, N_1
3Pyr	−NH···N_2	a, 1670	3Pyr:DITFB	Yes	C-I···N_1 C-I···N_2 N-H···O=C	3326, 1653	*, -17	N_1, N_2
3Pyr-I	−NH···N_2	a, 1669	3Pyr-I: DITFB	Yes	C-I···N_1 C-I···N_2 N-H···O=C	3324, 1650	*, -19	N_1, N_2
3Pyr-I	−NH···N_2	a, 1669	3Pyr-I:TITFB	Yes	C-I···N_1 C-I···N_2 N-H···O=C	3317, 1655	*, -14	N_1, N_2
4Pyr	−NH···N_2	A, 1684	4Pyr:DITFB	Yes	C-I···N_1 C-I···N_2 N-H···O=C	3298, 3271, 1669	*, -15	N_1, N_2
4Pyr	−NH···N_2	a, 1684	4Pyr:TITFB	Yes	C-I'···N_1 C-I···N_2 N-H···I'	3284, 1659	*, -25	N_1, N_2
4Pyr-Cl	−NH···N_2	a, 1678	4Pyr-Cl:TITFB	Yes	C-I···N_1 C-I···N_2 N-H···O=C	3388, 1693	*, +15	N_1, N_2
4Pyr-Br	−NH···N_2	a, 1680	4Pyr-Br:DITFB	Yes	C-I'···N_1 C-I···N_2 N-H···I'	3403, 1686	*, +6	N_1, N_2

In two of the three co-crystals from the Bz series the homomeric dimeric NH···N1 hydrogen bonding in the target structure was broken in co-crystal formation. In these two co-crystals

Bz:DITFB and Bz:TITFB the pyridyl nitrogen N_1 was selected by one of the XB donor atoms while the second donor site of XB donor bound to a different site (either carbonyl oxygen or □ cloud in the target molecule). The net change in O=C position in IR was higher when a NH···O=C interaction (-/Δ 13, in Bz:DITFB) in comparison to when a C-I···O=C (+/Δ 3, Bz:TITFB) was formed with the same target molecule. In the instance of Bz-I:DITFB, where the homometic HB remained unchanged, with I···O=C halogen bond formation there was no discernible changes observed in the amide region of co-crystal IR spectra while the carbonyl peak shifted by (+/Δ 5).Thus, in the two cases where the hydrogen bond motif was changed, the IR at amide position visibly altered by the emergence of an NH peak which was not seen in spectra of the individual target compound, Bz.

As expected, the intramolecular hydrogen bonding of the targets in 2Pyr series remained intact in co-crystal formation. Halogen bonding occurred to the vacant N1, nitrogen atom 5/6 times. In the one instance, 2Pyr-I:DITFB where a C-I···O occurred could be result of the higher negative charge of the carbonyl oxygen of the 2Pyr target in comparison to 2Pyr-Br and 2Pyr-I. Due to the difference in selected binding sites, although the ratio in the solution of target:co-former was 1:1 in all three cases, the co-crystal stoichiometry was 1:1, 2:1 and 2:1 in 2Pyr:DITFB, 2Pyr-Br:DITFB and 2Pyr-I:DITFB respectively. All three co-crystals were accompanied by a significant red shift of the amide NH of ~60.

In the crystal structures of 3Pyr:DITFB, 3Pyr-I:DITFB and 3Pyr-I:TITFB, the HB in the target was altered from −NH···N2 to N-H···O=C. Halogen bonding occurred at both pyridyl nitrogen sites N1 and N2. In all three co-crystals, the carbonyl peak in the IR spectrum was red shifted in the range of ~14-19 and lead to an emergence of NH peak which was not seen in spectra of individual target molecule.

In the crystal structures of 4Pyr:DITFB, 4Pyr:TITFB, 4Pyr-Cl:TITFB and 4Pyr-Br:DITFB, the 'parent' −NH···N_2 was broken and halogen bonding occurred to both N_1 and N_2 pyridyl binding sites. In two out of four co-crystals, an N-H···O=C hydrogen bond was formed and in the other two cases an N-H···I interaction was observed. Since the N-H···I bond occurred in combination with TITFB (in 4Pyr:TITFB) and DITFB (in 4Pyr-Br:TITFB) it cannot be related to the type of co-former. Although there was no structure directing interaction at the carbonyl oxygen, in 4Pyr:TITFB, a red shift of 15 cm^{-1} was observed and with 4Pyr-Br:DITFB, a blue shift of 6 cm^{-1} occurred. All four co-crystals were accompanied by the emergence of an amide peak in the IR spectra. The N-H···O=C interaction in 4Pyr:DITFB was accompanied by a red shift of the carbonyl stretch of 15 cm^{-1} while in 4PyrCl:TITFB it was accompanied by a blue shift of 15 cm^{-1}.

Based on the interactions at the carbonyl group we can categorize the co-crystals into three groups; those which formed a N-H···O=C interaction, those in which an I···O=C interaction was present and those in which no interaction was shown at the carbonyl oxygen. The summarized data (Figure 9) indicate that an C-I···O=C did not bring about a significant change in the carbonyl peak and was comparable in value to when the target did not have any structure directing interactions at the carbonyl. On the other hand, NH···O=C did bring about bigger shifts to the carbonyl stretching mode (Figure 4.10).

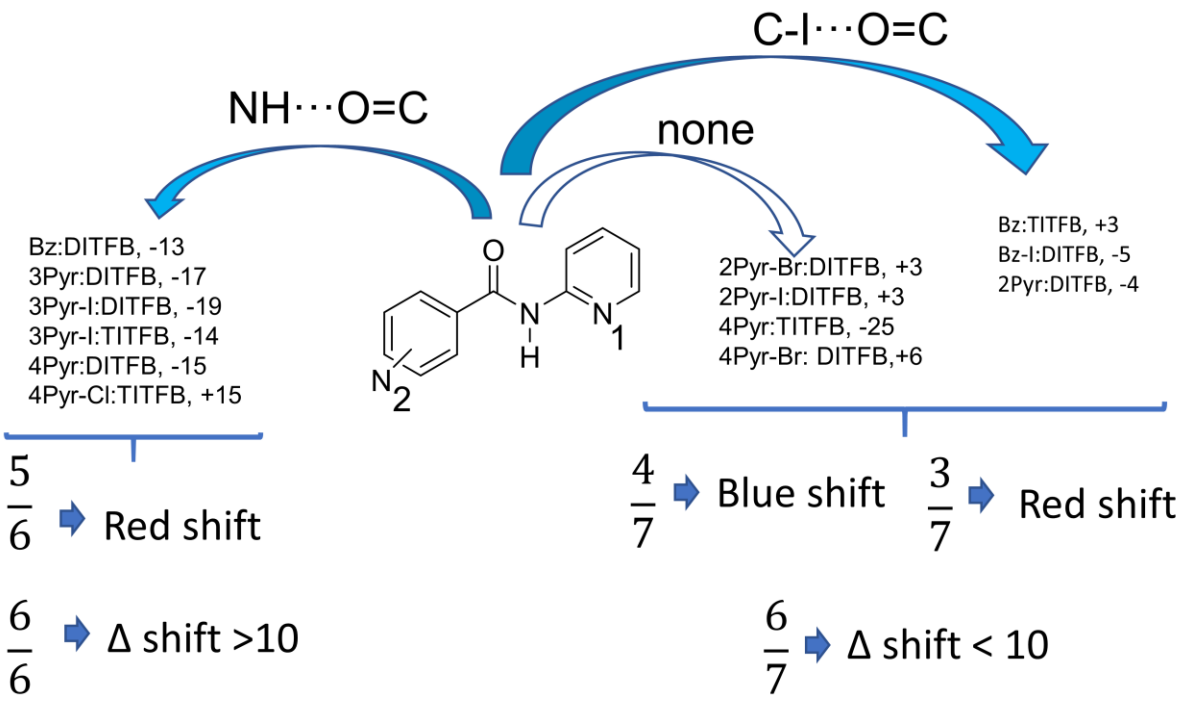

Figure 4.10. Summarized changes of carbonyl IR mode of co-crystal relative to respective target

4.5 Conclusions

A total of 13 co-crystals were analyzed by SCXRD. In all three of obtained from the 2Pyr series the homomeric intramolecular HB −NH···N_2 remained intact. In the 10 co-crystals obtained from the other three series, the intermolecular HB found in the self-assembly of the target was broken in 9/10 times. In all co-crystals combined the interaction between XB donor and target was either to a N(pyr)=77%, O=C(19%) or π (4%). Finally, we note that an C-I···O=C does not bring about a significant change to the carbonyl stretch in comparison to when a NH···O=C hydrogen bond is present. Therefore, vibrational spectroscopy offers a very indication as to whether the carbonyl moiety acts as an acceptor for either a hydrogen- or a halogen bond or to neither.

4.6 References

[1] Gellman, S. H. Introduction: Molecular Recognition. *Chem. Rev.* **1997**, *97*, 1231–1232

[2] Berger, G.; Frangville, P.; Meyer, F. Halogen Bonding for Molecular Recognition: New Developments in Materials and Biological Sciences. *ChemComm* **2020**, *56*, 4970–4981.

[3] A. Gautier, A.; Tebo, A. G. Sensing Cellular Biochemistry with Fluorescent Chemical–Genetic Hybrids. *Curr Opin Chem Bio.* **2020**, *57*, 58–64

[4] Zhang, Y.-M.; Xu, Q.-Y.; Liu, Y. Molecular Recognition and Biological Application of Modified β-Cyclodextrins. *Sci. China Chem.* **2019**, *62*, 549–560.

[5] Dervan, P. Molecular Recognition of DNA by Small Molecules. *Bioorg. Med. Chem.***2001**, *9*, 2215–2235

[6] Wang, K. B.; Dickerhoff, J.; Wu, G.; Yang, D. PDGFR-β Promoter Forms a Vacancy G-Quadruplex that Can Be Filled in by dGMP: Solution Structure and Molecular Recognition of Guanine Metabolites and Drugs *J. Am. Chem. Soc 142*, 5204-5211

[7] Grommet, A. B.; Lee, L. M.; Klajn, R. Molecular Photoswitching in Confined Spaces. *Acc. Chem. Res.* **2020**, *53*, 2600–2610

[8] Yamaguchi, H.; Kobayashi, R.; Takashima, Y.; Hashidzume, A.; Harada, A. Self-assembly of gels through molecular recognition of cyclodextrins: Shape selectivity for linear and cyclic guest molecules. *Macromolecules*. **2011**, *44*, 2395-2399.

[9] Zhou, J.; Yu, G.; Huang, F. Supramolecular Chemotherapy Based on Host–Guest Molecular Recognition: A Novel Strategy in the Battle against Cancer with a Bright Future. *Chem. Soc. Rev* **2017**, *46*, 7021–7053.

[10] Culver, H. R.; Clegg, J. R.; Peppas, N. A. Analyte-responsive hydrogels: intelligent materials for biosensing and drug delivery. *Acc. Chem. Res*, **2017**,*50*, 170-178.

[11] Jaegle, M.; Wong, E. L.; Tauber, C.; Nawrotzky, E.; Arkona, C.; Rademann, J. Protein-Templated Fragment Ligations—From Molecular Recognition to Drug Discovery. *Angew Chem Int Ed* **2017**, *56*, 7358–7378.

[12] Chen, W.; Tian, X.; He, W.; Li, J.; Feng, Y.; Pan, G. Emerging Functional Materials Based on Chemically Designed Molecular Recognition. *BMC Materials* **2020**, *2*,1-22.

[13] Yao, H.; Ke, H.; Zhang, X.; Pan, S. J.; Li, M. S.; Yang, L. P.; Schreckenbach. G.; Jiang, W. Molecular recognition of hydrophilic molecules in water by combining the hydrophobic effect with hydrogen bonding. *J. Am. Chem. Soc.* **2018,** *140*(41), 13466-13477

[14] Desiraju, G. R. Crystal engineering: a holistic view. *Angew Chem Int Ed*, **2017**,*46*, 8342-8356.

[15] Steiner, T.The hydrogen bond in the solid state. *Angew. Chem. Int. Ed.* **2002,** *41*, 48-76.

[16] G. R. Desiraju, P. S. Ho, L. Kloo, A. C. Legon, R. Marquardt, P. Metrangolo, P. Politzer, G. Resnati, K. Rissanen, *Pure Appl. Chem* **2013**, *85*, 1711-1713

[17] Alkorta, I.; Elguero, J.; Frontera, A. Not Only Hydrogen Bonds: Other Noncovalent Interactions. *Crystals* **2020**, *10*,

[18] Riley, K. E. Critical Comparison of RX···Y and RH···Y Directionality in Halogen and Hydrogen Bonds Using Modern Computational Chemistry Methods. Chemical Physics Letters. 2020, 744, 137221.

[19] M. Huber, S.; D. Scanlon, J.; Jimenez-Izal, E.; M. Ugalde, J.; Infante, I. On the Directionality of Halogen Bonding. *Physical Chemistry Chemical Physics* **2013**, *15*, 10350–10357

[20] Pfrunder, M. C.; Micallef, A. S.; Rintoul, L.; Arnold, D. P.; Davy, K. J.; McMurtrie, J. . *Cryst. Growth Des.* **2014** *14*, 6041-6047.

[21] V. Torubaev, Y.; V. Skabitsky, I. The Energy Frameworks of Aufbau Synthon Modules in 4-Cyanopyridine Co-Crystals. *CrystEngComm.* **2019**, *21*, 7057–7068

[22] D. Perera, M.; Desper, J.; S. Sinha, A.; B. Aakeröy, C. Impact and Importance of Electrostatic Potential Calculations for Predicting Structural Patterns of Hydrogen and Halogen Bonding. *CrystEngComm* **2016**, *18*, 8631–8636

[23] Aakeröy, C. B.; Wijethunga, T. K.; Desper, J.; Moore, C. Halogen-Bond Preferences in Co-Crystal Synthesis. *J Chem Crystallogr* **2015**, *45*, 267–276.

[24] Abeysekera, A. M.; Day, V. W.; Sinha, A. S.; Aakeröy, C. B.Mapping out the Relative Influence of Hydrogen and Halogen Bonds in Crystal Structures of a Family of Amide-Substituted Pyridines. *Cryst. Growth Des.* **2020**, 20, 7399-7410

[25] Nicolas, I.; Barrière, F.; Jeannin, O.; Fourmigué, M. Sequential halogen bonding with ditopic donors: σ-hole evolutions upon halogen bond formation. *Crystal Growth & Design*,**2016,** *16*, 2963-2971.
[26] Reza Khavasi, H.; Azhdari Tehrani, A. Effect of Halogen Bonding Interaction on Supramolecular Assembly of Halogen -Substituted Phenylpyrazinamides. *CrystEngComm* **2013**, *15*, 3222–3235.
[27] Metrangolo, P.; Resnati, G. Type II Halogen···halogen Contacts Are Halogen Bonds. *IUCrJ* **2013**, *1* (Pt 1), 5–7

Chapter 5 - Evaluating halogen bond binding preferences as a function of molecular electrostatic potentials

5.1 Introduction

In crystal engineering[1], calculated molecular electrostatic potentials (MEPs) serve as a useful tool for identifying the most likely, or the most prominent, (hydrogen/halogen/chalcogen)-bond donor and acceptor sites. The more positive the value of the MEP, the stronger the donor, and the more negative the value, the better the acceptor[2,3,4]

The MEP at the tip of a halogen atom is called a σ-hole[5,6,7] The magnitude of the σ- hole varies as a function of halogen atom; Cl<Br<I[8,9,10] In additiion, the σ-hole can be enhanced/increased by the presence of electron withdrawing atoms or functional groups such as flourine[11], nitrogen[12],[13] or nitro groups[14]. The MEP at the tip of a halogen also varies based on the hybridization of the associated carbon atom (sp^3<sp^2<sp) (Figure 5.1)[15]

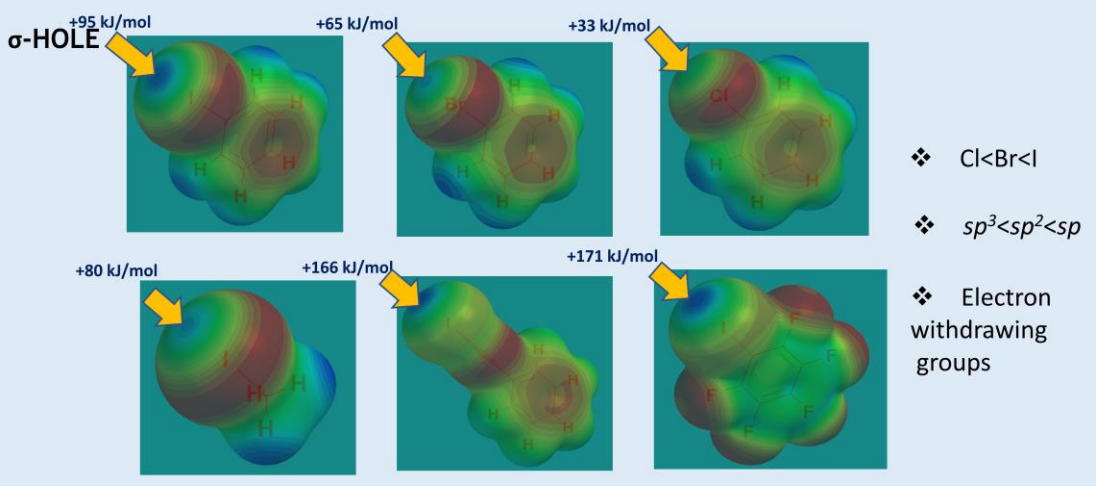

Figure 5.1. Factors which affect σ-hole value[16]

We recently explored the binding preferences of four series of compounds, N-(pyridin-2-yl)benzamide (Bz series), N-(pyridin-2-yl)picolinamides (2Pyr series), N-(pyridin-2-yl)nicotinamdes (3Pyr series), N-(pyridin-2-yl)isonicotinamdes (4Pyr series), functionalized with unactivated halogen atoms.[17] We found that halogen bonding was shown only by the iodinated compounds, which coincided with the halogen atom with the most positive σ- hole value. In this chapter, we deliberately increase the strength of the halogen bonding site by activating the three halogen atoms (Cl, Br, and I) to an *sp*-hybridized carbon atom. We hypothesize that this will lead to an increase in the occurrence of structure directing interactions produced by the respective halogen atoms. For comparison, we were also were interested in exploring the structural effects resulting from a similar activation of a hydrogen-bond donor, by decorating this series of compounds with an ethynyl hydrogen atom, (R-≡-H), in a series of new compounds (Figure 5.2).

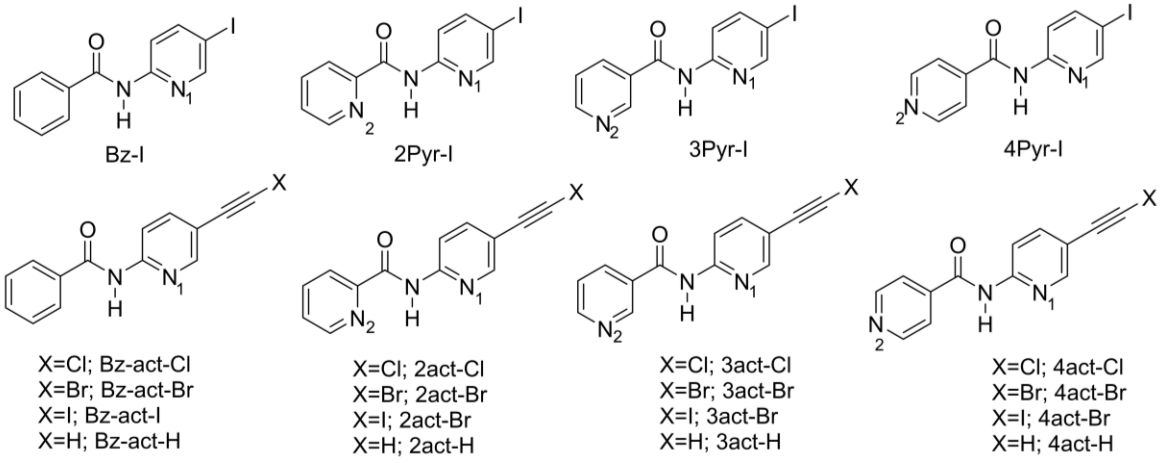

Figure 5.2. Target molecules in this study

Here we investigate the following;

- Can we expect the frequency of structure-directing interactions to be related to a threshod σ-hole value?

-Will halogen-bond donors, even though of different elemental origin, lead to synthon mimicry?

-Are there any fundamental differences between the acceptor sites selected by halogen-bond donors and an ethynyl-based hydrogen-bond donor with comparable electrostatic potential?

5.2 Experimental

5.2.1 General

All precursors, solvents were purchased from commercial sources and used without further purification. ^{1}H NMR spectra and ^{13}C NMR spectra were recorded on Brucker 400 spectrometer. Melting points were recorded on a Fisher-Johns melting point apparatus or a TA Instruments DSC Q20 differential scanning calorimeter. IR spectra were recorded with a Nicolet 380 FT-IR spectrometer using an attenuated total reflection (ATR) technique and ZnSe as the crystal. Electrostatic potentials were calculated with density functional B3LYP level of theory using 6-311++G** basis set in vacuum, using Spartan 08' software.

5.2.2 Synthesis

- Synthesis of N-(5-((trimethylsilyl)ethynyl)pyridin-2-yl)amides: Bz-TMS/2act-TMS/3Pyr TMS/4Pyr-X (Sections 5.2.2.1 - 5.2.2.4)

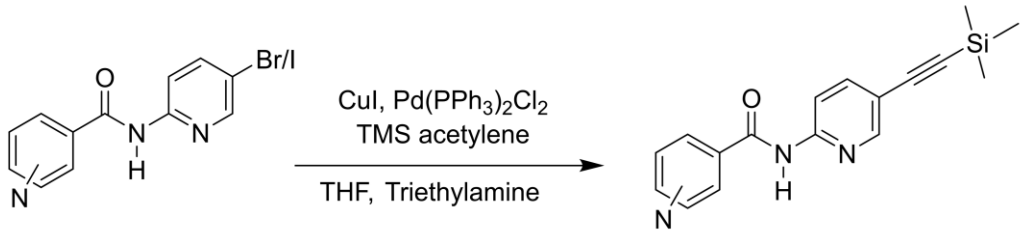

Bz-I/2Pyr-Br/3Pyr-Br/4Pyr-Br

Bz-TMS/2Pyr-TMS/3Pyr-TMS/4Pyr-TMS

The respective bromo or iodo amide (1 eq) was dissolved in trimethylamine: THF (1:1) and degassed with nitrogen. CuI (0.1 eq/ 0.5eq), bis(triphenylphosphine)palladium(II) dichloride (0.1 eq), and trimethylsilylacetylene (1.5 eq/2eq), was added and the reaction mixture was heated at 80°C under

nitrogen. The reaction completion was monitored by TLC. The reaction medium was filtered, and the filtrate evaporated to dryness and redissolved in methylene chloride. The organic layer was washed with 1M HCl, brine, water and dried with anhydrous magnesium sulfate and filtered. The organic layer was concentrated and the product purified by column chromatography (hexane followed by hexane: ethyl acetate 80:20).

-Synthesis of N-(5-(haloethynyl)pyridin-2-yl)amides: Bz-act-X/2act-X/3act-X/4act-X

(Sections 5.2.2.5 - 5.2.2.16)

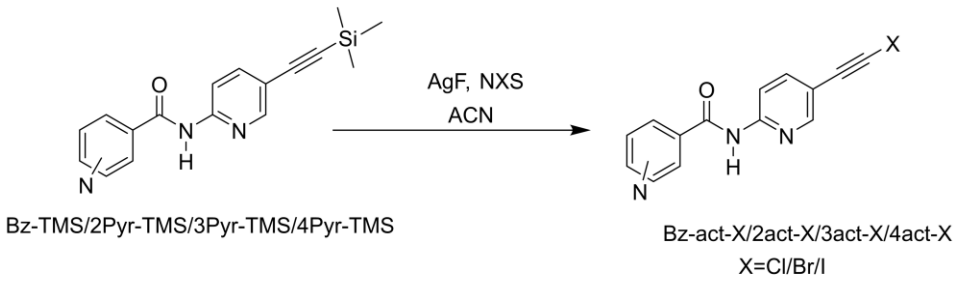

Bz-TMS/2Pyr-TMS/3Pyr-TMS/4Pyr-TMS

Bz-act-X/2act-X/3act-X/4act-X
X=Cl/Br/I

In a round bottomed flask covered with aluminum foil, acetonitrile (50 mL) was degassed with dinitrogen. The respective N-(5((trimethylsilyl)ethynyl)pyridin-2-yl)amide (1 eq) and AgF (1.1 eq/1.2 eq /1.5 eq) were added to acetonitrile and the mixture was covered with aluminum foil before the introduction of N-halosuccinimide (1.1 eq/1.2 eq /1.5 eq /2.0 eq/ 2.5 eq). The mixture was connected to a nitrogen inlet and stirred. Completion of the reaction was monitored with TLC and the resulting suspension was filtered. The filtrate was evaporated to dryness and redissolved in 150 mL ethylacetate:diethylether (4:1). The organic layer was washed with water and dried with anhydrous $MgSO_4$ and concentrated *in vacuo.* The resultant solid was purified by passing through a ~6 cm silica plug using hexane:ethyl acetate (10:1) to obtain the pure product.

- Synthesis of N-(5-ethynylpyridin-2-yl)amides: Bz-act-H/2act-H/3act-H/4act-H (Sections 5.2.2.17 - 5.2.2.20)

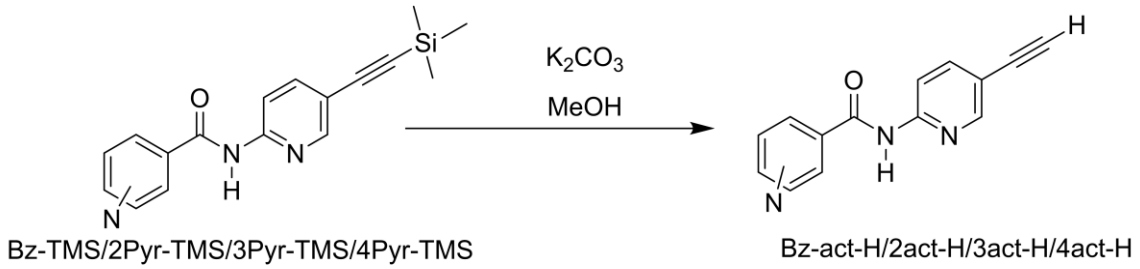

Bz-TMS/2Pyr-TMS/3Pyr-TMS/4Pyr-TMS

Bz-act-H/2act-H/3act-H/4act-H

The respective N-(5-((trimethylsilyl)ethynyl)pyridin-2-yl)amide (1 eq) was dissolved in methanol. Then, K_2CO_3 (~1 eq) was added into the solution. The mixture was stirred at room temperature. The reaction completion was monitored by TLC. Once the reaction was completed the solvent was evaporated to dryness and the solid was redissolved in ethyl acetate. The organic layer was washed with water and dried with anhydrous $MgSO_4$. The solid was purified by flash chromatography using hexane:ethyl acetate (10:1) to obtain the pure product.

5.2.2.1 Synthesis of N-(5-((trimethylsilyl)ethynyl)pyridin-2-yl)benzamide (Bz-TMS)

N-(5-iodopyridin-2-yl)benzamide/Bz-I (1.100 g, 3.3 mmol) was dissolved in 60 mL of trimethylamine: THF (1:1) and degassed with dinitrogen. CuI (0.064 g, 0.33 mmol), bis(triphenylphosphine)palladium(II) dichloride (0.216 g, 0. 0.33 mmol) and trimethylsilylacetylene (0.72 mL, 5.0 mmol), was added and the reaction mixture was heated overnight at 80°C under dinitrogen. The reaction was monitored by TLC. The reaction medium was filtered, and the filtrate evaporated to dryness and redissolved in methylene chloride. The organic later was washed with 1M HCl, brine, water and dried with anhydrous magnesium sulfate and filtered. The organic layer was concentrated, and the product purified by column

chromatography (hexane followed by hexane: ethyl acetate 80:20). Yield 80%, m.p 139-141°C. ^{1}H NMR (400 MHz, DMSO-d_6) δ 11.04 (s, 1H), 8.50 (dd, *J* = 2.4, 0.9 Hz, 1H), 8.24 (dd, *J* = 8.7, 0.9 Hz, 1H), 8.07 – 7.99 (m, 2H), 7.94 (dd, *J* = 8.7, 2.4 Hz, 1H), 7.66 – 7.57 (m, 1H), 7.57 – 7.48 (m, 2H), 0.26 (s, 9H). ^{13}C NMR (101 MHz, DMSO-d_6) δ 165.82, 151.45, 150.35, 140.60, 133.46, 131.79, 128.04, 127.74, 114.25, 113.57, 101.73, 96.36.

5.2.2.2 Synthesis of N-(5-((trimethylsilyl)ethynyl)pyridin-2-yl)picolinamide (2Pyr-TMS)

N-(5-bromopyridin-2-yl)picolinamide/2Pyr-Br (0.986 g, 3.5 mmol) was dissolved in 60 mL of trimethylamine: THF (1:1) and degassed with nitrogen. CuI (0.067 g, 0.35 mmol), bis(triphenylphosphine)palladium(II) dichloride (0.247 g, 0. 0.35 mmol) and trimethylsilylacetylene (0.97 mL, 7.0 mmol), was added and the reaction mixture was heated at 80°C under dinitrogen 3 days. The reaction was monitored by TLC. The reaction medium was filtered, and the filtrate evaporated to dryness and redissolved in methylene chloride. The organic later was washed with 1M HCl, brine, water and dried with anhydrous magnesium sulfate and filtered. The organic layer was concentrated, and the product purified by column chromatography (hexane followed by hexane: ethyl acetate 80:20). Yield 56%, m.p 139-141°C. ^{1}H NMR (400 MHz, DMSO-d_6) δ 10.54 (s, 1H), 8.78 – 8.72 (m, 1H), 8.48 (d, *J* = 2.2 Hz, 1H), 8.27 (d, *J* = 8.5 Hz, 1H), 8.24 – 8.17 (m, 1H), 8.11 (td, *J* = 7.7, 1.7 Hz, 1H), 7.99 (dd, *J* = 8.6, 2.3 Hz, 1H), 7.73 (ddd, *J* = 7.6, 4.7, 1.3 Hz, 1H), 0.26 (s, 9H) ^{13}C NMR (101 MHz, DMSO-d_6) δ 161.78, 150.85, 149.71, 148.48, 147.92, 141.19, 138.27, 127.45, 122.09, 114.82, 112.30, 101.52, 96.70.

5.2.2.3 Synthesis of N-(5-((trimethylsilyl)ethynyl)pyridin-2-yl)nicotinamide (3Pyr-TMS)

N-(5-bromopyridin-2-yl)nicotinamide/3Pyr-Br (1.468 g, 5.2 mmol) was dissolved in 80 mL of trimethylamine: THF (1:1) and degassed with dinitrogen. CuI (0.100 g, 0.52 mmol), bis(triphenylphosphine)palladium(II) dichloride (0.370 g, 0.52 mmol) and trimethylsilylacetylene (1.5 mL, 10.4 mmol), was added and the reaction mixture was heated at 80°C under dinitrogen 3 days. The reaction was monitored by TLC. The reaction medium was filtered, and the filtrate evaporated to dryness and redissolved in methylene chloride. The organic layer was washed with 1M HCl, brine, water and dried with anhydrous magnesium sulfate and filtered. The organic layer was concentrated, and the product purified by column chromatography (hexane followed by hexane: ethyl acetate 80:20). Yield 50%, 188-189°C. ^{1}H NMR (400 MHz, DMSO-d_6) δ 11.31 (s, 1H), 9.14 (s, 1H), 8.78 (s, 1H), 8.54 – 8.49 (m, 1H), 8.41 (s, 1H), 8.35 (dt, J = 8.0, 1.9 Hz, 1H), 8.23 (dd, J = 8.6, 0.9 Hz, 1H), 7.96 (dd, J = 8.6, 2.3 Hz, 1H), 7.56 (dd, J = 8.0, 4.7 Hz, 1H), 0.26 (s, 9H). ^{13}C NMR (101 MHz, DMSO-d_6) δ 164.60, 152.16, 151.20, 150.42, 148.74, 140.73, 135.50, 123.13, 114.54, 113.62, 101.65, 96.54

5.2.2.4 Synthesis of N-(5-((trimethylsilyl)ethynyl)pyridin-2-yl)isonicotinamide (4Pyr-TMS)

N-(5-bromopyridin-2-yl)isonicotinamide/4Pyr-Br (2.290 g, 8.2 mmol) was dissolved in 80 mL of trimethylamine: THF (1:1) and degassed with dinitrogen. CuI (0.078 g, 0.41 mmol), bis(triphenylphosphine)palladium(II) dichloride (0.288 g, 4.1 mmol) and trimethylsilylacetylene (2.30 mL, 16.4 mmol), was added and the reaction mixture was heated at 80°C under dinitrogen 3 days. The reaction was monitored by TLC. The reaction medium was filtered, and the filtrate evaporated to dryness and redissolved in methylene chloride. The organic later was washed with 1M HCl, brine, water and dried with anhydrous magnesium sulfate and filtered. The organic layer

was concentrated, and the product purified by column chromatography (hexane followed by hexane: ethyl acetate 80:20). Yield 48%,149-151°C. ^{1}H NMR (400 MHz, DMSO-d_6) δ 11.35 (s, 1H), 8.80 – 8.74 (m, 2H), 8.52 (d, *J* = 2.3 Hz, 1H), 8.22 (d, *J* = 8.7 Hz, 1H), 7.96 (dd, *J* = 8.7, 2.4 Hz, 1H), 7.93 – 7.87 (m, 2H), 0.25 (s, 9H). ^{13}C NMR (101 MHz, DMSO-d_6) δ 165.34, 151.79, 151.25, 150.70, 141.59, 122.30, 115.57, 114.55, 102.39, 97.47

5.2.2.5 N-(5-(chloroethynyl)pyridin-2-yl)benzamide (Bz-act-Cl)

In a round bottomed flask covered with aluminum foil, acetonitrile (50 mL) was degassed with dinitrogen. N-(5-((trimethylsilyl)ethynyl)pyridin-2-yl)benzamide (0.500 g, 1.69 mmol) and AgF (0.236 g, 1.86 mmol) were added before the introduction of N-chlorosuccinimide (0.249 g, 1.86 mmol). The mixture was connected to a nitrogen inlet and stirred for 6 days. Completion of the reaction was monitored with TLC and the resulting suspension was filtered. The filtrate was evaporated to dryness and redissolved in 150 mL of diethylether. The organic layer was washed with water and dried with anhydrous MgSO4 and concentrated *in vacuo* to obtain the pure product. Yield 34%, m.p 111-113°C. ^{1}H NMR (400 MHz, DMSO-d_6) δ 11.04 (s, 1H), 8.56 (s, 1H), 8.23 (d, *J* = 8.6 Hz, 1H), 8.05 – 7.96 (m, 3H), 7.61 (s, 1H), 7.52 (s, 2H). ^{13}C NMR (101 MHz, DMSO-d_6) δ 166.68, 152.42, 151.51, 141.71, 134.27, 132.63, 128.86, 128.58, 114.47, 113.91, 70.66, 67.27.

5.2.2.6 N-(5-(bromoethynyl)pyridin-2-yl)benzamide (Bz-act-Br)

In a round bottomed flask covered with aluminum foil, acetonitrile (50 mL) was degassed with dinitrogen. N-(5-((trimethylsilyl)ethynyl)pyridin-2-yl)benzamide (0.500 g, 1.69 mmol) and AgF (0.215 g, 1.69 mmol) were added to acetonitrile and the mixture was covered with aluminum foil before the introduction of N-bromosuccinimide (0.302 g, 1.69 mmol) The mixture was connected to a dinitrogen inlet and stirred for 4 days. Completion of the reaction was monitored with TLC and the resulting suspension was filtered. The filtrate was evaporated to dryness and redissolved

in 150 mL of diethylether (4:1). The organic layer was washed with water and dried with anhydrous MgSO4 and concentrated *in vacuo* to obtain the pure product. Yield 30%, m.p 111-113°C. ^{1}H NMR (400 MHz, DMSO-d_6) δ 11.02 (s, 1H), 8.53 (dd, *J* = 2.3, 1.0 Hz, 1H), 8.22 (d, *J* = 8.7 Hz, 1H), 8.01 (dd, *J* = 8.0, 1.6 Hz, 2H), 7.97 (dd, *J* = 8.7, 2.3 Hz, 1H), 7.65 – 7.56 (m, 1H), 7.56 – 7.47 (m, 2H). ^{13}C NMR (101 MHz, DMSO) δ 166.65, 152.28, 151.42, 141.61, 134.28, 132.62, 128.86, 128.58, 114.85, 114.44, 77.32, 55.65

5.2.2.7 N-(5-(iodoethynyl)pyridin-2-yl)benzamide (Bz-act-I)

In a round bottomed flask covered with aluminum foil, acetonitrile (80 mL) was degassed with dinitrogen. N-(5-((trimethylsilyl)ethynyl)pyridin-2-yl)benzamide (1.5 g, 5.0 mmol) and AgF (0.775 g, 6.1 mmol) were added to acetonitrile and the mixture was covered with aluminum foil before the introduction of N-iodosuccinimide (1.375g, 6.1 mmol). The mixture was connected to a dinitrogen inlet and stirred. Completion of the reaction was monitored with TLC and the resulting suspension was filtered. The filtrate was evaporated to dryness and redissolved in 250 mL of diethyl ether. The organic layer was washed with water and dried with anhydrous MgSO4 and concentrated *in vacuo.* The resultant solid was purified by passing through a ~6 cm silica plug using hexane:ethyl acetate (10:1) to obtain the pure product. Yield 29%, m.p 156-158°C .^{1}H NMR (400 MHz, DMSO-d6) δ 10.99 (s, 1H), 8.48 (dd, J = 2.3, 0.9 Hz, 1H), 8.20 (dd, J = 8.7, 0.9 Hz, 1H), 8.05 – 7.97 (m, 2H), 7.91 (dd, J = 8.7, 2.4 Hz, 1H), 7.64 – 7.55 (m, 1H), 7.51 (t, J = 7.5 Hz, 2H). ^{13}C NMR (101 MHz, DMSO-d6) δ 166.60, 152.07, 151.57, 141.70, 134.30, 132.60, 128.86, 128.56, 115.97, 114.35, 89.98, 21.15.

5.2.2.8 Synthesis of N-(5-(chloroethynyl)pyridin-2-yl)picolinamide (2act-Cl)

In a round bottomed flask covered with aluminum foil, acetonitrile (50 mL) was degassed with dinitrogen. N-(5-((trimethylsilyl)ethynyl)pyridin-2-yl)picolinamide (0.500 g, 1.69 mmol) and

AgF (0.429g, 3.38 mmol) were added to acetonitrile before the introduction of N-chlorosuccinimide (0.452 g, 3.38 mmol). The mixture was connected to a dinitrogen inlet and stirred for 6 days. Completion of the reaction was monitored with TLC and the resulting suspension was filtered. The filtrate was evaporated to dryness and redissolved in 150 mL ethylacetate:diethyl ether (4:1). The organic layer was washed with water and dried with anhydrous MgSO4 and concentrated *in vacuo.* The resultant solid was purified by passing through a ~6 cm silica plug using hexane:ethyl acetate (10:1) to obtain the pure product. Yield 9%, m.p 113-116°C 1H NMR (400 MHz, DMSO-d6) δ 10.56 (s, 2H), 8.76 (d, J = 4.8 Hz, 2H), 8.55 (d, J = 2.3 Hz, 2H), 8.29 (d, J = 8.7 Hz, 2H), 8.21 (d, J = 7.8 Hz, 2H), 8.16 – 8.02 (m, 4H), 7.74 (dd, J = 7.7, 4.7 Hz, 2H), 7.66 – 7.52 (m, 1H), 2.50 (d, J = 4.5 Hz, 2H). ^{13}C NMR (101 MHz, DMSO-d_6) δ 162.62, 151.98, 150.67, 149.28, 148.69, 142.29, 139.07, 128.26, 122.90, 114.48, 113.19, 70.95, 67.08.

5.2.2.9 Synthesis of N-(5-(bromoethynyl)pyridin-2-yl)picolinamide (2act-Br)

In a round bottomed flask covered with aluminum foil, acetonitrile (50 mL) was degassed with dinitrogen. N-(5-((trimethylsilyl)ethynyl)pyridin-2-yl)picolinamide (0.500 g, 1.69 mmol) and AgF (0.429g, 3.38 mmol) were added to acetonitrile before the introduction of N-bromosuccinimide (0.602 g, 3.38 mmol). The mixture was connected to a dinitrogen inlet and stirred for 4 days. Completion of the reaction was monitored with TLC and the resulting suspension was filtered. The filtrate was evaporated to dryness and redissolved in 150 mL ethylacetate:diethyl ether (4:1). The organic layer was washed with water and dried with anhydrous $MgSO_4$ and concentrated *in vacuo*. The resultant solid was purified by passing through a ~6 cm silica plug using hexane:ethyl acetate (10:1) to obtain the pure product. Yield 5% ^{1}H NMR (400 MHz, DMSO-d_6) δ 10.55 (s, 1H), 8.77 (s, 1H), 8.52 (s, 1H), 8.28 (d, J = 8.6 Hz, 1H), 8.21 (d, J = 7.8 Hz, 1H), 8.12 (s, 1H), 8.04 (d, J = 8.6 Hz, 1H), 7.74 (s, 1H). ^{13}C NMR (101 MHz, DMSO-d_6) δ 162.58, 151.86, 150.53, 149.33, 149.27, 148.69, 142.19, 139.14, 139.07, 128.25, 122.90, 115.40, 113.15, 77.12, 56.01.

5.2.2.10 Synthesis of N-(5-(iodoethynyl)pyridin-2-yl)picolinamide (2act-i)

In a round bottomed flask covered with aluminum foil, acetonitrile (50 mL) was degassed with dinitrogen. N-(5-((trimethylsilyl)ethynyl)pyridin-2-yl)picolinamide (0.500 g, 1.69 mmol) and AgF (0.253 g, 2.0 mmol) were added to acetonitrile before the introduction of N-iodosuccinimide (0.458 g, 2.0 mmol). The mixture was connected to a dinitrogen inlet and stirred overnight. Completion of the reaction was monitored with TLC and the resulting suspension was filtered. The filtrate was evaporated to dryness and redissolved in 150 mL ethylacetate:diethyl ether (4:1). The organic layer was washed with water and dried with anhydrous MgSO4 and concentrated *in vacuo.* The resultant solid was purified by passing through a ~6 cm silica plug using hexane:ethyl acetate (10:1) to obtain the pure product. Yield 5% ^{1}H NMR (400 MHz, DMSO-d_6) δ 10.52 (s, 1H), 8.76 (s, 1H), 8.47 (s, 1H), 8.24 (d, J = 20.6 Hz, 2H), 8.12 (s, 1H), 7.98 (s, 1H), 7.74 (s, 1H). ^{13}C NMR (101 MHz, DMSO-d_6) δ 162.55, 152.05, 150.33, 149.28, 148.72, 142.29, 139.06, 128.24, 122.89, 116.51, 113.06, 89.79, 21.64.

5.2.2.11 Synthesis of N-(5-(chloroethynyl)pyridin-2-yl)nicotinamide (3act-Cl)

In a round bottomed flask covered with aluminum foil, acetonitrile (50 mL) was degassed with dinitrogen. N-(5-((trimethylsilyl)ethynyl)pyridin-2-yl)nicotinamide (1.00 g, 3.38 mmol) and AgF (0.472 g, 6.7 mmol) were added to acetonitrile before the introduction of N-chlorosuccinimide (0.994 g, 6.7 mmol). The mixture was connected to a dinitrogen inlet and stirred for 7 days. Completion of the reaction was monitored with TLC and the resulting suspension was filtered. The filtrate was evaporated to dryness and redissolved in 150 mL ethylacetate:diethyl ether (4:1). The organic layer was washed with water and dried with anhydrous MgSO4 and concentrated *in vacuo.* The resultant solid was purified by passing through a ~6 cm silica plug using hexane:ethyl acetate (10:1) to obtain the pure product. Yield 8.5%, decomp. 199 – 201°C. ^{1}H NMR (400 MHz, DMSO-

d_6) δ 11.31 (s, 1H), 9.12 (s, 1H), 8.77 (s, 1H), 8.57 (s, 1H), 8.33 (s, 1H), 8.22 (s, 1H), 8.00 (s, 1H), 7.55 (s, 1H). 13C NMR (101 MHz, CDCl3) δ 167.60, 155.35, 154.52, 153.92, 151.92, 146.77, 144.21, 138.70, 132.51, 126.28, 116.87, 73.18, 69.56

5.2.2.12 Synthesis of N-(5-(bromoethynyl)pyridin-2-yl)nicotinamide (3act-Br)

In a round bottomed flask covered with aluminum foil, acetonitrile (50 mL) was degassed with dinitrogen. N-(5-((trimethylsilyl)ethynyl)pyridin-2-yl)nicotinamide (0.500 g, 1.69 mmol) and AgF (0.429g, 3.38 mmol) were added to acetonitrile before the introduction of N-bromosuccinimide (0.602 g, 3.38 mmol). The mixture was connected to a dinitrogen inlet and stirred for 7 days. Completion of the reaction was monitored with TLC and the resulting suspension was filtered. The filtrate was evaporated to dryness and redissolved in 150 mL ethylacetate:diethyl ether (4:1). The organic layer was washed with water and dried with anhydrous MgSO4 and concentrated *in vacuo.* The resultant solid was purified by passing through a ~6 cm silica plug using hexane:ethyl acetate (10:1) to obtain the pure product. Yield 4% ^{1}H NMR (400 MHz, DMSO-d_6) δ 11.30 (s, 1H), 9.12 (s, 1H), 8.77 (s, 1H), 8.54 (s, 1H), 8.34 (s, 1H), 8.21 (s, 1H), 8.00 (s, 1H), 7.53 (s, 1H). ^{13}C NMR (101 MHz, DMSO-d_6) δ 165.43, 152.99, 152.03, 151.49, 149.56, 141.75, 136.35, 130.17, 123.91, 115.15, 114.48, 55.85, 49.07.

5.2.2.13 Synthesis of N-(5-(iodoethynyl)pyridin-2-yl)nicotinamide (3act-I)

In a round bottomed flask covered with aluminum foil, acetonitrile (50 mL) was degassed with dinitrogen. N-(5-((trimethylsilyl)ethynyl)pyridin-2-yl)nicotinamide (0.500 g, 1.69 mmol) and AgF (0.215 g, 1.69 mmol) were added to acetonitrile before the introduction of N-iodosuccinimide (0.380 g, 1.69 mmol). The mixture was connected to a dinitrogen inlet and stirred for 7 days. Completion of the reaction was monitored with TLC and the resulting suspension was filtered. The filtrate was evaporated to dryness and redissolved in 150 mL ethylacetate:diethyl ether (4:1). The organic layer was washed with water and dried with anhydrous $MgSO_4$ and concentrated *in vacuo.* The resultant

solid was purified by passing through a ~6 cm silica plug using hexane:ethyl acetate (10:1) to obtain the pure product. Yield 10%, decomp. 192-194°C. ^{1}H NMR (400 MHz, DMSO-d_6) δ 11.27 (s, 1H), 9.12 (s, 1H), 8.76 (d, *J* = 4.9 Hz, 1H), 8.50 (d, *J* = 2.2 Hz, 1H), 8.33 (dt, *J* = 8.1, 1.9 Hz, 1H), 8.20 (d, *J* = 8.6 Hz, 1H), 7.93 (dd, *J* = 8.7, 2.3 Hz, 1H), 7.55 (dd, *J* = 8.0, 4.8 Hz, 1H). ^{13}C NMR (101 MHz, DMSO-d_6) δ 165.37, 152.95, 151.81, 151.63, 149.54, 141.83, 136.33, 130.19, 123.90, 116.25, 114.39, 89.92, 21.39.

5.2.2.14 Synthesis of N-(5-(chloroethynyl)pyridin-2-yl)isonicotinamide (4act-Cl)

In a round bottomed flask covered with aluminum foil, acetonitrile (80 mL) was degassed with dinitrogen. N-(5-((trimethylsilyl)ethynyl)pyridin-2-yl)isonicotinamide (1.000 g, 3.38 mmol) and AgF (1.06 g, 8.47 mmol) were added to acetonitrile before the introduction of N-chlorosuccinimide (1.127 g, 8.47 mmol). The mixture was connected to a dinitrogen inlet and stirred for 7 days. Completion of the reaction was monitored with TLC and the resulting suspension was filtered. The filtrate was evaporated to dryness and redissolved in 150 mL ethylacetate:diethyl ether (4:1). The organic layer was washed with water and dried with anhydrous MgSO4 and concentrated *in vacuo.* The resultant solid was purified by passing through a ~6 cm silica plug using hexane:ethyl acetate (10:1) to obtain the pure product. Yield 6.5%, decomp. 184-186°C. ^{1}H NMR (400 MHz, DMSO-d_6) δ 11.36 (s, 1H), 8.81 – 8.75 (m, 2H), 8.58 (dd, *J* = 2.3, 0.9 Hz, 1H), 8.23 (dd, *J* = 8.7, 0.9 Hz, 1H), 8.03 (dd, *J* = 8.7, 2.3 Hz, 1H), 7.93 – 7.87 (m, 2H), 1.23 (s, 1H). ^{13}C NMR (101 MHz, DMSO-d_6) δ 165.38, 151.93, 151.59, 150.70, 141.90, 141.42, 122.31, 114.63, 114.43, 70.88, 67.15.

5.2.2.15 Synthesis of N-(5-(bromoethynyl)pyridin-2-yl)isonicotinamide (4act-Br)

In a round bottomed flask covered with aluminum foil, acetonitrile (80 mL) was degassed with dinitrogen. N-(5-((trimethylsilyl)ethynyl)pyridin-2-yl)isonicotinamide (0.980 g, 3.32 mmol) and

AgF (1.180 g, 6.63 mmol) were added to acetonitrile before the introduction of N-bromosuccinimide (0.840 g, 6.63 mmol). The mixture was connected to a dinitrogen inlet and stirred for 6 days. Completion of the reaction was monitored with TLC and the resulting suspension was filtered. The filtrate was evaporated to dryness and redissolved in 150 mL ethylacetate:diethyl ether (4:1). The organic layer was washed with water and dried with anhydrous MgSO4 and concentrated *in vacuo.* The resultant solid was purified by passing through a ~6 cm silica plug using hexane:ethyl acetate (10:1) to obtain the pure product. Yield 10%, 179-181°C. ^{1}H NMR (400 MHz, DMSO-d_6) δ 11.34 (s, 1H), 8.76 (s, 2H), 8.56 (s, 1H), 8.22 (s, 1H), 8.01 (s, 1H), 7.89 (s, 2H).

5.2.2.16 Synthesis of N-(5-(iodoethynyl)pyridin-2-yl)isonicotinamide (4act-I)

In a round bottomed flask covered with aluminum foil, acetonitrile (50 mL) was degassed with dinitrogen. N-(5-((trimethylsilyl)ethynyl)pyridin-2-yl)isonicotinamide (0.800 g, 2.7 mmol) and AgF (0.375 g,2.98 mmol) were added to acetonitrile before the introduction of N-iodosuccinimide (0.667 g, 6.63 mmol). The mixture was connected to a dinitrogen inlet and stirred for 3 days. Completion of the reaction was monitored with TLC and the resulting suspension was filtered. The filtrate was evaporated to dryness and redissolved in 150 mL ethylacetate:diethyl ether (4:1). The organic layer was washed with water and dried with anhydrous MgSO4 and concentrated *in vacuo.* The resultant solid was purified by passing through a ~6 cm silica plug using hexane:ethyl acetate (10:1) to obtain the pure product. Yield 8%, decomp. 215-217°C. ^{1}H NMR (400 MHz, DMSO-d_6) δ 11.32 (s, 1H), 8.77 (s, 2H), 8.50 (s, 1H), 8.19 (s, 1H), 7.95 (s, 1H), 7.89 (s, 2H). ^{13}C NMR (101 MHz, DMSO-d_6) δ 165.29, 151.65, 151.57, 150.66, 141.88, 141.49, 122.32, 116.47, 114.52, 89.88, 21.59.

5.2.2.17 Synthesis of N-(5-ethynylpyridin-2-yl)benzamide (Bz-act-H)

N-(5-((trimethylsilyl)ethynyl)pyridin-2-yl)benzamide (0.294 g, 1 mmol) was dissolved in methanol. Then, K_2CO_3 (0.138g, 1 mmol) was added into the solution. The mixture was stirred at room temperature. The reaction completion was monitored by TLC. Once the reaction was completed the solvent was evaporated to dryness and the solid was redissolved in ethyl acetate. The organic layer was washed with water and dried with anhydrous $MgSO_4$. The solid was purified by flash chromatography using hexane:ethyl acetate (10:1) to obtain the pure product. 50% ^{1}H NMR (400 MHz, DMSO-d6) δ 11.02 (s, 1H), 8.51 (d, J = 2.3 Hz, 1H), 8.23 (d, J = 8.6 Hz, 1H), 8.06 – 7.99 (m, 2H), 7.96 (dd, J = 8.6, 2.4 Hz, 1H), 7.65 – 7.56 (m, 1H), 7.52 (t, J = 7.6 Hz, 2H), 4.37 (s, 1H). ^{13}C NMR (101 MHz, DMSO-d6) δ 166.65, 152.32, 151.24, 141.55, 134.29, 132.61, 128.86, 128.57, 114.64, 114.48, 83.60, 80.99.

5.2.2.18 Synthesis of N-(5-ethynylpyridin-2-yl)picolinamide (2act-H)

N-(5-((trimethylsilyl)ethynyl)pyridin-2-yl)picolinamide (0.321 g, 1.08 mmol) was dissolved in methanol. Then, K_2CO_3 (0.138g, 1.08 mmol) was added into the solution. The mixture was stirred at room temperature. The reaction completion was monitored by TLC. Once the reaction was completed the solvent was evaporated to dryness and the solid was redissolved in ethyl acetate. The organic layer was washed with water and dried with anhydrous $MgSO_4$. The solid was purified by flash chromatography using hexane:ethyl acetate (10:1) to obtain the pure product. 55% ^{1}H NMR (400 MHz, DMSO-d_6) δ 10.54 (s, 1H), 8.77 (s, 1H), 8.51 (s, 1H), 8.29 (d, *J* = 8.6 Hz, 1H), 8.22 (d, *J* = 7.8 Hz, 1H), 8.12 (s, 1H), 8.01 (d, *J* = 2.2 Hz, 1H), 7.74 (s, 1H), 4.39 (s, 1H). 13C NMR (101 MHz, DMSO-d6) δ 162.59, 151.75, 150.59, 149.28, 148.73, 142.11, 139.07, 128.25, 122.89, 115.19, 113.17, 83.87, 80.80.

5.2.2.19 Synthesis of N-(5-ethynylpyridin-2-yl)nicotinamide (3act-H)

N-(5-((trimethylsilyl)ethynyl)pyridin-2-yl)nicotinamide (0.275 g, 0.93 mmol) was dissolved in methanol. Then, K_2CO_3 (0.138g, 1 mmol) was added into the solution. The mixture was stirred at room temperature. The reaction completion was monitored by TLC. Once the reaction was completed the solvent was evaporated to dryness and the solid was redissolved in ethyl acetate. The organic layer was washed with water and dried with anhydrous $MgSO_4$. The solid was purified by flash chromatography using hexane:ethyl acetate (10:1) to obtain the pure product. 48% ^{1}H NMR (400 MHz, DMSO-d_6) δ 11.29 (s, 1H), 9.12 (s, 1H), 8.76 (s, 1H), 8.52 (s, 1H), 8.33 (s, 1H), 8.24 (s, 1H), 7.99 (s, 1H), 7.53 (s, 1H). ^{13}C NMR (101 MHz, DMSO-d_6) δ 165.37, 152.95, 151.81, 151.63, 149.54, 141.83, 136.33, 130.19, 123.90, 116.25, 114.39, 89.92, 21.39.

5.2.2.20 Synthesis of N-(5-ethynylpyridin-2-yl)isonicotinamide (4act-H)

N-(5-((trimethylsilyl)ethynyl)pyridin-2-yl)isonicotinamide (0.342 g, 1.15 mmol) was dissolved in methanol. Then, K_2CO_3 (0.138 g, 1.15 mmol) was added into the solution. The mixture was stirred at room temperature. The reaction completion was monitored by TLC. Once the reaction was completed the solvent was evaporated to dryness and the solid was redissolved in ethyl acetate. The organic layer was washed with water and dried with anhydrous $MgSO_4$. The solid was purified by flash chromatography using hexane:ethyl acetate (10:1) to obtain the pure product. 48% ^{1}H NMR (400 MHz, DMSO-d_6) δ 11.34 (s, 1H), 8.78 (s, 2H), 8.54 (s, 1H), 8.23 (s, 1H), 8.00 (s, 1H), 7.89 (s, 2H), 4.39 (s, 1H). ^{13}C NMR (101 MHz, DMSO-d_6) δ 165.34, 151.83, 151.32, 150.70, 141.73, 141.45, 122.31, 115.15, 114.64, 83.85, 80.86.

5.3 Results

5.3.1 Molecular electrostatic potentials (MEPs)

The MEPs of the twenty targets molecules are given (Figure 5.3)

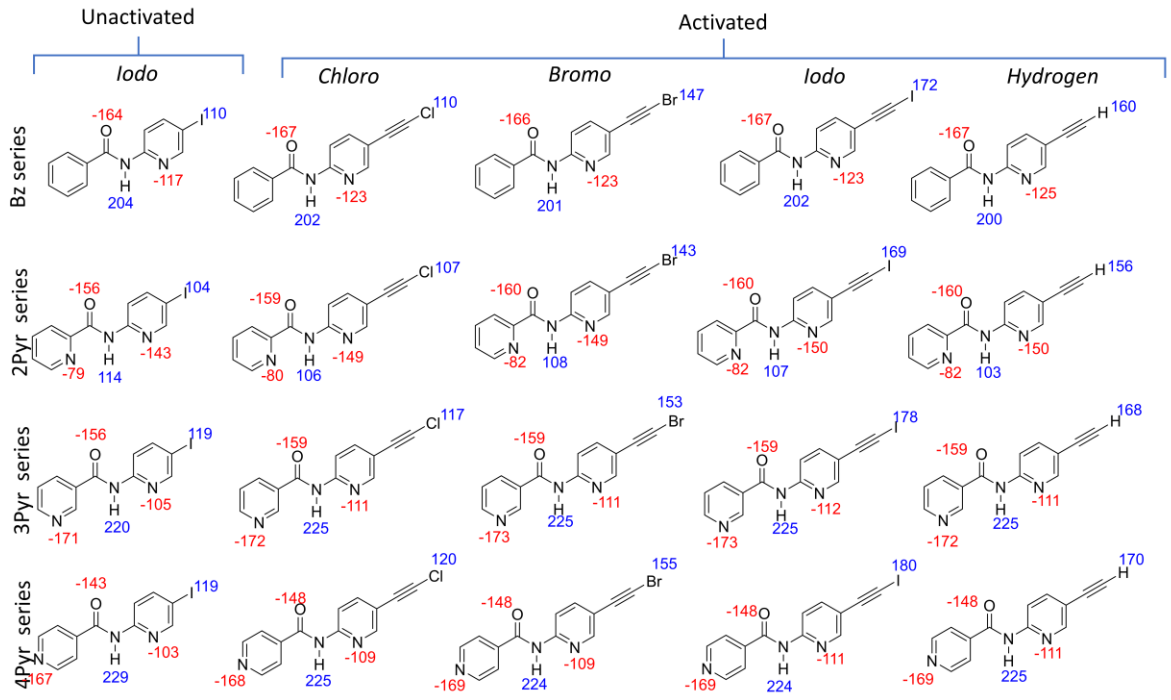

Figure 5.3. MEP values (kJ/mol) at most likely XB/HB donor and acceptor sites

5.3.2 Results from single crystal data

The four crystal strutures for the unactivated targets have been previously reported (see chapter 2).[17] Out of the sixteen new activated compounds crystallographic data were obtained for fourteen of them, as well as two polymorphs for Bz-act-I. The solvents used for cystal growth are listed in Table 5.1.

Table 5.1. Solvents used for crystal growth and crystal descriptions

Compound	Code	Solvent	Color and morphology
N-(5-(chloroethynyl)pyridin-2-yl)benzamide	Bz-act-Cl	Methanol	Colorless, plate
N-(5-(bromoethynyl)pyridin-2-yl)benzamide	Bz-act-Br	Methanol	Light yellow, plate
N-(5-(iodoethynyl)pyridin-2-yl)benzamide	Bz-act-I (Form 1)	Methanol	Yellow, block
	Bz-act-I (Form 2)	Methanol	Yellow, needle
N-(5-ethynylpyridin-2-yl)benzamide	Bz-act-H	Methanol	Colorless, block
N-(5-(chloroethynyl)pyridin-2-yl)picolinamide	2act-Cl	Acetone	Colorless, plate
N-(5-(bromoethynyl)pyridin-2-yl)picolinamide	2act-Br	Acetone	Colorless, needle
N-(5-ethynylpyridin-2-yl)picolinamide	2act-H	Methanol	Colorless, block
N-(5-(chloroethynyl)pyridin-2-yl)nicotinamide	3act-Cl	Acetonitrile:Ethyl acetate	Light yellow, needle
N-(5-(bromoethynyl)pyridin-2-yl)nicotinamide	3act-Br*	Methanol:Acetone	Colorless, needle
N-(5-(iodoethynyl)pyridin-2-yl)nicotinamide	3act-I	Methanol	Yellow, block
N-(5-ethynylpyridin-2-yl)nicotinamide	3act-H	Methanol	Colorless, plate
N-(5-(chloroethynyl)pyridin-2-yl)isonicotinamide	4act-Cl	Ethnyl acetate	Colorless, plate
N-(5-(bromoethynyl)pyridin-2-yl)isonicotinamide	4act-Br	Ethnyl acetate	Colorless, needle
N-(5-(iodoethynyl)pyridin-2-yl)isonicotinamide	4act-I	Acetone:THF	Yellow, block

*Preliminary structure

In the Bz series, the primary intermolecular interactions in the structure of the unactivated Bz-I, are a N-H···N_1(py)/N_1(py)···H-N synthon, and a C-I···π halogen bond (Figure 4a). In Bz-act-Cl and Bz-act-Br too, N-H···N(py)/N(py)···H-N synthons produce symmetry related dimers, accompanied by C-X···π halogen bonds. Both polymorphs of Bz-act-I displayed a C-I···N_1 halogen bond. In Bz-act-I (Form 1), surprisingly no hydrogen bonding was shown by the amide nitrogen, while in Form 2, an N-H···O=C interaction is present which links adject molecules. In

Bz-act-H, again the N-H···N(py)/N(py)···H-N synthon leads to dimers, and a -≡-C-H···O=C interaction is observed (Figure 5.4b-f). The relevant hydrogen- and halogen and bond geometries in the five crystal structures of these compounds are given in Table 5.2

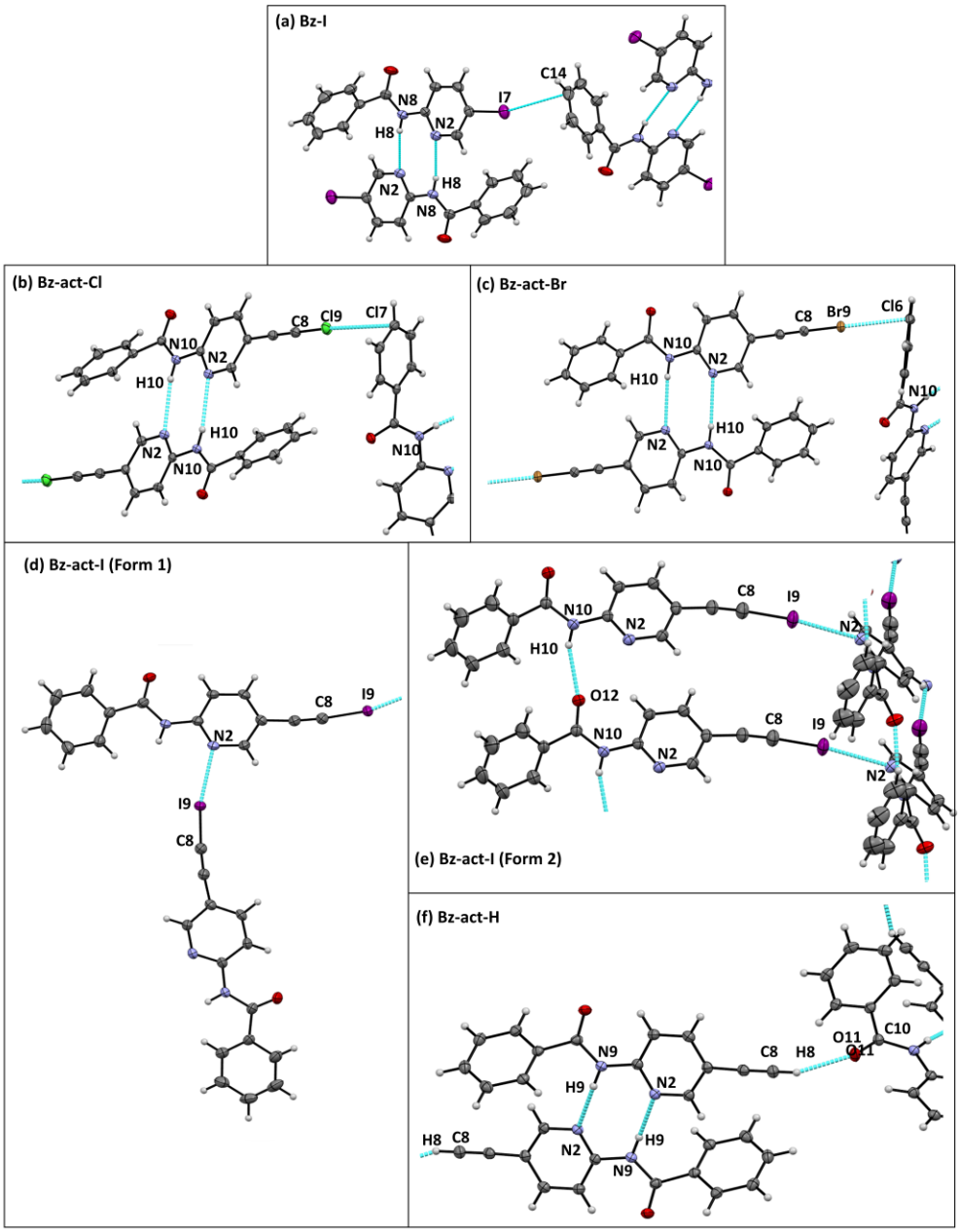

Figure 5.4. Primary interactions in single crystal structures of (a) Bz-I, (b) Bz-act-Cl, (c) Bz-act-Br (d) Bz-act-I (Form 1) (e) Bz-act-I (Form 2) and (f) Bz-act-H

Table 5.2. Hydrogen- and halogen-bond parameters of crystal structures for compounds in the Bz-act series

Code	D-H/I···A	D/I···A (A)	D-H···A (deg)
Bz-act-Cl	N10-H10···N2	3.204(6)	168.1(1)
	C8-Cl9···C17	3.346(1)	157.4(5)
Bz-act-Br	N10-H10···N2	3.208(2)	167(2)
	C8-Br9···C17	3.336 (2)	173.60(7)
Bz-act-I (Form 1)	C8-Cl9···N2	2.884(4)	167.4(2)
Bz-act-I (Form 2)	N10-H10···O12	3.693(2)	150.51(1)
	C8-Cl9···N2	2.886(1)	169.7(7)
Bz-act-H	N9-H9···N2	3.105(1)	158.8(6)
	C8-H8···O11	3.161(1)	154.6(7)

In the unactivated iodo compounds of the 2Pyr series, a N-H···N_2(py) intramolecular interaction is formed and structure directing C-I···N and C-I···I halogen bonds are present (Figure 5.5a). As expected, in 2act-Cl, 2act-Br and 2act-H, the N-H···N_2(py) intramolecular hydrogen bond is formed. In 2act-Cl an additional C-Cl···π halogen bond was present while in 2act-Br, an analogous C-Br···N was observed. In the crystal structure of 2act-H, the ethynyl hydrogen atom forms a C-H···O=C hydrogen bond (Figure 5.5). The relevant hydrogen- and halogen and bond geometries in the three crystal structures from these compounds are given in Table 5.3.

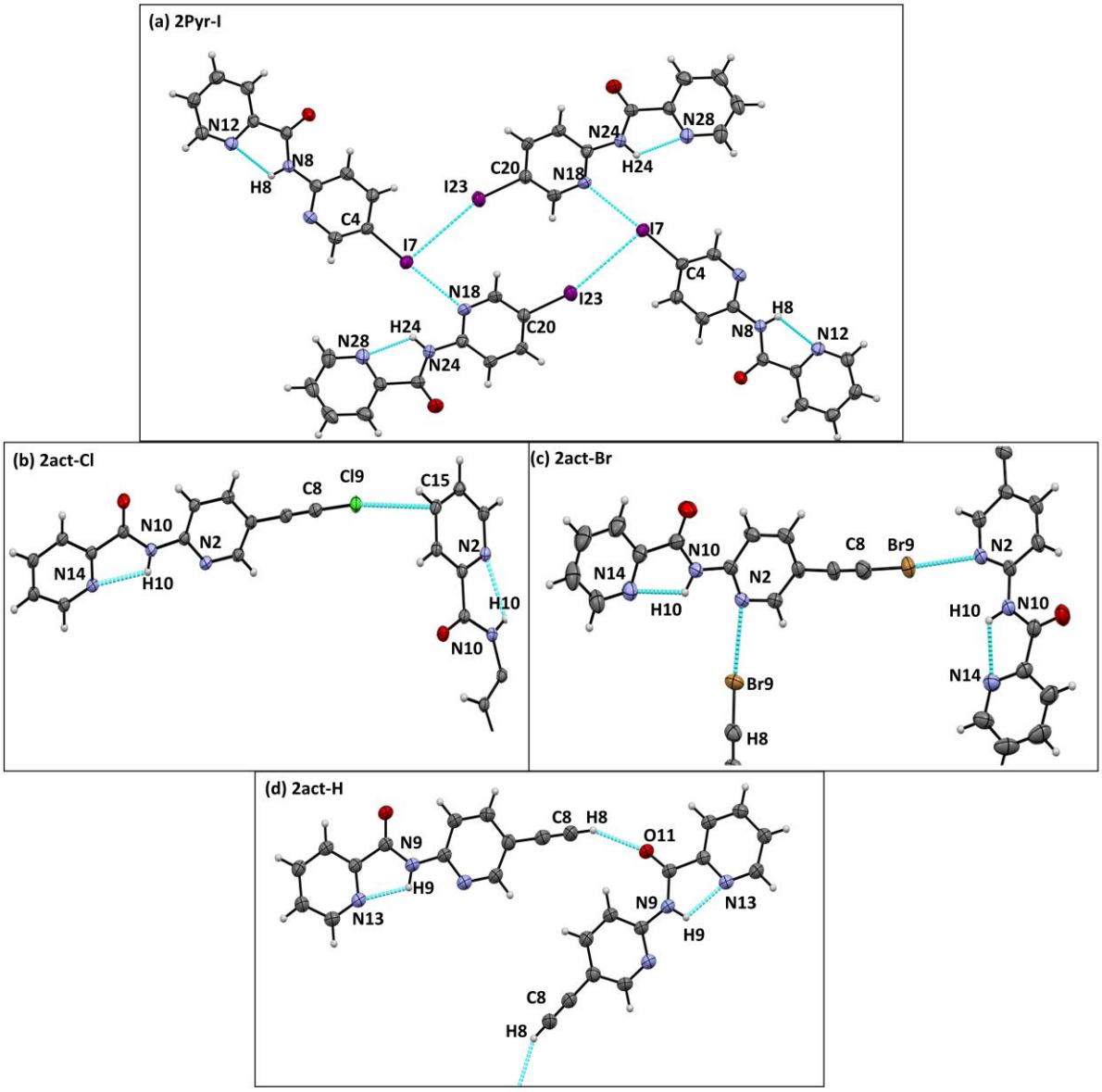

Figure 5.5. Primary interactions in the crystal structures of (a) 2Pyr-I, (b) 2act-Cl, (c) 2act-Br (d) Bz-act-H

Table 5.3. Hydrogen- and halogen-bond parameters in the crystal structures of 2act compounds

Code	**D-H/I···A**	**D/I···A (A)**	**D-H···A (deg)**
2act-Cl	N10-H10···N14	2.702(4)	110.47(1)
	C8-Cl9···C15	3.347(6)	167.14(2)
2act-Br	N10-H10···N14	2.689(1)	110.51(4)
	C8-Cl9···N2	2.940(1)	175.70(1)
2act-H	N9-H9···N13	2.626(6)	112.57 (1)
	C8-H8···O11	3.352(5)	150.982(4)

In the 3Pyr series, the primary non-covalent interaction in the unactivated iodo compound is a N-H···N_2(py) synthon and, surprisingly, no structure directing interactions are shown by the halogen atom. The same is true for both 3act-Cl and 3-act-Br; each present a N-H···N_2(py) synthon with no additional halogen bonds. In 3act-I, N-H···N_1(py)/N_1(py)···H-N hydrogen bonds lead to dimer formation. Additionally, a C-I···N_2 halogen bond is also formed. The N-H···N_2 interaction in the unactivated parent compound appears in 3act-H as well, and it is accompanied by a C-H···O=C interaction (Figure 6a-e). The relevant hydrogen- and halogen and bond geometries in these crystal structures are given in Table 5.4.

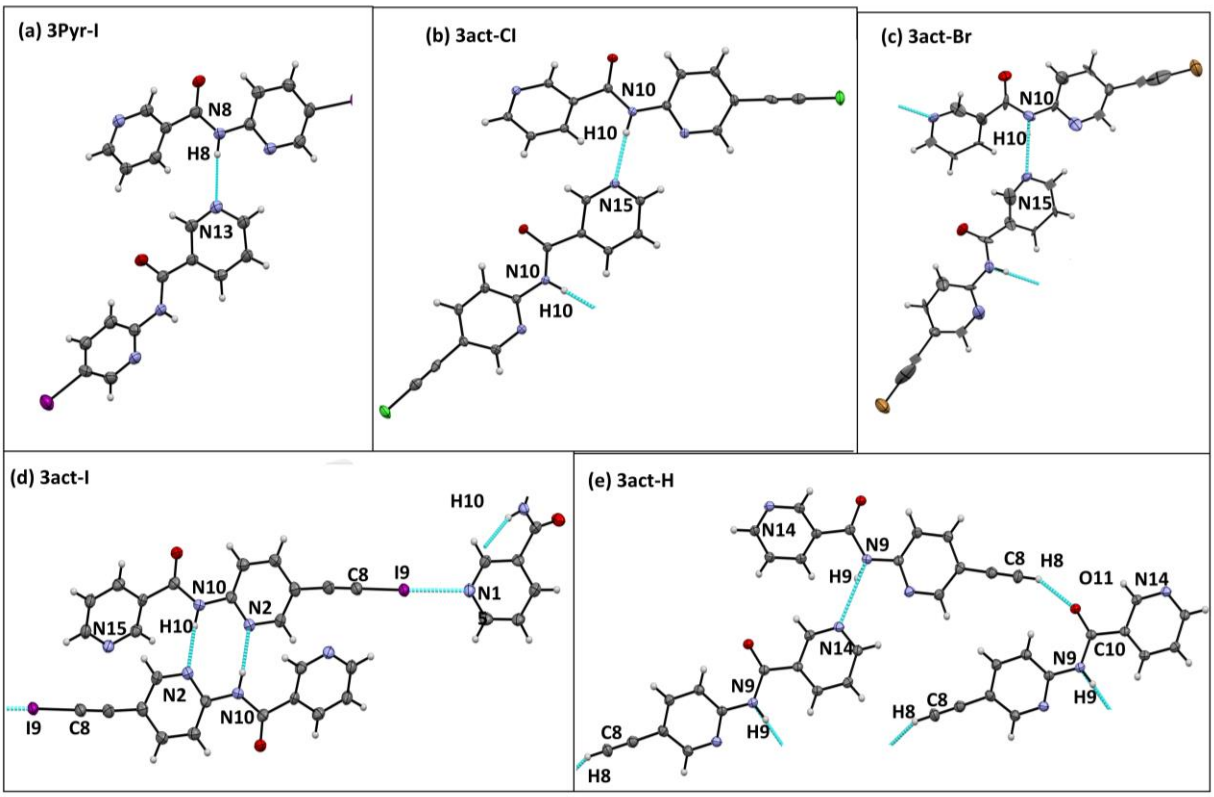

Figure 5.6. Primary interactions in the crystal structures of (a) 3Pyr-I, (b) 3act-Cl, (c) 3act-Br (d) 3act-H

Table 5.4. Hydrogen- and halogen-bond parameters of crystal structures of 3act targets

Code	**D-H/I···A**	**D/I···A (A)**	**D-H···A (deg)**
3act-Cl	N10-H10···N15	3.027(2)	164.04(1)
3act-Br	N10-H10···N15	3.050(3)	171.06(2)
3act-I	N10-H10···N2	3.156(5)	155.3(3)
	C8-Cl9···N15	2.793(4)	178.27(8)
3act-H	N9-H9···N14	3.106(1)	158.84(6)
	C8-Cl9···O11	3.161(1)	154.57(7)

In the 4Pyr targets, the unactivated iodo parent compound was the only compound where a halogen bond was competitive with a hydrogen bond. Two polymorphs of 4Pyr-I (Form 1 and Form 2) were obtained-i (Figure 5.7a and b) (See chapter 2) In both structures, a C-I···N_2(py) halogen bond was formed accompanied by either N-H···N_1(py)/N_1(py)···H-N or N-H···O=C, respectively. In

the activated 4act-Cl target, an N-H···N_2(py) hydrogen bond leads to infinite 1-D supramolecular chains. There are no notable halogen bonds. In 4act-Br, symmetry related dimers are produced by H···N_1(py)/N_1(py)···H-N synthon. Additionally, halogen bonding, C-Br···N_2(py) is also formed. In 4act-I too, once again the hydrogen bonding, H···N_1(py)/N_1(py)···H-N, resulted in dimer formation and C-I···N_2(py) occurred (Figure 5.7a-d). The relevant hydrogen- and halogen and bond geometries in these three crystals are given in Table 5.5.

Table 5.5. Hydrogen- and halogen-bond parameters of crystal structures of 4act targets

Code	**D-H/I···A**	**D/I···A (A)**	**D-H···A (deg)**
4act-Cl	N7-H7···N16	3.150(2)	167.25(1)
4act-Br	N10-H10···N2	3.099(2)	159.77(1)
	C8-Br9···N16	2.957(2)	172.06(8)
4act-I	N10-H10···N2	3.0346(5)	138.65(8)
	C8-Cl9···N16	2.787(5)	179.86(7)

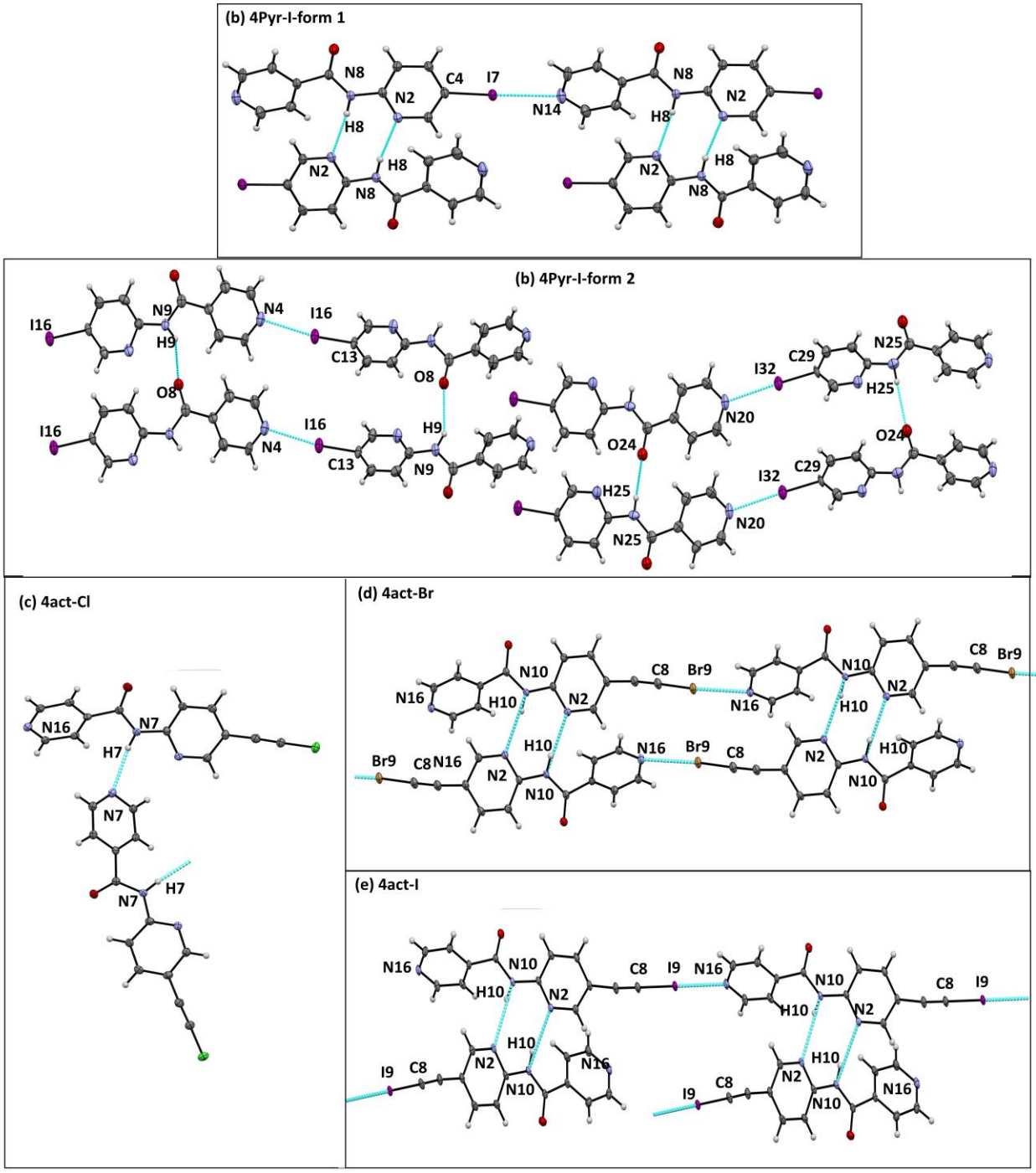

Figure 5.7. Primary interactions in the crystal structures of (a) 4Pyr-I (Form 1), (b) 4Pyr-I (Form 2) (c) 4Pyr-I (Form 2), (d) 4act-Cl (e) 4act-Cl (f) 4act-I

A summary of the halogen bonds in the parent compounds and the halogen and ethynyl hydrogen bonds in the activated analogues is given in Table 5.6.

Table 5.6. Halogen- and ethynyl hydrogen bonds in the structures of the twenty compounds analyzed herein.

	Unact-I	**Act-Cl**	**Act-Br**	**Act-I**	**Act-H**
Bz	C-X···π	C-X···π	C-X···π	C-X···N (Form I) C-X···N (Form 2)	C-H···O=C
2Pyr	C-X···N and C-X···X	C-X···π	C-X···N	No SXCRD data	C-H···O=C
3Pyr	none	none	none	C-X···N	C-H···O=C
4Pyr	C-X···N (Form I) C-X···N (Form 2)	none	C-X···N	C-X···N	No SXCRD data

5.4 Discussion

Within each series when the substituent X is ethynyl chloro, bromo, iodo or hydrogen, the MEPs at the acceptor sites (N, O) and amide H are very close to each other (within ≤ 2 units). Within each series, the MEPs of the acceptor sites (N, O) and amide H of activated targets, are also comparable to those of the unactivated parent compounds (within ≤ 10 units), Figure 5.8.

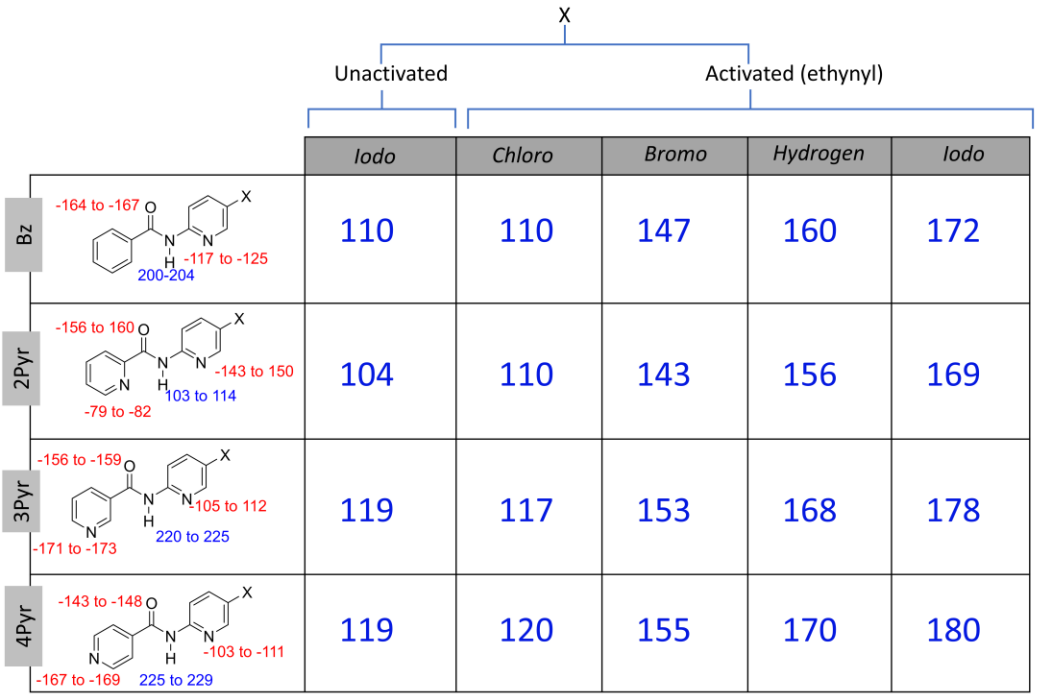

Figure 5.8. Summarized data of MEPs (in kJ/mol).

The MEP values of X within each series follows the trend of iodine < chloroethynyl < bromoethynyl< ethynyl hydrogen < iodoethynyl.

In the unactivated targets (see Chapter 2) halogen bonding was shown only with iodine while chlorine and bromine did not show any halogen bonding. This could be related to the MEP value of the halogen bond donor site (the unactivated iodine having the highest MEP site). Upon changing the connectivity of the halogen atoms to a sp carbon by attaching the halogens to an ethynyl arm, the MEP potentials of all the halogens increased. By this the σ-hole value of the least polarizable halogen (chlorine) was bought into the realm to that of iodine in the unactivated target. The SCXRD, demonstrates that this also led to the targeted increase in ability of the halogen atom to engage in structure directing interactions. With this structural modification (attachment to ethynyl group), the two halogens chlorine and bromine began to show structure directing interactions. In 2/4 cases (Bz-act-Cl and 2act-Cl) halogen bonding was observed with

chloroethynyl, and in 3/4 cases (Bz-act-Br, 2act-Br, and 4act-Br) halogen bonding was observed with bromoethynyl. The iodoethynyl compounds displayed halogen bonding in 4/4 cases. The frequency of halogen bond formation ranks in the order of chloroethynl<iodine~bromoethynyl<iodoethynyl. Both 3Pyr-I and 3act-Br were the only two cases where these two halogen bond donors (iodine and bromoethynyl) did not show any halogen bonding. Owing to the higher σ-hole value in bromoethynyl than iodine, it generally serves as a better halogen bond donor than iodine.[18]However, in 3act-Br, the bromoethynyl failed to function as a XB donor. The obstacles faced by the halogen bond donors of the series were however overcome by the iodoethynyl in 3act-I, making iodoethynyl the most superior halogen bond donor under investigation here. The frequency of halogen bond formation in the structures obtained along with MEP are considered. (Figure 5.9). Thus, in the presence of a halogen bond donor with MEP ~170 kJ/mol a structure directing interaction was guaranteed (Figure 5.9).

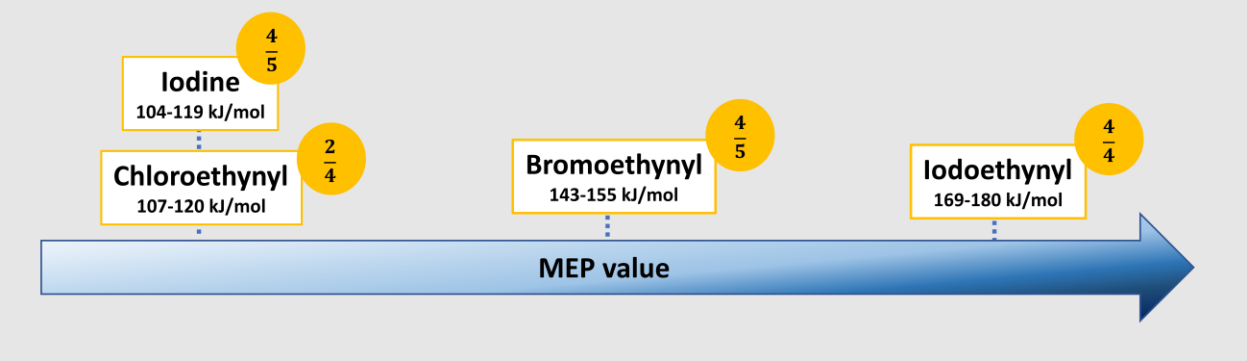

Figure 5.9. Trend in MEP of iodine and ethynyl substituent donor sites within each series and frequency of forming structure directing interactions.

The SXCRD of all four analogues pairs of unactivated iodo and chloroethynyl crystals were obtained (Table 5.6). Halogen bonding is not shown by either of the halogens in the 3Pyr targets (3Pyr-I and 3act-Cl). In the 4Pyr series, although competitive halogen bonding was shown in 4Pyr-

I no halogen bonding interactions were shown by 4act-Cl. In the Bz and 2Pyr targets both halogen donor sites formed halogen bonding. In the Bz-I and Bz-act-Cl pair, both halogens formed C-X···π interaction and lead to synthon mimicry. In the other pair, 2Pyr-I and 2act-Cl, while the iodine formed C-X···N and C-X···X halogen bonds, the ethynyl chlorine formed a C-X···π interaction and thus, synthon mimicry was not observed. The results indicate that although the σ- hole values of the two halogen atoms are very close to each other, they vary in their ability to form halogen bonds and may not necessarily pick the same acceptor site.

The halogen bonds either involved a pyridyl nitrogen or π (and negative belt of iodine in 2Pyr-I). The MEP value of the ethylnyl hydrogen lies between that of the σ- hole value of halogens in bromoethynyl and iodoethynyl compounds. Yet, in 3/3 cases the ethynyl hydrogen formed a C-H···O=C interaction. The selection of a 'different' type of acceptor site can be rationalized based on hydrogen atom being much smaller and harder, and preferring a harder acceptor site (carbonyl oxygen over nitrogen or π) than the halogen bond donors.

5.5 Conclusions

In our previous work (chapter 2), containing the unactivated halogens no structure directing interactions were shown by either chlorine (0/4) or bromine (0/4) while iodine did (4/5). Here, we increase the MEP of all three halogens by connecting to an ethynyl arm.

Upon activation, the σ-hole values rank in the order of chloroethynl~iodine < bromoethynyl < iodoethynyl. Though, the unactivated iodine and chloroethynyl targets had comparable σ- hole values the frequency of XB formation as well as the choice of acceptor sites were different for these two XB donors. Thus, the halogen bond forming frequency varies in the order of chloroethynyl < iodine~bromoethynyl < iodoethynyl. Chloroethynyl, iodine and bromoethynyl formed halogen bonds to π or N (and iodine in one example, 2Pyr-I). The iodoethynyl halogen-

bond donor (MEP 169 - 180 kJ) emerged as the most superior XB donor forming halogen bonds 4/4 times, and the interaction was always to a pyridyl nitrogen. The ethynyl hydrogen had a MEP between halogens of bromoethynyl and iodoethynyl, and selected a carbonyl oxygen as an acceptor site in 3/3 cases (Figure 5.10).

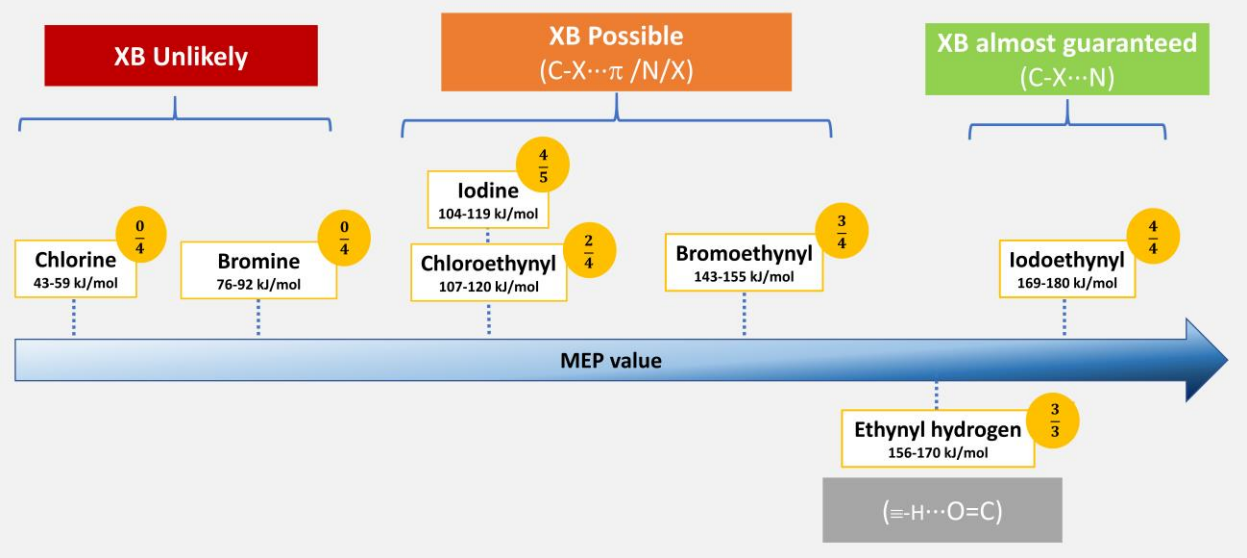

Figure 5.10. Frequency of structure directing interactions of XB donors and ethynyl hydrogen in this study with MEP variation.

5.6 References

[1] Desiraju, G. R. Crystal engineering: a holistic view. *Angew. Chem., Int. Ed.* **2007,** *46*, 8342-8356

[2] Etter, M. C. Encoding and decoding hydrogen-bond patterns of organic compounds. *Acc. Chem. Res.* **1990**, *23*, 120−126

[3] Aakeröy, C. B.; Chopade, P. D.; Desper, J. Avoiding "synthon crossover" in crystal engineering with halogen bonds and hydrogen bonds. *Cryst. Growth Des.***2011**, *11*, 5333-5336.

[4] Aakeröy, C. B.; Epa, K.; Forbes, S.; Schultheiss, N.; Desper, J. Ranking Relative Hydrogen-Bond Strengths in Hydroxybenzoic Acids for Crystal-Engineering Purposes. *Chem. **Eur**. J,* **2013**, *19*, 14998-15003.

[5] McDowell, S. A. Sigma-hole cooperativity in anionic [FX···CH3···YF]−(X,Y=Cl,Br) complexes. *Chem. Phys. Lett.* **2014**, *598*, 1-4.

[6] Lim, J. Y.Beer, P. D. Sigma-hole interactions in anion recognition. *Chem*.**2018**, 4, *4*731-783.

[7] Clark, T.; Hennemann, M.; Murray, J. S.; Politzer, P. Halogen bonding: the σ-hole. *J. **Mol**. Model*. **2007**, *13*, 291-296.

[8] Messina, M. T.; Metrangolo, P.; Panzeri, W.; Ragg, E.; Resnati, G. Perfluorocarbon-Hydrocarbon Self-Assembly. Part 3. Liquid Phase Interactions between Perfluoroalkylhalides and Heteroatom Containing Hydrocarbons. Tetrahedron Lett. **1998**, *39*, 9069−9072.

[9] Metrangolo, P.; Panzeri, W.; Recupero, F.; Resnati, G. Perfluorocarbon-Hydrocarbon Self-Assembly Part 16. 19F NMR Study of the Halogen Bonding between Halo-Perfluorocarbons and Heteroatom Containing Hydrocarbons. *J. Fluorine Chem*. **2002,** *114*, 27−33

[10] Desiraju, G. R.; Harlow, R. L. Cyano-Halogen Interactions and Their Role in the Crystal Structures of the 4-Halobenzonitriles. *J. Am. Chem. Soc*. **1989,** *111*, 6757−6764

[11] Kniep, F.; Stefan H.J.; Qi, Z.; Sebastian M. W,: Severin, S.; Ingo, S.; Eberhardt, H.; Stefan, M. H. "Organocatalysis by neutral multidentate halogen-bond donors. *Angew. Chem., Int. Ed.* 52, no. 27 **2013**, *52*, 7028-7032.

[12] Lange, A.; Heidrich, J.; Zimmermann, M. O.; Exner, T. E.; Boeckler, F. M. Scaffold effects on halogen bonding strength. J. *Chem. Inf. Model*. **2019,** *59*, 885-894.

[13] Khavasi, H. R.; Hosseini, M.; Tehrani, A. A.; Naderi, S. Strengthening N··· X halogen bonding via nitrogen substitution in the aromatic framework of halogen-substituted arylpyrazinamides. *CrystEngComm*. **2014,** *16*, 4546-4553.

[14] Aakeröy, C. B.; Wijethunga, T. K.; Desper, J.;Daković, M. Crystal engineering with iodoethynylnitrobenzenes: a group of highly effective halogen-bond donors. *Cryst. Growth Des.* **2015**. *15*, 3853-3861.

[15] Metrangolo, P.; Meyer, F.; Pilati, T.; Resnati, G.; Terraneo, G. Halogen Bonding in Supramolecular Chemistry. Angew. Chem., Int. Ed. **2008**, *47*, 6114−6127

[16] Electrostatic potentials were calculated with density functional B3LYP level of theory using 6-311++G** basis set in vacuum, using Spartan 08' software

[17] Abeysekera, A.M.; Day, V.W.; Sinha, A.S.; Aakeröy, C.B. Mapping out the Relative Influence of Hydrogen and Halogen Bonds in Crystal Structures of a Family of Amide-Substituted Pyridines. *Cryst. Growth Des.* **2020**, 20, 7399–7410.

[18] Aakeröy, C. B., Baldrighi, M., Desper, J., Metrangolo, P., Resnati, G. Supramolecular Hierarchy among Halogen-Bond Donors. *Chemistry–A European Journal*, **2013,** *19*, 16240-16247.

Chapter 6 - The role of non-polar components in self-assembly of 2-aminopyridines

6.1 Introduction

The hydrogen bond and other intermolecular interactions such as halogen, and chalcogen bonds are employed in the systematic construction of binary or even higher order molecular solids. There is general acceptance that the hierarchical nature, based on electrostatic component of these non-covalent interactions govern outcomes of intermolecular interactions. However, (electrostatically) non-interacting parts of a molecule can exert a great stabilizing[1,2] effect on molecular assembly. In addition, the ultimate conformation [3,4,5] of a molecule can be influenced by such "inert" parts of a molecule. Thus, subtle changes to a molecular framework can lead to significantly altered supramolecular assemblies. For example, carboxyl acids are well known for the formation of dimers[6], however, phenylpropiolic acid (QENSEK)[7] and acetic acid (ACETAC)[8] both form catemers.

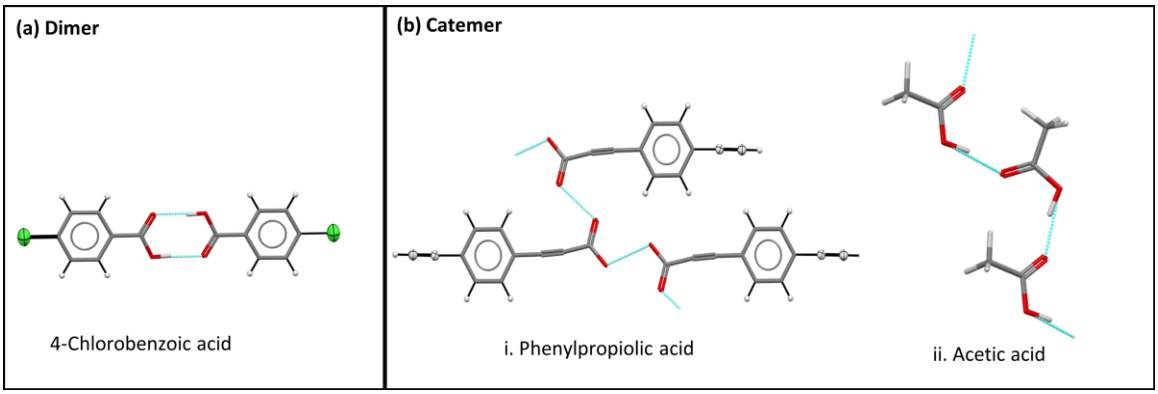

Figure 6.1. (a)Dimers (b) Catemer formed by carboxylic acid group

Another frequently employed vector in supramolecular chemistry is the amide moiety. The amide functional group predominantly occurs in the trans configuration. It is a very reliable synthon due the formation of amide ribbons/chains which has been utilized in constructing coordination polymers[9], hydrogels.[10,11] However, this particular motif can be disrupted by the presence of the bulky triphenylmethyl group in which case the chain is abandoned in favor of an N-H···π interaction.[12,13](Figure 6.2)

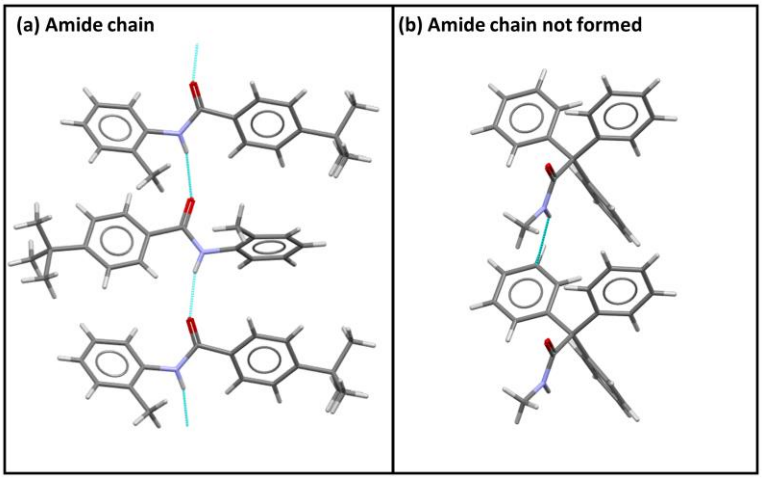

Figure 6.2. (a) amide chain formation [1] (b) amide chain not formed due to bulky group[13].

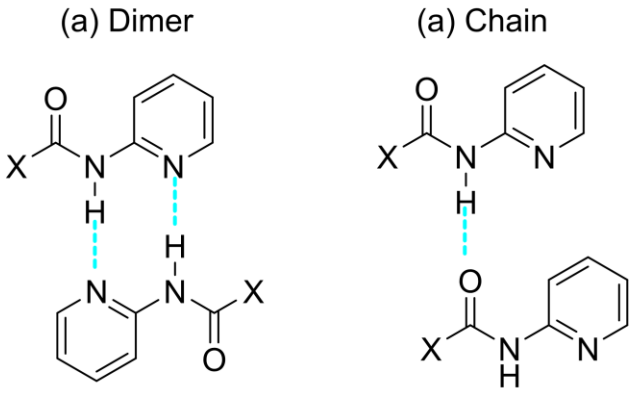

Figure 6.3. Two possible modes of self-aggregation of N-(pyridin-2-yl)alkylamides/2-acylaminopyridine.

In a study from 2010,[14] the self-aggregation in ten 2-acylaminopyridine decorated with non-electrostatically interacting groups as X and A substituents was reported. The X substituent was either an acetyl, propyl, *i*-Pr, t-Bu, 1-Ad group, while A was either a hydrogen or a methyl group. Each time (5/5 cases) that A was a methyl group, the molecules formed NH···O=C chain. When A=H in combination with X being *i*-Pr, t-Bu, 1-Ad, again NH···O=C chains were formed. In the remaining three cases (A=H and X= acetyl/propyl/*i*-Pr) NH···N_1 dimers were formed. The inference made was that NH···O=C chain formation is driven in order to prevent the steric clash with the bulky substituents (H<methyl while acetyl<propyl< i-Pr<t-Bu/1-Ad).The authors also noted that the C=O IR mode could be used as marker for which of the two motifs were formed in the solid state. In all cases where an NH···O=C chain was present, the C=O stretch was more red shifted (~1670 cm^{-1}) compared to when dimers were formed (~1690 cm^{-1}) (Figure 6.4).

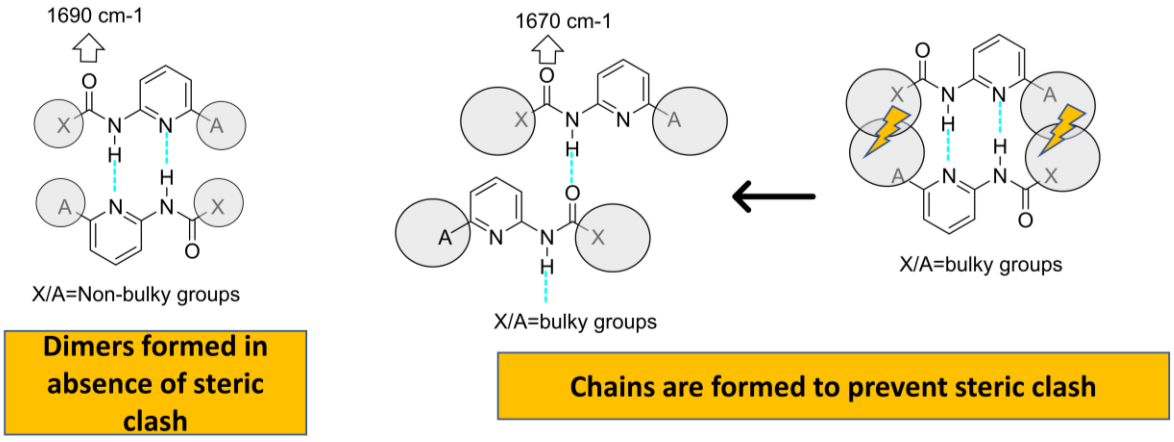

Figure 6.4. Proposed effect of sterics on chain vs. dimer formation.

However, recently obtained crystal structures, both published[15] and unpublished, show that chain formation can occur despite the absence of possible steric interference. In order to address this

unresolved conundrum, we set about to further map out the structural chemistry regarding the self-assembly of compounds containing the N-(pyridin-2-yl)acetamide functionality.

Part A.

First of all, we wanted to establish if/how a substituent at the Y position and at the X position influence supramolecular assembly in twenty closely related target compounds (Figure 6.5), (the structures of only three of these compounds have been published previously).[14,15]

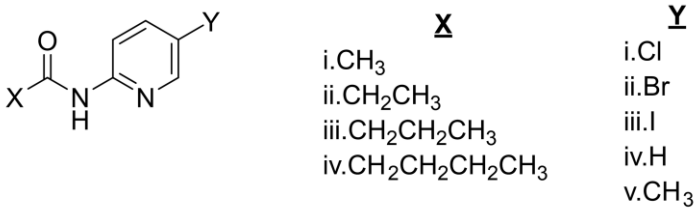

Figure 6.5. Target molecules in this study

We specifically wanted to address the following questions.

- Does the length of alkyl chain at the X position promote chain vs dimer?

- Does the size of the Y substituent affect assembly?

- Does the molecular electrostatic potential of the halogen-bond donor/acceptor affect assembly?

6.2 Experimental – Part A

6.2.1 General – Part A

All precursors, solvents were purchased from commercial sources and used without further purification. ^{1}H NMR spectra and ^{13}C NMR spectra were recorded on A Brucker 400 spectrometer. Melting points were recorded on a Fisher-Johns melting point apparatus or a TA Instruments DSC Q20 differential scanning calorimeter. IR spectra were recorded with a Nicolet 380 FT-IR

spectrometer using an attenuated total reflection (ATR) technique and ZnSe as the crystal. Electrostatic potentials were calculated with density functional B3LYP level of theory using 6-311++G** basis set in vacuum, using Spartan 08' software.

6.2.2 Synthesis – Part A

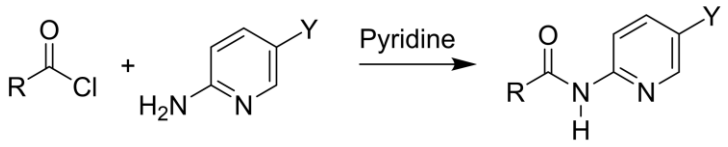

R/X= acetyl/propyl/butyl/pentyl

Y= Cl/Br/I/H/CH_3

6.2.2.1 Synthesis of N-(5-chloropyridin-2-yl)acetamide (Cl-acetyl)

2-Amino-5-chloropyridine (1.28 g, 10.0 mmol)) was dissolved in 50 mL of pyridine and cooled in an ice bath. Acetyl chloride (1.06 mL, 16.0 mmol) was added dropwise maintaining the temperature between 0-5 ºC. After the addition was complete the contents were stirred at room temperature until no further starting material (2-amino-5-chloropyridine) was detected by TLC. Upon completion, chilled water (100 mL) was added and stirred for 15 minutes. The reaction contents were extracted with dichloromethane and the organic layer was washed with saturated sodium bicarbonate solution, brine, water and dried with anhydrous magnesium sulfate, filtered, and concentrated *in vacuo* to isolate the pure product. Yield 88%, m.p 172 – 174 °C. ^{1}H NMR (400 MHz, DMSO-d6) δ 10.66 (s, 1H), 8.40 (s, 1H), 8.15 (s, 1H), 7.89 (s, 1H), 2.10 (s, 3H).

6.2.2.2 Synthesis of N-(5-chloropyridin-2-yl)propionamide (Cl-propyl)

2-Amino-5-chloropyridine (1.28 g, 10.0 mmol) was dissolved in 50 mL of pyridine and cooled in an ice bath. Propyl chloride (1.09 mL, 16.0 mmol) was added dropwise maintaining the temperature between 0-5 ºC. After the addition was complete the contents were stirred at room temperature until no further starting material (2-amino-5-chloropyridine) was detected by TLC.

Upon completion, chilled water (100 mL) was added and stirred for 15 minutes. The reaction contents were extracted with dichloromethane and the organic layer was washed with saturated sodium bicarbonate solution, brine, water and dried with anhydrous magnesium sulfate, filtered, and concentrated *in vacuo* to isolate the pure product. Yield 85%, m.p 126 – 128 °C. ^{1}H NMR (400 MHz, DMSO-d6) δ 10.59 (s, 1H), 8.34 (s, 1H), 8.13 (s, 1H), 7.85 (s, 1H), 2.38 (s, 2H), 1.05 (s, 3H).

6.2.2.3 Synthesis of N-(5-chloropyridin-2-yl)butyramide (Cl-butyl)

2-Amino-5-chloropyridine (1.28 g, 10.0 mmol) was dissolved in 50 mL of pyridine and cooled in an ice bath. Butyl chloride (1.54 mL, 16.0 mmol) was added dropwise maintaining the temperature between 0-5 ºC. After the addition was complete the contents were stirred at room temperature until no further starting material (2-amino-5-chloropyridine) was detected by TLC. Upon completion, chilled water (100 mL) was added and stirred for 15 minutes. The reaction contents were extracted with dichloromethane and the organic layer was washed with saturated sodium bicarbonate solution, brine, water and dried with anhydrous magnesium sulfate, filtered, and concentrated *in vacuo* to isolate the pure product. Yield 80%, m.p 104 – 106 °C. ^{1}H NMR (400 MHz, DMSO-d6) δ 10.61 (s, 1H), 8.35 (s, 1H), 8.12 (s, 1H), 7.86 (s, 1H), 2.36 (s, 2H), 1.58 (s, 2H), 0.88 (s, 3H).

6.2.2.4 Synthesis of N-(5-chloropyridin-2-yl)pentanamide (Cl-pentyl)

2-Amino-5-chloropyridine (1.28 g, 10.0 mmol) was dissolved in 50 mL of pyridine and cooled in an ice bath. Pentyl chloride (1.77 mL, 16.0 mmol) was added dropwise maintaining the temperature between 0-5 ºC. After the addition was complete the contents were stirred at room temperature until no further starting material (2-amino-5-chloropyridine) was detected by TLC. Upon completion, chilled water (100 mL) was added and stirred for 15 minutes. The reaction

contents were extracted with dichloromethane and the organic layer was washed with saturated sodium bicarbonate solution, brine, water and dried with anhydrous magnesium sulfate, filtered, and concentrated *in vacuo* to isolate the pure product. Yield 83%, m.p 103 – 105 °C ^{1}H NMR (400 MHz, DMSO-d6) δ 10.60 (s, 1H), 8.33 (s, 1H), 8.13 (s, 1H), 7.85 (s, 1H), 2.37 (s, 2H), 1.56 (s, 2H), 1.31 (s, 2H), 0.85 (s, 3H).

6.2.2.5 Synthesis of N-(5-bromopyridin-2-yl)acetamide (Br-acetyl)

2-Amino-5-bromopyridine (1.73 g, 10.0 mmol) was dissolved in 50 mL of pyridine and cooled in an ice bath. Acetyl chloride (1.06 mL, 16.0 mmol) was added dropwise maintaining the temperature between 0-5 ºC. After the addition was complete the contents were stirred at room temperature until no further starting material (2-amino-5-bromopyridine) was detected by TLC. Upon completion, chilled water (100 mL) was added and stirred for 15 minutes. The reaction contents were extracted with dichloromethane and the organic layer was washed with saturated sodium bicarbonate solution, brine, water and dried with anhydrous magnesium sulfate, filtered, and concentrated *in vacuo* to isolate the pure product. Yield 90%, m.p 174 – 176 °C. ^{1}H NMR (400 MHz, DMSO-d6) δ 10.65 (s, 1H), 8.42 (s, 1H), 8.07 (s, 1H), 7.97 (s, 1H), 2.09 (s, 3H).

6.2.2.6 Synthesis of N-(5-bromopyridin-2-yl)propionamide (Br-propyl)

2-Amino-5-bromopyridine (1.73 g, 10.0 mmol) was dissolved in 50 mL of pyridine and cooled in an ice bath. Propyl chloride (1.09 mL, 16.0 mmol) was added dropwise maintaining the temperature between 0-5 ºC. After the addition was complete the contents were stirred at room temperature until no further starting material (2-amino-5-bromopyridine) was detected by TLC. Upon completion, chilled water (100 mL) was added and stirred for 15 minutes. The reaction contents were extracted with dichloromethane and the organic layer was washed with saturated sodium bicarbonate solution, brine, water and dried with anhydrous magnesium sulfate, filtered,

and concentrated *in vacuo* to isolate the pure product. Yield 85 %, m.p 136 – 138 °C. ^{1}H NMR (400 MHz, DMSO-d6) δ 10.58 (s, 1H), 8.40 (s, 1H), 8.08 (s, 1H), 7.97 (s, 1H), 2.37 (s, 2H), 1.07 (s, 3H).

6.2.2.7 Synthesis of N-(5-bromopyridin-2-yl)butyramide (Br-butyl)

2-Amino-5-bromopyridine (1.73 g, 10.0 mmol) was dissolved in 50 mL of pyridine and cooled in an ice bath. Butyl chloride (1.54 mL, 16.0 mmol) was added dropwise maintaining the temperature between 0-5 ºC. After the addition was complete the contents were stirred at room temperature until no further starting material (2-amino-5-bromopyridine) was detected by TLC. Upon completion, chilled water (100 mL) was added and stirred for 15 minutes. The reaction contents were extracted with dichloromethane and the organic layer was washed with saturated sodium bicarbonate solution, brine, water and dried with anhydrous magnesium sulfate, filtered, and concentrated *in vacuo* to isolate the pure product. Yield 88 %, m.p 110 – 112 °C. ^{1}H NMR (400 MHz, DMSO-d6) δ 10.59 (s, 1H), 8.41 (s, 1H), 8.07 (s, 1H), 7.96 (s, 1H), 2.35 (s, 2H), 1.57 (s, 2H), 0.89 (s, 3H).

6.2.2.8 Synthesis of N-(5-bromopyridin-2-yl)pentanamide (Br-pentyl)

2-Amino-5-bromopyridine (1.73, 10.0 mmol) was dissolved in 50 mL of pyridine and cooled in an ice bath. Pentyl chloride (1.77 mL, 16.0 mmol) was added dropwise maintaining the temperature between 0-5 ºC. After the addition was complete the contents were stirred at room temperature until no further starting material (2-amino-5- bromopyridine) was detected by TLC. Upon completion, chilled water (100 mL) was added and stirred for 15 minutes. The reaction contents were extracted with dichloromethane and the organic layer was washed with saturated sodium bicarbonate solution, brine, water and dried with anhydrous magnesium sulfate, filtered, and concentrated *in vacuo* to isolate the pure product. Yield 80 %, m.p 109 – 111°C. ^{1}H NMR

(400 MHz, DMSO-d6) δ 10.59 (s, 1H), 8.41 (s, 1H), 8.06 (s, 1H), 7.96 (s, 1H), 2.38 (s, 2H), 1.56 (s, 1H), 1.28 (s, 2H), 0.87 (s, 3H).

6.2.2.9 Synthesis of N-(5-iodopyridin-2-yl)acetamide (I-acetyl)

2-Amino-5-iodopyridine (2.20 g, 10.0 mmol) was dissolved in 50 mL of pyridine and cooled in an ice bath. Acetyl chloride (1.06 mL, 16.0 mmol) was added dropwise maintaining the temperature between 0-5 ºC. After the addition was complete the contents were stirred at room temperature until no further starting material (2-amino-5-iodopyridine) was detected by TLC. Upon completion, chilled water (100 mL) was added and stirred for 15 minutes. The reaction contents were extracted with dichloromethane and the organic layer was washed with saturated sodium bicarbonate solution, brine, water and dried with anhydrous magnesium sulfate, filtered, and concentrated *in vacuo* to isolate the pure product. Yield 88 %, m.p 154 – 156°C. ^{1}H NMR (400 MHz, DMSO-d6) δ 10.60 (s, 1H), 8.51 (s, 1H), 8.10 (s, 1H), 7.96 (s, 1H), 2.08 (s, 3H).

6.2.2.10 Synthesis of N-(5-iodopyridin-2-yl)propionamide (I-propyl)

2-Amino-5-iodopyridine (2.20 g, 10.0 mmol) was dissolved in 50 mL of pyridine and cooled in an ice bath. Propyl chloride (1.09 mL, 16.0 mmol) was added dropwise maintaining the temperature between 0-5 ºC. After the addition was complete the contents were stirred at room temperature until no further starting material (2-amino-5-iodopyridine) was detected by TLC. Upon completion, chilled water (100 mL) was added and stirred for 15 minutes. The reaction contents were extracted with dichloromethane and the organic layer was washed with saturated sodium bicarbonate solution, brine, water and dried with anhydrous magnesium sulfate, filtered, and concentrated *in vacuo* to isolate the pure product. Yield 90 %, m.p 139 – 141°C. ^{1}H NMR (400 MHz, DMSO-d6) δ 10.53 (s, 1H), 8.50 (s, 1H), 8.09 (s, 1H), 7.98 (s, 1H), 2.37 (s, 2H), 1.05 (s, 3H).

6.2.2.11 Synthesis of N-(5-iodopyridin-2-yl)butyramide (I-butyl)

2-Amino-5-iodopyridine (2.20 g, 10.0 mmol) was dissolved in 50 mL of pyridine and cooled in an ice bath. Butyl chloride (1.54 mL, 16.0 mmol) was added dropwise maintaining the temperature between 0-5 ºC. After the addition was complete the contents were stirred at room temperature until no further starting material (2-amino-5-iodopyridine) was detected by TLC. Upon completion, chilled water (100 mL) was added and stirred for 15 minutes. The reaction contents were extracted with dichloromethane and the organic layer was washed with saturated sodium bicarbonate solution, brine, water and dried with anhydrous magnesium sulfate, filtered, and concentrated *in vacuo* to isolate the pure product. Yield 86, %, m.p 136 – 138°C ^{1}H NMR (400 MHz, DMSO-d6) δ 10.55 (s, 1H), 8.50 (s, 1H), 8.09 (s, 1H), 7.96 (s, 1H), 2.35 (s, 2H), 1.55 (s, 2H), 0.87 (s, 3H).

6.2.2.12 Synthesis of N-(5-iodopyridin-2-yl)pentanamide (I-pentyl)

2-Amino-5-iodopyridine (1.90 g, 11.0 mmol) was dissolved in 50 mL of pyridine and cooled in an ice bath. Pentyl chloride (1.77 mL, 16.0 mmol) was added dropwise maintaining the temperature between 0-5 ºC. After the addition was complete the contents were stirred at room temperature until no further starting material (2-amino-5-iodopyridine) was detected by TLC. Upon completion, chilled water (100 mL) was added and stirred for 15 minutes. The reaction contents were extracted with dichloromethane and the organic layer was washed with saturated sodium bicarbonate solution, brine, water and dried with anhydrous magnesium sulfate, filtered, and concentrated *in vacuo* to isolate the pure product. Yield 80, %, m.p 118 – 120°C ^{1}H NMR (400 MHz, DMSO-d6) δ 10.55 (s, 1H), 8.50 (s, 1H), 8.09 (s, 1H), 7.95 (s, 1H), 2.35 (s, 2H), 1.52 (s, 2H), 1.30 (s, 2H), 0.89 (s, 3H).

6.2.2.13 Synthesis of N-(pyridin-2-yl)acetamide (H-acetyl)

2-Amino-5-pyridine (0.94 g, 10.0 mmol) was dissolved in 50 mL of pyridine and cooled in an ice bath. Acetyl chloride (1.06 mL, 16.0 mmol) was added dropwise maintaining the temperature between 0-5 ºC. After the addition was complete the contents were stirred at room temperature until no further starting material (2-amino-5-pyridine) was detected by TLC. Upon completion, chilled water (100 mL) was added and stirred for 15 minutes. The reaction contents were extracted with dichloromethane and the organic layer was washed with saturated sodium bicarbonate solution, brine, water and dried with anhydrous magnesium sulfate, filtered, and concentrated *in vacuo* to isolate the pure product. Yield 80%, ^{1}H NMR (400 MHz, DMSO-d6) δ 10.45 (s, 1H), 8.29 (s, 1H), 8.05 (s, 1H), 7.74 (s, 1H), 7.04 (s, 1H).

6.2.2.14 Synthesis of N-(5-pyridin-2-yl)propionamide (H-propyl)

2-Amino-5-pyridine (0.94 g, 10.0 mmol) was dissolved in 50 mL of pyridine and cooled in an ice bath. Propyl chloride (1.09 mL, 16.0 mmol) was added dropwise maintaining the temperature between 0-5 ºC. After the addition was complete the contents were stirred at room temperature until no further starting material (2-amino-5-pyridine) was detected by TLC. Upon completion, chilled water (100 mL) was added and stirred for 15 minutes. The reaction contents were extracted with dichloromethane and the organic layer was washed with saturated sodium bicarbonate solution, brine, water and dried with anhydrous magnesium sulfate, filtered, and concentrated *in vacuo* to isolate the pure product. Yield 75%, ^{1}H NMR (400 MHz, DMSO-d6) δ 10.39 (s, 1H), 8.29 (s, 1H), 8.09 (s, 1H), 7.76 (s, 1H), 7.07 (s, 1H), 2.37 (s, 2H), 1.05 (s, 3H).

6.2.2.15 Synthesis of N-(5-pyridin-2-yl)butyramide (H-butyl)

2-Amino-5-pyridine (0.94 g, 10.0 mmol) was dissolved in 50 mL of pyridine and cooled in an ice bath. Butyl chloride (1.54 mL, 16.0 mmol) was added dropwise maintaining the temperature between 0-5 ºC. After the addition was complete the contents were stirred at room temperature until no further starting material (2-amino-5-pyridine) was detected by TLC. Upon completion, chilled water (100 mL) was added and stirred for 15 minutes. The reaction contents were extracted with dichloromethane and the organic layer was washed with saturated sodium bicarbonate solution, brine, water and dried with anhydrous magnesium sulfate, filtered, and concentrated *in vacuo* to isolate the pure product. Yield 60%, m.p 42 – 44 °C ^{1}H NMR (400 MHz, DMSO-d6) δ 10.40 (s, 1H), 8.29 (s, 1H), 8.07 (s, 1H), 7.76 (s, 1H), 7.07 (s, 1H), 2.36 (s, 2H), 1.55 (s, 2H), 1.32 (s, 1H), 0.86 (s, 3H).

6.2.2.16 Synthesis of N-(5-pyridin-2-yl)pentanamide (H-pentyl)

2-Amino-5-pyridine (0.94 g, 11.0 mmol) was dissolved in 50 mL of pyridine and cooled in an ice bath. Pentyl chloride (1.77 mL, 16.0 mmol) was added dropwise maintaining the temperature between 0-5 ºC. After the addition was complete the contents were stirred at room temperature until no further starting material (2-amino-5-pyridine) was detected by TLC. Upon completion, chilled water (100 mL) was added and stirred for 15 minutes. The reaction contents were extracted with dichloromethane and the organic layer was washed with saturated sodium bicarbonate solution, brine, water and dried with anhydrous magnesium sulfate, filtered, and concentrated *in vacuo* to isolate the pure product. Yield 55%, (Oil at room temperature) ^{1}H NMR (400 MHz, DMSO-d6) δ 10.40 (s, 1H), 8.29 (s, 1H), 8.07 (s, 1H), 7.73 (s, 1H), 7.05 (s, 1H), 2.36 (s, 2H), 1.57 (s, 2H), 1.31 (s, 2H), 0.90 (s, 3H).

6.2.2.17 Synthesis of N-(5-methylpyridin-2-yl)acetamide (Methyl-acetyl)

2-Amino-5-methylpyridine (1.08 g, 10.0 mmol) was dissolved in 50 mL of pyridine and cooled in an ice bath. Acetyl chloride (1.06 mL, 16.0 mmol) was added dropwise maintaining the temperature between 0-5 ºC. After the addition was complete the contents were stirred at room temperature until no further starting material (2-amino-5-methylpyridine) was detected by TLC. Upon completion, chilled water (100 mL) was added and stirred for 15 minutes. The reaction contents were extracted with dichloromethane and the organic layer was washed with saturated sodium bicarbonate solution, brine, water and dried with anhydrous magnesium sulfate, filtered, and concentrated *in vacuo* to isolate the pure product. Yield 75%, m.p 100 – 102 °C ^{1}H NMR (400 MHz, DMSO-d6) δ 10.36 (s, 1H), 8.12 (s, 1H), 7.97 (s, 1H), 7.58 (s, 1H), 2.23 (s, 3H), 2.06 (s, 3H).

6.2.2.18 Synthesis of N-(5-methylpyridin-2-yl) propionamide (Methyl-propyl)

2-Amino-5-methylpyridine (1.08 g, 10.0 mmol) was dissolved in 50 mL of pyridine and cooled in an ice bath. Propyl chloride (1.09 mL, 16.0 mmol) was added dropwise maintaining the temperature between 0-5 ºC. After the addition was complete the contents were stirred at room temperature until no further starting material (2-amino-5-methylpyridine) was detected by TLC. Upon completion, chilled water (100 mL) was added and stirred for 15 minutes. The reaction contents were extracted with dichloromethane and the organic layer was washed with saturated sodium bicarbonate solution, brine, water and dried with anhydrous magnesium sulfate, filtered, and concentrated *in vacuo* to isolate the pure product. Yield 70%, m.p 91 – 93°C. ^{1}H NMR (400 MHz, DMSO-d6) δ 10.36 (s, 1H), 8.12 (s, 1H), 7.97 (s, 1H), 7.55 (s, 1H), 2.23 (s, 3H), 2.06 (s, 3H).

6.2.2.19 Synthesis of N-(5-methylpyridin-2-yl)butyramide (Methyl-butyl)

2-Amino-5-methylpyridine (1.08 g, 10.0 mmol) was dissolved in 50 mL of pyridine and cooled in an ice bath. Butyl chloride (1.54 mL, 16.0 mmol) was added dropwise maintaining the temperature between 0-5 ºC. After the addition was complete the contents were stirred at room temperature until no further starting material (2-amino-5-methylpyridine) was detected by TLC. Upon completion, chilled water (100 mL) was added and stirred for 15 minutes. The reaction contents were extracted with dichloromethane and the organic layer was washed with saturated sodium bicarbonate solution, brine, water and dried with anhydrous magnesium sulfate, filtered, and concentrated *in vacuo* to isolate the pure product. Yield 65%, m.p 64 – 66°C ^{1}H NMR (400 MHz, DMSO-d6) δ 10.31 (s, 1H), 8.12 (s, 1H), 7.98 (s, 1H), 7.58 (s, 1H), 2.33 (s, 2H), 2.23 (s, 3H), 1.60 (s, 2H), 0.87 (s, 3H).

6.2.2.20 Synthesis of N-(5-methylpyridin-2-yl)pentanamide (Methyl-pentyl)

2-Amino-5-methylpyridine (1.08 g, 10.0 mmol) was dissolved in 50 mL of pyridine and cooled in an ice bath. Pentyl chloride (1.77 mL, 16.0 mmol) was added dropwise maintaining the temperature between 0-5 ºC. After the addition was complete the contents were stirred at room temperature until no further starting material (2-amino-5-methylpyridine) was detected by TLC. Upon completion, chilled water (100 mL) was added and stirred for 15 minutes. The reaction contents were extracted with dichloromethane and the organic layer was washed with saturated sodium bicarbonate solution, brine, water and dried with anhydrous magnesium sulfate, filtered, and concentrated *in vacuo* to isolate the pure product. Yield 60%, m.p 42 – 44°C ^{1}H NMR (400 MHz, DMSO-d6) δ 10.31 (s, 1H), 8.12 (s, 1H), 7.97 (s, 1H), 7.56 (s, 1H), 2.23 (s, 3H), 1.51 (s, 2H), 1.33 (s, 2H), 0.88 (s, 3H).

6.3 Results – Part A

6.3.1 Molecular electrostatic potentials (MEPs)

The calculated MEP values in kJ/mol are shown in Figure 6.6

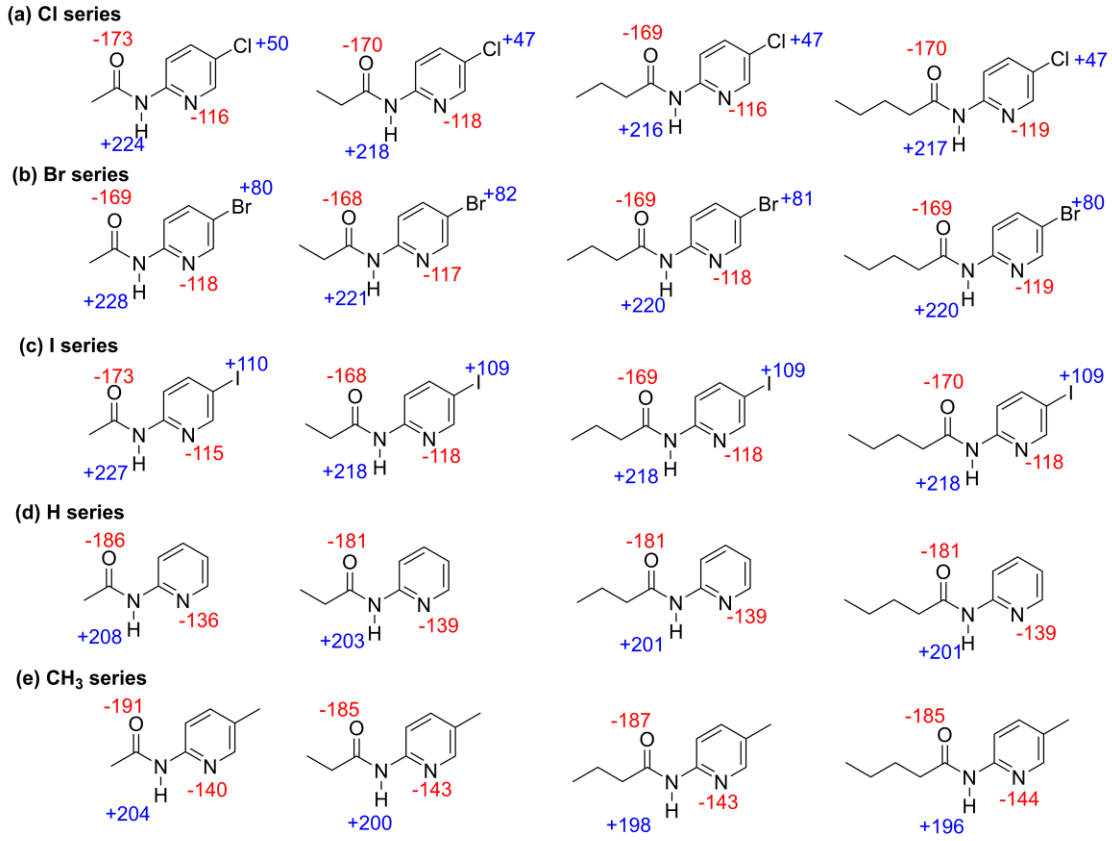

Figure 6.6. MEP values at most likely donor and acceptor sites in the twenty target compounds

6.3.2 IR spectroscopy results

The IR band for C=O mode in twenty target compounds are given (Table 6.1)

Table 6.1. Wave number of C=O mode in IR

		Y				
		-Cl	-Br	-I	-H	$-CH_3$
X	Acetyl	1659 cm^{-1}	1659 cm^{-1}	1674 cm^{-1}	1687 cm^{-1}	1694 cm^{-1}
	Propyl	1672 cm^{-1}	1669 cm^{-1}	1669 cm^{-1}	1687 cm^{-1}	1667 cm^{-1}
	Butyl	1692 cm^{-1}	1695 cm^{-1}	1692 cm^{-1}	1681 cm^{-1}	1691 cm^{-1} (minor) and 1672 cm^{-1} (major)
	Pentyl	1686 cm^{-1}	1691 cm^{-1}	1692 cm^{-1}	1666 cm^{-1}	1693 cm^{-1} (minor) and 1657 cm^{-1} (major)

6.3.3 X-ray crystallography results

Seven crystal structures and the solvents from which they were crystallized are listed (Table 6.2).

Table 6.2. Solvents used for crystal growth and crystal descriptions

Compound	Code	Solvent	Color and morphology
N-(5-chloropyridin-2-yl)acetamide	Cl-acetyl	Ethyl acetate	Colorless, needle
N-(5-bromopyridin-2-yl)acetamide	Br-propyl	Methanol	Colorless, needle
N-(5-bromopyridin-2-yl)pentanamide	Br-pentyl	Acetone	Colorless, plate
N-(5-iodopyridin-2-yl)acetamide	I-acetyl	Ethyl acetate	Brown, Rectangular
N-(5-iodopyridin-2-yl)propionamide	I-propyl	Methanol:acetone(1:1)	Colorless, plate
N-(5-iodopyridin-2-yl)butyramide	I-butyl	Acetone	White, needle
N-(5-iodopyridin-2-yl)pentanamide	I-pentyl	Methanol	Colorless, thin
N-(5-pyridin-2-yl)butyramide	H-butyl	Acetone	Colorless, block

The primary assembly in the seven crystal structures are given (Figure 6.7). Chains were formed by Cl-acetyl, Br-propyl[1], I-acetyl, I-propyl while dimers were formed by Br-Pentyl, I-butyl, I-pentyl and H-butyl.

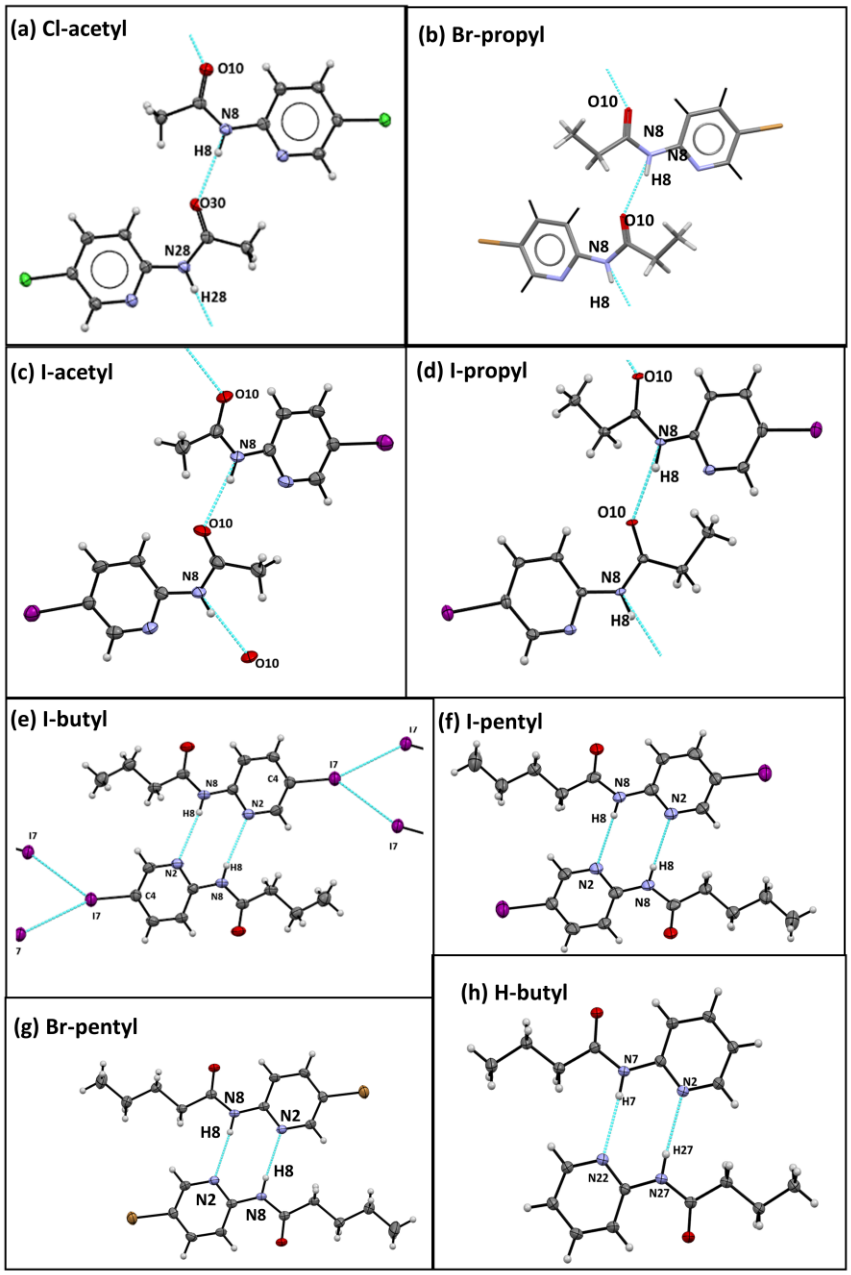

Figure 6.7. Primary assembly in the crystal structures of (a) Cl-acetyl, (b) I-acetyl, (c) I-propyl, (d) I-butyl, (e) I-pentyl, (f) (d) H-butyl and Br-propyl

[1] I wish to acknowledge former group member Dr. A.Rajbanshi for crystal growth of Br-propyl

The relevant hydrogen bond geometries of the crystal structures are given (Table 6.3)

Table 6.3. Bond parameters of crystal structures.

Compound	**D-H/I···A**	**D/I···A (Å)**	**D-H···A (deg)**
Cl-acetyl	N8-H8···O30	2.920(2)	175.37(7)
	N28-H28···O10	2.889(2)	171.01(6)
I-acetyl	N8-H8···O10	2.866(7)	168(7)
I-propyl	N8-H8···O10	2.852(3)	168.0
I-butyl	N8-H8···N2	3.267 (1)	172.47(4)
	C4-I7···I7	3.877(1)	159
I-pentyl	N8-H8··· N2	3.285(8)	174.(7)
Br-pentyl	N8-H8··· N2	3.234	170.6
H-Butyl	N7-H7··· N22	3.200(1)	174.68(6)
	N27-H27··· N2	3.208(1)	166.63(6)
	N47-H47··· N42	3.215(1)	159.85(6)
	N67-H67··· N62	3.234(1)	174.73(6)

6.4 Discussion – Part A

Since we have access to crystal structures for ten of the twenty compounds in this study, we are in a perfect position to try to establish if there are vibrational spectroscopic signatures that can help us to identify which of the two motifs, chain or dimer, that are present in the these solids, Table 6.4.

Table 6.4. Correlation between C=O stretch in IR, and primary hydrogen-bond motif

Compound	Code	Primary motif	C=O mode in IR
N-(5-chloropyridin-2-yl)acetamide	Cl-acetyl	Chain	1659 cm^{-1}
N-(5-bromopyridin-2-yl)acetamide	Br-acetyl	Chain[15]	1659 cm^{-1}
N-(5-bromopyridin-2-yl) propionamide	Br-propyl	Chain	1669 cm^{-1}
N-(5-bromopyridin-2-yl)pentanamide	Br-pentyl	Dimer	1695 cm^{-1}
N-(5-iodopyridin-2-yl)acetamide	I-acetyl	Chain	1674 cm^{-1}
N-(5-iodopyridin-2-yl)propionamide	I-propyl	Chain	1669 cm^{-1}
N-(5-iodopyridin-2-yl)butyramide	I-butyl	Dimer	1692 cm^{-1}
N-(5-iodopyridin-2-yl)pentanamide	I-pentyl	Dimer	1692 cm^{-1}
N-(pyridin-2-yl)acetamide	H-acetyl	Dimer [14]	1687 cm^{-1}
N-(5-pyridin-2-yl)propionamide	H-propyl	Dimer [14]	1687 cm^{-1}
N-(5-pyridin-2-yl)butyramide	H-butyl	Dimer	1681 cm^{-1}

Considering all these 10 structures we can see that IR data serves as a reliable tool to evaluate self-aggregation of the 8 new structures added for consideration here (Figure 6.8).

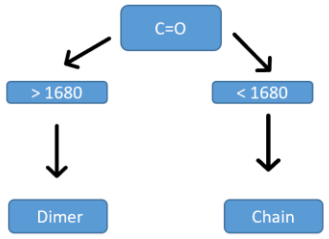

Figure 6.8. Cut-off C=O IR mode for assessing dimer or chain formation.

Since the IR data for our structures is consistent with crystallographic data, we can now make a confident assessment as to which type of assembly is present in the nine compounds where we do not have single-crystal data (Table 6.5)

Table 6.5. Primary motif of the twenty targets

		Y				
		-Cl	-Br	-I	-H	$-CH_3$
X	Acetyl	Chain	Chain	Chain	Dimer	Dimer
	Propyl	Chain	Chain	Chain	Dimer	Chain
	Butyl	Dimer	Dimer	Dimer	Dimer	Dimer (minor) and Chain (major)
	Pentyl	Dimer	Dimer	Dimer	Chain / oil	Dimer (minor) and Chain (major)

Based on the MEP values that were calculated, the target compounds can be clustered into two groups, halogenated or unhalogenated (Figure 6.9)

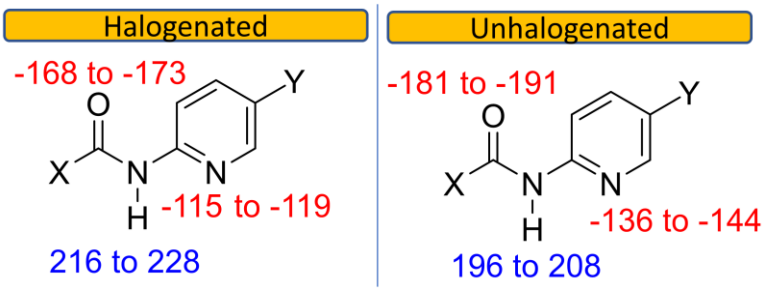

Figure 6.9. Summarized MEP values of acceptor and donor sites in target molecules

In the molecules of halogenated targets, the acceptor sites are weaker (less negative) while the donor NH is stronger in comparison to the unhalogenated targets. This can be explained by the electron withdrawing effect of the halogen atoms. Within each series, the length of the alkyl chain, substituent X, does not lead to significant changes of MEPs. The biggest contrast occurs at the amide hydrogen, with the switch from acetyl to propyl. However, the electrostatics are more or less unchanged within the molecules clustered into the above two groups (halogenated and unhalogenated).

There is no obvious obstruction to dimer formation in any of these twenty targets. When all five acetyl targets are considered, the three halogenated targets behave similarly forming chains while the H and methyl targets form dimers. The van der Waals radii of the "Y" substituents (in Å) are as follows. Cl=1.75, Br= 1.85, I= 1.98, H=1.20[16] and CH_3=1.70. In terms of size, the Cl, and CH_3 groups are most similar to each other and often are responsible for formation of isostructural assemblies. Yet, the Cl and CH_3 substituent led to different assemblies while all three halogenated targets (where there is a considerable difference in halogen size) led to identical assemblies. Thus, in the presence of the smallest X substituent, the molecules with similar electrostatic potentials at acceptor and donor sites lead to identical aggregation modes.

As for the five propyl targets, the three halogenated targets continue to form chains, the H-butyl target forms a dimer while the methyl-butyl target forms a chain. It is interesting to note that the MEP at the carbonyl oxygen of methyl-propyl is a slightly weaker acceptor (less negative) than in methyl-acetyl, yet chains were formed. Therefore, the switch from dimer to chain of the methyl target may be attributed to the influence of the increasing chain length going from acetyl to propyl in this methyl series.

The three butyl halogenated targets all form dimers and the H-butyl target also form dimers. Though, the electrostatic potentials of the three halogenated butyl targets were quite different to that of the H-butyl target, all four of these targets led to dimers. Methyl-butyl showed two carbonyl peaks indicating a high likelihood for polymorphism or the possibility of both synthons being present in the assembly. The three halogenated pentyl targets formed dimers. The H-pentyl target is an oil at room temperature but the C=O stretch indicates that chains are formed. Once again, the methyl target showed two carbonyl peaks. The targets, of all three halogenated series behaved similarly with variation of the X substituent forming chains with the acetyl and propyl and forming

dimers with the butyl and pentyl substituents. Despite the similarity of MEP charges in the H and CH_3 series, they produce similar aggregation modes only with acetyl as the X substituent. The two Y substituents, Cl and CH_3, similar in size, led to similar aggregation only with when X=propyl. Overall, our results indicate that very subtle changes to the Y and X substituents promote either chain or dimer formation. The halogenated acetyl and propyl targets formed chains (6/6 of these are supported by SCXRD data in addition to IR). Contrary to previously reported data this clearly indicates that chain formation is not solely the result of avoiding steric clash in molecular aggregation. However, decoding the driving force for dimer or chain formation will require the examination of an even deeper pool of targets. Overall, the shorter alkyl chain substituent led to a higher % of chain formation while the longer alkyl chain led to a higher % of dimer formation (Table 6.6)

Table 6.6. Summarized results based on alkyl chain length of X substituent

		Y
		-Cl, -Br, -I, -H and -CH_3
X	Acetyl and Propyl	Chain 7/10 Dimer 3/10
	Butyl and Pentyl	Dimer 7/10 Chain 1/10 Chain and Dimer 2/10

Part B. Can we deliberately change chains to dimers?

Despite the alteration in assembly (chain vs. dimer) we did not observe any structure directing interactions by the substituents at the Y position. Therefore, we next wanted to fully explore the structure directing interactions of Y position by introducing either a potential halogen or hydrogen bond donor. In part A, we observed that with the NH···O=C chain dominated (7/10) over the

NH···N dimer (3/10). We hypothesized that as long as the donor (Y) is of sufficient strength, it can effectively block the carbonyl position previously occupied by the amide NH, thereby converting chains into dimers (Figure 6.10).

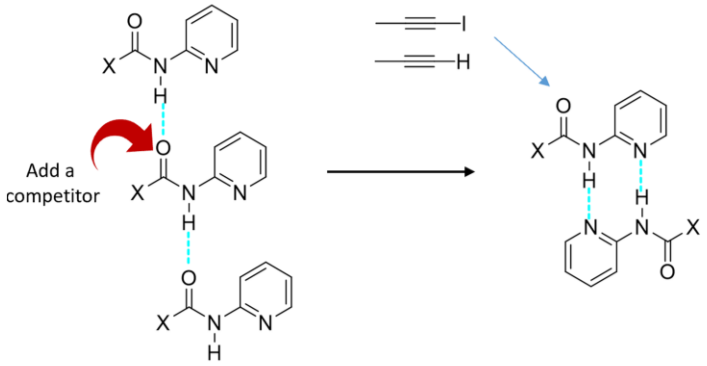

Figure 6.10. Proposed strategy for promoting dimer formation

Since dimers predominated (7/10) with the longer alkyl chains in Part A, we anticipated that dimers would occur even with changing the Y substituent to an ethynyl substituent. Additionally, we wanted to explore if the iodoethynyl and ethynyl hydrogen moieties display structural mimicry; i.e. do they form intermolecular interactions that deliver similar structural features. Accordingly, we selected eight target molecules for this part of the study (Figure 6.11)

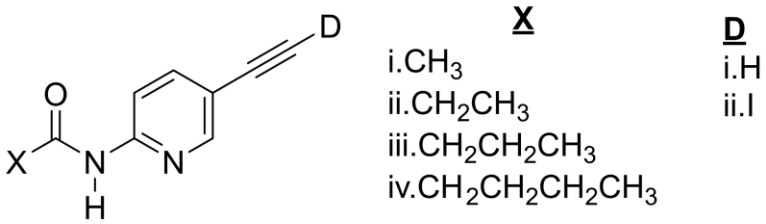

Figure 6.11. Target molecules in this study

6.5 Experimental – Part B

All precursors and solvents were purchased from commercial sources and used without further purification. ^{1}H NMR spectra and ^{13}C NMR spectra were recorded on a Brucker 400 spectrometer. Melting points were recorded on a Fisher-Johns apparatus or a TA Instruments DSC Q20. IR spectra were recorded with a Nicolet 380 FT-IR spectrometer using an attenuated total reflection (ATR) technique and ZnSe as the crystal. Electrostatic potentials were calculated with density functional B3LYP level of theory using 6-311++G** basis set in vacuum, using Spartan 08' software.

6.5.1 General

All precursors and solvents were purchased from commercial sources and used without further purification. ^{1}H NMR spectra were recorded on a Brucker 400 spectrometer. Melting points were recorded on a Fisher-Johns apparatus or a TA Instruments DSC Q20. IR spectra were recorded with a Nicolet 380 FT-IR spectrometer using an attenuated total reflection (ATR) technique and ZnSe as the crystal. Electrostatic potentials were calculated with density functional B3LYP level of theory using 6-311++G** basis set in vacuum, using Spartan 08' software.

6.5.2 Synthesis

-Synthesis of N-(5-((trimethylsilyl)ethynyl)pyridin-2-yl)alkylamides (Sections 6.5.2.1 – 6.5.2.4)

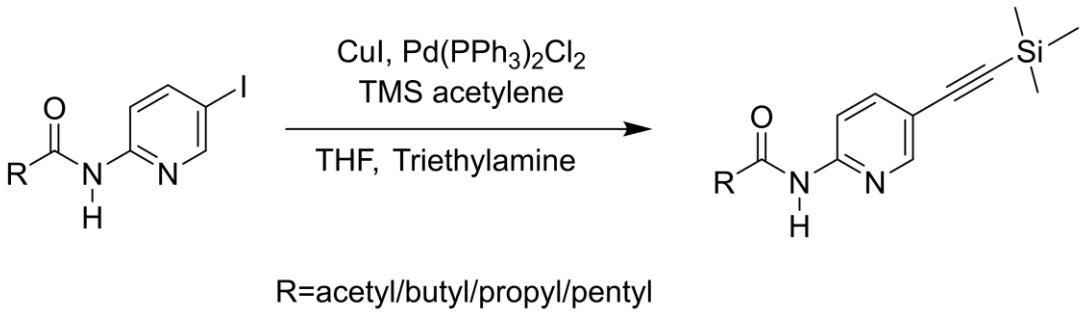

- Synthesis of N-(5-(iodoethynyl)pyridin-2-yl)alkylamides (Sections 6.5.2.5 – 6.5.2.8)

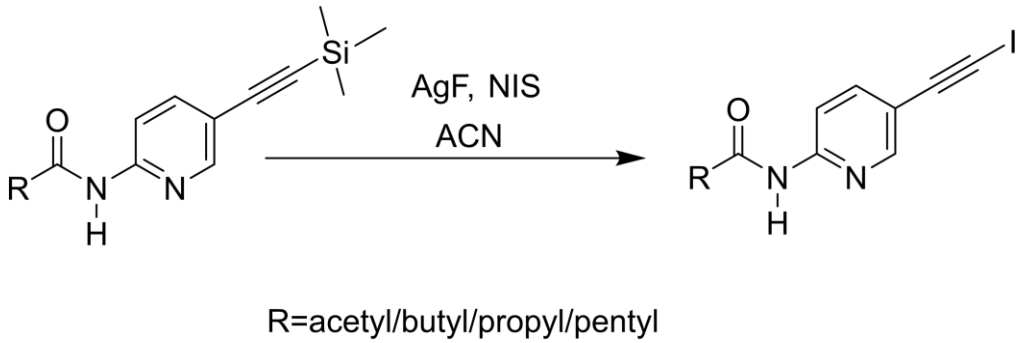

- Synthesis of N-(5-ethynylpyridin-2-yl)alkylamides (6.5.2.9– 6.5.2.12)

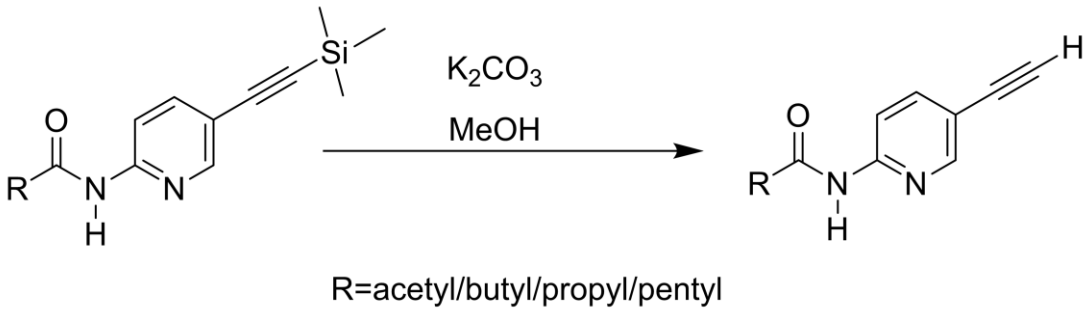

6.5.2.1 Synthesis of N-(5-((trimethylsilyl)ethynyl)pyridin-2-yl)acetamide

N-(5-iodopyridin-2-yl)acetamide(1.970 g, 7.5 mmol) was dissolved in 80 mL of Trimethylamine: THF (1:1) and degassed with nitrogen. CuI (0.143 g, 0.75 mmol), bis(triphenylphosphine)palladium(II) dichloride (0.527 g, 0.75 mmol) and trimethylsilylacetylene (2.07 mL, 15.0mmol), was added and the reaction mixture was heated overnight at 80°C under dinitrogen. The reaction was monitored by TLC. The reaction medium was filtered, and the filtrate evaporated to dryness and redissolved in methylene chloride. The organic layer was washed with 1M HCl, brine, water and dried with anhydrous magnesium sulphate and filtered. The organic layer was concentrated, and the product purified by column chromatography (hexane followed by hexane: ethyl acetate 80:20). m.p Yield 79% ^{1}H NMR (400 MHz, DMSO-d6) δ 10.70 (s, 1H), 8.39 (s, 1H), 8.09 (s, 1H), 7.85 (s, 1H), 2.10 (s, 3H), 0.23 (s, 9H).

6.5.2.2 Synthesis of N-(5-((trimethylsilyl)ethynyl)pyridin-2-yl)propionamide

N-(5-iodopyridin-2-yl)propionamide (2.070 g, 7.5 mmol) was dissolved in 80 mL of Trimethylamine: THF (1:1) and degassed with nitrogen. CuI (0.143 g, 0.75 mmol), bis(triphenylphosphine)palladium(II) dichloride (0.527 g, 0.75 mmol) and trimethylsilylacetylene (2.07 mL, 15.0mmol), was added and the reaction mixture was heated overnight at 80°C under nitrogen. The reaction was monitored by TLC. The reaction medium was filtered, and the filtrate evaporated to dryness and redissolved in methylene chloride. The organic layer was washed with 1M HCl, brine, water and dried with anhydrous magnesium sulphate and filtered. The organic layer was washed with 1M HCl, brine, water and dried with anhydrous magnesium sulphate and filtered. The organic later was concentrated and the product purified by column chromatography (hexane followed by hexane: ethyl acetate 80:20). Yield 75% ^{1}H NMR (400 MHz, DMSO-d6) δ 10.64 (s, 1H), 8.39 (s, 1H), 8.10 (s, 1H), 2.38 (s, 2H), 1.05 (s, 3H), 0.22 (s, 9H).

6.5.2.3 Synthesis of N-(5-((trimethylsilyl)ethynyl)pyridin-2-yl)butyramide

N-(5-iodopyridin-2-yl)butyramide (2.175 g, 7.5 mmol) was dissolved in 80 mL of Trimethylamine: THF (1:1) and degassed with nitrogen. CuI (0.143 g, 0.75 mmol), bis(triphenylphosphine)palladium(II) dichloride (0.527 g, 0.75 mmol) and trimethylsilylacetylene (2.07 mL, 15.0mmol), was added and the reaction mixture was heated overnight at 80°C under dinitrogen. The reaction was monitored by TLC. The reaction medium was filtered, and the filtrate evaporated to dryness and redissolved in methylene chloride. The organic later was washed with 1M HCl, brine, water and dried with anhydrous magnesium sulphate and filtered. The organic layer was concentrated, and the product purified by column chromatography (hexane followed by hexane: ethyl acetate 80:20). Yield 73% ^{1}H NMR (400 MHz, DMSO-d6) δ 10.65 (s, 1H), 8.39 (s, 1H), 8.11 (s, 1H), 7.83 (s, 1H), 2.37 (s, 2H), 1.62 (s, 1H), 0.91 (s, 2H), 0.23 (s, 9H).

6.5.2.4 Synthesis of N-(5-((trimethylsilyl)ethynyl)pyridin-2-yl)pentanamide

N-(5-iodopyridin-2-yl)pentanamide (2.280 g, 7.5 mmol) was dissolved in 80 mL of Trimethylamine: THF (1:1) and degassed with dinitrogen. CuI (0.143 g, 0.75 mmol), bis(triphenylphosphine)palladium(II) dichloride (0.527 g, 0.75 mmol) and trimethylsilylacetylene (2.07 mL, 15.0mmol), was added and the reaction mixture was heated overnight at 80°C under dinitrogen. The reaction was monitored by TLC. The reaction medium was filtered, and the filtrate evaporated to dryness and redissolved in methylene chloride. The organic layer was washed with 1M HCl, brine, water and dried with anhydrous magnesium sulphate and filtered. The organic layer was concentrated, and the product purified by column chromatography (hexane followed by hexane: ethyl acetate 80:20). Yield 73% ^{1}H NMR (400 MHz, DMSO-d6) δ 10.64 (s, 1H), 8.39 (s, 1H), 8.08 (s, 1H), 7.82 (s, 1H), 2.38 (s, 2H), 1.56 (s, 2H), 1.28 (s, 2H), 0.89 (s, 3H), 0.22 (s, 9H).

6.5.2.5 Synthesis of N-(5-(iodoethynyl)pyridin-2-yl)acetamide (Acetyl-act-I)

Acetonitrile (50 mL) was degassed with dinitrogen. N-(5-((trimethylsilyl)ethynyl)pyridin-2-yl)acetamide (0.440 g, 1.9 mmol) and AgF (0.267 g, 2.1 mmol) were added to acetonitrile and the mixture was covered with aluminum foil before the introduction of N-iodosuccinimide (0.470 g, 2.1 mmol). The mixture was connected to a dinitrogen inlet and stirred overnight. Completion of the reaction was monitored with TLC and the resulting suspension was filtered. The filtrate was evaporated to dryness and redissolved in 150 mL ethyl acetate:diethyl ether (4:1). The organic layer was washed with water and dried with anhydrous $MgSO_4$ and concentrated *in vacuo.* The resultant solid was purified by passed through a ~6 cm silica plug using hexane:ethyl acetate (10:1) to obtain the pure product. Yield 44%, decomposition ~200°C. ^{1}H NMR (400 MHz, DMSO-d6) δ 10.67 (s, 1H), 8.38 (s, 1H), 8.07 (s, 1H), 7.81 (s, 1H), 2.10 (s, 3H).

6.5.2.6 Synthesis of N-(5-(iodoethynyl)pyridin-2-yl)propionamide (Propyl-act-I)

Acetonitrile (50 mL) was degassed with dinitrogen. N-(5-((trimethylsilyl)ethynyl)pyridin-2-yl)propionamide (0.467 g, 1.9 mmol) and AgF (0.267 g, 2.1 mmol) were added to acetonitrile and the mixture was covered with aluminum foil before the introduction of N-iodosuccinimide (0.470 g, 2.1 mmol). The mixture was connected to a dinitrogen inlet and stirred overnight. Completion of the reaction was monitored with TLC and the resulting suspension was filtered. The filtrate was evaporated to dryness and redissolved in 150 mL ethyl acetate:diethyl ether (4:1). The organic layer was washed with water and dried with anhydrous $MgSO_4$ and concentrated *in vacuo.* The resultant solid was purified by passed through a ~6 cm silica plug using hexane:ethyl acetate (10:1) to obtain the pure product. Yield 40%, m.p. 171-173° C. ^{1}H NMR (400 MHz, DMSO-d6) δ 10.60 (s, 1H), 8.37 (s, 1H), 8.08 (s, 1H), 7.80 (s, 1H), 2.38 (s, 2H), 1.03 (s, 3H).

6.5.2.7 Synthesis of N-(5-(iodoethynyl)pyridin-2-yl)butyramide (Butyl-act-I)

Acetonitrile (50 mL) was degassed with dinitrogen. N-(5-((trimethylsilyl)ethynyl)pyridin-2-yl)butyramide, (0.494 g, 1.9 mmol) and AgF (0.267 g, 2.1 mmol) were added to acetonitrile and the mixture was covered with aluminum foil before the introduction of N-iodosuccinimide (0.470 g, 2.1 mmol). The mixture was connected to a dinitrogen inlet and stirred overnight. Completion of the reaction was monitored with TLC and the resulting suspension was filtered. The filtrate was evaporated to dryness and redissolved in 150 mL ethyl acetate:diethyl ether (4:1). The organic layer was washed with water and dried with anhydrous $MgSO_4$ and concentrated *in vacuo.* The resultant solid was purified by passed through a ~6 cm silica plug using hexane:ethyl acetate (10:1) to obtain the pure product. Yield, 57%, m.p. 157-157° C ^{1}H NMR (400 MHz, Chloroform-d) δ 8.33 (s, 1H), 8.20 (s, 1H), 7.73 (s, 1H), 2.37 (s, 2H), 1.79 (s, 2H), 1.03 (s, 3H).

6.5.2.8 Synthesis of N-(5-(iodoethynyl)pyridin-2-yl)pentanamide (Pentyl-act-I)

Acetonitrile (50 mL) was degassed with dinitrogen. N-(5-((trimethylsilyl)ethynyl)pyridin-2-yl)pentanamide (0.520 g, 1.9 mmol) and AgF (0.267 g, 2.1 mmol) were added to acetonitrile and the mixture was covered with aluminum foil before the introduction of N-iodosuccinimide (0.470 g, 2.1 mmol). The mixture was connected to a dinitrogen inlet and stirred overnight. Completion of the reaction was monitored with TLC and the resulting suspension was filtered. The filtrate was evaporated to dryness and redissolved in 150 mL ethyl acetate:diethyl ether (4:1). The organic layer was washed with water and dried with anhydrous $MgSO_4$ and concentrated *in vacuo.* The resultant solid was purified by passed through a ~6 cm silica plug using hexane:ethyl acetate (10:1) to obtain the pure product. Yield 50%, m.p. 143-146°. ^{1}H NMR (400 MHz, Chloroform-d) δ 8.32 (s, 1H), 8.27 – 8.16 (m, 2H), 7.71 (d, J = 2.1 Hz, 1H), 2.39 (s, 2H), 1.70 (s, 3H), 1.40 (s, 2H), 0.93 (s, 3H).

6.5.2.9 Synthesis of N-(5-ethynylpyridin-2-yl)alkylamides (Acetyl-act-H)

N-(5-((trimethylsilyl)ethynyl)pyridin-2-yl)acetamide (0.232 g, 1 mmol) was dissolved in 30 mL of methanol. Then, K_2CO_3 (0.138 g, 1 mmol) was added into the solution. The mixture was stirred at room temperature. The reaction completion was monitored by TLC. Once the reaction was completed the solvent was evaporated to dryness and the solid was redissolved in ethyl acetate. The organic layer was washed with water and dried with anhydrous $MgSO_4$. The solid was purified by flash chromatography using hexane:ethyl acetate (10:1) to obtain the pure product. Yield 65%, m.p. 183-185°. ^{1}H NMR (400 MHz, Chloroform-d) δ 8.32 (s, 1H), 8.27 – 8.16 (m, 2H), 7.71 (d, J = 2.1 Hz, 1H), 2.39 (s, 2H), 1.70 (s, 3H), 1.40 (s, 2H), 0.93 (s, 3H).

6.5.2.10 Synthesis of N-(5-ethynylpyridin-2-yl)propionamide (Propyl-act-H)

N-(5-((trimethylsilyl)ethynyl)pyridin-2-yl)propionamide (0.246 g, 1 mmol) was dissolved in 30 mL of methanol. Then, K_2CO_3 (0.138 g, 1 mmol) was added into the solution. The mixture was stirred at room temperature. The reaction completion was monitored by TLC. Once the reaction was completed the solvent was evaporated to dryness and the solid was redissolved in ethyl acetate. The organic layer was washed with water and dried with anhydrous $MgSO_4$. The solid was purified by flash chromatography using hexane:ethyl acetate (10:1) to obtain the pure product. Yield 60% m.p. 94-96°. ^{1}H NMR (400 MHz, Chloroform-d) δ 8.37 (s, 1H), 8.22 (s, 1H), 8.01 (s, 1H), 7.79 (s, 1H), 3.16 (s, 1H), 2.45 (s, 2H), 1.63 (s, 2H), 1.25 (s, 3H).

6.5.2.11 Synthesis of N-(5-ethynylpyridin-2-yl)butyramide (Butyl-act-H)

N-(5-((trimethylsilyl)ethynyl)pyridin-2-yl)butyramide (0.260 g, 1 mmol) was dissolved in 30 mL of methanol. Then, K_2CO_3 (0.138 g, 1 mmol) was added into the solution. The mixture was stirred at room temperature. The reaction completion was monitored by TLC. Once the reaction was completed the solvent was evaporated to dryness and the solid was redissolved in ethyl acetate. The organic layer was washed with water and dried with anhydrous $MgSO_4$. The solid was purified by flash chromatography using hexane:ethyl acetate (10:1) to obtain the pure product. Yield 62% m.p. 113-115°.

6.5.2.12 Synthesis of N-(5-ethynylpyridin-2-yl)pentanamide (Pentyl-act-H)

N-(5-((trimethylsilyl)ethynyl)pyridin-2-yl)pentanamide (0.274 g, 1 mmol) was dissolved in 30 mL of methanol. Then, K_2CO_3 (0.138 g, 1 mmol) was added into the solution. The mixture was stirred at room temperature. The reaction completion was monitored by TLC. Once the reaction was completed the solvent was evaporated to dryness and the solid was redissolved in ethyl acetate. The organic layer was washed with water and dried with anhydrous $MgSO_4$. The solid was purified by flash chromatography using hexane:ethyl acetate (10:1) to obtain the pure product. Yield 58% m.p. 110-112°. ^{1}H NMR (400 MHz, Chloroform-d) δ 8.42 (s, 1H), 8.36 (s, 1H), 8.20 (s, 1H), 7.76 (s, 1H), 3.16 (s, 1H), 2.40 (s, 2H), 1.39 (s, 2H), 0.93 (s, 3H).

6.6 Results – Part B

6.6.1 Molecular electrostatic potentials (MEPs)

The calculated MEP values in kJ/mol are shown in Figure 6.12

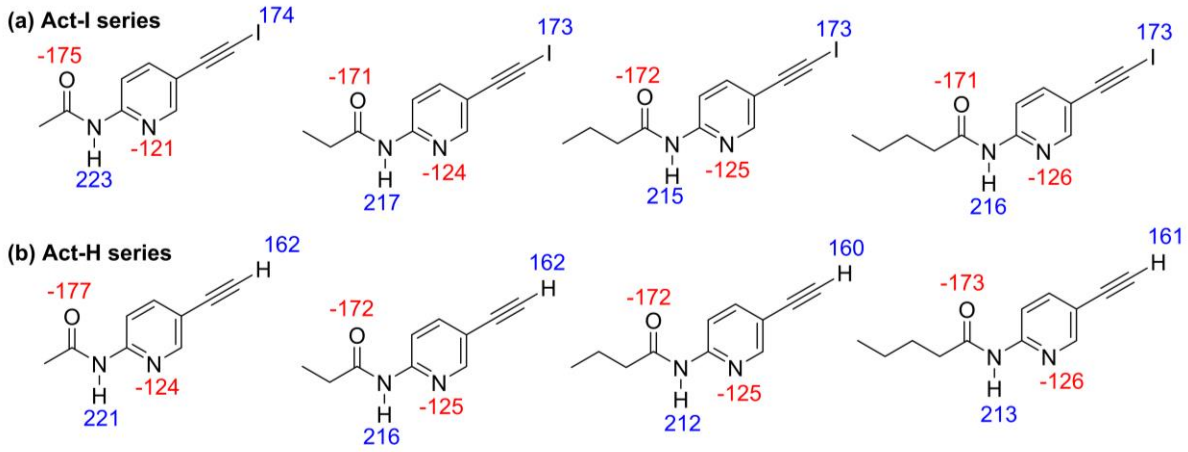

Figure 6.12. MEP values at most likely donor and acceptor sites in the eight target molecules.

6.6.2 X-ray crystallography results

Crystal structures of the eight targets are reported here. The solvents from which they were grown are given (Table 6.7).

Table 6.7. Solvents used for crystal growth and crystal descriptions

Compound	Code	Solvent	Color and morphology
N-(5-(iodoethynyl)pyridin-2-yl)acetamide	Acetyl-act-I	Acetone	Colorless, irregular
N-(5-(iodoethynyl)pyridin-2-yl)propionamide	Propyl-act-I	Methanol	Orange
N-(5-(iodoethynyl)pyridin-2-yl))butyramide	Butyl-act-I	Methanol	Colorless, irregular
N-(5-(iodoethynyl)pyridin-2-yl)pentanamide	Pentyl-act-I	Methanol	Yellow, tetragonal
N-(5-ethynylpyridin-2-yl)acetamide	Acetyl-act-H	Acetonitrile	Colorless, near
N-(5-ethynylpyridin-2-yl)propionamide	Propyl-act-H	Acetone	Colorless, plate
N-(5-ethynylpyridin-2-yl)butyramide	Butyl-act-H	Acetone	Yellow, Block
N-(5-ethynylpyridin-2-yl)pentanamide	Pentyl-act-H	Acetone	Colorless, plate

In all four crystal structures from the alkyl-act-I series, the primary intermolecular hydrogen bond is a N-H···N(py)/N(py)···H-N synthon led to dimers. In acetyl-act-I the targeted C-I···O=C interaction is seen. -The O=C···I angle is ~120° while the van de Waals reduction is ~16%. In propyl-act-I too the targeted C-I···O=C interaction is one again seen. The C-I···O=C angle is ~141°, with the van der Waals reduction of ~12%. In Butyl-act-I once again we see a C-I···O=C to carbonyl interaction. In addition, a C-I···I interaction is also present. Thus, there are two crystallographically unique molecules in this structure. In Pentyl-act-I, C-I···O=C halogen bond and C-I··· π interaction is seen (Figure 6.13).

In each of the four crystal structures from the alkyl-act-H series, again the primary intermolecular hydrogen bond interaction is a N-H···N(py)/N(py)···H-N synthon which produces dimers. The acetyl-act-H is the only target with a C-H···O=C interaction. There were no structure directing interaction shown by the ethynyl hydrogen atom in Propyl-act-H, butyl-act-H or Pentyl-act-H (Figure 6.14).

The relevant hydrogen bond geometries of the crystal structures from the acetyl-act-I and acetyl-act-H given (Table 6.8)

Table 6.8. Bond parameters in the crystal structures.

Compound	**D-H/I···A**	**D/I···A (Å)**	**D-H···A (deg)**
Acetyl-act-I	N10-H10···N2	3.321(6)	163.(6)
	C8-I9···O12	2.938(3)	166.49(17)
Propyl-act-I	N10-H10···N2	3.058(6)	178.(7)
	C8-I9···O12	3.087(4)	166.2(2)
Butyl-act-I	N10-H10···N22	3.248(8)	169.27(4)
	C8-I9···O32	2.920(5)	172.43(3)
	N30-H30···N2	3.251(8)	170.52(3)
	C68-2I9···I9	3.800(6)	171.92(1)
Pentyl-act-I	N7 H7 N18	3.237(8)	166.(7)
	C15-I16···O25	2.845(5)	171.1(3)
	N23-H23···N2	3.201(7)	176.(6)
	C11-I32···C21	3.648(10)	163.8(3)
Acetyl-act-H	N9-H9···N2	3.060(3)	166(3)
	N21-H21···N14	3.070(3)	169(3)
	C8-H8···O23	2.247(6)	159.35(5)
	C20-H20···O11	3.135	165.3
Propyl-act-H	N9-H9···N2	3.192(1)	165.99(8)
	N29-H29···N22	3.188(1)	165.42(8)
Butyl-act-H	N9-H9···N1	3.254 (7)	169.86(15)
	N23-H23···N15	3.262 (6)	171.54
Pentyl-act-H	N9-H9···N2	3.209(1)	171.80(6)

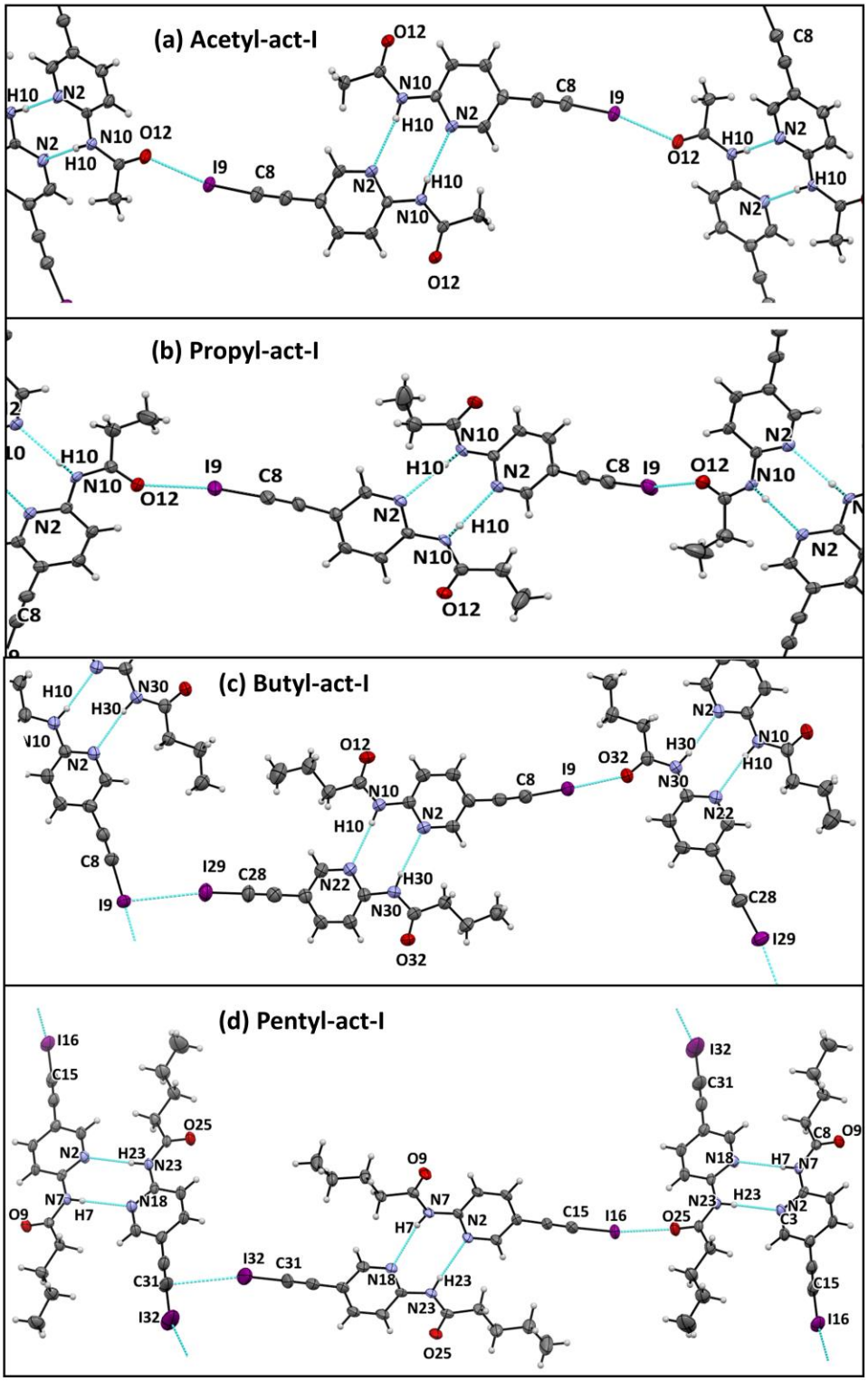

Figure 6.13. Primary assembly in the crystal structures of (a) Acetyl-act-I, (b) Propyl-act-I, (c) Butyl-act-I (d) Pentyl-act-I

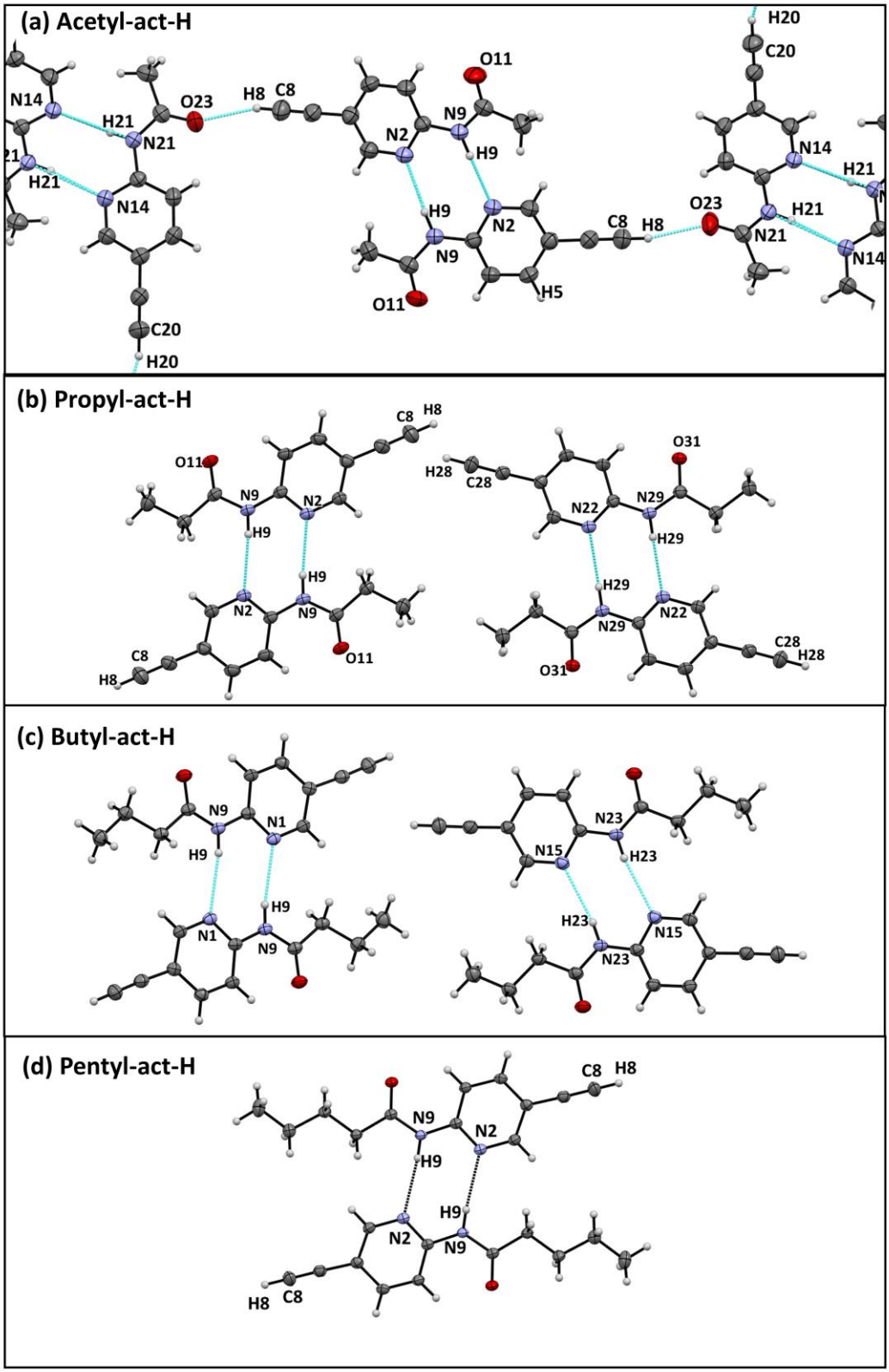

Figure 6.14. Primary assembly in the crystal structures of (a) Acetyl-act-H, (b) Propyl-act-H, (c) Butyl-act-H (d) Pentyl-act-H

6.7 Discussion – Part B

in part A we observed that chains predominated with the two shorter alkyl chain substituents while dimers predominated with the two longer alkyl chains. Here we observe dimer formation with both shorter and longer alkyl chains (8/8).

In both the acetyl-act-I and the acetyl-act-H targets, either a C-I···O=C or an -≡-H ···O=C interaction is formed, respectively. In part A, we hypothesized that chain formation could be promoted by the differing electrostatics (when X=acetyl), in the two groups (halogenated and non-halogenated).

The electrostatic profile of these molecules, in part B, are closer to the halogenated group of part A (which formed chains) (Figure 6.15, compare with Figure 6.9).

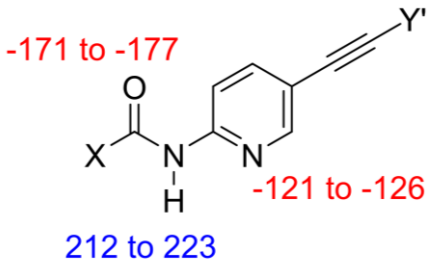

Figure 6.15. Summarized MEP data of targets in part B

Therefore, the strategy of "capping" the carbonyl group with a strongly competing iodoethynyl or ethynyl hydrogen atom worked as an effective approach to promote dimer formation. In propyl-act-I too a C-I···O interaction is formed.

Both butyl-act-I and pentyl-act-I form C-I···O=C interactions, while an additional C-I···I and C-I···π interaction is formed in the two targets respectively. Thus, when all four act-I compounds are considered, the halogen-bond donor interaction is influenced by the alkyl chain substituents.

The interactions shown by the iodoethynyl and ethynyl hydrogen atoms are summarized (Table 6.9)

Table 6.9. Intermolecular interactions by iodoethynyl and ethynyl moieties

		Act-I series	Act-H series
X	Acetyl	C-I···O=C	C-H···O=C
	Propyl	C-I···O=C	none
	Butyl	C-I···O=C and C-I···I	none
	Pentyl	C-I···O=C and C-I··· π	none

Therefore, there is no notable synthon mimicry between the iodoethynyl and ethynyl hydrogen moieties. In the previously published work on synthon mimicry of iodoethynyl and ethynyl hydrogen groups, a stronger acceptor, namely a pyridyl nitrogen was present[17]. Here however, since dimer formation occurred the weaker carbonyl oxygen does not attract the ethynyl hydrogen (Table 6.10).

6.8 Conclusions

The motivation for this work was driven by a need for investigation the self-aggregation of N-(pyridin-2-yl)alkylamides. Previous work indicated that dimer formation was the result of an attempt at preventing a steric clash.[14] Here we explored 20 different target molecules (two of which were considered in the previous work[14] in which there is no steric interference to dimer formation. Yet, dimers were not formed in all cases. The occurrence of dimer vs. chain formation for this group of molecules is actually very sensitive to small structural molecular changes. However, broadly speaking chains were formed in a higher frequency with shorter chains (acetyl and propyl) and dimers were formed in a higher percentage with the two longer alkyl chains.

In part B, we explored the strategy of promoting dimer formation by incorporating a potential hydrogen or halogen bond donor (Iodoethylnyl or ethynl hydrogen). This worked as an effective strategy to transition from chain to dimers with the smaller alkyl chain X substituents.

As a result of the work presented here, we have established in considerable detail how weaker intermolecular interactions are capable of ultimately tipping the balance between two dominant supramolecular motifs

6.9 References

[1] Adams, H.; Bernad Jr, P. L.; Eggleston, D. S.; Haltiwanger, R. C.; Harris, K. D.; Hembury, G. A., Kariuki McCabe, J. F. Substituent effects on aromatic interactions in the solid state. *Chem. Commun*. **2001**, 16, 1500-1501.

[2] Taborosi, A.; Yamaguchi, T.; Odani, A.; Yamauchi, O.; Kohzuma, T. The Role for the Weak Interaction on the Stabilization of Copper-Containing Complex: DFT Investigation of Noncovalent Interactions in Ternary-Cu (II)(DA)(AA) Complexes (DA= Diamine and AA= Amino Acids) as a Model of Metalloprotein. *Bull. Chem. Soc. Jpn*, **2019,** *92*, 1874-1882.

[3] Parra, N.; Guarda, L.; Belmar, J. B.; Hidalgo, P. I.; Jiménez, C. A.; Pasán, J.; Ruiz-Pérez, C. Conformational influence of quinoline moieties in the crystal packing of bis (quinolinecarboxamide) alkane derivatives. *CrystEngComm*. **2013**, *15*, 7212-7221.

[4] Bertolasi, V.; Hunter, N.; Vaughan, K.Crystal Structures of a Series of Bis {(2-Aminobenzoyl-) amino} alkanes. *J. Chem. Crystallogr*. **2009**, *39*, 372-376.

[5] Feng, Z.; Fan, A.; Valiyaveettil, S.; Vittal, J. J. Interplay of weak interactions and structural features in the solid state self-assembly of symmetric diamides. *Cryst. Growth Des*. **2003,** *3*, 555-565.

[6] D.El Sayed, *CSD Communication* **(2019)**

[7] Jing-Huo Chen, Cheng-Hua Deng, Sheng Fang, Jian-Gong Ma, Peng Cheng, *CSD Communication* (2018)

[8] Jones, R. E.; Templeton, D. H. The crystal structure of acetic acid. *Acta Cryst.* **1958**, *11*, 484-487

[9] Thapa, K. B.; Chen, J. D. Crystal engineering of coordination polymers containing flexible bis-pyridyl-bis-amide ligands. *CrystEngComm*. ***2015,*** *17*, 4611-4626.

[10] Zhou, Y.; Gu, Z.; Liu, J.; Huang, K.; Liu, G.; Wu, J. Arginine based poly (ester amide)/hyaluronic acid hybrid hydrogels for bone tissue Engineering. *Carbohydr. Polym.* **2020**, *230*, 115640.

[11] Radwan, M. A.; Al-Sweasy, O. H.; Elazab, H. A. Preparation of hydrogel based on acryl amide and investigation of different factors affecting rate and amount of absorbed water. *Agricultural Sciences*. **2017**, *8*, 161.

[12] Bendzińska-Berus, W.; Warżajtis, B.; Gajewy, J.; Kwit, M.; Rychlewska, U. Trityl Group as an Crystal Engineering Tool for Construction of Inclusion Compounds and for Suppression of Amide NH⋯ O=C Hydrogen Bonds. *Cryst. Growth Des.* **2017**. *17*, 2560-2568.

[13] McQuade, D. T.; McKay, S. L.; Powell, D. R.; Gellman, S. H. Indifference to hydrogen bonding in a family of secondary amides. *J. Am. Chem. Soc*, **1997**, *119*, 8528-8532.

[14] Osmiałowski, B.; Kolehmainen, E.; Dobosz, R.; Gawinecki, R.; Kauppinen, R.; Valkonen, A.; Koivukorpi. J.; Rissanen, K. Self-organization of 2-acylaminopyridines in the solid state and in solution. *J. Phys. Chem. A.* ***2010****, 114*, 10421-10426.

[15] Fun, H. K.; Shahani, T.; Kumar, R.; Isloor, A. M.; Shivananda, K. N. N-(5-Bromopyridin-2-yl) acetamide. *Acta Crystallographica Section E: Structure Reports Online*. **2011**, *67*, o2043.

[16] Batsanov, S. S. Van der Waals radii of elements. *Inorganic materials*, **2001**,*37*, 871-885.

[17] Aakeröy, C. B.; Welideniya, D.; Desper, J. Ethynyl hydrogen bonds and iodoethynyl halogen bonds: a case of synthon mimicry. *CrystEngComm*, 2017, *19*, 11-13.

Chapter 7 - Making ternary co-crystals

7.1 Introduction

In order to bring bottom-up[1]synthesis of new organic materials to a higher level of sophistication and functionality, it is essential that we can combine more than two different building blocks within a single crystalline lattice. However, multicomponent co-crystal synthesis is very challenging, simply because of the increased number of possible outcomes of interactions[2], as the number of different molecules is increased (Figure 7.1)

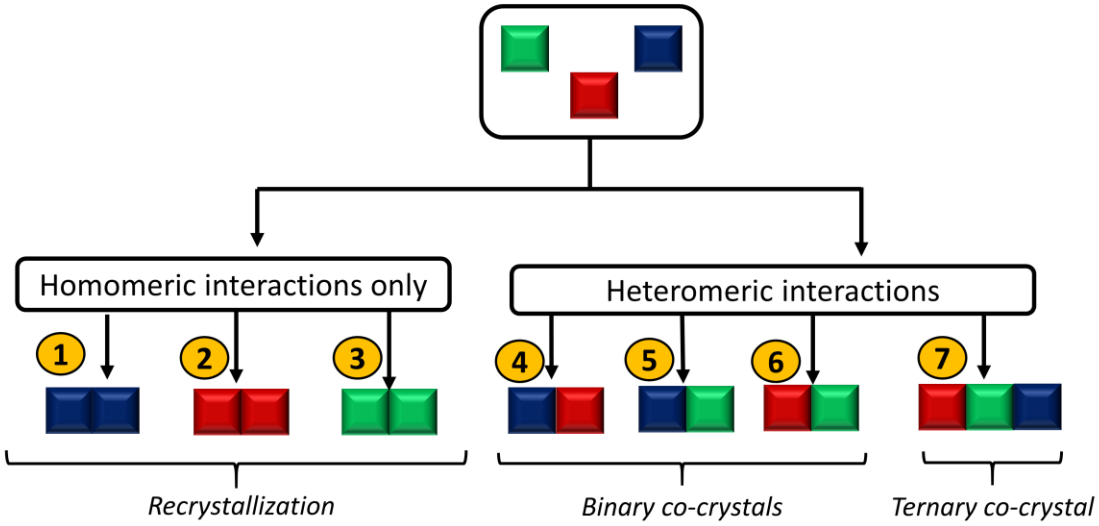

Figure 7.1. Schematic representation of possible outcomes of a multi component supramolecular synthesis

To synthesize ternary co-crystals, it is necessary to make a careful selection of functional groups (to satisfy chemical interactions) and molecule characteristics (to meet geometric requirements) in order to achieve targeted synergistic assembly of different molecular building blocks. One strategy which has been used includes a hierarchical approach[3] based on a best donor-best acceptor ranking of intermolecular interactions.[4,5,6] Another strategy has been based on a size and shape template

approach[7] to deliver very rare quaternary[8] and quintenary[9] co-crystals. Despite these advances, the pool of multicomponent co-crystals in still limited where only ~120 were documented in the CSD by 2019 (out of close to a million crystal structures).[10] There are a few reports of halogen bonds being used in combination with hydrogen bonds for ternary co-crystal synthesis.[11,12] Structural studies on the possible hierarchical nature of halogen bonds and hydrogen bonds in multicomponent co-crystal comprising crown ether, thio-urea and perfluoro halocarbons have been reported recently.[13,14] Additionally, the experimental outcome of any crystallization and co-crystallization is going to be influenced by solvent.[15]

Because of the similarities between hydrogen and halogen bonds, they can compete for the same binding sites. We hypothesize that carboxylic acids, which are well known to form dimers in the solid state, would preferentially form an interaction where the –OH group can act as a donor, whilst the carbonyl oxygen atom can simultaneously function as an acceptor, rather than forming a single point hydrogen bond to an acceptor (Figure 7.2).

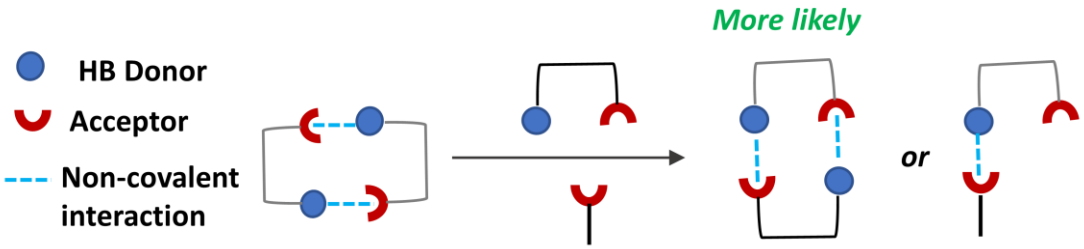

Figure 7.2. Postulated preferences in co-crystallization for a carboxylic acid-type moiety

Thus, if a halogen bond donor is brought into the midst of the reaction components above and if heteromeric interactions proceeded we can expect the halogen bond donor to bind to the molecule with an acceptor site only.

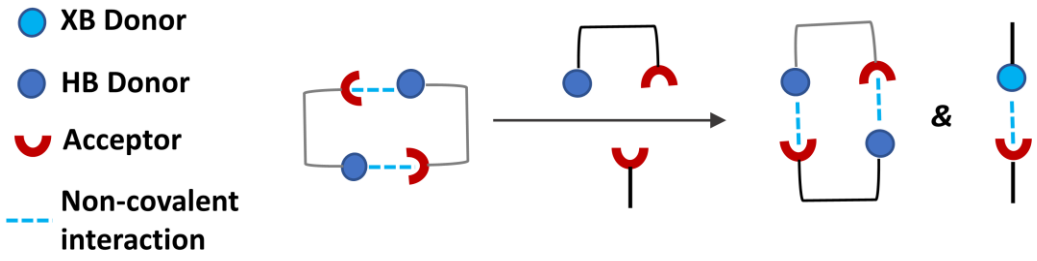

Figure 7.3. Postulated preference in co-crystallization for a carboxylic acid-type moiety and halogen bond donor containing moiety

In this chapter, we pursue a design strategy for ternary co-crystal formation of a system bearing a XB donor which could also offer a complementary binding site to a molecule which assembles by complimentary hydrogen bonding (such as carboxylic acid) (Figure 7.4).

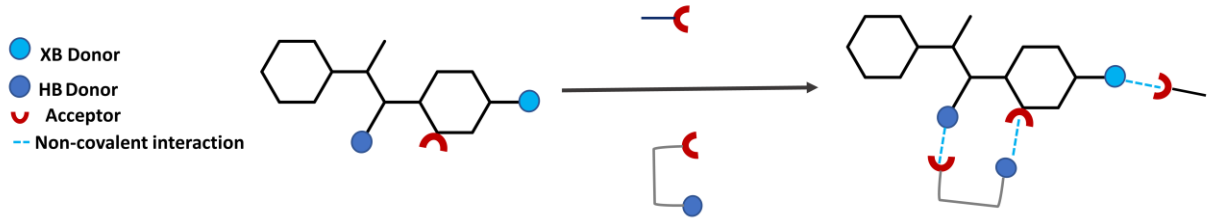

Figure 7.4. Proposed design strategy for ternary co-crystal formation

In Chapter 3[16], and in previous work[17] we have reported that the -N(py)-NH pocket can serve as a reliable recognition point forming –COOH···N(py)-NH synthon with carboxylic acids. In Chapter 5, we showed that the iodoethynyl group can function as an effective recognition point by reliably forming R-≡-I···N(py) halogen bonds. Thus, here we explore a proposed strategy for ternary co-crystal synthesis by combining the -N(py)-NH and the iodoethynyl group as assembly sites (Figure 7.5).

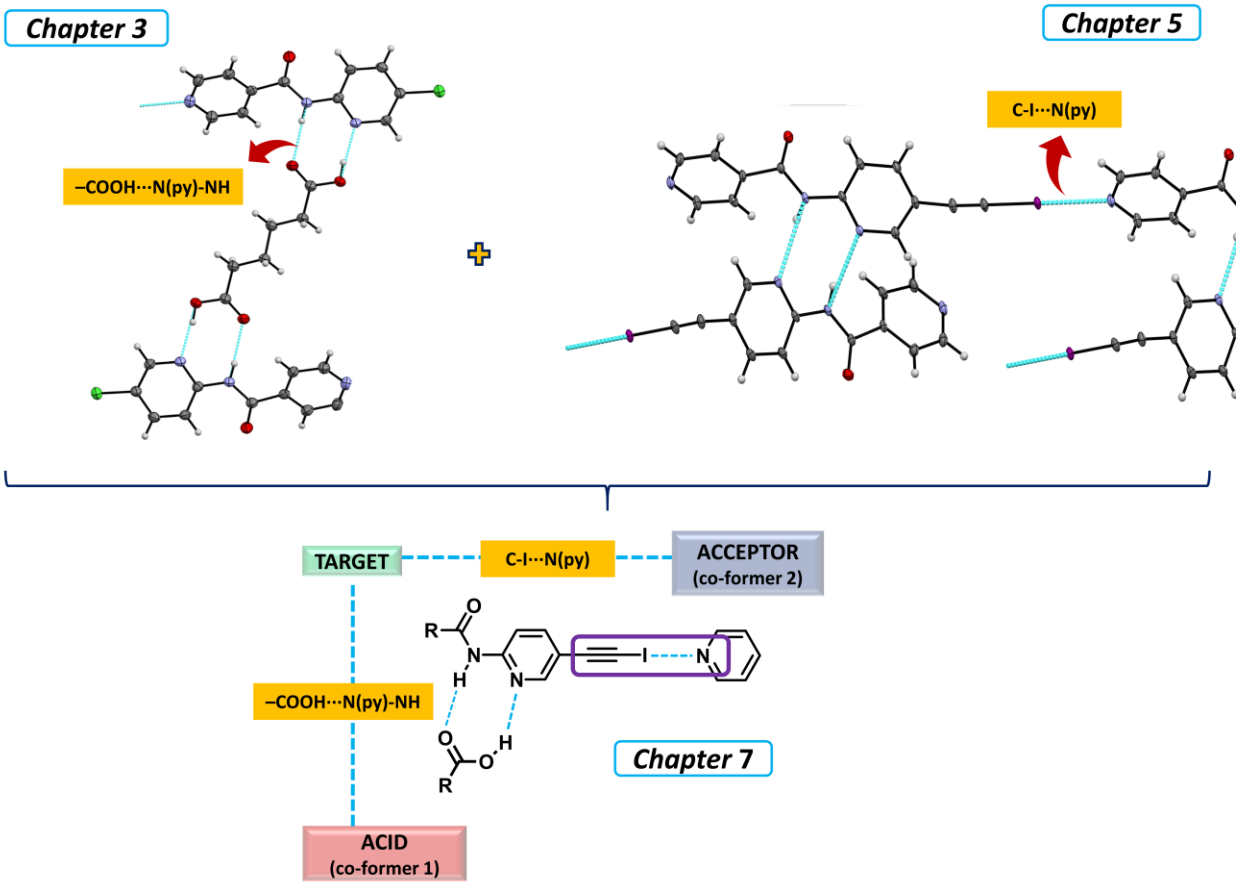

Figure 7.5. Principle of synthon selection for ternary co-crystal design in this study

Accordingly, two targets, three acids and seven acceptor molecules were selected (Figure 7.6), with the goal of forming ternary co-crystals through a combination of two-point hydrogen bonds and single-point halogen bonds.

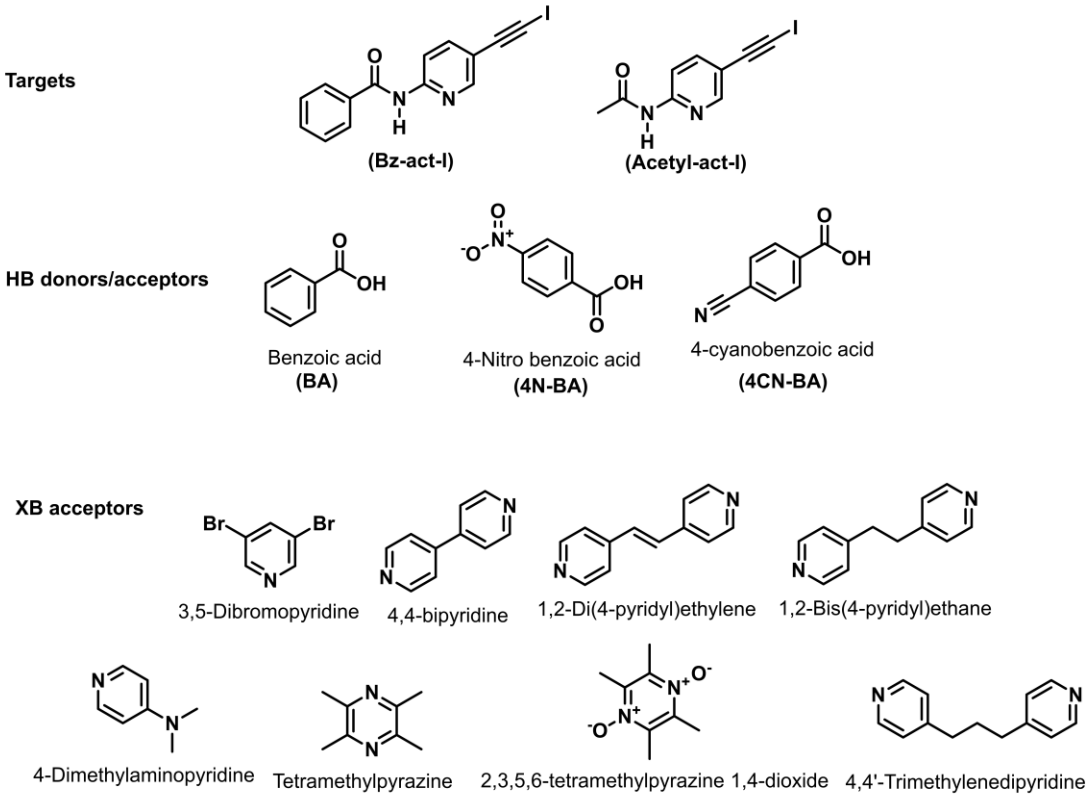

Figure 7.6. Targets (top) halogen-bond acceptors (bottom), hydrogen-bond donors/acceptors (middle)

7.2 Experimental

All acceptors and acids were purchased from commercial sources and used without further purification. The two target compounds were synthesized as mentioned in Chapter 5 (Bz-act-I) and Chapter 6 (Acetyl-act-I). Melting points were recorded on DSC Q20 differential scanning calorimeter. IR spectra were recorded with a Nicolet 380 FT-IR spectrometer using an attenuated total reflection (ATR) technique and ZnSe as the crystal.

First, each of the targets were screened to confirm co-crystal formation of the binary combinations by liquid assisted grinding followed by IR analysis. Next, the ternary combinations were subjected to liquid assisted grinding.

- Bz-act-I targets were screened in combination with three acids and 7 acceptors (21 experiments).
- Acetyl-act-I targets were screened in combination with three acids and 5 acceptors (15 experiments).

The target and acid were always in a 1:1 stoichiometric ratio. The acceptor was either in a 1:2 (4,4-bipyridine, 1,2-di(4-pyridyl)ethylene, 1,2-*bis*(4-pyridyl)ethane, tetramethylpyrazine, 2,3,5,6-tetramethylpyrazine 1,4-dioxide, 4,4'-trimethylenedipyridine) or 1:1 (3,5-bromopyridine, 4-dimethylaminopyridine) molar ratio to acid and target.

The DSC profiles were used to assess the crystallinity (sharp melting points of the sample). A positive hit was confirmed by IR and DSC analyses, where melting points of the ground mixture was different to any of the individual or binary components.

7.2.1 DSC and IR data

The DSC and IR data of ternary co-crystal screens done with Bz-act-I are given in Tables 7.1-7.3.

The DSC and IR data of ternary co-crystal screens done with Acetyl-act-I are given in Tables 7.4-7.6.

Table 7.1. Ternary co-crystal screen data of Bz-act-I+4CNBA+7 acceptors

Target	**Acid**	**Target + Acid**		**Acceptor**		**Target + Acceptor**	**Acid + Acceptor**	**All three combined**	✗/ ✓
BZ-act-I m.p	*4-CNBA* m.p	m.p		Name	m.p	m.p	m.p	m.p	
IR, cm^{-1}	*IR, cm^{-1}*	*IR, cm^{-1}*			*IR, cm^{-1}*	*IR, cm^{-1}*	*IR, cm^{-1}*	*IR, cm^{-1}*	
156-158 °C followed by exothermic peak	219-221 °C	154-156 °C and no degradation	**1**	**3,5 Bromopyridine**	110 - 112 °C (87.3 J/g)	93-94 °C (36.05 J/g)	121-123 °C (149 J/g), 216-218 °C (94 J/g)*	90-92 °C (25 J/g). 112-114 °C (1 J/g)** 133- 135 °C (11.47 J/g)*	✗
3427, 1686, 1502, 1486, 1365	2230, 1689, 1609, 1430, 1322, 1302, 1286, 1182	2439, 2224, 1897, 1692, 1606, 1581, 1316, 1296, 1269			3004,1540, 1407,1083	3428, 1690, 1508, 1298. 1258	2228, 1711, 1547, 1410, 1312, 1277	2224, 1692, 1533, 1269	
			2	**4,4-Bipyridine**	111 - 113 °C (126.7 J/g)	152-154 °C (102.2 J/g) followed by exothermic peak at 158	188-190 °C (83 J/g), 201 – 203 °C (8 J/g)*	142-144 °C, 146-148 °C (59 J/g) *150-**(164)**-170 °C*	✓
					3023, 1585, 1529, 1404, 1217, 987	1666, 1592, 1573, 1368	2449, 1701, 1598, 1283	2339, 1875, 1679, 1508, 1406, 1372, 1067	
			3	**1,2-Di(4-pyridyl)ethylene**	151 - 153 °C (133.1 J/g)	156 - 158 °C (48.90 J/g) followed by exothermic peak 161	209 - 211 °C (147 J/g)	142 - 144 °C (38 J/g) followed by small exothermic peak	✓
					1592, 1409, 1551, 1300, 978	1678, 1596, 1488, 1418, 1371,1305	2222, 1710, 1425, 1312, 1296, 1004	1710, 1687, 1608, 1508, 1487, 1367	
			4	**1,2-Bis(4-pyridyl)ethane**	111 - 113 °C (143.4 J/g)	121 -124 °C (69-39 J/g) followed by exothermic peak	152 – 154 °C (5 J/g)* 185 -187 °C (90 J/g)	131 - 133 °C (49 J/g) followed by exothermic peak	✓
					1592, 1565, 1453, 1416, 1077	1686, 1572, 1508, 1437, 1301, 1129	1707, 1696,	1708, 1687, 1509, 1415, 1254, 1019	

							1416, 1292, 1065, 1016		
			5	**Tetramethyl pyrazine**	85 - 87 °C (201.5 J/g)	153 - 156 °C (5.826 J/g) followed by exothermic peak	216 - 218 °C (42 J/g)	124 - 126 °C (28 J/g)	✓
					1437, 1406, 1357, 1199, 986	1688, 1508, 1365, 1255, 1135	1702, 1232, 1171, 865, 773	2748, 1905, 1678, 1600,1272, 1115	
			6	**2,3,5,6-tetramethylpyrazine 1,4-dioxide**	229 - 231 °C (137 J/g)	121-124 °C (0.366 J/g) followed by exothermic peak	138 -140 °C (47 J/g)	124 - 126 °C (56 J/g)	✓
					1522, 1302, 1114,1102	1670, 1698, 1508, 1115, 1024	1711, 1405, 1231, 1093, 1013	2154, 1894, 1689, 1507, 1172	
			7	**4,4'-Trimethylenedipyridine**	60 - 62 °C (88.16 J/g)	91 - 93 °C (26.48 J/g)	121-123 °C (2 J/g r)* 152 - 154°C (84 J/g)	122 -124 °C (52 J/g) followed by exothermic peak	✓
					1600, 1555, 1226, 1215, 900	1667, 1505, 1384, 1255, 1021	1706, 1609, 1420, 1219, 1066	2363, 1693, 1502, 1293,1039	

Table 7.2. Ternary co-crystal screen data of Bz-act-I+BA+7 acceptors

Target	Acid	Target + Acid		Acceptor		Target + Acceptor	Acid + Acceptor	All three combined	×/ ✓
BZ-act-I m.p	*BA* m.p	m.p		Name	m.p	m.p	m.p	m.p	
IR, cm^{-1}	*IR, cm^{-1}*	*IR, cm^{-1}*			*IR, cm^{-1}*	*IR, cm^{-1}*	*IR, cm^{-1}*	*IR, cm^{-1}*	
156-158 °C followed by exothermic peak	121-123 °C (209.9 J/g)	118-120 °C (59.8 J/g) and no degradation	**1**	**3,5 Bromopyridine**	110 - 112 °C (87.3 J/g)	93-94 °C (36.05 J/g)	74-76 °C (43.84 J/g)	78-80 °C (45.75 J/g) Some additional peaks above 200.	×
3427, 1686, 1502, 1486, 1365	1677, 1600, 1418, 1286, 1179, 927	3429, 1675, 1602, 1295, 1274, 1026			3004,1540, 1407,1083	3428, 1690, 1508, 1298. 1258		1681, 1582, 1413, 1351, 1317,	
			2	**4,4-Bipyridine**	111 - 113 °C (126.7 J/g)	152-154 °C (102.2 J/g) followed by exothermic peak at 158	114 -116 °C (108.3 J/g)	123-125 °C (6.493 J/g)* 132-134 °C (56.72 J/g)	✓
					3023, 1585, 1529, 1404, 1217, 987	1666, 1592, 1573, 1368	2428, 1685,1596, 1535, 1313, 1266	1672, 1600, 1592, 1450, 1371, 1272	
			3	**1,2-Di(4-pyridyl)ethylene**	151 - 153 °C (133.1 J/g)	156 - 158 °C (48.90 J/g) followed by exothermic peak 161	125-127 °C (181.9 J/g)	129-131 °C (58.94 J/g)	✓
					1592, 1409, 1551, 1300, 978	1678, 1596, 1488, 1418, 1371,1305	1670, 1599, 1415, 1308, 1270, 1067	1674, 1578, 1491, 1371, 1292	
			4	**1,2-Bis(4-pyridyl)ethane**	111 - 113 °C (143.4 J/g)	121 -124 °C (69-39 J/g) followed by exothermic peak	87 – 89 °C (65.89 J/g)	110 – 112 °C (44.25 J/g) 121-123 °C (2.620 J/g)	✓
					1592, 1565, 1453, 1416, 1077	1686, 1572, 1508, 1437, 1301, 1129	1682, 1610, 1434, 1316, 1122	1671, 1509, 1370, 1320, 1293	
			5	**Tetramethylpyrazine**	85 - 87 °C (201.5 J/g)	153 - 156 °C (5.826 J/g)	76 – 78 °C (97.88 J/g)	78 – 80 °C (29.68 J/g),	✓

						followed by exothermic peak		161 – 162 °C (48.89 J/g),	
					1437, 1406, 1357, 1199, 986	1688, 1508, 1365, 1255, 1135	1496, 1448, 1408, 1312, 1252, 1113	2410, 1905, 1678, 1367, 1295, 1257	
			6	**2,3,5,6-tetramethylpyrazine 1,4-dioxide**	229 - 231 °C (137 J/g)	121-124 °C (0.366 J/g) followed by exothermic peak	88-90 °C (40.91 J/g), 125- 127 °C (9.517 J/g) minor	91 – 93 °C (32.51 J/g)	✓
					1522, 1302, 1114,1102	1670, 1698, 1508, 1115, 1024	1689, 1524, 1297, 1271, 1089	1681, 1487, 1448, 1367, 1259,	
			7	**4,4'-Trimethylenedipyridine**	60 - 62 °C (88.16 J/g)	91 - 93 °C (26.48 J/g)	46-48 °C (132.2 J/g)	96 – 98 °C (32.89 J/g)	✓
					1600, 1555, 1226, 1215, 900	1667, 1505, 1384, 1255, 1021	1683, 1600 1580, 1446, 1418	1690, 1571, 1487, 1368, 1254	

Table 7.3. Bz-act-I+4N-BA+7 acceptors

Target	**Acid**	**Target + Acid**		**Acceptor**		**Target + Acceptor**	**Acid + Acceptor**	**All three combined**	✗ / ✓
BZ-act-I m.p	*4N-BA* m.p	m.p		Name	m.p	m.p	m.p	m.p	
IR, cm^{-1}	*IR, cm^{-1}*	*IR, cm^{-1}*			*IR, cm^{-1}*	*IR, cm^{-1}*	*IR, cm^{-1}*	*IR, cm^{-1}*	
156-158 °C followed by exothermic peak	236 – 238 °C (295 J/g)	167 – 169 °C (51 J/g)	**1**	**3,5 Bromopyridine**	110 - 112 °C (87.3 J/g)	93-94 °C (36.05 J/g)	237-239 °C (89.38 J/g), 103-105 °C (39.33 J/g)	96 – 99 °C (17.47 J/g), 165 – 167 °C (24. 65 J/g)	✓
3427, 1686, 1502, 1486, 1365	1681, 1598, 1533, 1422, 1273	1681, 1602, 1582, 1521, 1372, 1267			3004,1540, 1407,1083	3428, 1690, 1508, 1298. 1258		1691, 1533, 1522, 1310, 1286, 1105	
			2	**4,4-Bipyridine**	111 - 113 °C (126.7 J/g)	152-154 - °C (102.2 J/g) followed by exothermic peak at 158	219 – 221 °C (49 J/g), 232 – 234 °C (130 J/g)	141-143 °C (20.17 J/g), 150 – 153 °C (7.949 J/g)*	✓
					3023, 1585, 1529, 1404, 1217, 987	1666, 1592, 1573, 1368	1700, 1601, 1526, 1405, 1310,	1692, 1669, 1532, 1513, 1303	
			3	**1,2-Di(4-pyridyl)ethylene**	151 - 153 °C (133.1 J/g)	156 - 158 °C (48.90 J/g) followed by exothermic peak 161	222- 224 °C (139.5 J/g), 192-195 °C (10.92 J/g)	122-124 °C (1.607 J/g), 148-150 °C (16.33 J/g), 161-163 °C (6.26J/g), 167 – 169 °C (3.509 J/g), multiple peaks ~10 from 250 – 300 °C	✗
					1592, 1409, 1551, 1300, 978	1678, 1596, 1488, 1418, 1371,1305	1703, 1605, 1519, 1312,1102	1690, 1603, 1370, 1298, 1267	
			4	**1,2-*Bis*(4-pyridyl)ethane**	111 - 113 °C (143.4 J/g)	121 -124 °C (69-39 J/g) followed by exothermic peak	188 – 190 °C (29 J/g), 198-200 °C (87 J/g)	133 – 135 °C (13.08 J/g), 141 – 143 °C (9.422 J/g),	✗

								155-157 °C (6.953 J/g),	
					1592, 1565, 1453, 1416, 1077	1686, 1572, 1508, 1437, 1301, 1129	1698, 1606, 1522,1314, 1251, 1025	1692, 1509, 1488, 1417, 1296	
			5	**Tetramethylpyrazine**	85 - 87 °C (201.5 J/g)	153 - 156 °C (5.826 J/g) followed by exothermic peak	238 – 240 °C (91.86 J/g)	165 – 167 °C (42.68 J/g),	✓
					1437, 1406, 1357, 1199, 986	1688, 1508, 1365, 1255, 1135	1697, 1515, 1410, 1342, 1234	1691, 1602, 1520, 1371, 1267	
			6	**2,3,5,6-Tetramethylpyrazine 1,4-dioxide**	229 - 231 °C (137 J/g)	121-124 °C (0.366 J/g) followed by exothermic peak	162 – 164 °C (154.4 J/g)	140 – 143 °C (51.11 J/g) followed by exotherm.	✓
					1522, 1302, 1114,1102	1670, 1698, 1508, 1115, 1024	1686, 1520, 1343, 1255, 1081	1687, 1677, 1372, 1296, 1099	
			7	**4,4'-Trimethylenedipyridine**	60 - 62 °C (88.16 J/g)	91 - 93 °C (26.48 J/g)	166 – 168 °C (122.4 J/g)	123 – 125 °C (32.75 J/g)	✓
					1600, 1555, 1226, 1215, 900	1667, 1505, 1384, 1255, 1021	2418, 1714, 1607, 1514, 1471	1690, 1607, 1570, 1417, 1065,	

Table 7.4. Ternary co-crystal screen with Acetyl-act-I + 4CNBA + 5 acceptors

Target	**Acid**	**Target + Acid**		**Acceptor**		**Target + Acceptor**	**Acid + Acceptor**	**All three combined**	✗/ ✓
Act-I m.p	*4-CNBA* m.p	m.p		Name	m.p	m.p	m.p	m.p	
IR, cm^{-1}	*IR, cm^{-1}*	*IR, cm^{-1}*			*IR, cm^{-1}*	*IR, cm^{-1}*	*IR, cm^{-1}*	*IR, cm^{-1}*	
199-200 °C	219-221 °C 118.4 J/g	168- 170 °C (6.4 J/g, minor), 174 – 176 °C (58.1 J/g)	**1**	**4-Dimethylaminopyridine**	111-113 °C (199.3 J/g)	147-149 °C (30.47 J/g) , followed by degradation peaking at 149	107 – 109 °C (1.603 J/g)*, broad 150 – 160 °C peaking at 158 °C	142-144 °C (77 J/g), Degradation *148 – 153 °C (58 J/g) peaking at 150 °C*	✗
1672, 1587, 1506, 1380, 1365	2230, 1689, 1609, 1430, 1322, 1302, 1286, 1182	1702, 1673, 1288, 1255			1585, 1536, 1442, 1344, 1220,	1696, 1605, 1586, 1437, 1360		1673, 1650, 1555, 1292, 1201	
			2	**4,4-Bipyridine**	111 - 113 °C (126 J/g)	185 – 187 °C (218 J/g)	188-190 °C (83 J/g), 201 – 203 °C (8 J/g)*	163 – 165 °C (123 J/g), Degradation 165- 175 °C, peaking at 172 °C, 85 J/g)	✓
					3023, 1585, 1529, 1404, 1217, 987	1666, 1592, 1573, 1368	1678, 1596, 1488, 1418, 1371,1305	1672, 1507, 1316, 1288, 1004	
			3	**1,2-Di(4-pyridyl)ethylene**	151 - 153 °C (133.1 J/g)	121 – 123 °C (25 J/g), followed by degradation 170 – 200 °C leaking at 184 °C)	209 - 211 °C (147 J/g)	166 – 169 °C (104 J/g), Followed by degradation 170- 175 °C, peaking at 172 °C, 29 J/g)	✓
					1592, 1409, 1551,	1663, 1599, 1572, 1518, 1297	2222, 1710, 1425,	1709, 1672, 1608, 1518, 1425, 1171	

		1300, 978		1312, 1296, 1004		
4	**1,2-*Bis*(4-pyridyl)ethane**	111 - 113 °C (112 J/g)	151 -155 °C degradation peaking at 153 °C (114 J/g), broad melting point 168- 175 °C (17.18 J/g)	152 – 154 °C (5 J/g)* 185 -187 °C (90 J/g)	148 – 150 °C (75 J/g), Followed by exotherm 150 – 155 °C (65 J/g),	✗
		1592, 1565, 1453, 1416, 1077	1663, 1603, 1509, 1296, 1066	1707, 1696, 1416, 1292, 1065, 1016	1667, 1603, 1584, 1518, 1367,1124	
5	**2,3,5,6-Tetramethylpyrazine 1,4-dioxide**	229 - 231 °C (137 J/g)	Degradation 160 - 200 °C peaking at 171 °C	138 -140 °C (47 J/g)	119 - 123 °C (25 J/g), 131 - 133 °C (22 J/g), 152 -169 °C (32 J/g)	✓
		1522, 1302, 1114,1102	1673, 1515, 1382, 1116	1711, 1405, 1231, 1093, 1013	1714, 1511, 1445, 1405, 1298,	

Table 7.5. Ternary co-crystal screen with Acetyl-act-I + 4BA + 5 acceptors

Target	**Acid**	**Target + Acid**		**Acceptor**		**Target + Acceptor**	**Acid + Acceptor**	**All three combined**	×/ ✓
Act-I	*BA* m.p			Name	m.p	m.p	m.p	m.p	
IR, cm^{-1}	*IR, cm^{-1}*	*IR, cm^{-1}*			*IR, cm^{-1}*	*IR, cm^{-1}*	*IR, cm^{-1}*	*IR, cm^{-1}*	
199-200 °C	121-123 °C (209.9 J/g)	139-141 °C (87.3 J/g, *200-202 °C (201.6 J/g)*	**1**	**4-Dimethylaminopyridine**	111-113 °C (199.3 J/g)	147-149 °C (30.47 J/g) , followed by degradation peaking at 149	83 – 84 °C (4 J/g), 101 – 103 °C (73 J/g)	104 – 106 °C (26 J/g)	×
1672, 1587, 1506, 1380, 1365	1677, 1600, 1418, 1286, 1179, 927	1683, 1602, 1585, 1367, 1320			1585, 1536, 1442, 1344, 1220,	1696, 1605, 1586, 1437, 1360	1641, 1539, 1376, 1214, 1444	1674, 1642, 1529, 1320, 1215	
			2	**4,4-Bipyridine**	111 - 113 °C (126 J/g)	185 – 187 °C (218 J/g)	113 – 116 °C (108 J/g)	101 – 103 °C (9.3 J/g), 127 – 129 °C (4.1 J/g)	✓
					3023, 1585, 1529, 1404, 1217, 987	1666, 1592, 1573, 1368	2428, 1685,1596 , 1535, 1313, 1266	1684, 1602, 1525, 1449	
			3	**1,2-Di(4-pyridyl)ethylene**	151 - 153 °C (133.1 J/g)	121 – 123 °C (25 J/g), followed by degradation 170 – 200 °C leaking at 184 °C)	125 – 127 °C (182 J/g)	108 – 110 °C (14.14 3 J/g), 126 – 128°C (32 J/g)	✓
					1592, 1409, 1551, 1300, 978	1663, 1599, 1572, 1518, 1297	1703, 1605, 1519, 1312,1102	1671, 1517, 1449, 1277	

				4	**1,2-*Bis*(4-pyridyl)ethane**	111 - 113 °C (112 J/g)	151 -155 °C degradation peaking at 153 °C (114 J/g), broad melting point 168- 175 °C (17.18 J/g)	87 – 89 °C (65 J/g)	92 – 94 °C (8 J/g), 117- 119 °C (9 J/g), several peaks above 150 °C	✗
						1592, 1565, 1453, 1416, 1077	1663, 1603, 1509, 1296, 1066	1682, 1610, 1434, 1316, 1122	1667, 1584, 1518, 1417, 1367	
				5	**2,3,5,6-Tetramethylpyrazine 1,4-dioxide**	229 - 231 °C (137 J/g)	Degradation 160 - 200 °C peaking at 171 °C	88 -90 °C (40 J/g), 129 – 131 °C (9.5 J/g)	82 – 84 °C (8 J/g), 102 – 104 °C (13 J/g),	✓
						1522, 1302, 1114,1102	1673, 1515, 1382, 1116	1689, 1524, 1297, 1271, 1089	1681, 1506, 1448, 1295, 1259	

Table 7.6. Ternary co-crystal screen with Acetyl-act-I + 4NBA + 5 acceptors

Target	**Acid**	**Target + Acid**		**Acceptor**		**Target + Acceptor**	**Acid + Acceptor**	**All three combined**	✗/ ✓
Act-I m.p	*4N-BA* m.p	m.p		Name	m.p	m.p	m.p	m.p	
IR, cm^{-1}	*IR, cm^{-1}*	*IR, cm^{-1}*			*IR, cm^{-1}*	*IR, cm^{-1}*	*IR, cm^{-1}*	*IR, cm^{-1}*	
199-200 °C	236 – 238 °C (1029 J/g)	174 – 176 °C (249.5 J/g), 189 – 191 °C (46.0 J/g, minor)	**1**	**4-Dimethylaminopyridine**	111-113 °C (199.3 J/g)	147-149 °C (37 J/g) , followed by degradation peaking at 149	189 – 191 °C (30.47 J/g), 196 – 200 °C (42 J/g)	136 – 138 °C (3 J/g), Followed by degradation 150 – 153 °C (94 J/g),	✓
1672, 1587, 1506, 1380, 1365	1681, 1598, 1533, 1422, 1273	1534, 1557, 1438, 1335, 1201			1585, 1536, 1442, 1344, 1220,	1696, 1605, 1586, 1437, 1360	1636, 1557, 1514, 1335, 1201	1697, 1517, 1364, 1293, 1203	
			2	**4,4-Bipyridine**	111 - 113 °C (126 J/g)	185 – 187 °C (218 J/g)	219 – 221 °C (49 J/g), 232 – 234 °C (130 J/g)	175 – 177 °C (20 J/g), followed by degradation 177 – 185 °C peaking at 179 °C	✓
					3023, 1585, 1529, 1404, 1217, 987	1666, 1592, 1573, 1368	1700, 1601, 1526, 1405, 1310,	1704, 1673, 1524, 1342, 1295	
			3	**1,2-Di(4-pyridyl)ethylene**	151 - 153 °C (133.1 J/g)	121 – 123 °C (25 J/g), followed by degradation 170 – 200 °C leaking at 184 °C)	192 – 194 ° (10 J/g), 222 – 224 °C (140 J/g)	162 – 164 °C (39 J/g)	✓
					1592, 1409, 1551, 1300, 978	1663, 1599, 1572, 1518, 1297	1703, 1605, 1519, 1312,1102	1674, 1519, 1340, 1314, 1218	

			4	**1,2-*Bis*(4-pyridyl)ethane**	111 - 113 °C (112 J/g)	151 -155 °C degradation peaking at 153 °C (114 J/g), broad melting point 168- 175 °C (17.18 J/g)	201 °C (303 J/g) 188 – 190 °C (29 J/g), 198-200 °C (87 J/g)	157 – 159 °C (80 J/g) followed by degradation 160 – 162 °C (80 J/g)	✓
					1592, 1565, 1453, 1416, 1077	1663, 1603, 1509, 1296, 1066	1698, 1606, 1522,1314, 1251, 1025	1674, 1557, 1514, 1438, 1317	
			5	**2,3,5,6-Tetramethylpyrazine 1,4-dioxide**	229 - 231 °C (137 J/g)	Degradation 160 - 200 °C peaking at 171 °C	161 – 163 °C (155 J/g))	142 – 144 °C (90 J/g)	✓
					1522, 1302, 1114,1102	1673, 1515, 1382, 1116	1686, 1520, 1343, 1255, 1081	1674, 1518, 1367, 1294, 1227	

7.2.2 X-ray crystallography results

We obtained SXCRD for the ternary co-crystal comprising Bz-act-I, benzoic acid and 4,4-Bipyridine grown from chloroform. The intended assembly of the three components were observed. The -N(py)-NH pocket of the target interacted with the carboxylic acid forming –COOH···N(py)-NH synthon. The iodoethynyl halogen bond donor formed C-I···N(py) halogen bonds to both nitrogen atoms of the 4,4-bipyridine (Figure 7.7).

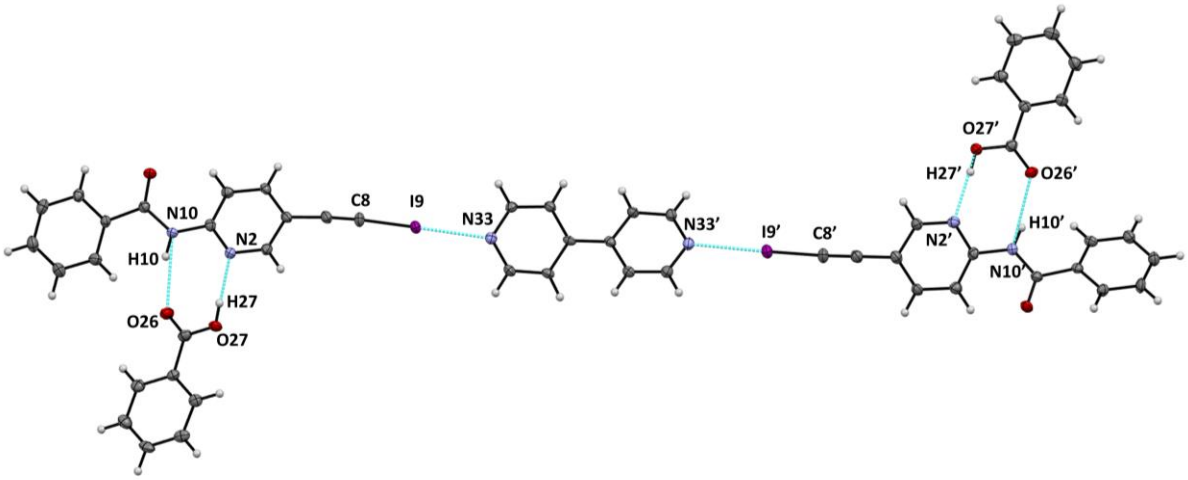

Figure 7.7. Primary interactions seen in ternary co-crystal of Bz-act-I, benzoic acid and 4-4'-Bipyridine

Table 7.7. Hydrogen- and halogen bond-bond parameters of ternary co-crystal Bz-act-I, benzoic acid and 4,4'-Bipyridine

D-H/I···A	**D/I···A (A)**	**D-H···A (deg)**
N10-H10···O26	2.904(5)	162.1(3)
O27-O27···N2	2.700(5)	176.7
C8-I9···N33	2.740(5)	179.40(17)
N10'-H10'···O26'	2.885(5)	164.4
O27'-O27'···N2'	2.736(5)	175.7
C8'-I9'···N33'	2.832(5)	178.36(18)

7.2.3 Discussion and conclusions

In some cases, more than one sharp melting point, different to any of the individual or binary components, was observed. This could possibly arise due to another solid phase wherein only one of the pyridyl nitrogen atoms bind to iodine to form a halogen bond (Figure 7.8).

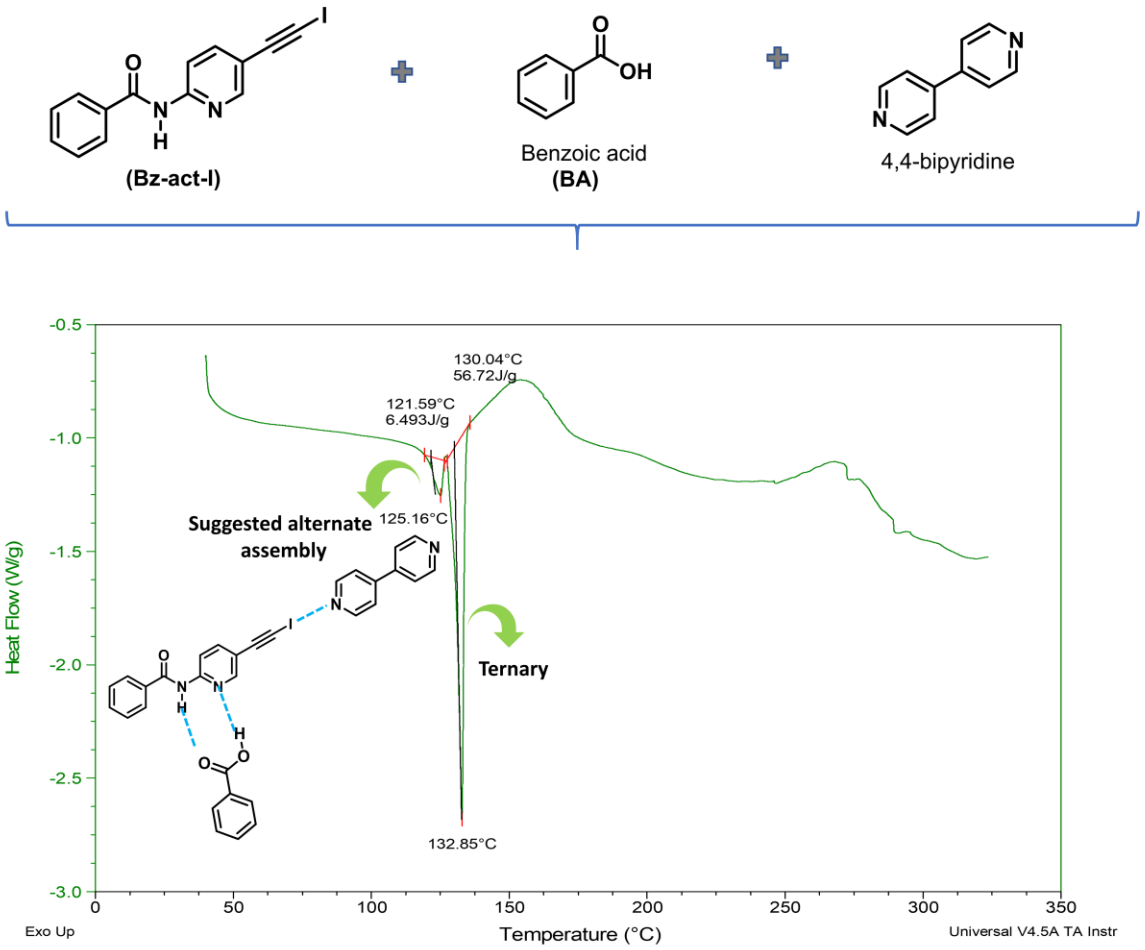

Figure 7.8. A suggested possible mode of assembly when more than one peak is seen in the DSC trace.

The overall success rate in ternary co-crystal formation was 80% with both Bz-act-I (17/21) and acetyl-act-I (12/15) targets. From the 29 hits obtained one crystal suitable for SXCRD was grown. Crystal growth is affected by solvent and the relative solubility of these components. If the solubilities are not closely similar to one another, one of the individual components may precipitate or one of the three possible binary co-crystals may nucleate first. In short, the experimental space which allows for a successful crystal growth from solution of ternary (or higher order) co-crystals is small (Figure 7.9).

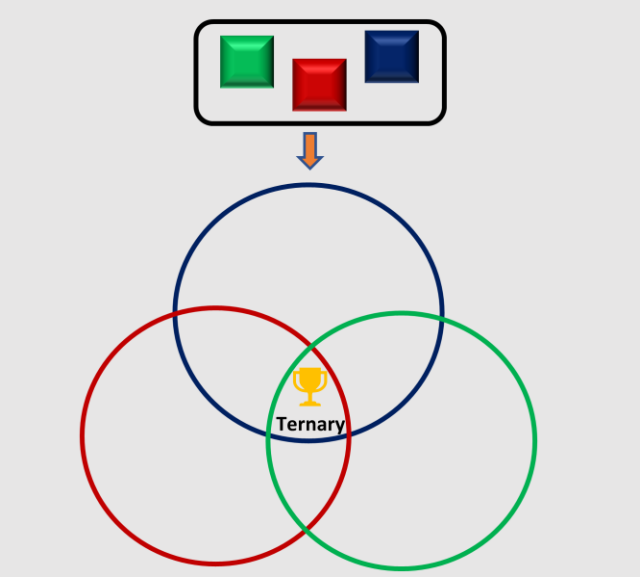

Figure 7.9. Schematic representation of the challenge of solubility in ternary crystal growth.

Based on our previous systematic structural studies of multicomponent (Chapter 2) and single component systems (Chapter 5), here we employ two functional groups, N(py)-NH and R-≡-I into the same target molecule to form –COOH···N(py)-NH and R-≡-I···N(py) synthons with carboxylic acids (co-former 1) and a pyridyl (co-former 2) acceptor respectively. In conclusion, the designed system proved to be a high yielding (80% success rate) for the synthesis of ternary co-crystals.

7.3 References

[1] Gunawardana, C. A.; Aakeröy, C. B. Co-crystal synthesis: fact, fancy, and great expectations. *Chem. Commun*, **2018**, *54*, 14047-14060.

[2] Bolla, G.; Nangia, A. Binary and ternary cocrystals of sulfa drug acetazolamide with pyridine carboxamides and cyclic amides. **2016**, *IUCrJ*, *3*, 152-160.

[3] Etter, M. C. Encoding and decoding hydrogen-bond patterns of organic compounds. Acc. Chem. Res. **1990**, *23*, 120−126.

[4] Aakeröy, C. B., Desper, J., Smith, M. M. Constructing, deconstructing, and reconstructing ternary supermolecules. *ChemComm*. **2007**, *38*, 3936-3938.

[5] Aakeröy, C. B.; Beatty, A. M.; Helfrich, B. A. "Total synthesis" supramolecular style: Design and hydrogen-bond-directed assembly of ternary supermolecules. *Angew. Chem. Int. Ed*. **2001**, *40*, 3240-3242.

[6] Adsmond, D. A.; Sinha, A. S.; Khandavilli, U. R.; Maguire, A. R.; Lawrence, S. E. Design and synthesis of ternary cocrystals using carboxyphenols and two complementary acceptor compounds. *Cryst. Growth Des.* 2016, *16*, 59-69.

[7] Tothadi, S.; Mukherjee, A.; Desiraju, G. R. Shape and size mimicry in the design of ternary molecular solids: towards a robust strategy for crystal engineering. *ChemComm*, **2011,** *47*, 12080-12082.

[8] Dubey, R. Mir, N. A.; Desiraju, G. R. Quaternary cocrystals: combinatorial synthetic strategies based on long-range synthon Aufbau modules (LSAM). **2016**, *IUCrJ*, *3*, 102-107.

[9] Mir, N. A., Dubey, R., Desiraju, G. R. Four-and five-component molecular solids: crystal engineering strategies based on structural inequivalence.**2016**, *IUCrJ*, *3*(2), 96-101.

[10] Mir, N. A., Dubey, R., Desiraju, G. R. Strategy and methodology in the synthesis of multicomponent molecular solids: The quest for higher cocrystals. Acc. Chem. Res, **2019**, *52*(8), 2210-2220.

[11] Tothadi, S.; Desiraju, G. R. Designing ternary cocrystals with hydrogen bonds and halogen bonds. *ChemComm*, **2013**, 49, 7791−7793

[12] Tothadi, S.; Sanphui, P.; Desiraju, G. R. Obtaining synthon modularity in ternary cocrystals with hydrogen bonds and halogen bonds. *Cryst. Growth Des*, **2014**, *14*, 5293-5302.

[13] Topić, F.; Rissanen, K. Systematic construction of ternary cocrystals by orthogonal and robust hydrogen and halogen bonds. *J. Am. Chem. Soc*, **2016**, *138*, 6610-6616.

[14] Mandal, S.: Mukhopadhyay, T. K.: Mandal, N.; Datta, A. Hierarchical Noncovalent Interactions between Molecules Stabilize Multicomponent Cocrystals. *Cryst. Growth Des*, **2019**, *19*, 4802-4809.

[15] Lombard, J.; le Roex, T.; Haynes, D. A. Competition between Hydrogen and Halogen Bonds: The Effect of Solvent Volume. *Cryst. Growth Des*, ***2020***, *20*, 7384-7391.

[16] Abeysekera, A. M.; Sinha, A. S.; Aakeroy, C. B. The Impact of Halogen Substituents on the Synthesis and Structure of Co-Crystals of Pyridine Amides. *Molecules*. ***2021***, *26*, 1147.

[17] Aakeröy, C.B.; Panikkattu, S.V.; DeHaven, B.; Desper, J. Establishing supramolecular control over solid-state architectures: A simple mix and match strategy. *Cryst. Growth Des.* **2012**, 12, 2579–2587

Chapter 8 - Evaluating structure-property relationship in a new family of mechanically flexible co-crystals

8.1 Introduction

The response of a crystalline material to external mechanical stress can range from brittleness, plastic (bending/shearing), and elastic bending. While all materials have a certain degree of elasticity[1], a crystalline solid in which either elastic or plastic deformation can be observed easily as a macroscopic property is termed 'flexible'.[2] Thus, mechanical flexibility of crystalline materials is a rare phenomenon as such solids typically have a brittle nature[3]. Applications based on mechanically flexible crystals could deliver new luminescent materials,[4] organic actuators, optoelectronics, molecular machinery, and pharmaceuticals with improved processing features.[5] Over the last three decades, there has been a shift in focus of crystal engineering to proceed from a targeted assembly (structure) of molecules, towards assemblies that yield desired functions and performance.[6]

The response to mechanical stress is highly dependent on crystal packing features.[7] Plastic bending is typically associated with the existence of weak anisotropic interactions in the lattice, and the presence of active slip planes.[8,9,10] In contrast, elastic crystals show dispersive isotropic interactions and are devoid of slip planes.[11] However, both plastic (bending) and elastic crystals exhibit corrugation. A crystal with a layered assembly can be brittle or show plastic shearing if intralayer interactions are strong enough to overcome the mechanical stress. A crystal bearing an interdigitated packing of molecules will invariably be brittle.[12] For a crystal to exhibit mechanical flexibility, both topological[13] and energetic requirement must be met[14] (Figure 8.1). In cases where visual inspection does not offer an easy assessment of relative interaction strengths, energy

frameworks calculations of crystal explorer[15] can serve as a useful tool to unravel structure property relationships.[16,17]

During the characterization of a previously synthesized co-crystal, N-(5-iodopyridin-2-yl)propionamide:benzoic acid, (used initially as a candidate for ternary co-crystal screening), we found that it displayed remarkable mechanical flexibility (Figure 8.1). Given the broad interest in improving our understanding of how flexibility of crystalline materials is related to structure (packing features), we decided to explore possible structure-property relationships of similar co-crystals i.e. those formed by N-(pyridin-2-yl)alkylamides and carboxylic acids.

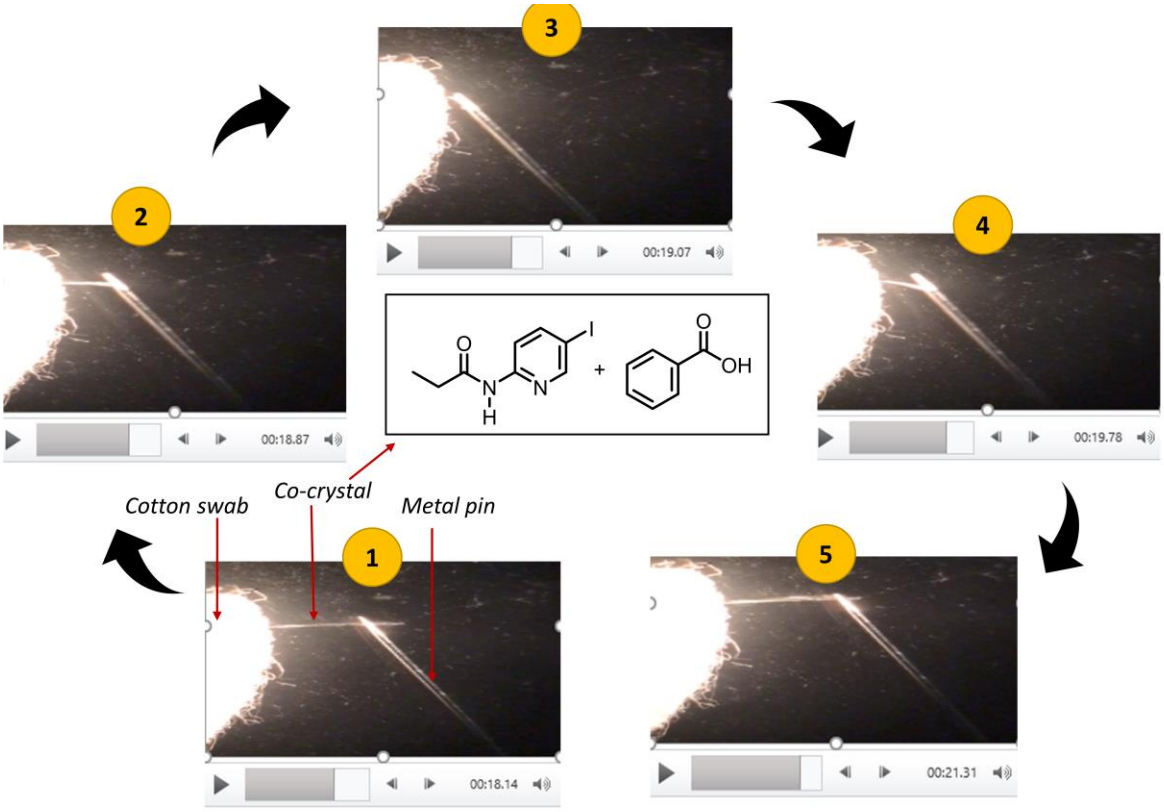

Figure 8.1. Snapshots of the different staged of the N-(5-iodopyridin-2-yl) propionamide:benzoic acid co-crystal being bent.

8.2 Experimental

8.2.1 General

The three co-formers (benzoic acid, 4-chlorobenzoic acid and 3,5-dimethyl benzoic acid), were obtained from commercial sources and used without further purification. Target compounds were synthesized as described in Chapter 6. In order to synthesize the desired co-crystals, the target and co-former were combined in a 1:1 stoichiometric ratio, and subsequently crystallized from ethyl acetate (Table 8.1).

Table 8.1. Composition and crystal descriptions and response to mechanical stress

Composition	**Code**	**Color and morphology**	**Response to mechanical stress**
N-(5-iodopyridin-2-yl)acetamide:benzoic acid	I-acetyl:BA	Colorless, Parallelepiped	Brittle
N-(5-iodopyridin-2-yl)acetamide:3,5-dimethyl benzoic acid	I-acetyl:3,5-MBA	Colorless, Parallelepiped	Brittle
N-(5-chloropyridin-2-yl)acetamide: benzoic acid	I-acetyl:4Cl-BA	Colorless, Parallelepiped	Brittle
N-(5-iodopyridin-2-yl)propionamide:benzoic acid	I-propyl:BA	Colorless, Rectangular	Elastic
N-(5-bromopyridin-2-yl)propionamide:benzoic acid	Br-propyl:BA	Colorless, needle	Elastic
N-(5-iodopyridin-2-yl)butyramide:benzoic acid	I-butyl:BA	Colorless, Rectangular	Elastic
N-(5-iodopyridin-2-yl)propionamide:4-chloro benzoic acid	I-propyl:4Cl-BA	Colorless, Rectangular	Elastic
N-(5-pyridin-2-yl)propionamide:4-chloro benzoic acid	H-propyl: 4Cl-BA	Colorless, needle	Elastic
N-(5-iodopyridin-2-yl)propionamide: 3,5-dimethyl benzoic acid	I-propyl:3,5-MBA	Colorless, plate	Plastic
N-(5-bromopyridin-2-yl)propionamide: 3,5-dimethyl benzoic acid	Br-propyl:3,5-MBA	Colorless, needle	Plastic

A simple qualitative mechanical testing was done by examining if the crystal would “fold” by pushing at a crystal with a metal needle on one end, while having the other end secured with forceps or a cotton bud (Figure 8.1). Upon removing the needle, if the bent crystal regained its original position it was categorized as elastic. If it did not spring back after releasing pressure it

was categorized as plastic. A brittle crystal was one which could not be bent, and simply cracked. The typical appearances of these are shown (Figure 8.2).

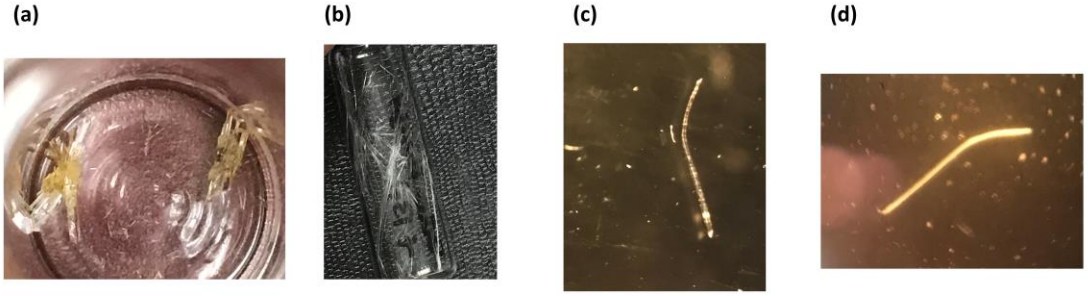

Figure 8.2. Images of (a) Typical appearance of brittle crystals (b) Typical appearance of flexible crystals (c) Plastic crystal Br-propyl:3,5-MBA (d) Plastic crystal I-propyl:3,5-MBA

8.2.2 SCXRD analysis

8.2.2.1 Primary intermolecular interaction in the co-crystals.

In all ten co-crystals, the primary hydrogen bond motif was the same. The NH-N pocket of the target interacted with a carboxylic acid forming a –COOH···N(py)-NH synthon (Figure 8.3). In the two co-crystals I-propyl:3,5-MBA, and Br-propyl:3,5-MBA additional structure directing X···O(OH) interactions occurred (Figure 8.4). The relevant hydrogen- and halogen and bond geometries in these crystal structures are given in Table 8.2.

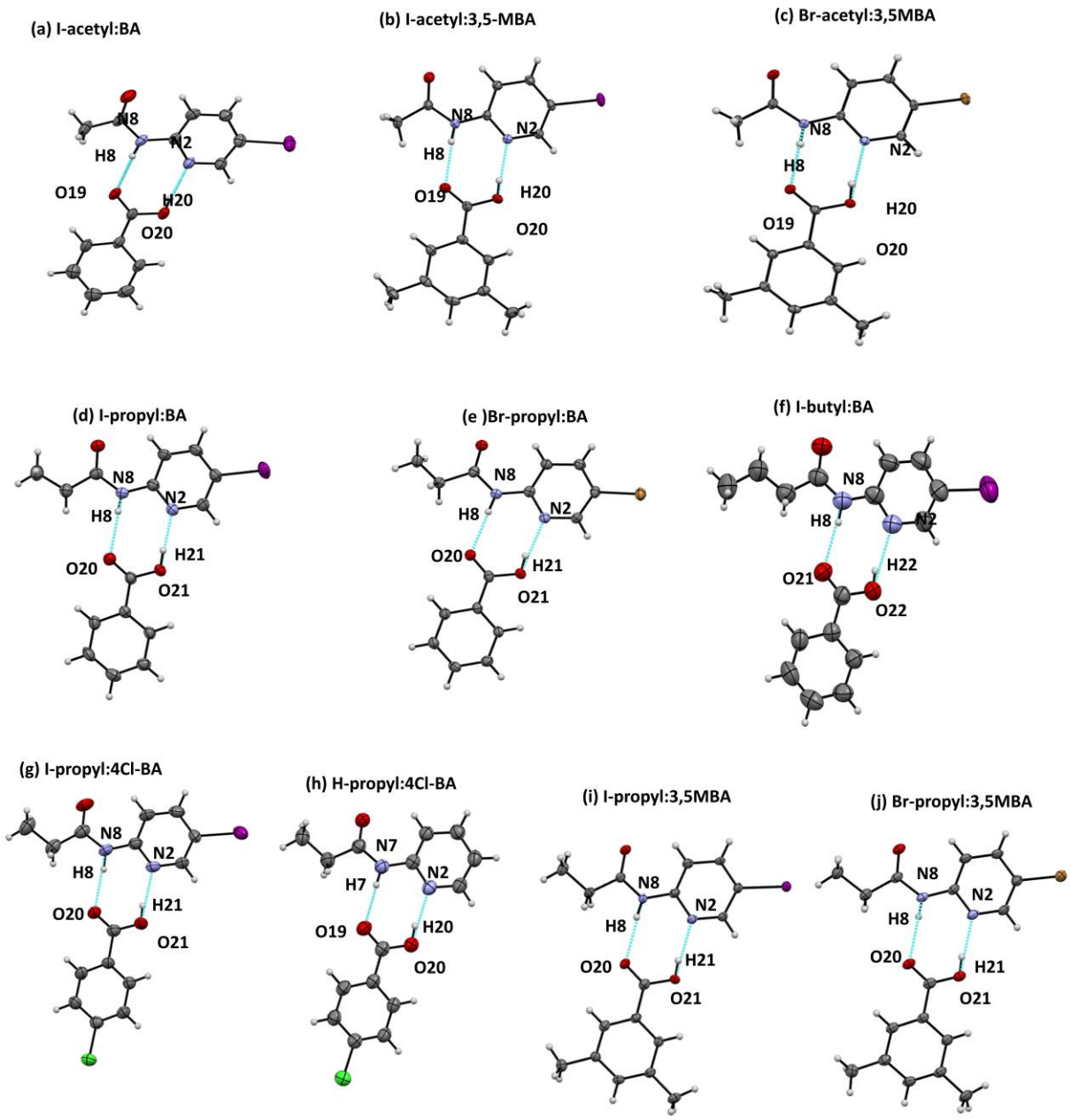

Figure 8.3. Primary hydrogen-bond interaction interactions in (a) I-acetyl:BA (b) I-acetyl:3,5-MBA (c) I-acetyl:4Cl-BA (d) I-propyl:BA (e) Br-propyl:BA (f) I-butyl:BA (g) I-propyl:4Cl-BA (h) H-propyl:4Cl-BA (i) I-propyl:3,5-MBA (j) I-propyl:3,5-MBA

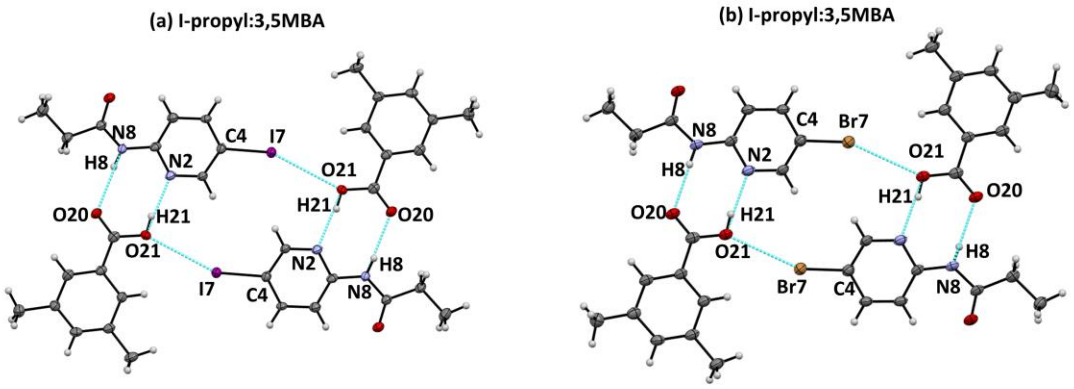

Figure 8.4. Primary hydrogen- and halogen bond interactions in (a) I-propyl:3,5MBA and (b) I-propyl:3,5MBA

Table 8.2. The relevant hydrogen- and halogen and bond geometries in these co-crystals

Code	D-H/I···A	D/I···A (A)	D-H···A (deg)
I-acetyl:BA	N8-H8···O19	2.889(6)	173.(6)
	O20-H20···N2	2.664(6)	167.(8)
I-acetyl:3,5-MBA	N8-H8···O19	2.879(4)	161(5)
	O20-H20···N2	2.683(4)	174(7)
I-acetyl: 4Cl-BA	N8-H8···O19	2.958(6)	171.1(3)
	O20-H20···N2	2.648(5)	147.8(3)
I-propyl:BA	N8-H8···O20	2.913(4)	176.(4)
	O21-H21···N2	2.678(4)	174.(5)
Br-propyl:BA	N8-H8···O20	2.924(4)	177.32(12)
	O21-H21···N2	2.681	169.3(13)
I-butyl:BA	N8-H8···O21	2.886(6)	173.(7)
	O22-H22···N2	2.715(6)	162.(8)
I-propyl:4Cl-BA	N8-H8···O20	2.894(10)	173.(9
	O21-H21···N2	2.643(10)	166.(13)
H-propyl:4Cl-BA	N7-H7···O19	2.8619(3)	178(5)
	O20-H20···N2	2.638(7)	173(8)
I-propyl:3,5-MBA	N8-H8···O19	2.898 (4)	161.32(9)
	O20-H20···N2	2.687(4)	171.1(7)
	C4-I7···O21	3.324	156.51(10)
Br-propyl:3,5-MBA	N8-H8···O20	2.887(2)	163.84(18)
	O21-H21···N2	2.672(4)	170.76(2)
	C4-Br7···O21	3.228(2)	157.08(11)

8.2.2.2 Secondary intermolecular interactions in the co-crystals

In all ten co-crystals, the dimers formed between target and acid are linked by CH···O=C interactions to produce tetramers (Figure 8.5).

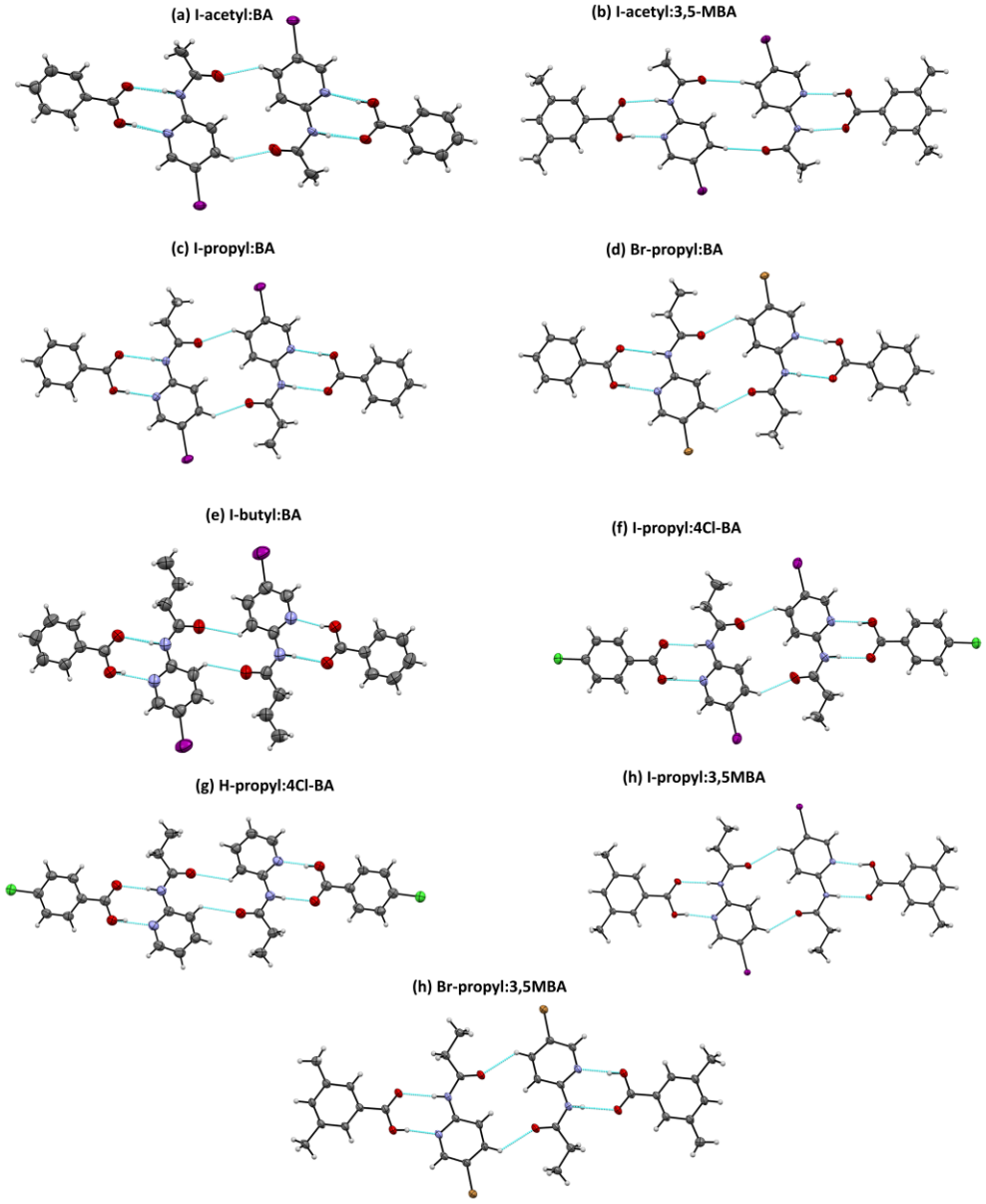

Figure 8.5. Tetramers in the crystal structures of (a) I-acetyl:BA (b) I-acetyl:3,5-MBA (c) I-acetyl: 4Cl-BA (d) I-propyl:BA (e) Br-propyl:BA (f) I-butyl:BA (g) I-propyl:4Cl-BA (h) H-propyl:4Cl-BA (i) I-propyl:3,5-MBA (j) I-propyl:3,5-MBA

8.2.3 Establishing structure-property correlations using crystal packing features

As shown in sections 8.2.2.1 and 8.2.2.2, the main supramolecular interactions in these ten co-crystals are the same. A tetrameric unit can be identified at the larger building block or "supermolecule" in these co-crystals. To understand the distinct types of responses to mechanical stress, we next look at the packing features in each co-crystal.

8.2.3.1 N-(5-iodopyridin-2-yl)acetamide:benzoic acid (I-acetyl:BA)

The tetrameric building blocks of I-acetyl undergo π-π stacking. These π stacked column do not show any corrugation and, instead, a layered arrangement of the tetramers is observed. In each layer, apart from the hydrogen bond interactions which lead to the tetrameric assembly, there are no additional strong intralayer interactions. The building blocks in each layer are thus, relatively 'isolated'. These packing features correlate with the brittleness of the crystals.

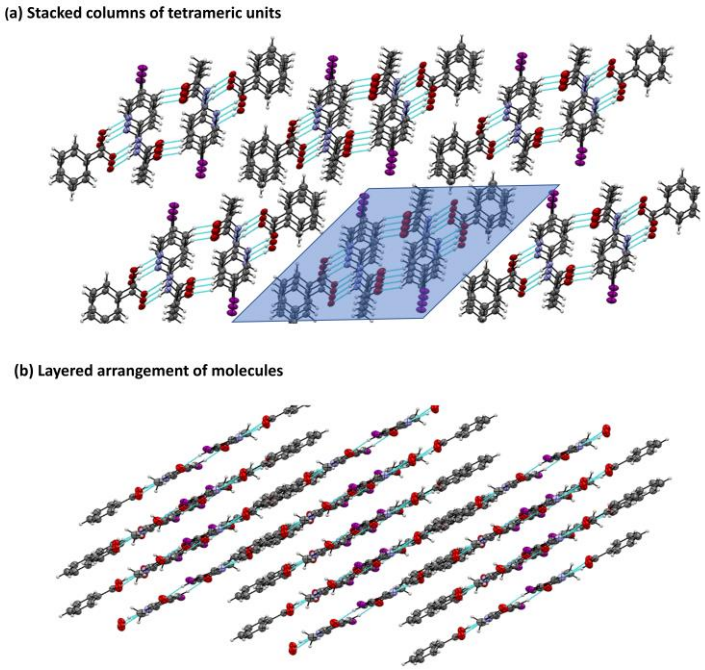

Figure 8.6. Packing features of I-acetyl:BA (a) Stacked column of tetrameric units (b) layered arrangement of molecules

8.2.3.2 N-(5-iodopyridin-2-yl)acetamide:3,5-dimethyl benzoic acid (I-acetyl:3,5-MBA)

The tetrameric units of I-acetyl:3,5-MBA arrange in a displaced fashion *i.e* like molecules do not stack one above the other. The molecules showed a layered arrangement. Apart from the hydrogen bonds which lead to tetrameric units there are no strong intralayer interaction. These features result in macroscopically brittle crystals.

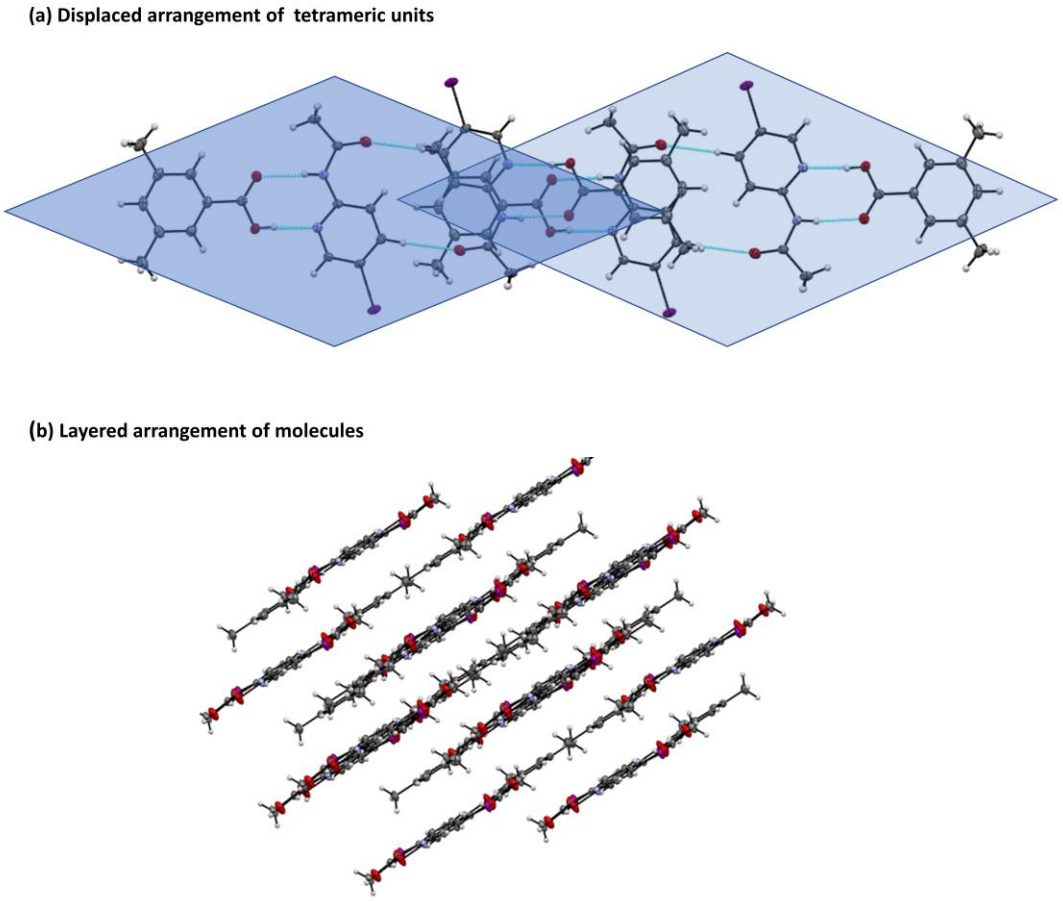

Figure 8.7. Packing features of I-acetyl: 3,5-MBA (a) Displaced arrangement of tetrameric units (b) layered arrangement of molecules.

8.2.3.3 N-(5-iodopyridin-2-yl)acetamide:4-chloro benzoic acid (I-acetyl:4Cl-BA)

The tetrameric building blocks of I-acetyl undergo π-π stacking leading to a layered arrangement. Apart from the hydrogen bond interactions within the tetrameric building blocks there are no strong intralayer interactions and, thus, the crystals are brittle.

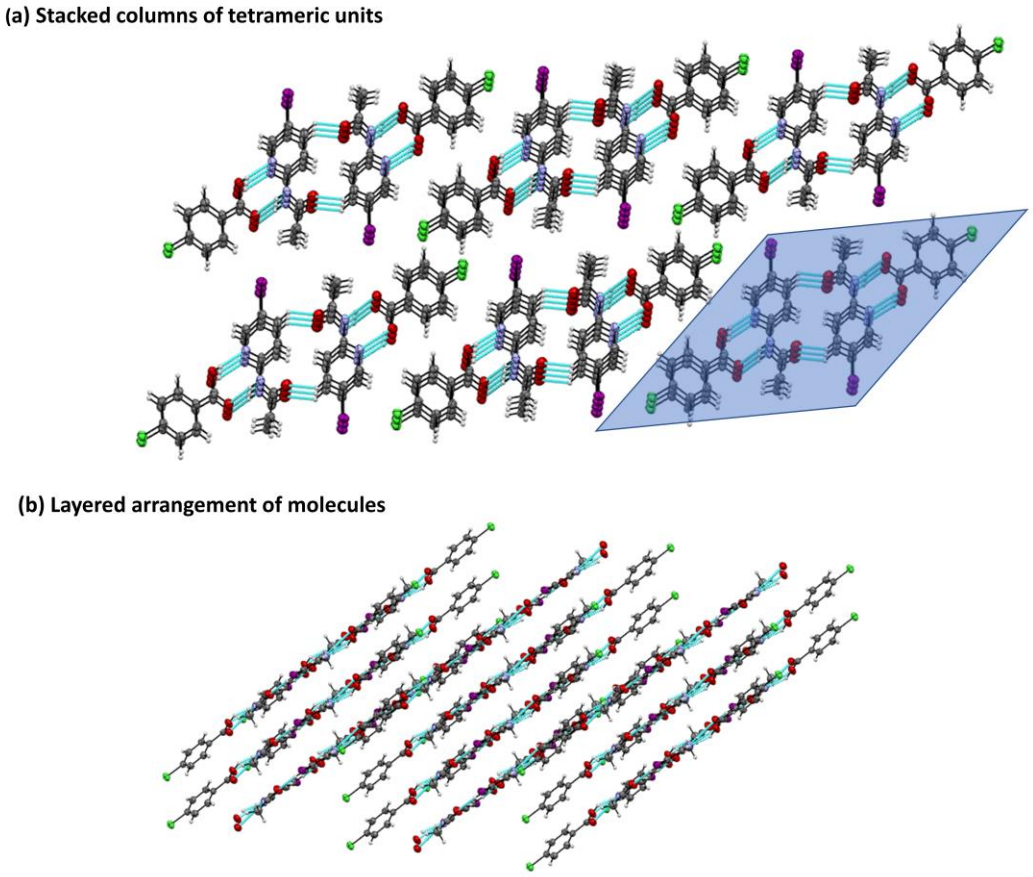

Figure 8.8. Packing features of I-acetyl:4Cl-BA (a) Stacked column of tetrameric units (b) layered arrangement of molecules.

8.2.3.4 N-(5-iodopyridin-2-yl)propionamide:benzoic acid (I-propyl:BA)

In I-propyl:BA, the tetrameric building blocks undergo π-π stacking. These π stacked column are tilted, which leads to corrugation and there are no slip planes. In addition, the propyl chains of the tetrameric units which are tilted in opposite directions, align and likely function as 'strain buffers' along with the CH···π interactions which facilitate mechanical flexibility in these crystals.

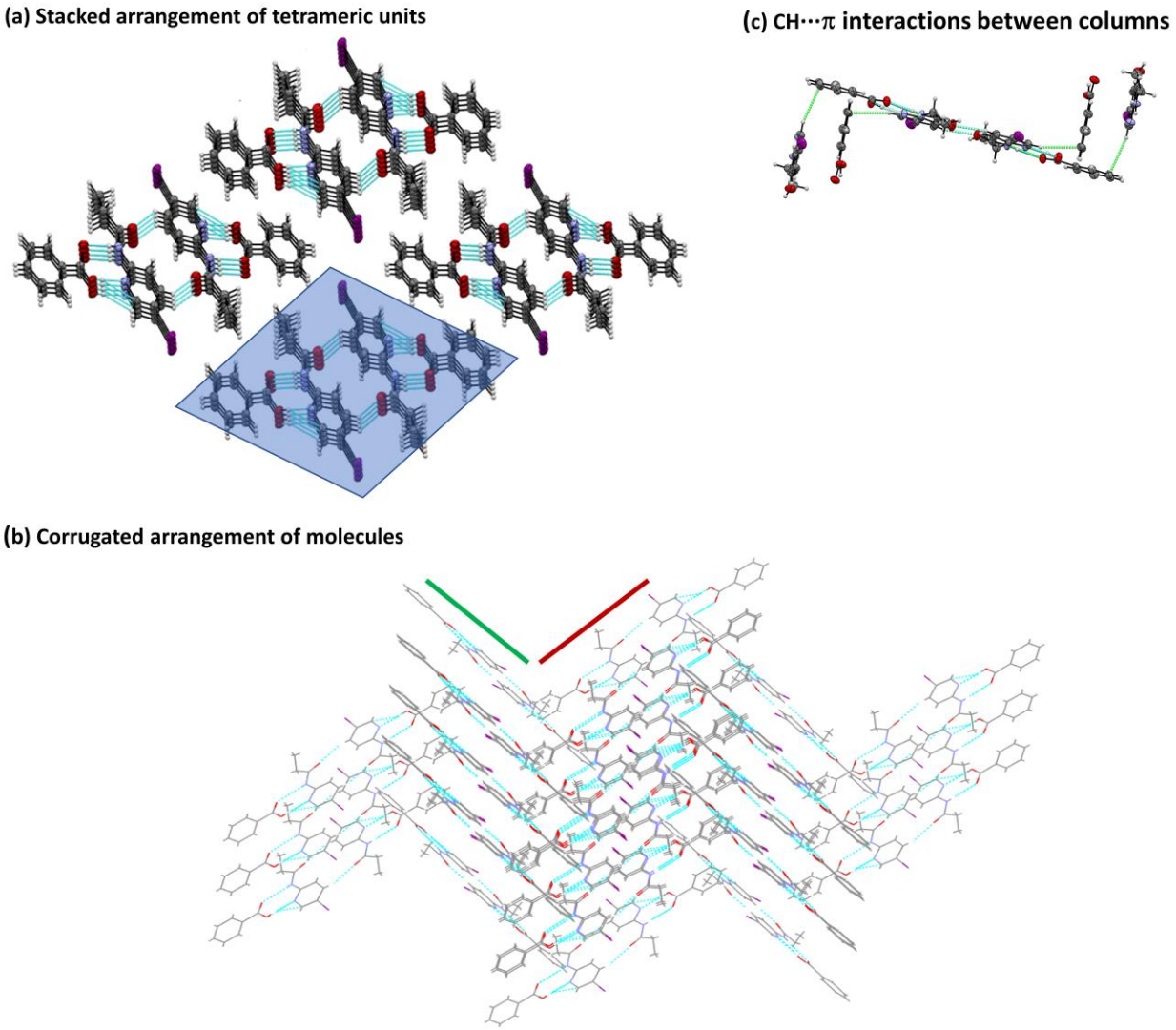

Figure 8.9. Packing features of I-propyl:BA (a) Stacked tetrameric units (b) Corrugated arrangement of molecules (c) CH···π interactions between columns

8.2.3.5 N-(5-bromopyridin-2-yl)propionamide:benzoic acid (Br-propyl:BA)

The tetrameric building blocks undergo π-π stacking and lead to corrugation by tilting of the columns. There are no slip planes. Dispersive alkyl-alkyl and CH···π interactions are present and, thus, the structure displays all the characteristics which facilitate elastic bending.

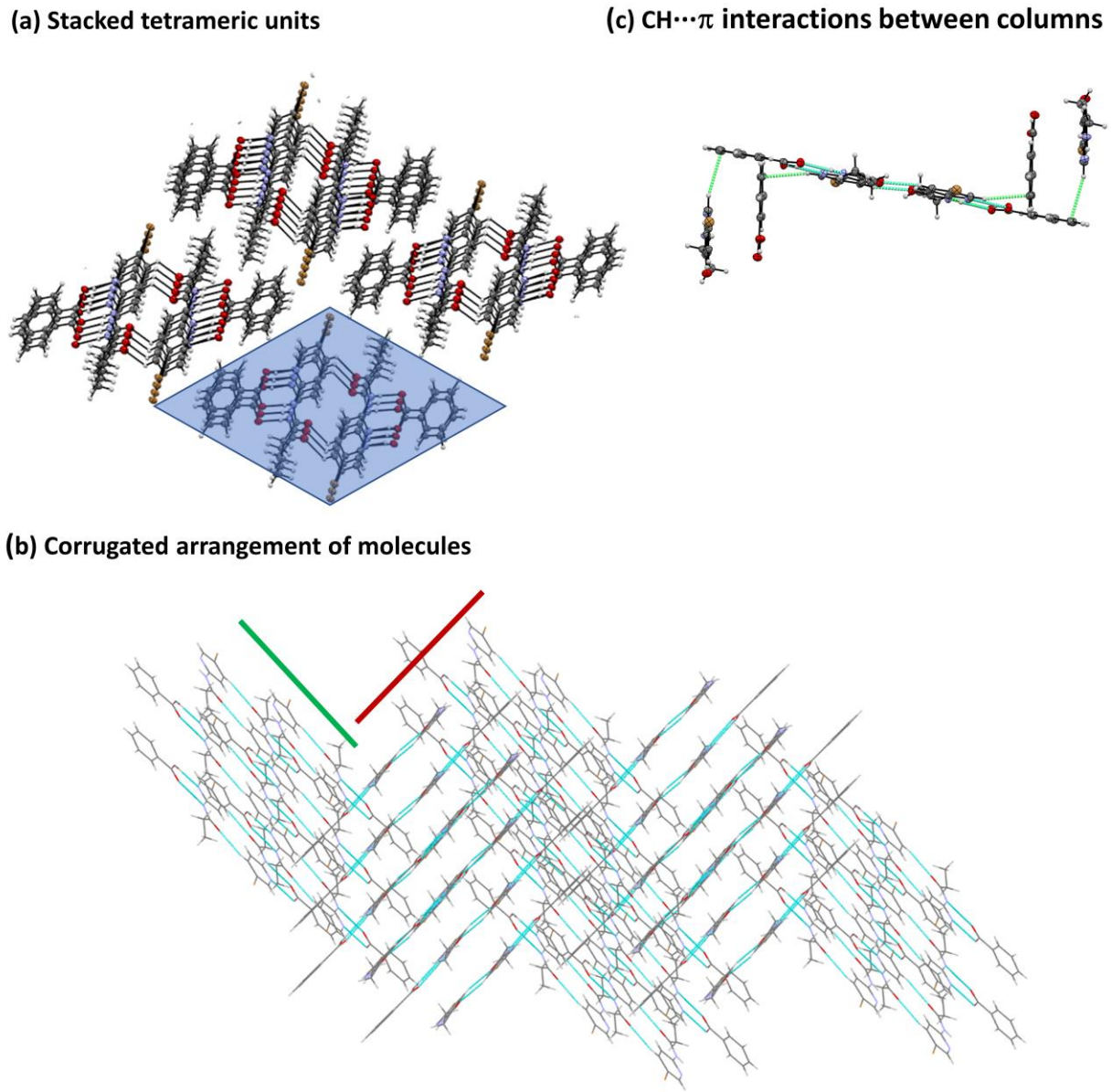

Figure 8.10. Packing features of Br-propyl:BA (a) Stacked tetrameric units (b) Corrugated arrangement of molecules (c) CH···π interactions between columns

8.2.3.6 N-(5-iodopyridin-2-yl)butyramide:benzoic acid (I-butyl:BA)

The tetrameric building blocks are π-π stacked and corrugated due to tilting of the columns. There are no slip planes. Dispersive alkyl-alkyl and CH···π interactions contribute to the structural characteristics which facilitate elastic bending.

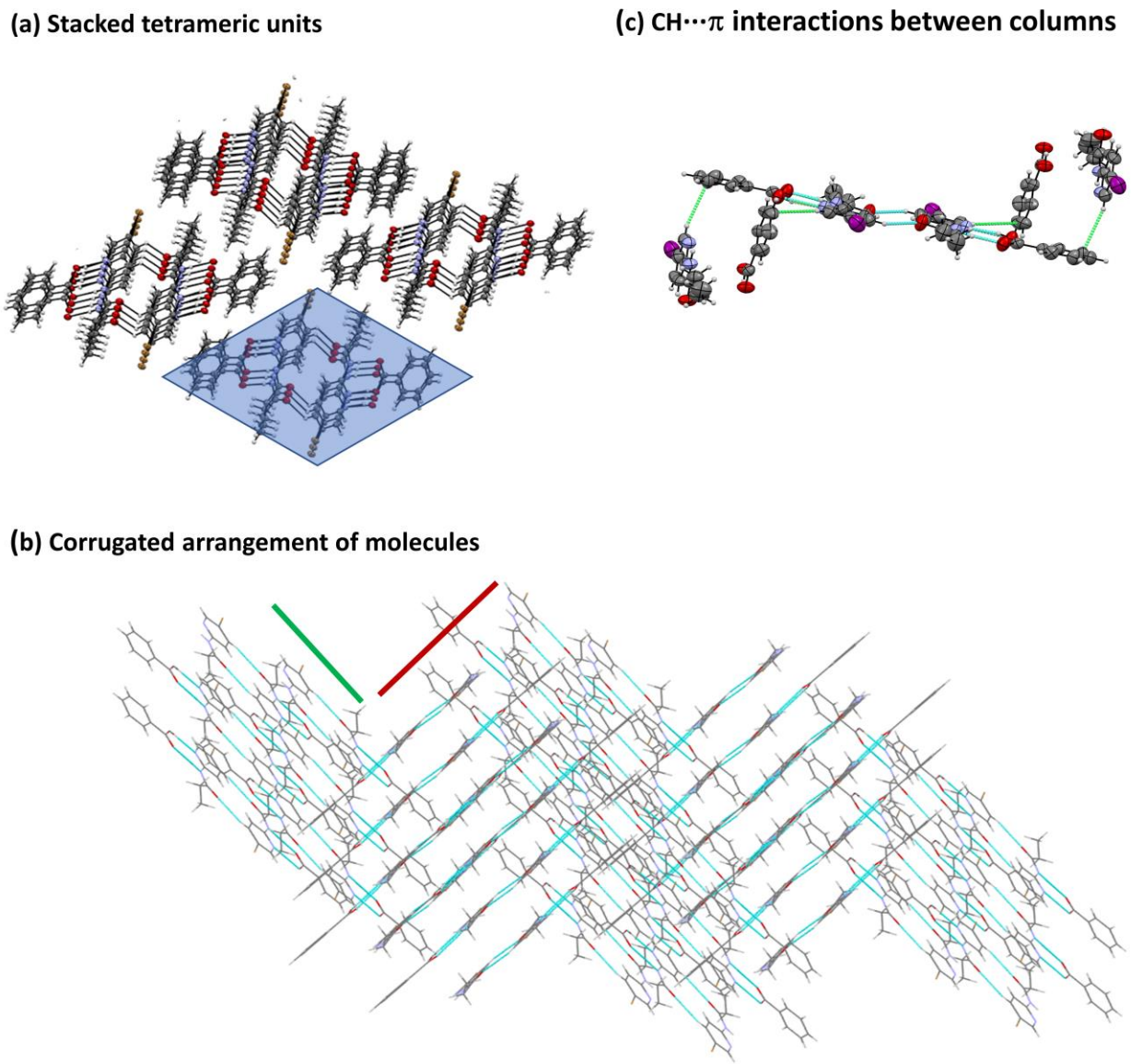

Figure 8.11. Packing features of I-butyl:BA (a) Stacked tetrameric units (b) Corrugated arrangement of molecules (c) CH···π interactions between columns

8.2.3.7 N-(5-iodopyridin-2-yl)propionamide:4-chloro benzoic acid, I-propyl:4Cl-BA

In I-propyl:4Cl-BA, corrugated columns are formed by tetrameric units which π-π stack. No slip planes are present but weak dispersive C-I···Cl and CH···Cl interactions are observed. These interactions provide a buffering to mechanical stress which enables notable elastic bending.

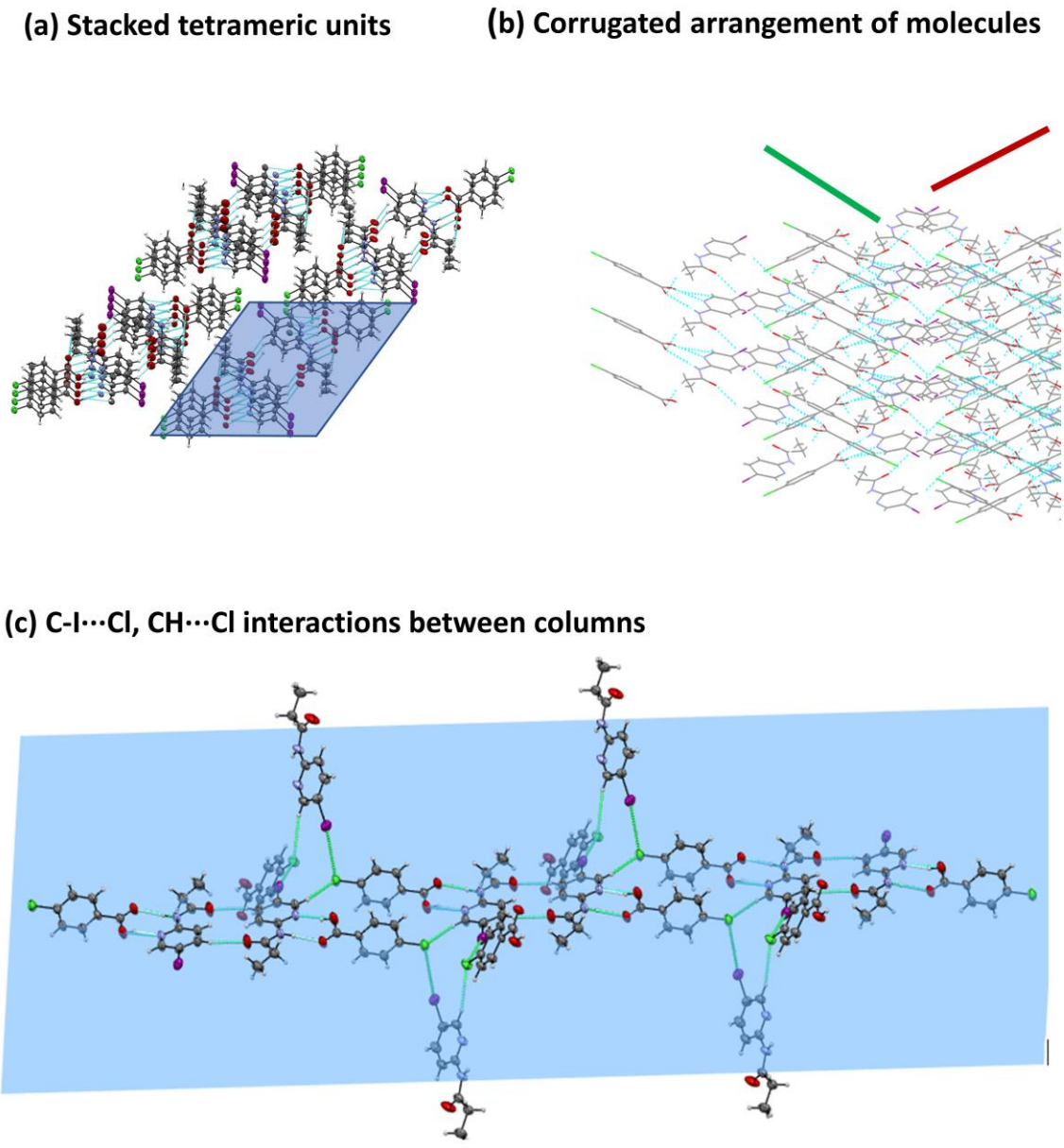

Figure 8.12. Packing features of I-propyl:4Cl-BA (a) Stacked tetramers (b) Corrugated arrangement of molecules (c) C-I···Cl, C-H···Cl interactions between columns

8.2.3.8 N-(5-pyridin-2-yl)propionamide:4-chloro benzoic acid (H-propyl:4Cl-BA)

Packing in H-propyl:4Cl-BA, displays corrugated stacks of tetrameric units which interact via dispersive alkyl-alkyl and Cl···Cl interactions. There are no slip planes and, thus these crystals show elastic behavior.

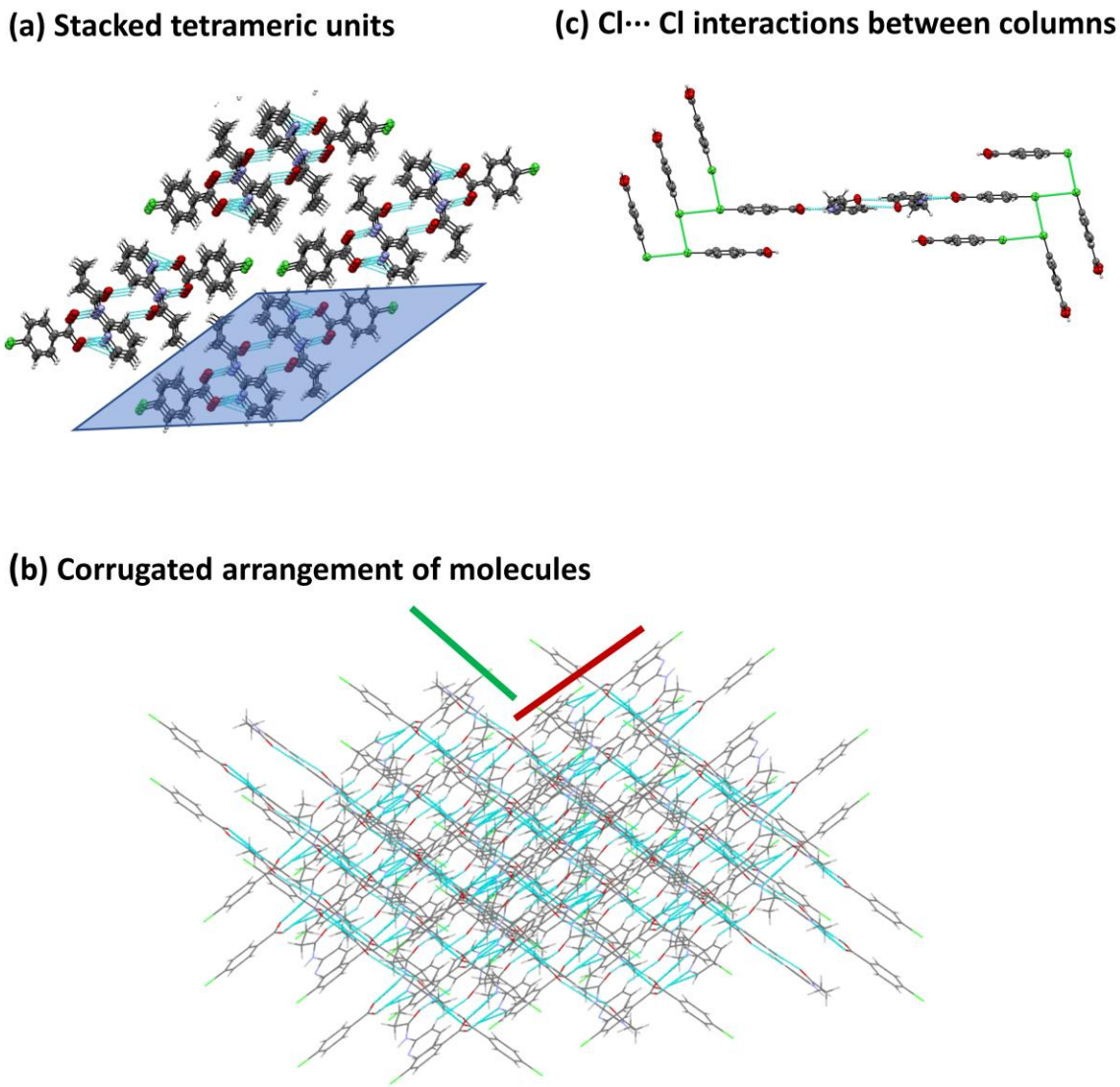

Figure 8.13. Packing features of H-propyl:4Cl-BA (a) Stacked tetrameric units (b) Corrugated arrangement of molecules (c) Cl···Cl interactions between columns.

8.2.3.9 N-(5-iodopyridin-2-yl)propionamide:3,5-dimethyl benzoic acid (I-propyl:3,5-MBA)

The tetramers in I-propyl:3,5-MBA π-π stack in a linear manner and tetramers within the layers are connected by halogen bonds. When subjected to pressure, these units undergo synchronized/ordered movement, leading to notable plastic (sheer) deformation.

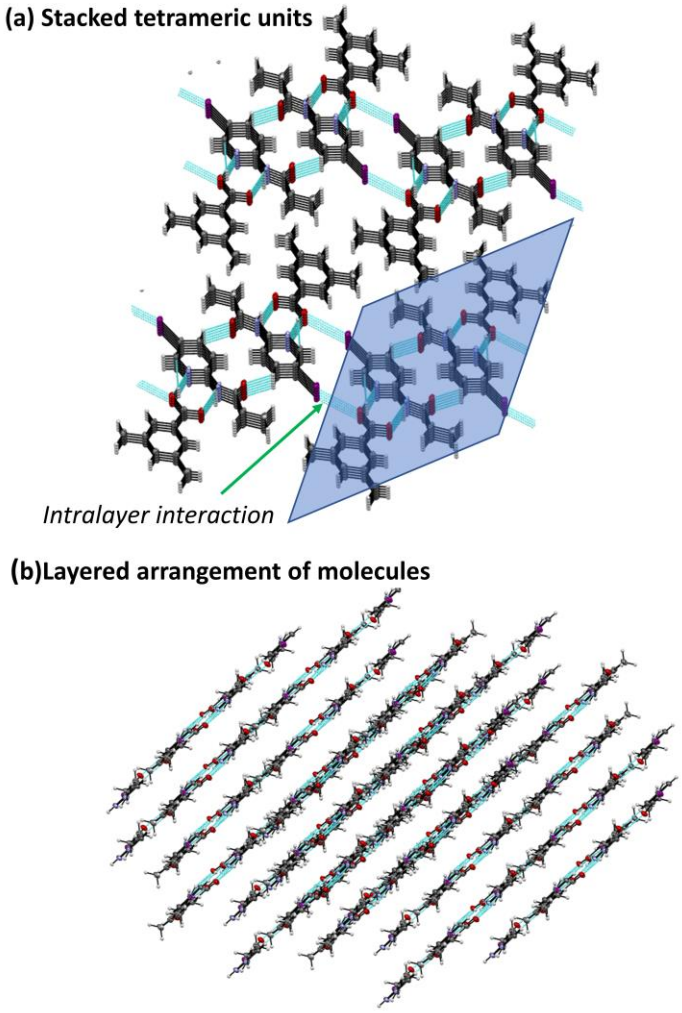

Figure 8.14. Packing features of I-propyl:3,5-MBA (a) Stacked column of tetrameric units interlinked by halogen bonding (b) layered arrangement of molecules

8.2.3.10 N-(5-bromopyridin-2-yl)propionamide: 3,5-dimethyl benzoic acid (Br-propyl:3,5-MBA)

In Br-propyl:3,5-MBA, the tetramers π-π stack in a linear arrangement. The halogen bonds connect the tetrameric units, facilitating the plastic (sheer) deformation observed in the macroscopic crystals.

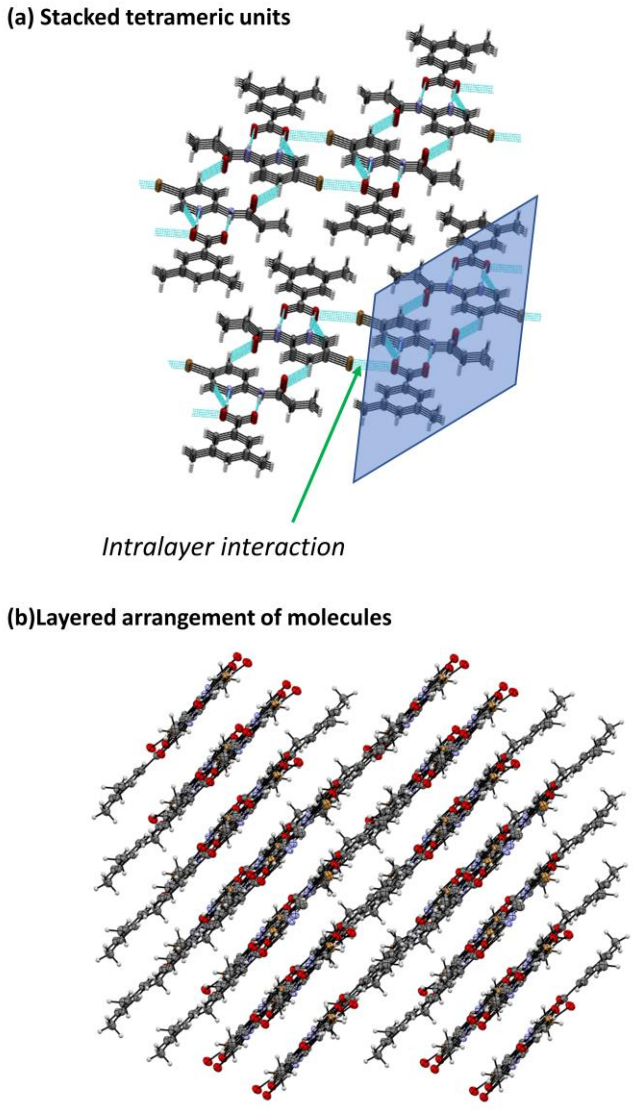

Figure 8.15. Packing features of Br-propyl:3,5-MBA (a) Stacked column of tetrameric units interlinked by halogen bonding (b) layered arrangement of molecules

8.2.4 Establishing structure-property correlations using energy framework calculations

To complement the crystallographic structural analysis in 8.2.3, we carried out energy framework calculations. Representations of the Coulombic and dispersive interactions in the three co-crystals I-acetyl:BA, I-propyl-BA and I-propyl are shown. (Figure 8.16).

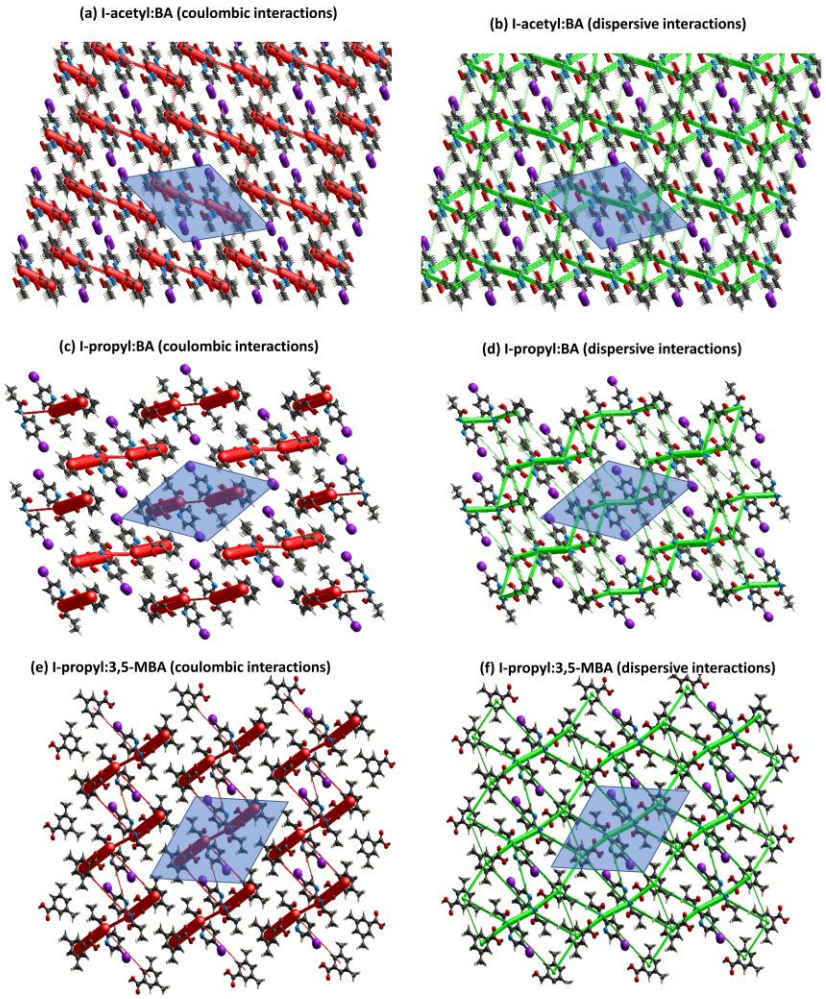

Figure 8.16. Coulombic and dispersive interactions in I-acetyl:BA (a),(b), I-propyl:BA (c),(d), and I-propyl:3,5-MBA (e),(f).

The three examples shown in Figure 8.15, represent one example from each other three groups of compounds, as classified by their respective response to external mechanical stimuli ((brittle/elastic/plastic sheering). In all cases, hydrogen-bonded tetramers units are held together by strong Coulombic interactions. Molecular slippage is unlikely by way of disrupting a Coulombic/electrostatic interaction, Thus, our assumption that these tetramers can be considered as the supramolecular "building block" of these co-crystals in validated. In I-acetyl:BA, the Coulombic interactions linking the supramolecules are not as prominent as compared to those in I-propyl:3,5-MBA. This is reflected in the macroscopic flexibility of I-propyl:3,5-MBA, and the contrasting brittleness of I-acetyl:BA. Dispersive interactions, which enable the relative movement between adjacent π=π stacks (formed by the tetramers) are seen in I-propyl:BA.

8.3 Conclusions

The syntheses of all ten co-crystals were achieved via identical intermolecular recognition points (NH-N and -COOH). The basic building block or "supermolecule"[18] was the same tetrameric unit. Yet, mechanical responsiveness could be grouped into three distinctly different categories; brittle, elastic and plastic (sheering).

All three brittle crystals were obtained in combination with targets that carried an acetyl chain. The other seven were substituted with longer alkyl chain length. Thus, in this "class" of co-crystals, a longer alkyl chain promotes flexible mechanical behavior (Figure 8.17).

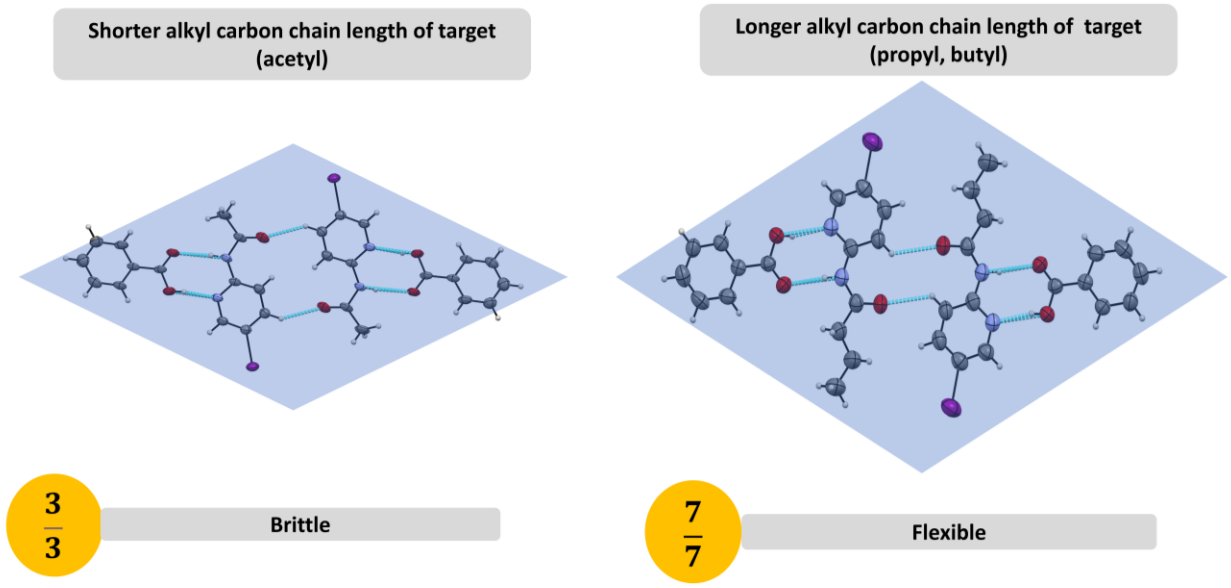

Figure 8.17. Correlation between alkyl chain length on target and observed physical properties.

The two co-crystals that showed plastic deformation comprised 3,5-dimethyl benzoic acid with I-propyl and Br-propyl, respectively. The X···O(OH) halogen bonds are identified as instrumental in promoting plastic flexibility, as sheering would not be possible given the presence of layered topologies in these crystals. However, none of the other seven co-crystals obtained with halogenated targets (all bearing either bromine or iodine atoms) displayed any halogen-bond interactions. In fact, the halogen atoms are not in close proximity to the O(OH) group. The methyl group thus seems to function as a steric factor which enables a shorter contact between the halogen atom and O(OH) groups. This, in turn, facilitates the formation of a halogen bond which is instrumental in creating a structural feature which is critically important to the observed plastic deformation.

In all ten co-crystals examined herein, the observed response to mechanical stimuli could be related to pre-requisite criterion or models resulting in a road map for connecting, and even predicting, mechanical behavior (Figure 8.18).

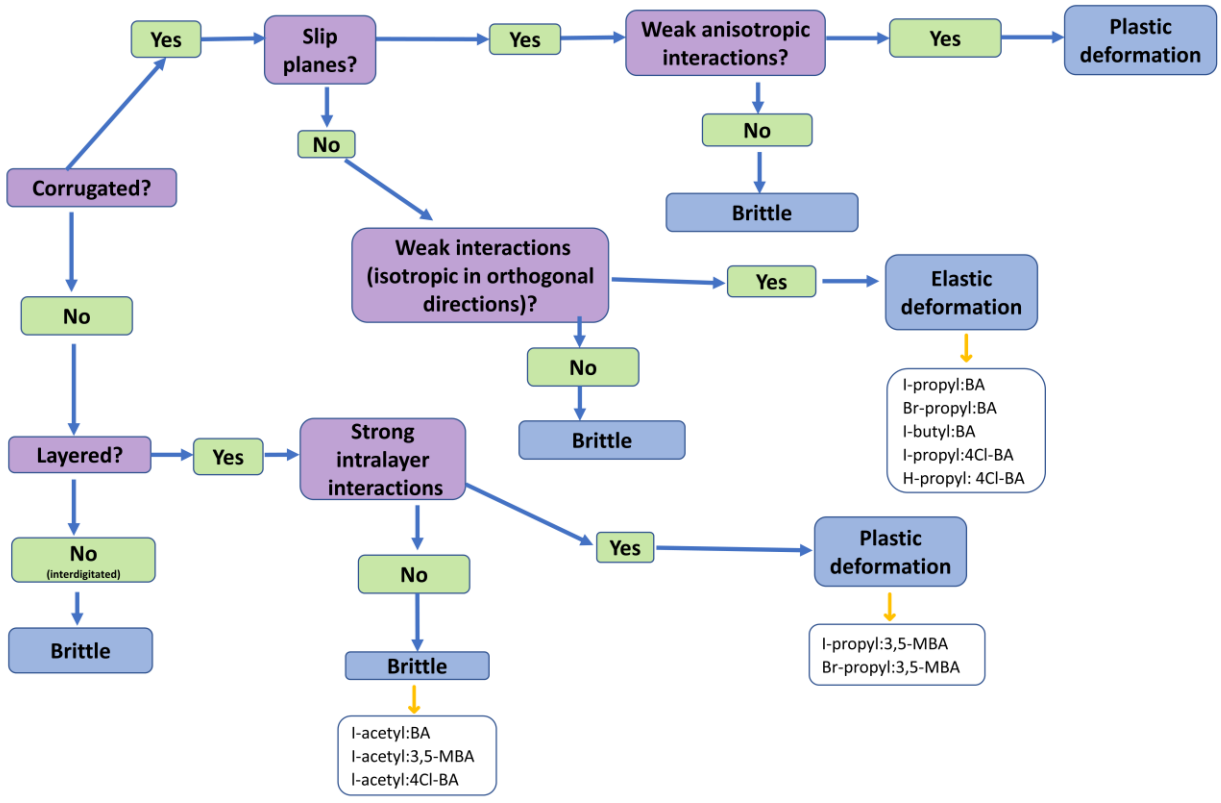

Figure 8.18. Road map to assess responsiveness of crystalline solid to mechanical stress and corresponding co-crystal obtained

It is important to note that currently, there are no universally accepted models or theories for how mechanical behavior in the organic solid state as well as in crystalline coordination polymers can be explained. However, it is clear that systematic structure-property studies, such as what we present in this chapter, can offer considerable insight and a degree of predictability for assessing, in advance, whether a certain crystalline material will be likely to be brittle, elastic, or elastic.

This is an essential towards being able to realize practical and reliable ‘bottom-up’ synthesis of materials with desirable macroscopic properties.

8.4 References

[1] Commins, P.; Karothu, D. P.; Naumov, P. Is a Bent Crystal Still a Single Crystal?. *Angew. Chem., Int. Ed*. **2019**, *58*, 10052-10060.
[2] Saha, S.; Mishra, M. K.; Reddy, C. M.; Desiraju, G. R. From molecules to interactions to crystal engineering: mechanical properties of organic solids. *Acc. Chem. Res*, **2018**, *51*, 2957-2967.
[3] Liu, H.; Bian, Z.; Cheng, Q.; Lan, L.; Wang, Y.; Zhang, H. Controllably realizing elastic/plastic bending based on a room-temperature phosphorescent waveguiding organic crystal. *Chem. Sci*. **2019**, *10*, 227-232.
[4] Hayashi, S.; Koizumi, T. Elastic Organic Crystals of a Fluorescent π-Conjugated Molecule. *Angew. Chem., Int. Ed*. **2016**, *128*, 2751-2754.
[5] Khandavilli, U. R.; Yousuf, M.; Schaller, B. E.; Steendam, R. R.; Keshavarz, L.; McArdle, P.; Frawley, P. J. Plastically bendable pregabalin multi-component systems with improved tabletability and compressibility. *CrystEngComm*. **2020**, *22*, 412-415.
[6] Mishra, M. K.; Ramamurty, U.; Desiraju, G. R. Mechanical property design of molecular solids. *Curr Opin Solid State Mater Sci*. **2016**, *20*, 361-370.
[7] Ahmed, E.; Karothu, D. P.; Naumov, P. Crystal adaptronics: mechanically reconfigurable elastic and superelastic molecular crystals. *Angew. Chem., Int. Ed*. **2018**, *57*, 8837-8846.
[8] Reddy, C. M.; Kirchner, M. T.; Gundakaram, R. C.; Padmanabhan, K. A.; Desiraju, G. R. Isostructurality, polymorphism and mechanical properties of some hexahalogenated benzenes: the nature of halogen··· halogen interactions. *Chem. Eur. J.* **2006**, *12*, 2222-2234.
[9] Reddy, C. M.; Padmanabhan, K. A.; Desiraju, G. R. Structure− property correlations in bending and brittle organic crystals. *Cryst. Growth Des*. **2006**, *6*, 2720-2731.
[10] Panda, M. K.; Ghosh, S.; Yasuda, N.; Moriwaki, T.; Mukherjee, G. D.; Reddy, C. M.; Naumov, P. Spatially resolved analysis of short-range structure perturbations in a plastically bent molecular crystal. *Nat. Chem.* **2015**. *7*, 65-72.
[11] Mishra, M. K.; Mishra, K.; Asif, S. S.; Manimunda, P. Structural analysis of elastically bent organic crystals using in situ indentation and micro-Raman spectroscopy. *Chem. Commun*, **2017**, *53*, 13035-13038.
[12] Raju, K. B.; Ranjan, S.; Vishnu, V. S. Bhattacharya, M.; Bhattacharya, B.; Mukhopadhyay, A. K.; Reddy, C. M. Rationalizing distinct mechanical properties of three polymorphs of a drug adduct by nanoindentation and energy frameworks analysis: Role of slip layer topology and weak interactions. *Cryst. Growth Des*. **2018**, *18*, 3927-3937.
[13] Bryant, M. J., Maloney, A. G. P., Sykes, R. A. Predicting mechanical properties of crystalline materials through topological analysis. *CrystEngComm*, 2018, *20*, 2698-2704.
[14] Devarapalli, R.; Kadambi, S. B.; Chen, C. T.; Krishna, G. R.; Kammari, B. R.; Buehler, M. J.; Ramamurty, U; Reddy, C. M. Remarkably Distinct Mechanical Flexibility in Three Structurally Similar Semiconducting Organic Crystals Studied by Nanoindentation and Molecular Dynamics. *Chem. Mater.* **2019**, *31*, 1391-1402.
[15] Turner, M. J.; Thomas, S. P.; Shi, M. W.; Jayatilaka, D.; Spackman, M. A. Energy frameworks: insights into interaction anisotropy and the mechanical properties of molecular crystals. *Chem. Commun.* **2015**, *51*, 3735-3738.
[16] Wang, C.; Sun, C. C. Identifying slip planes in organic polymorphs by combined energy framework calculations and topology analysis. *Cryst. Growth Des*, **2018**, *18*, 1909-1916.
[17] Mishra, M. K.; Mishra, K.; Narayan, A.; Reddy, C. M.; Vangala, V. R. Structural Basis for Mechanical Anisotropy in Polymorphs of a Caffeine–Glutaric Acid Cocrystal. *Cryst. Growth Des*. **2020**, *20*, 6306-6315.
[18] Desiraju, G. R. Supramolecular synthons in crystal engineering—a new organic synthesis. *Angew. Chem., Int. Ed*.**1995,** *34*, 2311-2327.

Appendix A - Additional information for Chapter 1

A.1 Copyright permission for Chapter 1

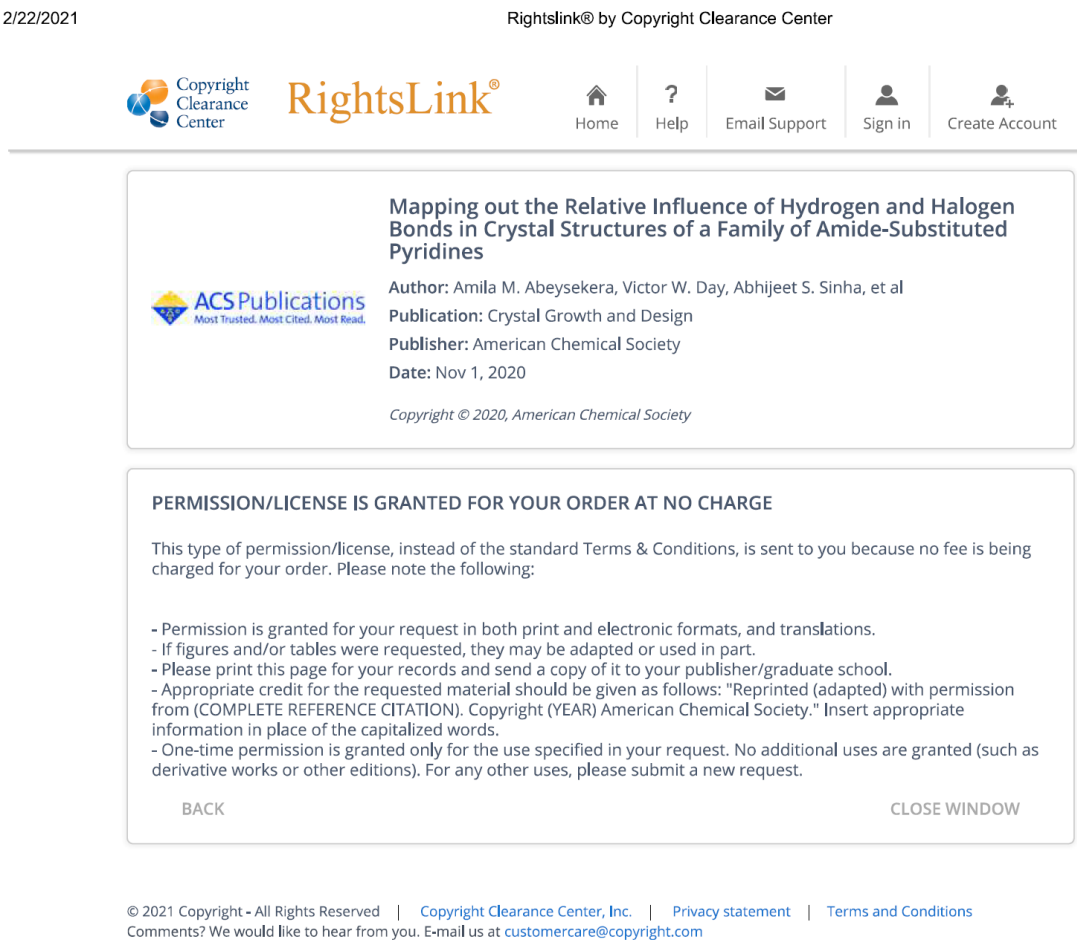

2/22/2021 Rightslink® by Copyright Clearance Center

Copyright Clearance Center RightsLink®

Home | Help | Email Support | Sign in | Create Account

ACS Publications
Most Trusted. Most Cited. Most Read.

Mapping out the Relative Influence of Hydrogen and Halogen Bonds in Crystal Structures of a Family of Amide-Substituted Pyridines

Author: Amila M. Abeysekera, Victor W. Day, Abhijeet S. Sinha, et al
Publication: Crystal Growth and Design
Publisher: American Chemical Society
Date: Nov 1, 2020

Copyright © 2020, American Chemical Society

PERMISSION/LICENSE IS GRANTED FOR YOUR ORDER AT NO CHARGE

This type of permission/license, instead of the standard Terms & Conditions, is sent to you because no fee is being charged for your order. Please note the following:

- Permission is granted for your request in both print and electronic formats, and translations.
- If figures and/or tables were requested, they may be adapted or used in part.
- Please print this page for your records and send a copy of it to your publisher/graduate school.
- Appropriate credit for the requested material should be given as follows: "Reprinted (adapted) with permission from (COMPLETE REFERENCE CITATION). Copyright (YEAR) American Chemical Society." Insert appropriate information in place of the capitalized words.
- One-time permission is granted only for the use specified in your request. No additional uses are granted (such as derivative works or other editions). For any other uses, please submit a new request.

BACK CLOSE WINDOW

A.2 FT-IR spectrum of 2Pyr-I

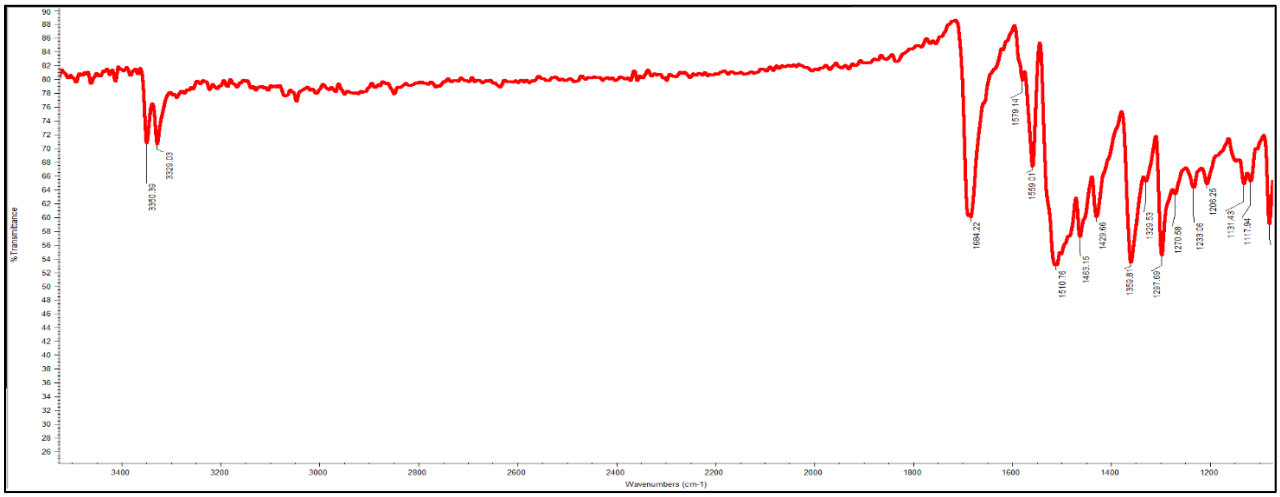

Figure A.1 FT-IR spectrum of 2Pyr-I

A.3 PXRD data of 3Pyr-I

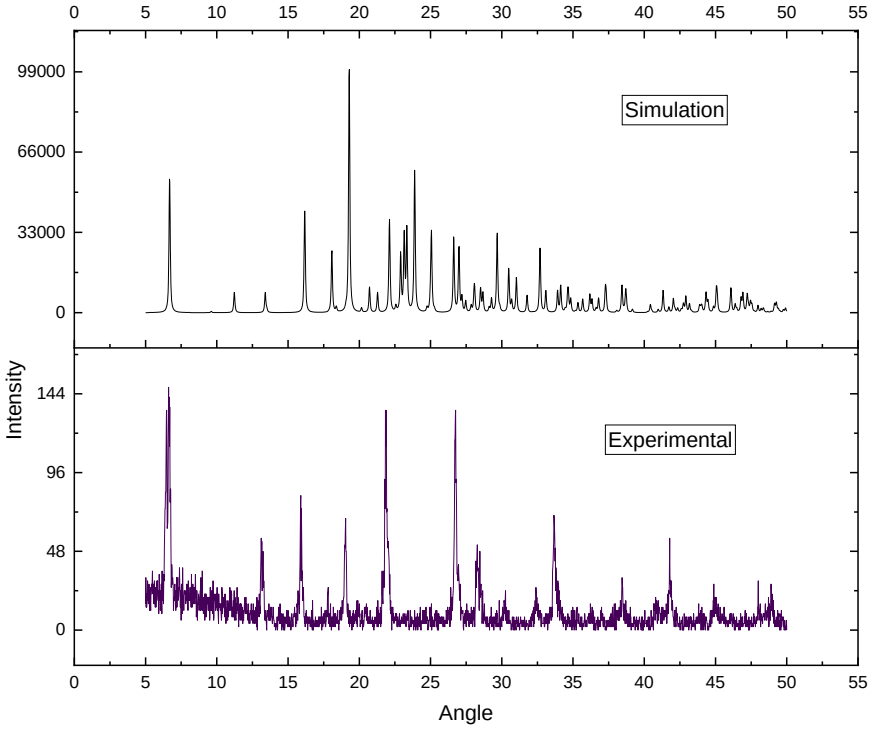

Figure A.2 Comparison of simulated and experimental PXRD data of 3Pyr-I

A.4 REF codes of N-(pyridin-2-yl)benzamide structures from CCDC

Table A.1 REF codes of N-(pyridin-2-yl)benzamide structures from CCDC

	REF CODE	Compound name	Observed assembly
1	GOXNIT	N-(pyridin-2-yl)anthracene-9-carboxamide	Dimers
2	YOVKIG01	4-chloro-N-(pyridin-2-yl)benzamide	
3	YOVKUS	3-chloro-N-(pyridin-2-yl)benzamide	
4	YOVLAZ	2-chloro-N-(pyridin-2-yl)benzamide	
5	CUBRIC	N-(pyridin-2-yl)-9H-fluorene-2-carboxamide	
6	DOKZUZ	2-Iodo-N-(6-methyl-2-pyridyl)benzamide	
7	ETEKAR	N-(pyridin-2-yl)-4-(trifluoromethyl)benzamide	
8	FAFBIZ	3-Methyl-N-(pyridin-2-yl)benzamide	
9	FAFBOF	2-Methyl-N-(pyridin-2-yl)benzamide	
10	FAFBOF01	2-Methyl-N-(pyridin-2-yl)benzamide	
11	FATNET	N-(4,6-Dimethylpyridin-2-yl) benzamide	
12	HAXLID	4-Fluoro-N-(pyridin-2-yl)benzamide	
13	HAXLOJ	3-Fluoro-N-(pyridin-2-yl)benzamide	
14	HAXLUP	2-Fluoro-N-(pyridin-2-yl)benzamide	
15	IDALAA	N-(2-Pyridyl)-pentafluorobenzamide	
16	JIXCUO	3-Benzamido-5,6,7,8-tetrahydro-5,8-methanoisoquinoline	
17	JIXDAV	3-(m-Chlorobenzamido)-5,6,7,8-tetrahydro-5,8-methanoisoquinoline	
18	KIZRUJ	N-(5-bromopyridin-2-yl)benzamide	
19	OGENOE	2,3-Difluoro-N-(2-pyridyl)benzamide	
20	XIFNIK01	4-Methyl-N-(pyridin-2-yl)benzamide	
21	YOVKIG	4-chloro-N-(pyridin-2-yl)benzamide	Chains
22	JIXDEZ	3-(p-Methylbenzamido)-5,6,7,8-tetrahydro-5,8-methanoisoquinoline	
23	JIXDID	3-(p-Nitrobenzamido)-5,6,7,8-tetrahydro-5,8-methanoisoquinoline	

Appendix B - Additional data for Chapter 3

B.1 IR data of co-crystal screen

Table B.1 IR data of co-crystal screen

		Malonic acid	**Glutaric acid**	**Pimelic acid**	**Azelaic acid**	**Fumaric acid**	**Succinic acid**	**Adipic acid**	**Suberic acid**	**Sebacic acid**	**Dodecanedioic acid**
	c=o	1689	1677	1683	1686	1659	1679	1864	1685	1686	1684
		OH---N stretch wave number if present									
		C=O									
2Pyr	1686	x	x	x	x	x	x	x	x	x	x
2Pyr-Cl	1692	x	x	x	x	x	x	x	x	x	x
2Pyr-Br	1692	x	x	x	x	x	x	x	x	x	x
2Pyr-I	1689	x	x	x	x	x	x	x	x	x	x
3Pyr-Cl	1687	2489, 1919	x	2551, 1924	x	x	2486, 1942	2495, 1847	2507, 1944	x	x
		1716, 1694, 1680		1692			1701, 1680	1719, 1686	1683		
3Pyr-Br	1687	2440, 1883	2561, 1940	x	x	2459, 1872	2481, 1897	2538, 1868	2517, 1879	x	x
		1715, 1679	1682			1681	1700, 1682	1717, 1686	1683		
3Pyr-I	1669	2438, 1895	2454, 1895	x	x	2444, 1866	2484, 1889	2484, 1913	2,331	2516, 1901	x
		1678	1676			1677	1684, 1699	1695, 1683	1692, 1662	1685	
4Pyr-Cl	1676	2452, 1889	2457, 1934	2505, 1913	2499, 1896	2473, 1870	2480, 1905	2519, 1894	2504, 1911	2522, 1904	2456, 1885
		1753, 1680	1679	1697, 1681	1702, 1689, 1674	1665	1681	1689	1688	1692	1690
4Pyr-Br	1680	2470, 1892	2472, 1298	2503, 1904	2499, 1896	2443, 1887	2384, 1896	2457, 1861	2452, 1893	2528, 1905	2411, 1900
		1756, 1678	1698, 1680	1687	1703, 1675	1673	1670	1689	1687	1701, 1682	1690
4Pyr-I	1658	2489, 1897	2495, 1902	2516, 1942	2495, 1890	2394, 1888	2412, 1889	2438, 1933	2512, 1892	2551, 1904	x
		1686	1698, 1678	1696, 1687	1704, 1674	1673	1686, 1670	1686, 1676	1688	1698, 1674	

B2. 3Pyr-I:SeA with all crystallographically unique molecules displayed

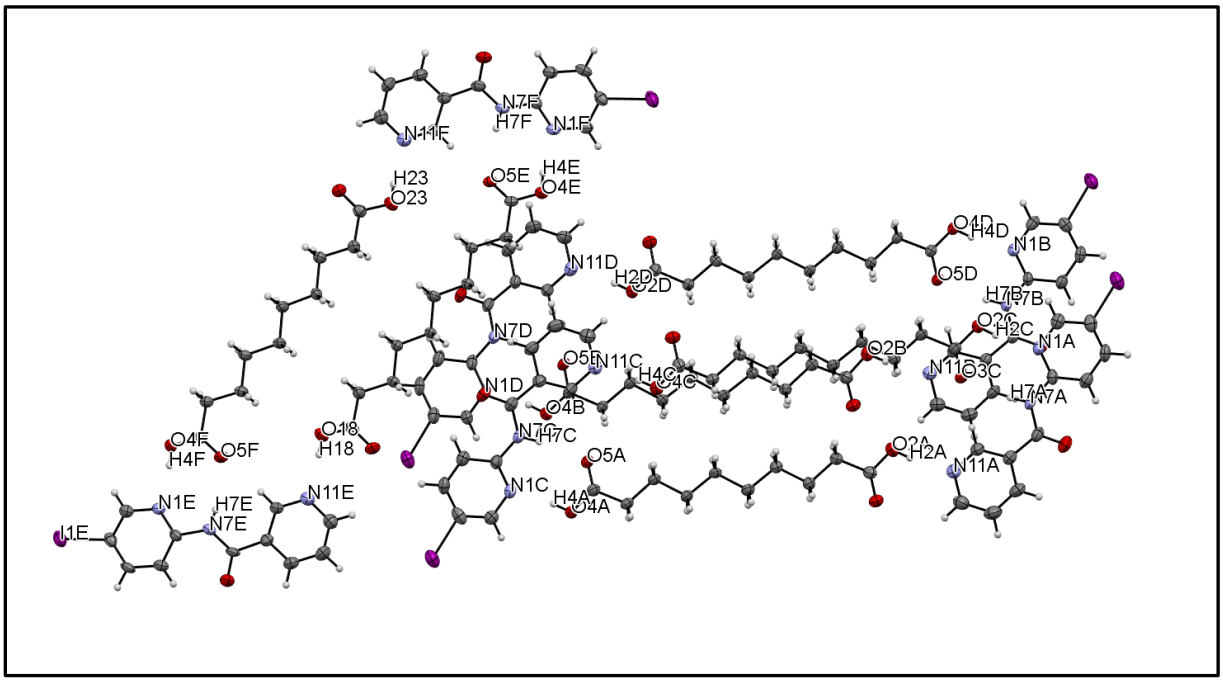

Figure B.1. 3Pyr-I:SeA with all crystallographically unique molecules displayed

B3. 4Pyr-I:AA with all crystallographically unique molecules displayed

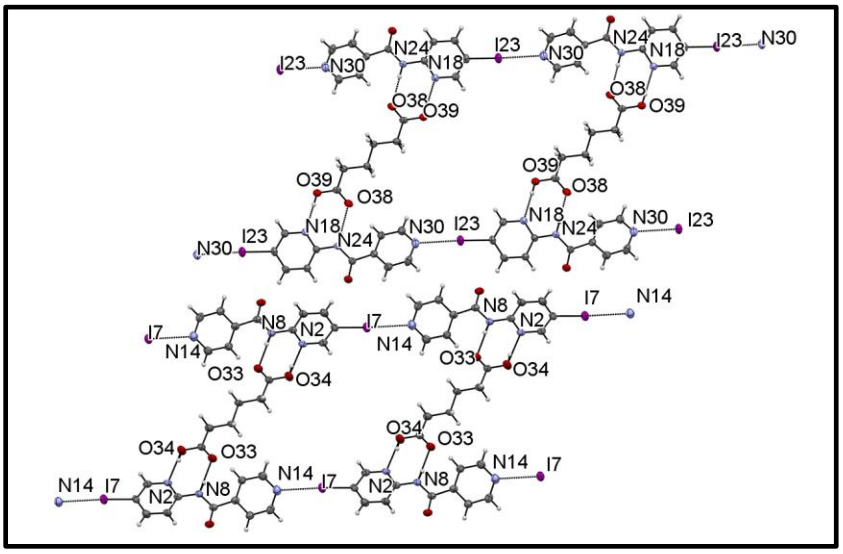

Figure B.2. 4Pyr-I:AA with all crystallographically unique molecules displayed

Appendix C - IR data for Chapter 4

C.1 IR data of co-crystal screen.

	Location of IR bands for N-H, and C=O modes, respectively.	DITFB Key IR peak positions in co-crystal (ground mixture) for NH and O=C. (cm^{-1})	TITFB Key IR peak positions in co-crystal (ground mixture) for NH and O=C. (cm^{-1})
Bz-Bz	No sharp peak	3338	3410
	1669	1656	1672
Bz-Cl	No sharp peak	3242	3390
	1674	1679	(1674) 1657
BZ-Br	No sharp peak	*	3386
	1677	1670	(1674) 1656
Bz-I	No sharp peak	*	3391
	1672	1667	(1673) 1656
2Pyr	3342	3285	*
	1686	1684	1682
2Pyr-Cl	3445	3289	3274
	1692	1695	1675
2Pyr-Br	3343	3286	3343, 3270
	1691	1694	(1693),1675
2Pyr-I	3350, 3331	3290	NH sharpness lost
	1689, 1683	1692	1681
3Pyr	No sharp peak	3326	3304
	1670	1653	1653
3Pyr-Cl	No sharp peak	3336	3388
	1686	(1686),1650	1692
3Pyr-Br	No sharp peak	3336	3518
	1686	1649	1689
3Pyr-I	No sharp peak	3324	3317
	1669	1650	1655
4Pyr	No sharp peak	3298, 3271	3293
	1684	1669	1659
4Pyr-Cl	No sharp peak	3308	3388
	1676	1681, 1656	1693
4Pyr-Br	No sharp peak	3403	3390
	1680	1655	1692, 1662
4Pyr-I	No sharp peak	3407	3393
	1680	1686	1693
*=No change, ( )=unreacted/residual target			